The role of the *C. elegans* Aryl hydrocarbon receptor in environmentally-driven aging

Inaugural-Dissertation

zur Erlangung des Doktorgrades
der Mathematisch-Naturwissenschaftlichen Fakultät
der Heinrich-Heine-Universität Düsseldorf

vorgelegt von

Vanessa Brinkmann
aus Senden (Westfalen)

Düsseldorf, 24. Juli 2018

aus dem Leibniz Institut für umweltmedizinische Forschung (IUF)
an der Heinrich-Heine-Universität Düsseldorf

Gedruckt mit der Genehmigung der
Mathematisch-Naturwissenschaftlichen Fakultät der
Heinrich-Heine-Universität Düsseldorf

Berichterstatter:

1. Prof. Dr. Charlotte Esser

2. Prof. Dr. William Martin

Co-Betreuerin: Dr. Natascia Ventura

Tag der mündlichen Prüfung: 24.09.2018

Table of contents

Abstract 1

1. Introduction 2

Caenorhabditis elegans as a model organism for aging research 3

General features of *C. elegans* 3

Aging features of *C. elegans* 5

Age-associated neurodegenerative disease models 9

Modulation of aging in *C. elegans* 10

Genetic interventions 11

Nutritional interventions 15

The aryl hydrocarbon receptor (AhR) 19

AhR structure and function 19

Modulation of AhR activity 21

AhR in aging and diseases 23

AHR-1, the AhR ortholog of *C. elegans* 24

2. Hypothesis and aims 28

3. Material and Methods 30

E. coli 30

C. elegans 31

Methods for Aim 1: Treatment with AhR modulators 35

Methods for Aim 2: Assessing aging 38

Methods for Aim 3: Identification of AHR-1 target gene expression 41

Box plots 46

Statistical analysis 46

4. Results 47

Benzo(a)pyrene (BaP) affects development and lifespan in an AHR-1-dependent manner, under specific conditions 47

Curcumin extends *C .elegans* healthspan in an AHR-1-dependent manner 48

AHR-1 protects against UVB-induced apoptosis in the germline 51

Loss of AHR-1 function extends lifespan and healthspan on an *E. coli* HT115 diet 53

Loss of AHR-1 function affects lifespan and healthspan in a diet-dependent manner 55

Loss of AHR-1 function influences lifespan and healthspan in a temperature-dependent manner 62

Loss of AHR-1 function does not affect lifespan, healthspan, and heat stress resistance on killed bacteria.....63

Mass spectrometry analysis reveals that HT115 might produce higher levels of tryptophan and indole-containing compounds.....66

AHR-1 regulates genes responsible for the detoxification response.....81

AHR-1 is required in the nervous system to regulate lifespan 85

Curcumin treatment leads to the differential expression of cytochrome P450 genes in an AHR-1-dependent manner.....89

Genes induced by curcumin are mainly AHR-1-dependent.....91

5. Discussion.....98

AIM 1 Identification of potential AHR-1 modulators 98

Benzo(a)pyrene (BaP) affects development and lifespan in an AHR-1-dependent manner, under specific conditions.....98

Curcumin extends healthy lifespan in an AHR-1-dependent manner 99

AHR-1 protects against UVB stress 100

AHR-1 influences lifespan in a diet-dependent manner.....101

Mass spectrometry analysis reveals that HT115 might produce higher levels of tryptophan and indole-containing compounds.....103

AIM 2 Impact of AHR-1 deficiency on aging and age-associated phenotypes.....105

AHR-1 influences polyQ accumulation and toxicity independent of the diet 105

AHR-1 affects aging in a temperature-depending manner 106

ahr-1 RNAi and *ahr-1(ju145)* have opposing effects on lifespan 107

AIM 3 Identification of AHR-1 target genes in response to AHR-1 modulators 108

AHR-1 regulates genes responsible for the detoxification response.....108

AHR-1 is required in the nervous system to regulate lifespan 109

Potential crosstalk between AHR-1 and other pathways 109

6. Summary.....111

7. Zusammenfassung.....112

8. Bibliography 114

Statutory Declaration 125

Contribution to scientific publications 126

Supplement 127

Abstract

Aging is the highest risk factor for death and disease, and it is concurrently shaped by extrinsic and intrinsic factors. It is of great importance to understand the molecular mechanisms underlying these factors to prevent aging-associated diseases. In mammals, the hazardous effects of many environmental toxicants are mediated by the aryl-hydrocarbon receptor (AhR). The AhR is a highly conserved transcription factor of the bHLH/PAS protein family, which is activated through the binding of specific classes of ligands in mammals. Both, chemicals of anthropogenic origin (xenobiotics) and natural compounds were identified as AhR modulators. Specifically, AhR modulators can be divided into four classes: environmental, dietary, host-mediated, and microbial factors.

In *C. elegans*, the well-known AhR ligand 2,3,7,8-tetrachlorodibenzo-p-dioxin does not bind the AhR homolog AHR-1 and no other AHR-1 modulating compounds had been identified to date. Also, besides xenobiotic ligands, no other potential modulators of AHR-1 signaling have been tested for their ability to influence *C. elegans* life traits through AHR-1. Therefore, in this study, I addressed the question whether the *C. elegans* AHR-1 responds to any of the known classes of mammalian AhR modulators (either as ligands or ligand-independent) and whether AHR-1 influences the aging process. I specifically looked for health-associated parameters and gene expression in response to representatives of the four different classes. The environmental pollutant benzo(a)pyrene affected health and *cyp* (Cytochrome P450 monooxygenase) expression mainly independent of AHR-1. As a host-mediated factor, I used UVB, which produces a highly potent AhR ligand *in vivo*. I found that *ahr-1* mutants are more sensitive against the UVB-induced reduction of fertility and that apoptosis is induced in *ahr-1* mutants, while there was no significant induction of *cyp*s. The dietary factor curcumin increased health and induced gene expression in an AHR-1-dependent manner. As microbial factors, I used different *E. coli* diets (HT115 vs. OP50), which I found to differentially impact on the health span of the *ahr-1 C. elegans* mutant. While assessing the function of AHR-1 in age-associated neurodegenerative diseases, I found that AHR-1 has an impact on the progression of polyglutamine aggregation.

In conclusion, I showed that *C. elegans* is a good model for studying conserved AhR functions since it appears to be involved in the response to three out of four classes of mammalian AhR modulators. Moreover, AHR-1 affects aging and age-associated diseases.

1. Introduction

Aging is defined as the time-dependent biological deterioration of physiological functions. It is accompanied by an increased risk of death and morbidity. Pathologies with a higher incidence in old age are diabetes, cardiovascular diseases, neurodegenerative diseases, and cancer [1, 2]. There are many theories about the aging process, and they can be mainly divided into two categories: the programmed theory of aging and the damage or error theory of aging. Each of these theories is further divided into several sub-categories. The programmed theory states that the activity of specific genes (Programmed Longevity), hormones (Endocrine Theory), or the immune system (Immunological Theory) define the aging process. The damage or error theory instead assumes that the primary factor contributing to aging and age-associated diseases is caused by cellular damages. These damages might occur due to the repeated use of specific tissues (Wear and tear theory), the accumulation of cross-linked proteins (Cross-linking theory), Free radicals (Free radicals theory), or DNA damage (Somatic DNA damage theory) [3]. While these theories try to explain aging by either genetic or environmental factors, it has been proposed that both, genes and environment interact to shape the aging process [4, 5]. From the genetic point of view, nutrient sensing pathways like the Insulin/Insulin-like growth factor signaling (IIS) pathway, the AMP-activated protein kinase (AMPK) pathway, sirtuins and the mechanistic target of rapamycin (mTOR) signaling pathway have evolutionarily conserved functions in the regulation of aging. While the impact of genetic factors is estimated to be one quarter, environmental and epigenetic factors account for the rest and therefore have a fundamental impact on aging. Environmental factors affecting aging are pollutants, diet, radiation, stress, and temperature [5]. More recently, also host-microbiota interactions have been considered important contributors to aging [5].

Aging is complex, and none of the above-mentioned theories is sufficient to explain it fully. Nevertheless, there are common mechanisms and features, which shape the aging process in an evolutionarily conserved fashion. Lopez-Otin [2] and colleagues have identified nine hallmarks of aging, which are 1) genomic instability, 2) telomere attrition, 3) epigenetic alterations, 4) loss of proteostasis, 5) deregulated nutrient sensing, 6) mitochondrial dysfunction, 7) cellular senescence, 8) stem cell exhaustion and 9) altered intercellular communication. Most of these aging hallmarks are evolutionary conserved, and therefore model organisms are of specific importance for the field of aging research. In fact, apart from telomere attrition, all mentioned hallmarks can be observed in vertebrate as well as invertebrate model organisms [1]. Because of the conservation of aging features and their short lifespan, the yeast *Saccharomyces cerevisiae*, the nematode *Caenorhabditis elegans*, and the fruit fly *Drosophila melanogaster* have become elected model organisms of aging research [4, 6]. In the section below, I will point out some of the advantageous features of *C.*

elegans as a model organism in aging research as well as mention some of the evolutionary conserved intrinsic and extrinsic factors involved in aging.

Caenorhabditis elegans as a model organism for aging research

General features of *C. elegans*

In 1974 [7] Sydney Brenner introduced the nematode *Caenorhabditis elegans* as a model organism for developmental biology and neurobiology. Since then, *C. elegans* has become a favorable model organism in many fields of biology and toxicology. *C. elegans* is a free-living nematode, which lives on rotten fruit and feeds mainly on different bacteria species. While feeding on a variety of species in the wild, in the laboratory it is cultured on agar plates and commonly feeds on a single bacterial strain, the proteobacterium *Escherichia coli* [7]. Alongside the easy cultivation *C. elegans* comprises several features, which make it an attractive model organism: the occurance of self-fertilizing hermaphrodites, the short developmental and reproductive cycles, its short lifespan, small size, transparency, the existence of big libraries for mutant strains and RNAi, and the conservation of core metabolic and aging pathways [7-9].

C. elegans exists in two sexes: hermaphrodites and males. Hermaphrodites carry two X chromosomes while males have only one X chromosome. In the wild and the laboratory, the self-fertilizing hermaphrodite occurs with a frequency of approx. 99.9 %. The self-fertilization of hermaphrodites allows the cultivation of populations with low genetic variability in the laboratory, while the presence of males enables the cross between different *C. elegans* strains in the laboratory and increases the genetic variability in the wild. Both sexes have a constant number of somatic cells, a phenomenon called eutely. Hermaphrodites have 959 somatic cells, while males count 1031 somatic cells [10]. This constant cell number allows the tracking of cell fates from fertilization to adulthood [8]. Another advantage of using *C. elegans* as a model organism is its small size and the transparency of the body. Adult hermaphrodites reach an average length of 1 mm, while the male is smaller and thinner. Besides the smaller size, the male can be easily identified by the shape of its tail, which has a blunt end compared to the pointed end of the hermaphrodite (Figure 1) [10]. Although *C. elegans* is small, it is a complex multicellular organism. Through its transparent body, the organization of the animals can be studied on a cellular level in the living organism [11]. *C. elegans* is composed of an epidermis, muscles, a digestive system, a reproductive system, and a nervous system [8].

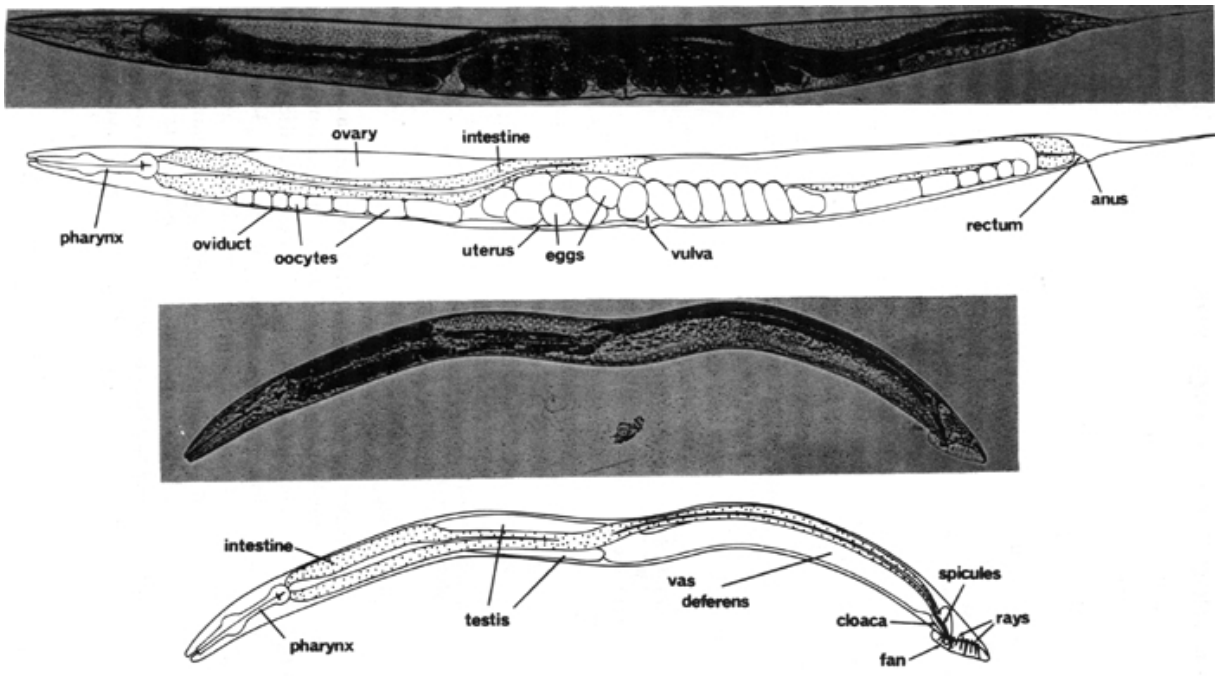

Figure 1 Anatomical features of a hermaphrodite and a male *C. elegans*. Both sexes are composed of an epidermis, muscles, a digestive system, a reproductive system, and a nervous system. Due to the transparency of the nematode, the single tissues can be observed *in vivo* using a stereomicroscope [12, 13]. Reprinted from [12], © 1977, with permission from Elsevier.

At 20 °C, the development of *C. elegans* takes 3 days from fertilized eggs to adults. After the fertilization, the embryo develops *in utero* until it leaves the uterus in the 24-cell stage. After the eggs are laid the embryo stays inside the egg, which is covered by an impermeable egg-shell, for approx. 10 h. After hatching, the nematode undergoes the postembryonic development, which contains 4 larval stages (L1 to L4). Each larval stage ends with a molting process. During the first 16 h after hatching, the 250 µm long L1 larva starts the development of postembryonic neurons and the reproductive system. In the L2 stage, which arises 26 h after hatching, the organization of the gonad starts and its development continues during the larval stages L3 and L4. In L4 larvae, the germ cells differentiate, and a short period of sperm production starts. The L4 stage ends with the worm's final molt, the L4/adult molt. In the phase of young adulthood, which begins approx. 56 h after birth, the worm generates oocytes and the egg-laying apparatus. Approx. 12 h after the L4 molt, the adult worm starts to lay eggs for 2 to 4 days [11]. After the fertile phase, the adult lives for a couple of weeks before it dies of senescence.The lifespan of *C. elegans* is very short compared to mammals. It is dependent on the culturing conditions, and when cultured on a standard diet at 20 °C, *C. elegans* lives approx. 16 days. Especially for aging studies, the short lifespan is very advantageous. Moreover, similar to mammals, *C. elegans* shows a progressive decline in functions and undergoes morphological changes during the aging process. Of note, many longevity pathways are very well conserved in *C. elegans*. These features are discussed more detailed in the following chapters.

Besides the physiological features of the worm, the existence of standard procedures and big libraries for mutant strains and RNA interference (RNAi) further strengthens its use as a model organism for aging studies. Conventional methods include the long-term storage of viable nematodes in liquid nitrogen [8, 14]. One of the libraries mentioned above is the Caenorhabditis Genetics Center (CGC) (https://cgc.umn.edu/), which collects, maintains and distributes *C. elegans* strains. At the moment, more than 40,000 Caenorhabditis strains are available from the CGC. Another big library is the *C. elegans* RNAi Collection (Ahringer Library), which counts almost 20,000 *E. coli* clones to conduct RNAi feeding in *C. elegans*. By this, it covers 87 % of annotated *C. elegans* genes. The significance of *C. elegans* as a model organism is further underlined by the facts that its genome was the first multicellular genome wholly sequenced (*C. elegans* Sequencing Consortium, 1998) and that 4 Nobel Prizes were awarded to *C. elegans* researchers in the past 20 years [15].

Aging features of *C. elegans*

Like in humans, aging is correlated to behavioral, physiological and biochemical changes and an increased incidence of death in *C. elegans*. Behavioral changes include the decline in pharyngeal pumping rate, locomotion, and chemotaxis, while physiological changes include a decrease in the organization of different tissues (*e.g.* body wall muscles and gonad), a progressive reduction of the reproductive rate and the accumulation of bacteria in the gut. Besides others accumulation of lipofuscin, increase in DNA damage, and changes in gene expression can be considered age-related biochemical changes [16].

Age-related behavioral changes

Probably one of the easiest accessable changes during aging is the decline in locomotion. The alternation of dorsal and ventral body wall muscle contractions causes *C. elegans* to move in a sinusoidal pattern. This process is controlled by motor neurons [17]. During aging, a drop in motoric functions is observable. It is characterized by slower and less coordinated movement (Figure 2A) and can be assessed by measuring the locomotion frequency or by analyzing the quality of movement [16, 18]. The deterioration of the body wall muscles (sarcopenia) and the functional decline in motor neuron functionality play a fundamental role in the decay of motility during aging [18, 19]. The ability of nematodes to move is correlated to lifespan and pharyngeal pumping activity and can be used to predict the lifespan of an animal [16, 20].

Comparable to a reduced ability to move, the pharyngeal pumping activity declines during aging (Figure 2B) [16, 20]. The pharynx is a neuromuscular organ, consisting of 20 neuronal cells and 20 non-striated muscle cells. It is required for food uptake and crushing. Due to the transparency of *C. elegans*, the pharyngeal pumping activity can be easily studied using a stereoscope. A young adult shows a pharyngeal pumping activity between 200 to 300 pumps per minute. This frequency is modulated by the neurotransmitters acetylcholine and serotonin.

During aging, the pharyngeal pumping activity progressively declines until there is hardly any pumping observable anymore. This deterioration appears most likely due to the degeneration of the pharyngeal muscles and a lesser extent due to plugging of the pharynx by bacteria [19-21]. Although neuronal inputs are relevant for the regulation of the pharyngeal pumping frequency, the functionality of the pharyngeal nervous system is not essential for the pumping activity [22]. The pharyngeal pumping activity is used as an indicator of health and a parameter to predict the lifespan of *C. elegans* [20]. However, this parameter has been lately criticized as a poor factor to assess the healthspan since neither protection against the age-associated decline in pharyngeal pumping in long-lived mutants was found, nor do short-lived mutants show an earlier decrease in pumping [23, 24]. The nematode's pharynx has been proposed to be orthologous to the vertebrate heart due to 1) a similar function as a material-transporting organ, 2) similarities in the electrical circuits regulating pharyngeal pumping and the contractions of the vertebrate heart, and 3) the dependency on NKX transcription factors [25].

Another behavioral change during aging is the decline in chemotaxis towards food and chemical attractants [26-28]. Chemotaxis is the movement in the direction of a particular substance. In *C. elegans*, this behavior is regulated by ciliated sensory neurons, and is, similar to movement and pharyngeal pumping, a neuromuscular behavior. The chemotaxis behavior is influenced by both, the nervous system and the muscles, and can be therefore used as a parameter to study aging of the muscles and the nervous system. Interestingly, studies have shown that there are no morphological changes in sensory neurons, but that sensory neurons are implicated in the determination of lifespan [29].

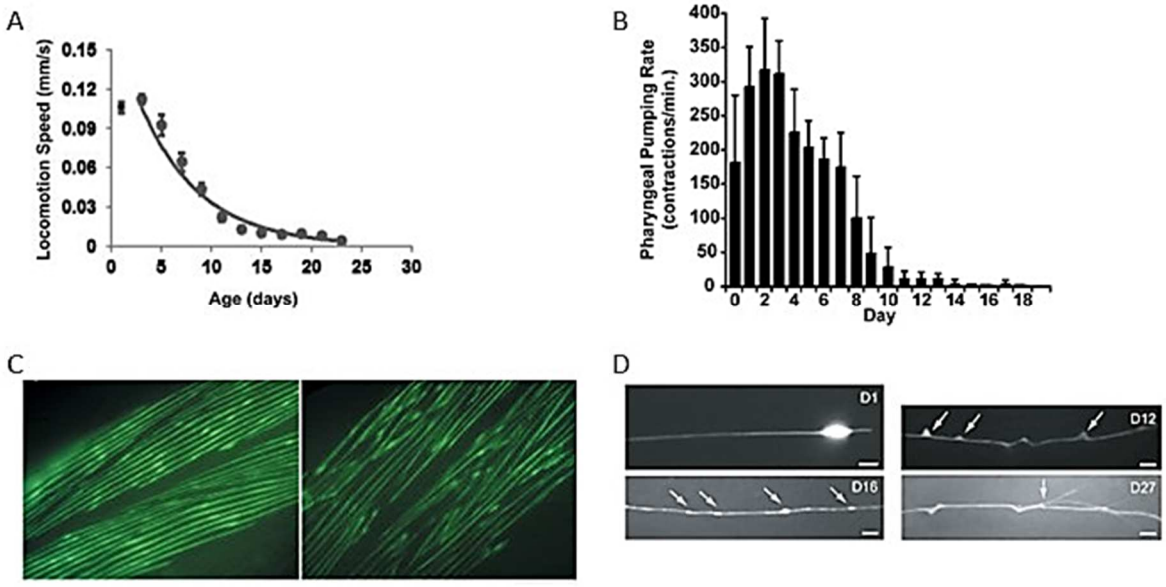

Figure 2 Aging features of *C. elegans*. A) During aging, worms undergo a progressive decay in motor activity, beginning in early life. Reprinted from [18], © 2013, with permission from Elsevier. B) Age-related changes in pharyngeal pumping rate starting from L4 larvae (day 0). Reprinted from [20] (© 2004 National Academy of Sciences). C) Deterioration of the muscle structure during aging in Pmyo-3-myo-3-GFP worms at day 4 (left) and day 18 (right). Reprinted by permission from Springer Customer Service Centre GmbH: Springer Nature, Nature,

[19], © 2002. D) Age-dependent defects in *C. elegans* touch receptor neurons. Top left: a healthy touch neuron; bottom left: a touch neuron with beads; top right a touch neuron with blebs; bottom right: a touch neuron with ectopic branches. Reprinted from [30].

Morphological changes during aging

Age-related morphological changes in different organs have a high impact on above-mentioned behavioral changes and are reliable markers of the health status of *C. elegans*. In the following, I will focus on the age-dependent changes occurring in the body wall muscles, the nervous system, the intestine and the reproductive system.

C. elegans hermaphrodites have 95 body wall muscle cells, which are similar to the skeletal muscle cells of vertebrates. These striated muscles are innervated by the cholinergic and GABAergic neurons of the ventral nerve cord and mediate the movement of *C. elegans* [31]. The muscle structure can be easily visualized by using transgenic strains expressing the GFP under the promoter of genes expressed in the muscles (Figure 2C). During the aging process, *C. elegans* shows symptoms of sarcopenia starting from mid-life (day 11): disorganization of the sarcomeres, reduced number of myosin thick filaments, bends and breaks of the filaments, increased misshapen nuclei and bigger nucleoli, increased mitochondrial fragmentation, and a decrease in mitochondrial volume and activity [19, 21, 32]. The degree of sarcomere disorganization is correlated to a decline in the motility.

The *C. elegans* nervous system is one of the more complex systems in the nematode. It contains 302 neurons in the hermaphrodite and 473 neurons in the male. As in vertebrates, it consists of cholinergic, GABAergic, glutamatergic, dopaminergic, and serotonergic neurons. The neurons can be divided into 4 functional categories: motor neurons, sensory neurons, interneurons and polymodal neurons. The motor neurons are responsible for locomotion and reproduction. The sensory neurons instead recognize environmental stimuli as mechanical stimuli, toxic and harmful stimuli, chemicals, temperature, light, and oxygen. Interneurons link neuronal networks in the worm and function as processors of information. They form the largest functional group of neurons in the nematode. Polymodal neurons are neurons, which have more than one function (*e.g.,* motor and sensory function) [33]. As the nervous system ages, morphological and functional changes in the organization of the neurons appear. Similar to the human brain, aging does not cause neuronal death or axonal degeneration in *C. elegans* [19]. Instead, beads, blebs, ectopic branches, and a decline in synaptic signaling appear in the aging *C. elegans* nervous system (Figure 2D) [34, 35]. The structural changes can be studied by expressing a fluorescent protein (*e.g.,* GFP) under the promoter of specific neuronal genes (*e.g., mec-4* or *unc-47*): beads can be observed as bubble-like enlargements with a dark, fluorescence-free center [34]; blebs as triangular protrusions from the processes [30, 34]; ectopic branches are found in some, but not all the mechanosensory neurons and GABAergic neurons [35, 36]. A decline in the number and size of synapses and a shrinkage of the axon

diameter can be also observed during aging [21, 35]. Together with the degeneration of the muscles, the decline in motor neuron functionality plays a vital role in the deterioration of motility during aging [18]. Moreover, the nervous system has been proposed to be a central regulator of longevity [37]. Its effect on the determination of the lifespan is mediated by the sensory neurons and involves the Insulin/IGF-1 pathway [29, 38].

The intestine of *C. elegans* is a large organ consisting of 20 epithelial cells, which form a long tube around the intestinal lumen. Many microvilli form a brush border at the apical membrane. The intestine is connected to the pharynx and the rectum through valves [39]. It is responsible for the digestion of food and the synthesis and storage of macromolecules. Beside its function in absorption and metabolism, the intestine is the principal organ involved in the response towards environmental stressors like toxins and chemicals. Therefore, it is not surprising that many genes responsible for the detoxification process in *C. elegans* are exclusively expressed in the intestine. These genes include metallothionein genes, cytochrome P450 (cyp) genes, and p-glycoprotein genes [40]. Moreover, the intestine has an essential function in the interaction of host-pathogen interactions and the interaction between *C. elegans* and its microbiota [40, 41]. Compared to other organs and tissues, the age-associated changes in the *C. elegans* intestine are poorly understood. One of the first changes, which has been observed in the aging *C. elegans* digestive system, is the accumulation of bacteria in the pharynx and intestine [42]. The reasons for this accumulation are not yet fully understood, but the age-dependent reduction in the pharyngeal pumping and grinder activity and the decline of the immune system have been suggested as possible causes [21, 43]. The bacteria accumulation has been proposed to contribute to the mortality of *C. elegans* and recent studies show that the lifespan of *C. elegans* is inversely correlated to the accumulation of bacteria in the intestine [42, 43]. But the bacteria are not harmful *per se* and metabolically active bacteria are needed for healthy growth, fertility, and aging of the worm. Interestingly, the relationship between *C. elegans* and its gut microbiota has been suggested to change during the aging process: while *C. elegans* is the predator in early life, it becomes prey later in life [41]. The accumulation of bacteria in the intestine has been moreover proposed to be responsible for another age-related phenomenon, the loss of microvilli [44]. Other age-related changes in the intestine are the variability in the shape and size of the intestinal lumen, the reduction in microvilli length, the loss of intestinal nuclei, and the accumulation of yolk in the intestinal lumen [21, 44].

The reproductive system of the hermaphrodite can be divided into 3 parts: the somatic gonad, the germline, and the egg-laying apparatus. The somatic gonad is composed of the distal tip cells (DTCs), the gonadal sheath, the spermatheca, the spermatheca-uterine valve, and the uterus. The germline produces oocytes and sperm. While the sperm cells are exclusively produced during the L4 larval stage, the oocytes are produced throughout adult life. The egg-

laying apparatus consists of the uterus, the uterine muscles, the vulva, the vulval muscles, and the egg-laying neurons [45]. As an effect of aging, the self-fertile reproduction declines early in life, and wild-type *C. elegans* have an average reproductive span of 5.8 days [20]. Therefore, similar to humans, reproductive aging precedes the aging of the somatic tissues [46]. The fertility of a hermaphrodite is mainly limited by the amount of sperm, but also independent of self-fertilization the production of progeny declines with aging [16]. This decline is mainly due to the age-dependent reduction in oocyte quality [47]. During aging, unfertilized oocytes accumulate in the uterus, resulting in the swelling of the mid-body. Degradation products of these oocytes also block the vulva and impair the egg-laying muscles. In very old animals even germline tumors can appear [21]. Similar to the nervous system and the intestine, also the germline plays a vital role in the aging process. While on the one hand, somatic signaling pathways implicated in longevity influence reproductive aging (*e.g.*, IIS and TGF-β), on the other hand, germline signals affect somatic aging [47].

Age-associated neurodegenerative disease models

Although *C. elegans* itself does not develop pathologies similar to human age-associated neurodegenerative diseases, there are different transgenic strains available to study diseases like Alzheimer's disease (AD), Parkinson's disease (PD), and Huntington's disease (HD). AD is among the top 10 causes leading to death in humans. In 2015 almost 50 million people worldwide were affected by AD or related dementias, and the number is predicted to increase to more than 130 million by 2050 [48]. The disease is characterized by memory loss, but the severity of symptoms increases drastically during the disease's progression, reaching from memory lapses and forgetfulness in early stages to the loss of the ability to speak or respond to the surroundings in late stages [49]. One of the characterizing features of AD is the accumulation of β-Amyloid (Aβ) plaques in the brain, which have been shown to contribute to the development of AD [50]. In *C. elegans* models for AD a peptide of 42 aa of the human Aβ ($A\beta_{1-42}$) is expressed in the muscles of *C. elegans* causing age-dependent paralysis and Aβ accumulation (Figure 3A) [51]. By now, several strains expressing human Aβ peptides exist, including strains with Aβ in the nervous system [52, 53].

Parkinson's disease (PD) is another neurodegenerative disease, which affects more than 10 million people worldwide [54]. It is characterized by the accumulation of Lewy bodies containing aggregated alpha-synuclein (α-syn) proteins and the degeneration of dopaminergic neurons. Symptoms vary among patients but mainly affect motoric ability leading from light impairment in motoric function and mild tremors in early stages to the loss of the capacity to walk independently in later stages. Also, cognitive disabilities are described [54]. *C. elegans* possesses orthologues for many genes involved in PD, which are parkin (*pdr-1*), PINK1 (*pink-1*), DJ-1 (*djr-1.1, 1.2*), LRRK2 (*lrk-1*), ATP13A2 (*capt-6*), and GBA (*F11E6.1, TO4A8.7*),

making it a suitable model to study PD [55]. Interestingly, similar to humans, mutations in some of these genes lead to the degeneration of dopaminergic neurons [55-57], which can be observed in strains expressing fluorophores in the dopaminergic neurons [58]. On the other hand, strains expressing α-syn fused to fluorophores can be used to study the age-dependent accumulation of α-syn in muscle cells [59, 60] or in neurons [61].

Besides Aβ plaques and Lewy bodies, the expansion of polyglutamine (polyQ) is involved in the progression of neurodegenerative diseases in humans. The expansion of polyQ in the protein huntingtin, for example, leads to HD, a heritable progressive brain disorder which leads to uncontrolled movements and a decline in cognitive functions [62]. Up to date, besides HD, 8 other polyQ related neurodegenerative diseases are known. To model polyQ disorders, *C. elegans* strains expressing fluorescence-tagged polyQ fusion products serve as models [63]. Several transgenic *C. elegans* strains expressing fluorescentl polyQ residues of different length in the body wall muscles exist [63, 64]. Other strains express fluorescentl polyQ repeats in the nervous system [65]. Due to the fusion of polyQ to fluorophores, the aggregation can be observed by fluorescence microscopy *in vivo* (Figure 3B). The accumulation of polyQ is age-dependent and leads to paralysis, toxicity, and disruption of protein-folding homeostasis (proteostasis) [63, 66]. Therefore, additionally to modeling polyQ disorders, the mentioned *C. elegans* polyQ expressing strains can be used as a model for proteostasis [66]. Besides above-mentioned strains, many other strains to model the specified and other neurodegenerative diseases (*e.g.*, Amyotrophic lateral sclerosis (ALS)) are available in *C. elegans* [67].

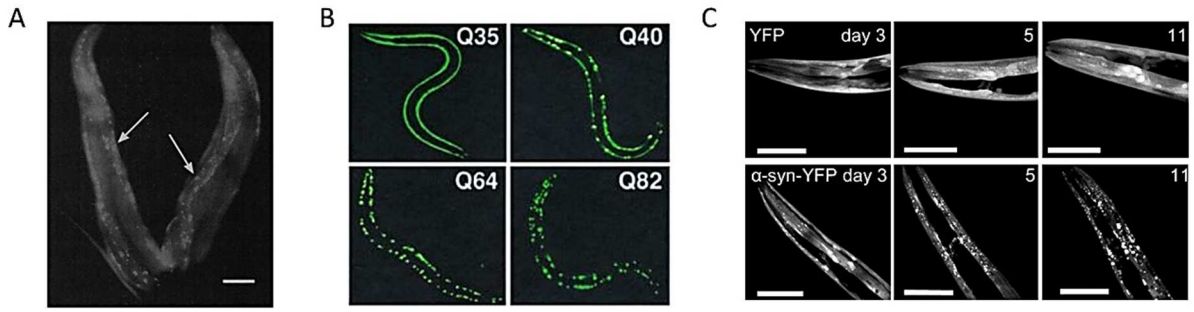

Figure 3 Different *C. elegans* models for age-associated neurodegenerative diseases. A) A *C. elegans* model for AD. Muscle-specific Aβ deposits in transgenic Aβ-expressing worms (strain CL1019) stained with an anti-Aβ antibody [51] (©1995 National Academy of Sciences). B) Models for polyQ disorders showing aggregation of polyQ-YFP fusion proteins of different lengths [63] (©National Academy of Sciences).C) A model for PD shows age-dependent accumulation of α-syn-YFP (strain NL5901). Panel taken from [59].

Modulation of aging in *C. elegans*

Aging is modulated by intrinsic and extrinsic factors (*e.g.,* environment and nutrients) and thanks to the ease of mutagenesis and RNAi screening in *C. elegans*, many of the genes and interventions modulating aging have been initially discovered in *C. elegans* [2, 68]. In the following chapters, I will focus on 1) the major genetic pathways involved in the regulation of lifespan: IIS pathway, the TOR pathway, mitochondrial signaling, germline signaling, quality

control mechanisms, and 2) on the influence of diet as an extrinsic factor modulating the aging process.

Genetic interventions

The IIS pathway

The *C. elegans* Insulin/Insulin-like growth factor (IGF-1) signaling pathway (IIS) is the evolutionary most conserved signaling pathway influencing the aging process from nematodes to mammals and has been extensively studied. It is a nutrient sensing pathway which plays a crucial role in linking environmental stimuli and physiological outputs. It is modulated by the activation or inactivation of the IGF/Insulin receptor, DAF-2 in *C. elegans*. Ligands influencing the activity of the IIS by binding to DAF-2 are insulin-like peptides (ILPs). *C. elegans* possesses 40 ILPs which are different in their structures and work as either activators or inhibitors of the IIS. They are mainly expressed in the nervous system but can also be found in other tissues. The activation of DAF-2 by ligand binding results in the activation of the phosphatidylinositol 3-kinase AGE-1. In turn, AGE-1 activates AKT-1 and AKT-2 by phosphorylation, which then form a complex with the serum- and glucocorticoid-inducible kinase SGK-1. This complex phosphorylates the Forkhead box O (FOXO) transcription factor DAF-16 preventing its nuclear translocation (Figure 4a). Unfavorable conditions like stress or the absence of ILPs prevent the phosphorylation of DAF-16, which, in turn, enters the nucleus and initiates the transcription of target genes. Besides physiological stimuli, also the loss of DAF-2 function causes the nuclear translocation of DAF-16. Genes regulated by DAF-16 include stress-responsive genes coding for heat-shock proteins, antioxidant enzymes, and detoxification genes (*e.g., cyps*, UDP-glucuronosyltransferases (*ugts*), and glutathione S-transferases (*gsts*)) [4, 5, 69]. The nuclear translocation of DAF-16 extends lifespan, increases resistance to different types of stressors (*e.g.,* heat, hypoxia, heavy metals, high osmolarity, UV, and pathogens) and protects against age-associated diseases [70, 71]. Besides DAF-16, the bZIP transcription factor SKN-1 and the heat-shock transcription factor HSF-1 are downstream targets of the IIS. Also, the interaction between the IIS and another important nutrient-sensing pathway, the mTOR pathway is known [38, 72, 73].

The TOR pathway

Similar to the IIS pathway, the TOR (target of rapamycin) pathway is an evolutionarily conserved nutrient-sensing pathway, which affects aging in model organisms from yeast to mice [69]. The *C. elegans* homolog of the TOR kinase is encoded by *let-363* [74]. It has a critical function in the worms' development and worms which lack LET-363, arrest their development at the L3 stage [74]. LET-363 can be found in two functional complexes, the TOR complex 1 (TORC1) and the TOR complex 2 (TORC2). TORC1 is composed of LET-363, the LST8 homolog MLST-8, and the Raptor homolog DAF-15. TORC2 instead is formed by LET-363, MLST-8, and the Rictor homolog RICT-1 [75]. TORC1 is activated by different cues,

including amino acids and growth signals (Figure 4b). The activation of TORC1 includes its translocation to the lysosomal surface and the activation by GTP-bound Rheb. TORC1 regulates metabolic processes like protein and lipid synthesis, and autophagy, while TORC2 is involved in cell survival, apoptosis, and proliferation. TORC2 is activated by growth signals and activates AKT, SGK, and related kinases. The molecular mechanisms of TORC2 activation are far less known than the ones of TORC1, but it has been proposed that ribosomes play a role [73].

Down-regulation of TOR signaling activity can be either achieved by genetic or pharmacological interventions. The most famous compound regulating the activity of the TOR pathway is the immunosuppressant rapamycin, which inhibits TOR signaling. While it was first assumed that rapamycin inhibits explicitly TORC1, it was more recently found to inhibit both TOR complexes [76]. The specific inactivation of only one TOR complex requires either the genetic inactivation of *daf-15* or *rict-1* [73]. Inactivation of TORC1 leads to an increase in autophagy, and the activation of the transcription factors SKN-1 and DAF-16, which in turn promote a longevity response [76]. Through the activation of SKN-1, TORC1 regulates its transcription in a positive feedback loop, since SKN-1 activation leads to the transcription of TORC1 [76]. DAF-16 activation instead, acts as a negative feedback loop by inhibition of *daf-15* expression [73, 77]. Besides DAF-16 and SKN-1, the FOXA homolog PHA-4 is required for the lifespan extension of worms with reduced TORC1 signaling [78]. PHA-4 is a transcription factor regulating genes involved in autophagy. While DAF-16 is required for the lifespan-extending effects associated with inactivation of TORC1, TORC2 inactivation prolongs lifespan independent of DAF-16 [76]. Interestingly, the lifespan extension of animals with reduced TORC2 activity through *rict-1* RNAi is dependent on the bacterial diet [79].

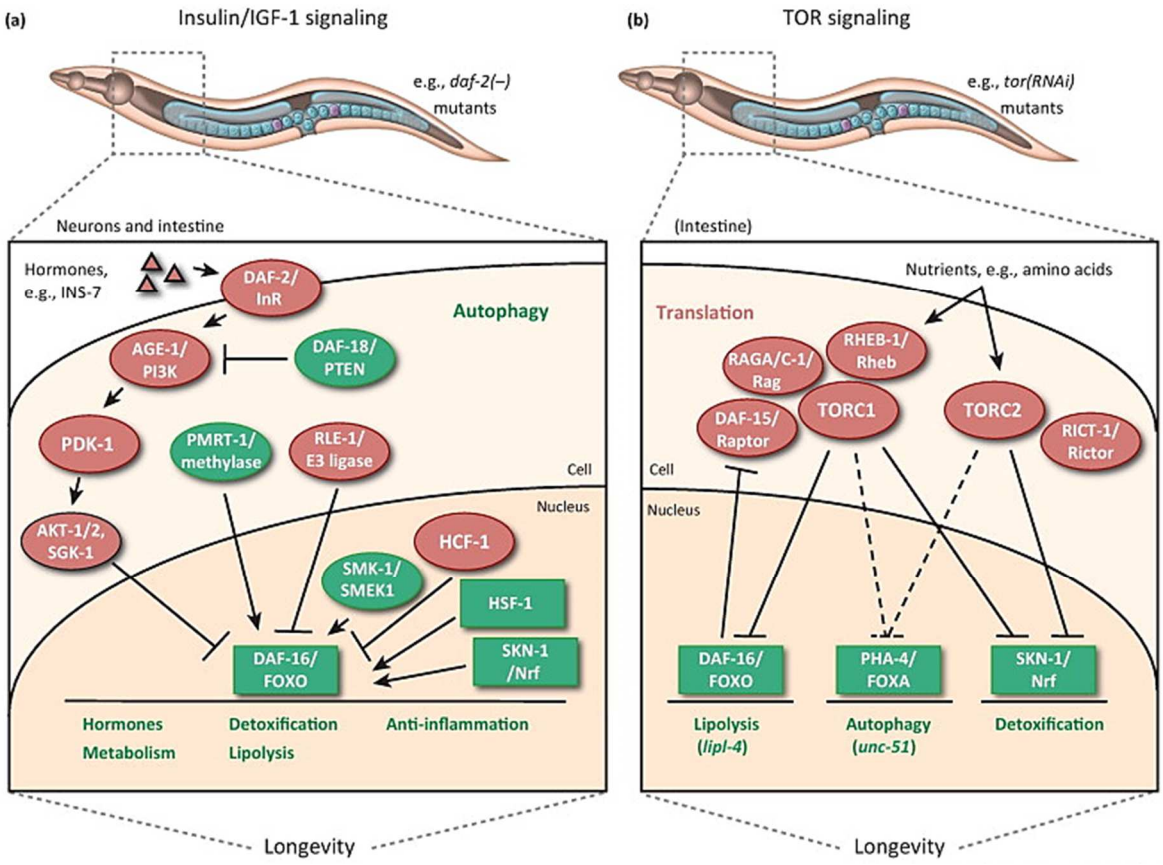

Figure 4 IIS and TOR signaling in *C. elegans*. (a) DAF-2 ligands (*e.g.*, INS-7) activate the IIS pathway, which enables a downstream cascade containing AGE-1, AKT-1, and AKT-2 and prevents DAF-16 from entering the nucleus. Besides the canonical IIS signaling pathway, DAF-16 is regulated by ubiquitination (RLE-1/E3 ligase) and arginine methylation (PMRT-1/methylase). (b) Nutrients influence TOR signaling. The TOR kinase can be found in two different complexes, TORC1 and TORC2. TORC1 interacts with DAF-15, RAGA-1, RAGC-1, and RHEB-1/Rheb. TORC2 interacts with RICT-1. TORC1 and TORC2 inhibit the transcription factors DAF-16 and SKN-1, and PHA-4. Reprinted from [80], © 2012, with permission from Elsevier.

Mitochondrial signaling

Mitochondria are the power generators of the cell and play an essential role in cellular homeostasis [68]. The relationship between mitochondria and aging is two-sided: on the one hand aging impacts mitochondria by reducing the activity of the respiratory chain, on the other hand, the mitochondrial function has a profound impact on the rate of aging. Not only does mitochondrial dysfunction contribute to numerous age-related diseases like diabetes, cardiomyopathy, and neurodegeneration, but a mild reduction of mitochondrial function extends the lifespan in different species from yeast to mammals. Indeed, it has been shown that while a strong reduction in mitochondrial function has deleterious effects, a mild reduction extends lifespan. This phenomenon is referred to as mitohormesis and can be achieved either by genetic or pharmaceutical interventions in *C. elegans* [2, 68]. The lifespan extension comes for the price of a slower development, and a smaller body and brood size. The mechanisms by which mild mitochondrial dysfunction delays aging are not yet completely understood but the induction of specific quality control mechanisms like the mitochondrial unfolded protein response (UPR^{mit}), autophagy and mitophagy play an important role [81-84].

Germline signaling

Aging and reproduction are correlated as the reproductive activity declines with aging. As described above, the reproductive system undergoes changes as the animal ages. But not only does aging influence the reproduction but the germline also affects aging. The removal of the germ cells increases the lifespan of *C. elegans* hermaphrodites by approx. 60 %. For this, the removal of the proliferating germline stem cells (GSC) but not of intact somatic germline tissues (uterus and spermatheca) is crucial [4, 85]. Coherent with the complete ablation of GSCs, the genetic reduction of GSC number (*e.g.,* by *glp-1* downregulation) is associated with an increased lifespan, while over-proliferation (*e.g.,* by *gld-1* downregulation) shortens lifespan [38, 86]. Loss of the GSC leads to the activation of DAF-16 in the intestine via an IIS independent mechanism, which is required for the lifespan extension [87]. Besides DAF-16 activation, reduced germline signaling activates autophagy [38]. Also, the transcription factors SKN-1, HSF-1, and nuclear hormone receptors play an important role in longevity mediated by germline signaling [85]. Effects of the germline on the aging process can also be observed in mice, where the transplantation of ovaries from young mice into old mice increases the recipients' lifespans [88, 89].

Autophagy

All of the above-mentioned signaling pathways converge on a common mechanism: autophagy, a conserved recycling process with a crucial role in aging and diseases [38]. Increased autophagy has been shown to have lifespan-extending effects in *C. elegans*, Drosophila, and mice. Autophagy can be divided into at least 3 different sub-types: microautophagy, chaperone-mediated autophagy, and macroautophagy. Of these types, only macroautophagy (herein referred to as autophagy) has been linked to aging in *C. elegans*. The process of autophagy includes different steps, starting with the formation of the autophagosome, which is a double membrane vesicle. These vesicles encapsulate cytosolic components, which are marked for degradation. The autophagosome then fuses with the acidic lysosome and forms the autolysosome, which degrades the cargo. According to the cargo, autophagy can be divided into further sub-types, of which especially mitophagy (autophagy of mitochondria) and lipophagy (autophagy of lipids) are relevant for the aging process. Autophagy is regulated by the transcription factors HLH-30, a basic helix-loop-helix (bHLH) transcription factor, and PHA-4. Besides the genetic induction of autophagy also pharmacological interventions activate autophagy (*e.g.,* resveratrol and spermidine). In *C. elegans* the LC3 homolog LGG-1 is commonly used as a marker for autophagy. In transgenic lines, fluorophore-labeled LGG-1 foci are counted for the quantification of autophagy. LGG-1 is associated with the membrane of the autophagosome and plays a role in autophagosome elongation, cargo recognition and fusion to the lysosome. Another commonly used marker for autophagy is the p62 homolog SQST-1, which is a cargo receptor that recognizes and binds

proteins labeled for degradation [90]. Studies have revealed that the autophagic activity decreases with age in the *C. elegans'* intestine, body-wall muscle, pharynx, and neurons [91].

Protein homeostasis (Proteostasis)

One of the hallmarks of aging is the loss of proteostasis [2]. It is the balance between protein synthesis, folding, repair, and degradation [92]. A disbalance in proteostasis leads to the aggregation of unfolded or misfolded proteins, aging, and age-associated diseases. To protect the organism from cell-damaging protein aggregation, organisms have evolved mechanisms to detect, repair and degrade unfolded proteins. The response to the occurrence of unfolded proteins is specific for the sub-cellular compartment and is composed of a repair system, a degradation system and a disposal system [92, 93]. In the cytosol, the aggregation of unfolded proteins activates the heat shock transcription factor HSF-1 for activation of the repair system. The repair system is composed of members of the heat shock response. One of them is the 16-kDa heat shock protein gene *hsp-16.2*. It is a stress-induced chaperone, which is induced by the aggregation of human Aβ and polyQ in *C. elegans*. HSP-16.2 binds the unfolded proteins and prevents their aggregation [93]. Besides the repair system, the degradation system has a vital role in proteostasis. The major system for the degradation of unfolded proteins is the ubiquitin/proteasome system (UPS). This system uses ubiquitin as a marker for proteins to be degraded by the proteasome. Aging leads to a decline in the UPS activity and in turn, facilitates the aggregation of proteins [92]. The UPS is effective for single misfolded proteins, while large amounts of misfolded proteins and aggregates are handled by autophagy [94]. Therefore, it is not surprising that inactivation of autophagy genes accelerates the aggregation phenotype of polyQ and Aβ-expressing worms [95, 96].

Nutritional interventions

Dietary restriction (DR)

Dietary restriction is defined as reduced intake of food without malnutrition. It includes on the one hand caloric restriction, which is characterized by a reduced amount of calorie intake. On the other hand, DR also includes the limitation of specific nutrients (*e.g.,* decreased uptake of lipids or carbohydrates). It is a very well conserved, and well-studied intervention for lifespan extension and prevention of age-associated diseases from yeast to mammals [97]. In mice, DR is protective against AD and other neurodegenerative diseases [1]. Even in rhesus monkeys, DR has a health-promoting effect and leads to a lower incidence of diabetes, obesity, cardiovascular disease, and cancer [1, 98, 99].

In *C. elegans* there are at least 20 different protocols to study DR including genetic mutations (*e.g.*, mutations of *eat-2*), pharmacological interventions, and dilutions of bacterial food. The vast amount of protocols results in significant differences in the magnitude of lifespan extension, ranging from 25 % and 268 %, depending on the method. The different DR methods

address both, common and specific signaling pathways [38, 100]. At least 2 major pathways are involved in mediating the pro-longevity effects of DR, the IIS pathway, and the TOR pathway. The mediation of pro-longevity effects by these pathways is conserved from worms to mammals [69]. Besides these 2 highly conserved signaling pathways, many others have been identified as crucial factors for extending lifespan under different DR regimens. Among others, these factors are the bZIP transcription factor SKN-1, the heat-shock inducible transcription factor HSF-1, the hypoxia-inducible transcription factor HIF-1, and nuclear hormone receptors (NHRs) [100]. Interestingly, although the different DR regimens used in *C. elegans* work partially through distinct mechanisms, many of them induce autophagy [38, 97].

Nutraceuticals

Like DR, dietary supplementation with nutraceuticals influences aging and other physiological parameters in *C. elegans*. Nutraceuticals are nutritional products which are additionally used as pharmaceuticals. One of these nutraceuticals is curcumin, which in mammals has been shown to also act as AhR modulator. Curcumin extends the nematode's lifespan and increases its stress resistance towards oxidative and thermal stress [101, 102]. Moreover, it ameliorates the paralysis phenotype of *C. elegans* models for neurodegenerative diseases (AD and polyQ disorders) and protects *C. elegans* against pathogenic bacteria [101, 103, 104]. The molecular mechanisms of these health-promoting effects are mainly unknown, but it is proposed that curcumin activates stress response pathways and that *osr-1, sek-1, mek-1, skn-1, unc-43,* and *sir-2.1* are required for the lifespan-extending effects [101, 102]. Similar effects of curcumin are reported for the polyphenol quercetin, which can act through AhR in mammals, too. Quercetin inhibits Aβ-mediated paralysis in a *C. elegans* model for AD, delays aging and increases stress response [105-107]. The lifespan-extending effect of quercetin is dose-dependent and in line with the principle of hormesis [108]. The lifespan extension involves TGF-β signaling, Insulin-like signaling, and the p38 MAPK pathway, while the protection against Aβ accumulation requires autophagy [105, 109]. Other natural compounds with lifespan-extending effects and protection against age-associated diseases are resveratrol [110, 111], cranberry extract [112, 113], Ginkgo biloba extract (EGb 761) [52, 114], blueberry phenols [115], spermidine [116], and many others [117].

Bacterial diet

While the principles of DR and supplementation with nutraceuticals are well-established and highly conserved between species, more recently, the effect of different *E. coli* diets on *C. elegans* life traits have been in focus. For this work, especially the differences between the two most commonly used *E. coli* diets, *E. coli* OP50 and *E. coli* HT115, are of relevance. The *E. coli* B strain OP50 was initially employed by Sydney Brenner and is frequently used as a bacterial food source for *C. elegans* [7]. The *E. coli* K-12 strain HT115 instead is mainly used

in RNAi studies. Although these bacterial strains are commonly utilized and lead to differences in many life traits, many differences in their composition or their metabolites are still unknown. Only a few studies describing the difference in the bacterial composition revealed that the higher carbohydrate content of HT115(DE3) is the main difference in macronutrients between these *E. coli* strains [118]. Moreover, the composition of the lipopolysaccharide structure (LPS), the main component of the outer bacterial membrane, is different in these *E. coli* strains [119]. Even less is known about the production of bacterial metabolites. Up to my knowledge, the only differences in metabolites described are that *E. coli* OP50 produces a higher amount of the polysaccharide colanic acid [120] and a lower amount of vitamin B12 [121].

One of the first studies on different *E. coli* strains as a food source for *C. elegans* used the *E. coli* strains OP50 and HT115(DE3) to elucidate the influence of the bacterial food source on fat storage [118]. The authors of this study found that feeding on OP50 led to an increased fat content in young wild-type *C. elegans*. The difference in the fat accumulation is dependent on the intestinal peptide transporter PEPT-1 [122]. Besides the differences in fat content [118, 122], changes in the metabolic profile and the mitochondrial copy are described [123]. While the *E. coli* diet did not affect the lifespan in some studies [79, 118, 124] in other studies an increased lifespan on HT115 is reported [119]. One essential factor which for the differences in the lifespan of worms feeding on HT115 or OP50 is the neuromedin U receptor, NMUR-1 [119]. Worms with a mutation in *nmur-1* are long-lived on OP50 but have a normal lifespan on HT115(DE3) [119]. This difference occurs because of the differences in the LPS structure of OP50 and HT115 [119] (Figure 5). Moreover, together with *ahl-6*, a mitochondrial proline catabolism gene, *nmur-1* is required for the maintenance of mitochondrial homeostasis and aging on an OP50 diet [124]. It is proposed that dietary information is processed by NMUR-1, leading to the activation of proline catabolism in the mitochondria [124]. In the absence of AHL-6, the activation of proline catabolism disrupts mitochondrial homeostasis due to an accumulation of the toxic proline derivate P5C [124]. Another vital complex regulating changes in lifespan is TORC2. One component of the TORC2 is rictor (*rict-1*), which modulates lifespan on the different *E. coli* diets by affecting feeding and metabolism (Figure 5) [79]. *rict-1* loss of function mutants have a normal lifespan on HT115, but a shortened lifespan on OP50 at 25 °C [79]. The diet-dependent effect of *rict-1* on lifespan is as well temperature-dependent since *rict-1* affects aging in a diet-dependent manner at 25 °C but not at 20 °C and 15 °C [125]. Moreover, *rict-1* is also responsible for differences in the development, oxygen consumption and ATP production of *C. elegans* feeding on OP50 and HT115 [122]. Aging is not only influenced by the different bacterial strains. Also, single gene mutations in the same bacterial strain have tremendous effects on the host aging process, including the progression of age-associated neurodegenerative diseases and cancer [120]. In total 3983 *E. coli* mutants were screened for their effect on longevity in their host *C. elegans*. Out of these, deletion in 29

bacterial genes, increased *C. elegans* lifespan acting either on the IIS pathway, the TOR signaling pathway, through DR or mitochondrial dynamics and unfolded protein response [120].

Besides the effects of the different *E. coli* diets on physiological aging, diet also influenced the progression of neurodegenerative diseases in *C. elegans* models for AD, PD, and polyQ disorders [126]. Specifically, they showed that the onset of paralysis in an Aβ expressing strain (AD model), the aggregation of α-syn (PD model) and Q40 aggregation were faster on OP50 than on HT115(L4440) [126]. Also, a connection between diet and activation of the EGFR-Ras-ERK signaling pathway has been proposed [127]. Another diet-dependent phenotype has been observed in loss of function mutants for NHR-114, a ligand-activated nuclear hormone receptor. In the absence of *nhr-114*, *C. elegans* was sterile on an OP50 diet but not on an HT115 diet, a phenotype which could be rescued by the supplementation of OP50 with tryptophan [128]. Potentially both, tryptophan and NHR-114 protect *C. elegans* against potential insults of the OP50 diet by triggering the detoxification response by activating *cyps*, *ugts*, C-type lectins (*clecs*) and *gsts* (Figure 5) [128]. It has been suggested that the beneficial effect of tryptophan supplementation is dependent on the activation of SKN-1 [125].

In conclusion, the comparison of *C. elegans* feeding on either HT115 or OP50, showed that an *E. coli* HT115 diet leads to a lower fat content, a faster development, a higher oxygen consumption and ATP production, an increased mitochondrial copy number, differences in the metabolic profile, and a slower progression of paralysis in *C. elegans* models for neurodegenerative diseases [118, 122, 123, 126]. The influence on lifespan, instead, is controversially discussed [79, 118, 119, 123]. A general weakness of most of these studies is that the presence of antibiotics, IPTG and empty vector was not considered as being potentially relevant for the observed differences.

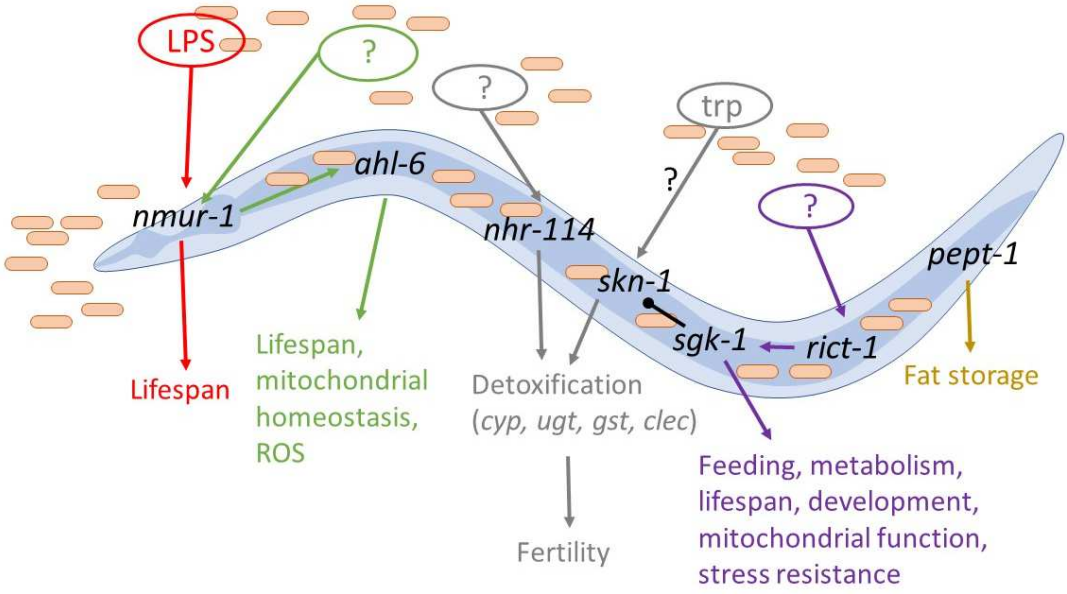

Figure 5 The bacterial diet influences *C. elegans* life traits. Model of known gene-diet interactions. The neuromedin U receptor, NMUR-1, mediates LPS-dependent changes in lifespan [119] and senses bacterial cues of an OP50 diet which activate proline catabolism. In the absence of AHL-6, the activated proline catabolism leads to the accumulation of ROS, mitochondrial dys-homeostasis and a shorter lifespan [124]. Tryptophan and the nuclear hormone receptor NHR-114 activate the detoxification response in response to an OP50 diet [128]. This activation is required for normal fertility on OP50 [128]. The activation of the detoxification response by tryptophan metabolites is probably mediated by SKN-1 [125]. Rictor, *rict-1*, influences many physiological parameters relevant for the aging process dependent on the bacterial food source [79, 122, 125]. It works in a pathway with SGK-1 and SKN-1 [125]. The peptide transporter PEPT-1 regulates fat storage in response to different bacterial diets [122].

The aryl hydrocarbon receptor (AhR)

AhR structure and function

The aryl hydrocarbon receptor (AhR), previously known as dioxin receptor, was discovered in 1976 by Poland et al. [129] as a dioxin-binding protein. It is a highly conserved ligand-activated transcription factor of the bHLH PAS family. Vertebrate AhR proteins have a molecular weight between 95 and 125 kDa and consist of a basic helix-loop-helix domain (bHLH), two Per-ARNT-Sim (PAS) domains and a transcriptional activation domain (TAD). The bHLH domain is located close to the amino-terminal end of the protein, and it is involved in DNA binding, binding of heat shock protein 90 (HSP90), and dimerization with the AhR nuclear translocator (Arnt) [130, 131]. Moreover, the nuclear localization signal (NLS) and the nuclear export signal (NES) are located in the bHLH domain [130, 132]. Together with the bHLH domain, the PAS A domain is required for binding of Arnt, while the PAS B domain is involved in ligand binding and interaction with the AhR-associated protein (AIP (also XAP2)). Also, together with the bHLH domain, the PAS B domain is required for the interaction with HSP90. The TAD is located at the carboxy-terminal end of AhR and is needed for transcriptional activation [130, 131].

In the absence of ligands, AhR is bound by HSP90, AIP, and p23, which retain it in the cytoplasm (Figure 6). There is evidence that also the tyrosine kinase c-Src is part of this

cytosolic complex [133]. Ligand binding of an AhR agonist leads to the dissociation of the AhR binding complex and conformational changes, which result in the exposition of the nuclear localization signal (NLS) and AhR nuclear translocation [130, 132]. It is proposed that the phosphorylation of the AhR NLS by the protein kinase C (PKC) prevents the nuclear localization of the AhR and that dephosphorylation of the NLS and inhibition of PKC is required for the nuclear translocation of the AhR [134]. Once in the nucleus, AhR dimerizes with Arnt, another transcription factor of the bHLH PAS superfamily. The AhR-Arnt heterodimer then binds to the xenobiotic responsive elements (XREs) (core sequence 5'-GCGTG-3') of AhR target genes [130]. There are many genes influenced by the activity of the AhR, but typical target genes of the AhR upon activation by xenobiotic ligands are phase-I detoxification genes like cyps (*e.g.*, CYP1A1 or CYP1B1), phase-II detoxification genes like ugts (*e.g.,* UGT1A1 or UGT1A6), and gsts (*e.g.,* GSTA1 or GSTA2) [130, 135, 136]. To avoid the constant activation of the AhR, negative feedback loops regulate the AhR cascade pathway. Up to date, three types of feedback loops have been described: 1. the proteasomal degradation of AhR after the binding of AhR to the DNA, 2. the induction of negative regulators of the AhR like the AhR repressor (AHRR), which itself is a target gene of the AhR, and 3. the degradation of AhR ligands by detoxification enzymes [136, 137].

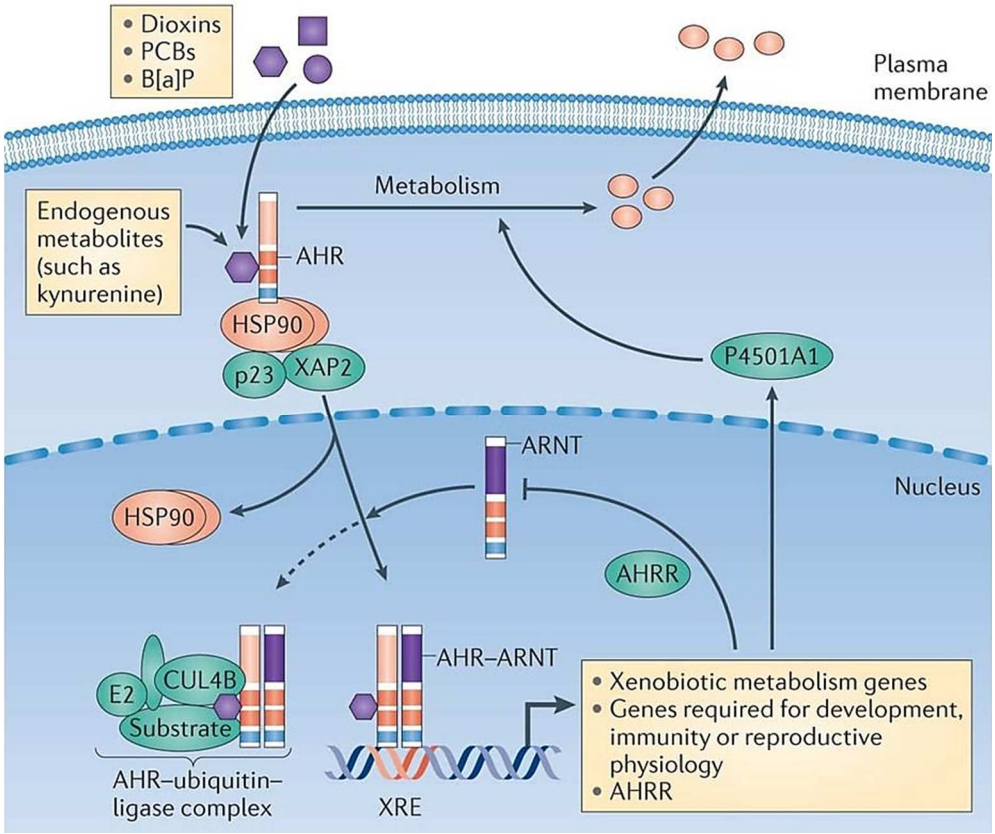

Figure 6 The canonical AhR signaling pathway. The activation of the AhR signaling pathway is dependent on ligand binding. In the absence of ligands, AhR is kept in the cytoplasm by binding to the co-chaperones HSP90, XAP2 and p23. Upon binding of exogenous ligands (*e.g.*, benzo[a]pyrene (B[a]P)) or endogenous ligands (*e.g.*, kynurenine) the AhR translocates to the nucleus, where the chaperones are exchanged for the AHR nuclear translocator (ARNT). The AHR–ARNT dimer binds to XREs of specific target genes (*e.g.,* CYP1A1 (P4501A1)) and

initiates their transcription. CYP1A1 and other AhR target genes are required for the metabolism of xenobiotics. The metabolism of xenobiotics is one of three negative feedback loop mechanisms controlling the AhR pathway. The expression of AHRR, a target gene of the AhR, presents another negative feedback loop mechanism. AHRR can dimerize with ARNT to form a transcription-repressing complex, which competes with AHR–ARNT. The third negative feedback loop is mediated by the degradation of the AhR by the AHR-ubiquitin-ligase complex. Reprinted by permission from Springer Customer Service Centre GmbH: Springer Nature, Nature Reviews Cancer, [138], © 2013.

The interaction between the AhR pathway and multiple other pathways have been discovered. In response to UVB light, a crosstalk between the AhR and the EGFR pathway has been reported. The exposure to UVB radiation leads to the formation of FICZ. The activation of the AhR by FICZ leads to the dissociation of AhR co-factors. One of these, the src kinase $pp60^{scr}$, activates the EGFR through a not yet defined mechanism. This leads to the activation of the downstream ERK1/2 signaling cascade [139, 140]. A target gene controlled by the crosstalk between the AhR and the EGFR pathway is the cyclooxygenase *Cox-2* [139], a known mediator of cancer [140]. Another crosstalk has been reported between AHR and the NF-κB pathway. The NF-κB pathway is involved in immune and inflammatory responses but has also been proposed as a critical modulator of the aging process. It takes part in the progression of age-associated neurodegenerative diseases and cardiovascular diseases [141]. The canonical NF-κB pathway can be activated by diverse stress stimuli (*e.g.*, inflammatory stimuli) [142]. Crosstalk between the NF-κB and the AhR signaling pathway has been described in response to UVB [143] and TCDD [142]. Also, AhR interacts with the Nrf2 pathway, a major pathway involved in the response to various stressors which is associated with longevity in invertebrate model organisms [144]. The interaction between AhR and Nrf2 is believed to be due to two different mechanisms: 1. the transcriptional activation of *Nrf2* by AhR, 2. the production of ROS by CYPs, which are activated by AhR. As a transcription factor, Nrf2 binds to antioxidant elements (AREs) in the promoter region of its target genes. There are a couple of target genes, namely *Nqo1*, *Gsta2,* and *Ugt1a6*, which are regulated by both, Nrf2 and AhR [145]. Moreover, there is evidence that AhR is also localized inside the mitochondria, where its localization is dependent on the presence of ligands. It is mostly localized in the intermembrane space [146]. AhR was found to interact with ATP5α1, a subunit of the mitochondrial ATP synthase and it has an essential function in the regulation of mitochondrial homeostasis after TCDD exposure [146, 147].

Modulation of AhR activity

Besides the anthropogenic ligands which activate the AhR signaling pathway other AhR modulators are known. In general, AhR modulators can be divided into four categories, which are xenobiotic modulators, dietary modulators, endogenous modulators produced by the host and ligands generated by the microbiota.

Xenobiotic compounds

Xenobiotic compounds are defined as chemical substances within an organism, which are not produced by this organism. Such compounds are, for example, environmental toxicants and some of them are potent activators of the AhR. One of these is 2,3,7,8-tetrachlorodibenzo-p-dioxin (TCDD). TCDD is a chemical, often of anthropogenic origin, which belongs to the class of halogenated aromatic hydrocarbons (HAHs) and is carcinogenic. It is mainly produced by incineration and accumulated in the food (mostly in meat, fish, and eggs), drinking water, the air and the soil [148]. Depending on the dose and the exposure times, TCDD causes chloracne, liver damage, reproductive toxicity, neurotoxicity, immunosuppression, cancer, and cardiovascular diseases in humans [148, 149]. Other HAHs, which are AhR ligands are polychlorinated biphenyls (PCBs), dibenzo-p-furans (PCDF) and dibenzo-p-dioxins (PCDD) [131]. Besides HAHs, polycyclic aromatic hydrocarbons (PAHs) like benzo[a]pyrene (BaP), 3-methylcholanthrene (3MC), and 7,12-dimethyl-benz[a]xanthracene are classical xenobiotic ligands of the AhR. Other, well-characterized ligands of xenobiotic origin are the synthetic flavone β-naphthoflavone, which is an AhR activator, α-naphthoflavone and 3'-methoxy-4'-nitroflavone (MNF), which are instead considered to be AhR antagonists [130, 131]. Many of these xenobiotic ligands influence aging and lead to age-associated diseases in different vertebrate species. BaP for example negatively affects the lifespan in mice [150], and promotes neurodegeneration in zebrafish [151].

Dietary interventions/factors

In an *in vitro* screening for vegetable constituents inhibiting the dioxin-induced AhR activation Amakura *et al.* [152] found various naturally occurring dietary AhR ligands. The most potent class of AhR antagonists were flavonoids, but also anthraquinones were identified as effective AhR antagonists. In fact, the most robust inhibition of AhR activation was noticed for the anthraquinones emodin and Aloe-emodin followed by the flavonoids chrysin, luteolin, apigenin, kaempferol and quercetin [152]. All these compounds can be found in a variety of different fruits and vegetables. Many of these dietary factors have life- and health-extending effects. Curcumin, for example, shows protective effects on age-related neurodegenerative diseases in nematodes [101], flies [153] and mice [154], but whether this is due to its effect on AhR signaling is unknown.

Endogenous factors

Besides modulation by exogenous ligands, like xenobiotics and dietary components, AhR is also activated by endogenous ligands. A well-described endogenous high-affinity ligands is 6-formylindolo[3,2-b]carbazole (FICZ), a photoproduct of tryptophan, which is known to be produced in response to UVB light [139, 155]. The toxicological effects of FICZ are not very well investigated. A recent study shows that FICZ can be generated inside the cell independent

of light exposure by hydrogen peroxide (H_2O_2) [156]. This process is of relevance since the formation of H_2O_2 frequently occurs *in vivo*. Other endogenous but low-affinity ligands of AhR are kynurenine, kynurenic acid, cinnabarinic acid and ITE (2-(1′*H*-indole-3′-carbonyl)-thiazole-4-carboxylic acid methyl ester) [157-160].

Bacteria can generate AhR ligands

Other than the endogenous ligands produced by the organism itself, its microbiota also provides AhR modulators. These are mainly derivatives of tryptophan. AhR activating tryptophan metabolites produced by the gut bacteria are indole, indoxyl-3-sulfate, indole-3-propionic acid, indole-3-aldehyde, indole-3-acetate, and tryptamine [161, 162]. Microbial pigment virulence factors were also described as potent AhR ligands produced by some microbes. Recently AhR was found to have a major role in the recognition of the phenazines from *Pseudomonas aeruginosa* and the naphthoquinone phthiocol from *Mycobacterium tuberculosis* and in the induction of the antimicrobial defense of the host [163].

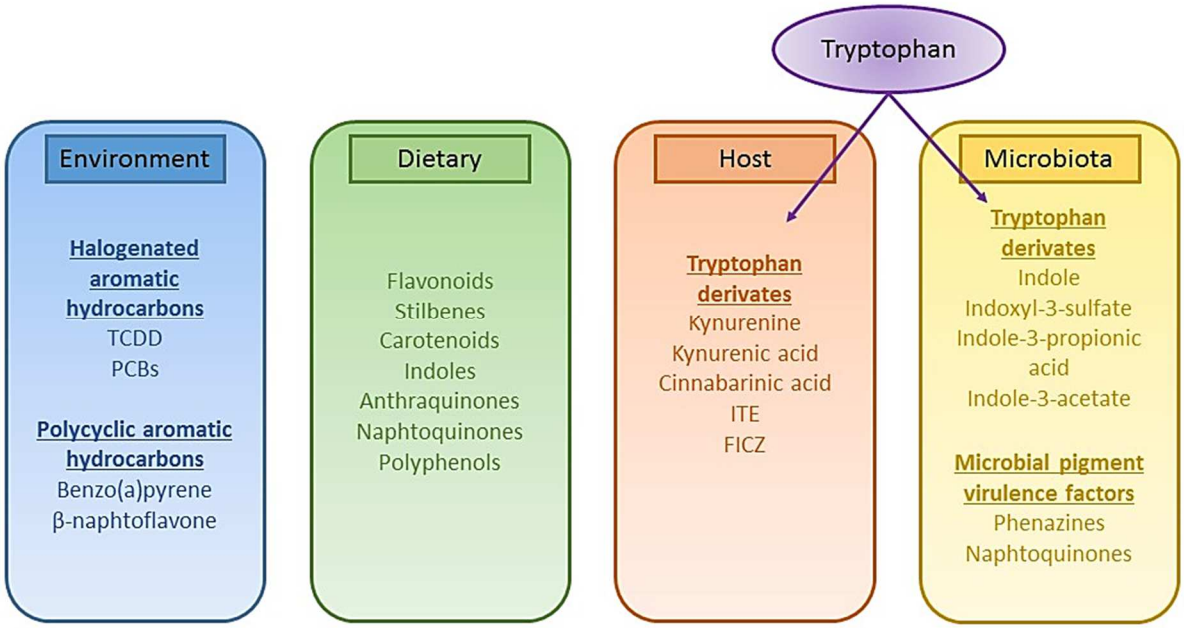

Figure 7 Classes of AhR ligands. 1) Environmental toxicants like halogenated aromatic hydrocarbons and polycyclic aromatic hydrocarbons are well-known AhR activators. 2) The diet of an organism contains AhR ligands of different classes (*e.g.,* flavonoids, carotenoids, and polyphenols). 3) Endogenous AhR ligands formed by the organism itself are mainly tryptophan derivatives. Some of them are produced in the kynurenine pathway. 4) Also, the microbiota provides AhR ligands. These microbiota mediated AhR ligands are either metabolites of tryptophan, like indole and its derivates or microbial pigment virulence factors. Figure modified and adjusted from [164].

AhR in aging and diseases

There is a growing body of evidence indicating a role of the AhR in the aging process. A recent epidemiological study in Chinese people showed for instance that single nucleotide polymorphisms in the *AhR* gene are correlated to skin aging [165]. Interestingly, both pro- and anti-aging effects are reported for the AhR. The anti-aging effect of AhR is suggested by a study showing that loss of AhR function induces premature aging of hematopoietic stem cells

[166]. Additionally, AhR loss of function resulted in a short lifespan, the development of age-related macular degeneration, and an increased risk for metabolic diseases in mice [166-168]. Also, the decrease in AhR activity and AhR protein expression in human retinal pigment epithelial cells from old donors compared to young donors supports the hypothesis of AhR-dependent anti-aging effects [167]. On the other hand, studies suggesting a pro-aging effect of the AhR were often based on the use of AhR ligands. The exposure of human skin cells towards PAHs in polluted air and tobacco smoke caused aging [169, 170]. This effect was dependent on the AhR and can be abolished by AhR knockout and inhibition of the AhR activity by AhR antagonists [169, 170]. Exposure to AhR activating xenobiotic ligands also causes age-related pathologies like cancer and cardiovascular diseases and lead to a reduced life-expectancy [148-150, 171]. Moreover, AhR inactivating polyphenolic ligands have a protective effect against various age-associated diseases, namely cardiovascular diseases, cancer and neurodegenerative disorders [136]. Somehow surprisingly, the dependency of this health-promoting effects on the AhR is not yet investigated [136]. Independent of the exposure to extrinsic ligands, the theory of pro-aging effects associated with the AhR is supported by the observation of an increase in AhR expression in murine splenocytes during aging and the fact that AhR expression is correlated parameters of vessel aging [172, 173]. In cross-species studies, together with others, I could show that the AhR promotes aging phenotypes in human, mice and *C. elegans* [173].

AHR-1, the AhR ortholog of *C. elegans*

The *C. elegans* orthologs of AhR and ARNT, which are AHR-1 and AHA-1 respectively, were identified in 1998 with homologies of 38 % (AHR-1) and 45 % (AHA-1) to their human counterparts [174]. The *ahr-1* gene is located on chromosome I and encodes for a protein, AHR-1, with two isoforms. Isoform a is 620 aa long and has an estimated weight of 68.2 kDa, while isoform b is shorter (560 aa) with a predicted molecular weight of 63.2 kDa. Like the mammalian AhR, AHR-1a consists of a bHLH domain with signals for nuclear localization and nuclear export and two PAS domains (Figure 8 and Figure 9). In isoform b instead, parts of the bHLH domain, as well as the nuclear localization signal, are missing (Figure 8 and Figure 9).

AHR-1, isoform a

MYASKRRQRNFKRVRDPPKQLTNTNPSKRHRERLNGELETVAMLLPYDSSTISRLDKLSVLRLAVSFLQCKAHFQACLHNSQFLSAGFP
MSTHSYSYQPHPPIPFSNKVPTIFDLRIGTPMLDPEESNFEEISLKSLGGFILVLNDNGEIYYASENVENYLGFHQSDVLHQPVYDLIHSEDR
DDIRQQLDSNFHIPTSSASNQFDVFAPQNSKYLERNVNARFRCLLDNTCGFLRIDMRGKLMSLHGLPSSYVMGRTASGPVLGMICVCTP
FVPPSTSDLASEDMILKTKHQLDGALVSMDQKVYEMLEIDETDLPMPLYNLVHVEDAVCMAEAHKEAIKNGSSGLLVYRLVSTKTRRTYF
VQSSCRMFYKNSKPESIGLTHRLLNEVEGTMLLEKRSTLKAKLLSFDDSFLQSPRNLQSTAALPLPSVLKDDQDCLEPSTSNSLFPSVPVPT
PTTTKANRRRKENSHEIVPTIPSIPIPTHFDMQMFDPSWNHGVHPPAWPHDVYHLTQYPPTYPHPPGTVGYPDVQIAPVDYPGWHPN
DIHMTQLPHGFTPDAQKLVPPHPQMSHFTEYPTPSTHHDLHHHPLKQDNFHLISEVTNLLGT

PAS Domain
bHLH domain
Murine Nuclear Export Signal: LDKLSVLRL
Nuclear Localization Signal: RRQRNFKRVRDPPKQLTNTNPSKRHRER

AHR-1, isoform b

MLLPYDSSTISRLDKLSVLRLAVSFLQCKAHFQACLHNSQFLSAGFPMSTHSYSYQPHPPIPFSNKVPTIFDLRIGTPMLDPEESNFEEISLK
SLGGFILVLNDNGEIYYASENVENYLGFHQSDVLHQPVYDLIHSEDRDDIRQQLDSNFHIPTSSASNQFDVFAPQNSKYLERNVNARFRCL
LDNTCGFLRIDMRGKLMSLHGLPSSYVMGRTASGPVLGMICVCTPFVPPSTSDLASEDMILKTKHQLDGALVSMDQKVYEMLEIDETDL
PMPLYNLVHVEDAVCMAEAHKEAIKNGSSGLLVYRLVSTKTRRTYFVQSSCRMFYKNSKPESIGLTHRLLNEVEGTMLLEKRSTLKAKLLS
FDDSFLQSPRNLQSTAALPLPSVLKDDQDCLEPSTSNSLFPSVPVPTPTTTKANRRRKENSHEIVPTIPSIPIPTHFDMQMFDPSWNHGV
HPPAWPHDVYHLTQYPPTYPHPPGTVGYPDVQIAPVDYPGWHPNDIHMTQLPHGFTPDAQKLVPPHPQMSHFTEYPTPSTHHDLHH
HPLKQDNFHLISEVTNLLGT

PAS Domain
bHLH domain
Murine Nuclear Export Signal: LDKLSVLRL
Nuclear Localization Signal: RRQRNFKRVRDPPKQLTNTNPSKRHRER

Figure 8 AHR-1 protein sequence and features. Isoform a contains one bHLH domain, two PAS domains and potential signals for nuclear import (NLS) and export (NES). Isoform b has two PAS domains but misses the bHLH domain as well as the NLS.

There are two *ahr-1* loss of function alleles available to study the role of AHR-1: *ia03* and *ju145*. The allele *ia03* carries a 1517 bp deletion in the PAS A domain, leading to a premature stop codon [175]. The other allele, *ju145*, carries a point mutation (C to T nucleotide transition) in the PAS B domain, leading to a stop codon [176]. Both alleles could potentially result in the expression of truncated proteins (Figure 9B and C), but their existence has not been verified yet. The potential expression of the truncated proteins might allow the binding to XREs without activation and could lead to a repressor-like function [177] or the constant nuclear localization as described for truncated human AhR protein, missing the PAS domains [132]. In general, both AHR-1 loss of function strains appear healthy with only minor abnormalities like a slightly slower larval development (especially in reaching the L4 larval stage), a slightly reduced egg number, increased embryonic lethality, slow and uncoordinated movement and a longer defecation cycle [178].

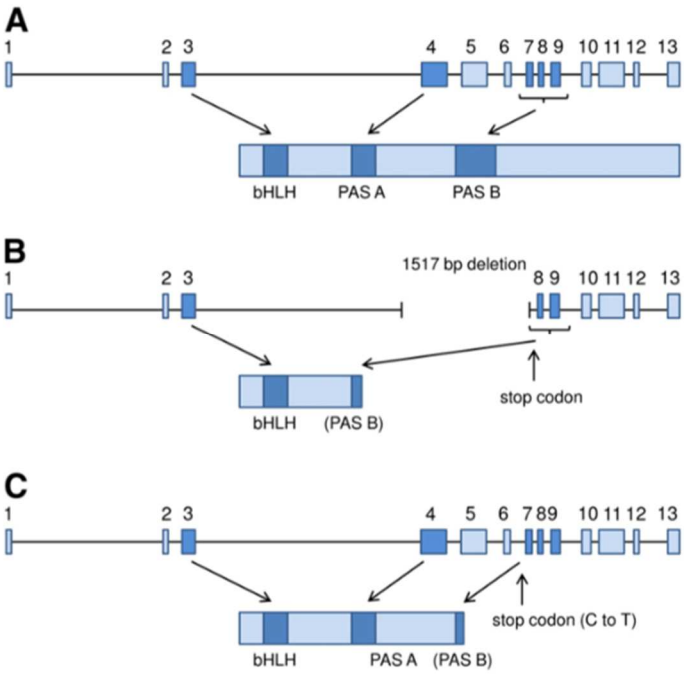

Figure 9 Predicted protein models of AHR-1 (isoform a) in the wild-type and AHR-1 loss of function strains. (A) The wild-type *ahr-1* gene consists of 13 exons coding for a protein with a bHLH domain and two PAS domains. (B) In *ahr-1(ia03)* exon 4 to 7 are deleted, leading to a premature stop codon in exon 8. The corresponding truncated protein, if translated, would miss both PAS domains and other carboxyterminal domains. (C) *ahr-1(ju145)* carries a C to T substitution in exon 7, which leads to a stop codon. If a truncated protein were translated, it would consist of the bHLH domain and the PAS A domain, while the PAS B domain and any other carboxyterminal domains would be missing. Figure taken from [177].

Like their mammalian homologs, AHR-1 and AHA-1 can form a heterodimer, which binds to XREs [174]. This dimerization of AHR-1 and AHA-1 is required for the transcriptional activity of AHR-1 [174], while, unlike in mammals, daf-21/HSP90 is not [176, 179]. Another difference between mammalian and *C. elegans* AhR is that mammalian AhR is bound by AIP, which does not show any binding to AHR-1 in co-immunoprecipitation assays [180]. Moreover, no ligands have been found so far to bind to the *C. elegans* AHR-1 [174, 175] and knocking down AHR-1 by RNAi does not inhibit the induction of *cyp, gst* and *ugt* transgenes after exposure to different xenobiotics [181]. Also, the existence of an active ligand binding domain has not been proven in *C. elegans*. These findings might suggest that AHR-1 does not bind ligands at all and that the ancestral role of the AhR is not the response to xenobiotics [174]. The role of AHR-1 is, in general, mostly unexplored. There are a couple of studies, showing that AHR-1 has relevant functions in the *C. elegans* nervous system, where it is expressed in several types of neurons: sensory neurons and neurons controlling feeding behavior and hypoxia avoidance [175, 176, 179, 182]. Interestingly, although a function of the AhR in neurodevelopment was found in *C. elegans*, only a few studies showing a connection between the AhR and neuronal development in mammals [164]. Besides its role in neurodevelopment, AHR-1 is involved in regulating long-chain unsaturated fatty acid synthesis, causing a shift towards shorter fatty acid chain lengths and higher proportions of fatty acid methyl esters (FAME) in AHR-1 deficient

animals [178]. Additionally, it has been shown that AHR-1, together with PHA-4, NHR-8 and AHA-1 mediates DR like lifespan extension by *mekk-3/drl-1* RNAi [183]. It is hypothesized that AHR-1 is required for the induction of phase I (*cyps*) and phase II (*ugts*) detoxification enzymes in worms with reduced MEKK-3/DRL-1 function [183]. Microarray studies showed indeed differences in *cyp-13A4*, *ugt-19*, *gst-21*, but also in genes involved in lipid metabolism (*fat-7*, *elo-5*, *nhr-49,* and *mdt-15)* [178]. RNA-seq data showed instead that soluble guanylate cyclase genes (*gcy-32* and *gcy-36*), the neuropeptide-like protein gene *nlp-20*, the F-box A protein genes *fbxa-191, fbxa-192* and *fbxa-193*, catalase genes *ctl-1* and *ctl-3,* the insulin-related peptide gene *ins-35,* and collagen genes (*col-176* and *dpy-3)* are the strongest differentially expressed genes upon *ahr-1* loss of function [177].

Although there are differences between mammalian AhR and the *C. elegans* AHR-1, our and other recent studies showed conserved functions of AHR-1. One of these is the involvement of AHR-1 and AHA-1 in the Wnt signaling pathway [184], which is regulated by AhR/ARNT as well in mammals [185, 186]. Direct comparison studies showed that AHR-1 has as well a conserved function in the regulation of movement [187] and aging [173]. More specifically, these studies showed a higher spontaneous movement activity of *C. elegans*, *Drosophila melanogaster* and mice with reduced *Ahr* expression [187] as well as a longer life- and health-span in *C. elegans* with loss of AHR-1 function, a better vessel functionality in aging mice and a negative correlation between vessel functionality and AhR expression [173]. The existence of conserved AhR functions suggests that investigations in *C. elegans* might reveal important novel information about the AhR in humans.

2. Hypothesis and aims

My doctoral thesis aims to investigate how the AhR influences physiological and environmental-induced aging using the *C. elegans* model. This topic is of high relevance because understanding the mechanisms of environmentally/nutritionally-induced aging is crucial to prevent and treat age-associated diseases. Based on (1) my previously published findings showing that AhR promotes aging in *C. elegans* [173] and (2) preliminary data from my Master thesis indicating that *C. elegans ahr-1* loss-of-function differentially affects healthspan in a bacterial diet-dependent manner, I hypothesized that besides the general effect of AHR-1 on healthy aging, AHR-1-dependent metabolism of environmental or nutritional factors may also regulate the aging process (Figure 10A). To address this hypothesis, I wanted (1) to investigate whether AHR-1 mediates responses to different classes of mammalian AhR modulators, (2) to characterize the role of AHR-1 in the aging process, and (3) to identify AHR-1 target genes in response to environmental and/or dietary interventions (Figure 10B).

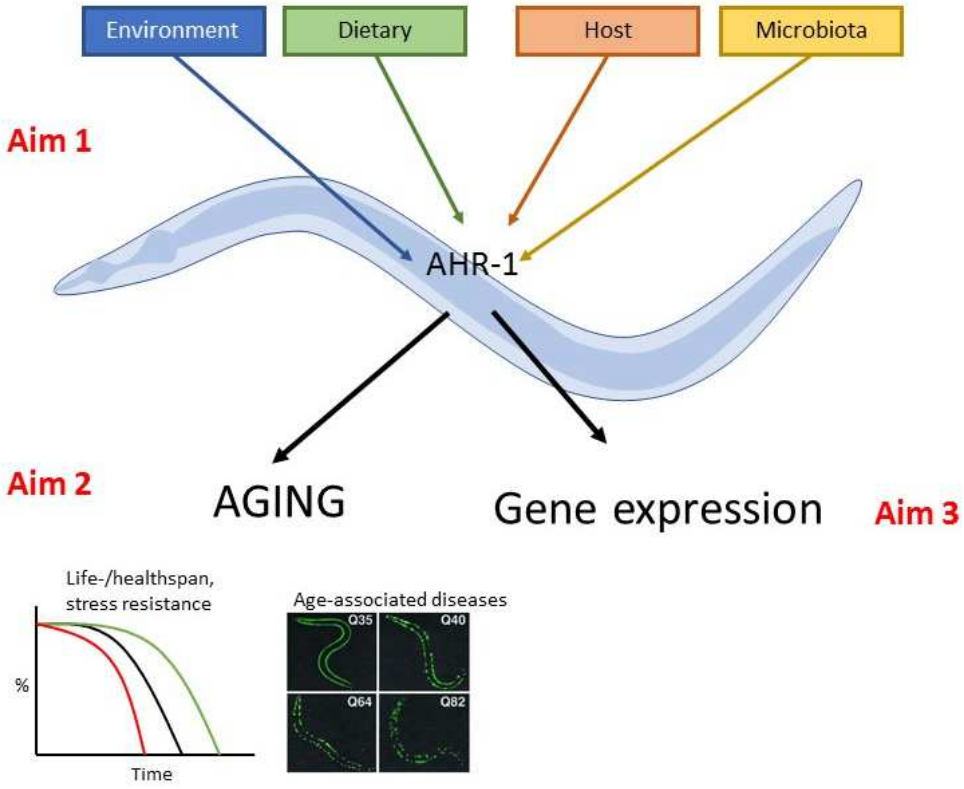

Figure 10 Hypothesis and aims of the project. Hypothesis: The *C. elegans* AHR-1 modulates the effect of specific compounds on the aging process. Aims: Firstly, I will test whether different classes of mammalian AhR modulators affect *C. elegans* depending on AHR-1 (aim 1). Then, the role of the AHR-1 in healthy aging will be assessed in response to specific modulators (aim 2). In the final step, AHR-1 target genes which respond to identified modulators in an AHR-1-dependent manner and affect aging will be determined.

Aim 1. Identification of potential AHR-1 modulators

The primary goal of the first part of the project was to validate *C. elegans* as a model to study conserved functions of the AhR. In this context, I wanted to identify compounds acting through the AHR-1 pathway to influence the aging process. Since it is not known whether AHR-1 binds any ligands, in this context also modulators of the AHR-1 signalling pathway, which are no direct ligands of AHR-1 were of interest. Therefore, I investigated the different classes of mammalian AhR modulators on their ability to affect *C. elegans* life traits in an AHR-1-dependent manner.

Aim 2. Impact of AHR-1 deficiency on aging and age-associated phenotypes

In the second part of the project, I wanted to systematically characterize age-associated features in AHR-1 loss of function worms to understand the role of AHR-1 in the aging process. Although my previous studies already revealed that AHR-1 is affecting lifespan and movement, further age-associated parameters like pharyngeal pumping and stress resistance in aged animals were not assessed. Additionally, my previous studies suggested that AHR-1 loss of function might affect healthy aging dependent on the bacterial food source. Therefore, one primary aim was to elucidate the AHR-1-dependent relevance of different *E. coli* diets as well as other potential AHR-1 modulators on aging and age-associated features.

Aim 3. Identification of AHR-1 target genes in response to AHR-1 modulators

In the final part of the project, I wanted to identify AHR-1 target genes to understand how AHR-1 and AHR-1 modulators affect aging. Therefore, I tried to find target genes of AHR-1 and then test potential AHR-1 ligands on the expression of these target genes. In a next step, the interventions leading to an AHR-1-dependent modulation of these genes should be tested for their ability to influence the aging process in AHR-1 proficient or deficient animals.

3. Material and Methods

E. coli

***E. coli* strains and growth**

E. coli HT115(L4440), HT115(*ahr-1*), and OP50 were obtained from the Ahringer *C. elegans* RNAi library [188]. *E. coli* OP50*(xu363)* [122] was kindly provided by the Xu laboratory (University of Michigan). For this study, I created OP50(L4440) and OP50(*ahr-1*). Bacteria were grown in LB medium at 37 °C overnight. When using *E. coli* carrying vectors the LB medium was supplemented with 0.01 % of ampicillin (amp) and 0.0005 % of tetracycline (tet).

Transformation of *E. coli* OP50*(xu363)*

E. coli OP50(*xu363*) were transformed by PEG transformation according to methods described previously with adjustments [189]. To get competent cells, bacteria were grown at 37 °C in LB medium to an optical density of OD_{595} = 0.6 and then pelleted by centrifugation at 4 °C. The pellet was resuspended in 1:10 of the original volume of ice-cold TSB (10 % PEG (MW 3500), 10 mM $MgCl_2$, 10 mM $MgSO_4$, 5 % DMSO in LB medium) and incubated on ice for 10 min. Afterward, competent cells were aliquoted and stored at - 80 °C.

For the transformation, competent cells were thawed on ice. Afterward, 100 µl of bacteria were incubated (30 min on ice) with 100 pg of the plasmid. Plasmids isolated from the HT115(DE3) strains (Ahringer Library) were used. After incubation, bacterial cells were exposed to heat shock (60 s at 42 °C) and then cooled down on ice for 2 min for permeabilization. Bacterial cells were then transferred to 900 ml TSBG (TSB + 0.2 % Glucose) and incubated at 37 °C shaking for 1 h. Then cells were seeded on LB plates containing 0.01 % amp and 0.0005 % tet for selection. After overnight incubation at 37 °C, colonies grown on the LB plates were cultured in LB medium, and the plasmids were isolated for verification.

Plasmid isolation

Plasmids were isolated using the QIAprep Spin Miniprep Kit (Qiagen, 27104) according to the instructions. 5 ml of a bacterial overnight culture was pelleted and dissolved in a resuspension buffer including RNase A (Buffer P1). The bacterial cells were then lysed by adding lysis buffer (Buffer P2). After an incubation time, the reaction was neutralized by adding Buffer N3. The lysate was cleared by centrifugation, and applied to the QIAprep 2.0 spin column, for plasmid DNA binding. After centrifugation, the membrane was washed with a wash buffer (Buffer PE), and DNA was eluted in nuclease-free water.

Killing bacteria prior to seeding

When seeding killed *E. coli* onto the NGM, the bacteria were pelleted (10 min at 4000 rpm), the supernatant was removed, and the pellet was suspended in s-basal to a final concentration

of OD_{595} = 3.6. Then the bacteria suspension was irradiated with a UVB lamp (Type: Waldmann UV 236 B) for 1 h to kill the bacteria. The suspension of the dead bacteria was seeded to NGM plates and let dry at room temperature overnight.

Killing bacteria on plates

Bacteria (OD_{595} = 0.9) were seeded to the NGM plates and let grow for 2 days at room temperature. The bacterial lawn was then killed by exposure to UVB light (Waldmann UV 236 B) for 45 min.

Using killed bacteria with switched media

The bacteria were killed before seeding as described above. Instead of discarding the LB media in which the bacteria were grown, the media were kept in a separate centrifuge tube. After the bacteria were killed they were centrifuged again, the s-basal was removed, and the bacteria were dissolved in the LB medium kept apart in a concentration of OD_{595} = 3.6.

C. elegans

***C. elegans* strains and maintenance**

Some of the *C. elegans* strains used for the experiments were obtained from the Caenorhabditis Genetics Center, which is funded by the NIH Office of Research Infrastructure Programs (P40 OD010440). cyp35A2, cyp35A3, cyp35A5, and cyp33E2 were kindly provided by the laboratory of Ralph Menzel (University of Berlin). NL2098 and NL2550 were kindly provided by the laboratory of Björn Schumacher (University of Cologne). BC20306 and BC20334 were kindly provided by the laboratory of David Depomerai (University of Nottingham). I created the following strains for this study by crossing CZ2485 with transgenic strains: NV33/NV33a: *ahr-1(ju145); cyp-35B1p::GFP + gcy-7p::GFP*, NV33wt: *cyp-35B1p::GFP + gcy-7p::GFP*, NV35a: *ahr-1(ju145); (pAF15)gst-4p::GFP::NLS*, NV35wt: *(pAF15)gst-4p::GFP::NLS*, NV38b: *ahr-1(ju145); unc-54p::Q40::YFP*, NV38wt: *unc-54p::Q40::YFP*. Strains used in this study are listed in Table 1.

Table 1 *C. elegans* strains used in this study. Strains are sorted alphabetically.

Strain name	Genotype		Strain name	Genotype
AM141	unc-54p::Q40::YFP		NL2550	ppw-1(pk2505)
BC14926	dpy-5(e907); sEx14926[rCes K09A11.4::GFP + pCeh361]		NR222	rde-1(ne219); kzIs9[lin-26p::nls::GFP + lin-26p::rde-1 + rol-6(su1006)]
BC15044	dpy-5(e907); sEx15044[rCes F01D5.9::GFP + pCeh361]		NV33	ahr-1(ju145); cyp-35B1p::GFP + gcy-7p::GFP
BC20306	Pcyp-34A9::GFP		NV33a	ahr-1(ju145); cyp-35B1p::GFP + gcy-7p::GFP
BC20334	Pcyp-29A2::GFP		NV33wt	cyp-35B1p::GFP + gcy-7p::GFP
CL6114	nre-1(hd20) lin-15b(hd126)		NV35a	ahr-1(ju145); (pAF15)gst-4p::GFP::NLS
CY573	cyp-35B1p::GFP + gcy-7p::GFP		NV35wt	(pAF15)gst-4p::GFP::NLS

cyp35A2	Pcyp-35A2::GFP		NV38b	ahr-1(ju145); unc-54p::Q40::YFP
cyp35A3	Pcyp-35A3::GFP		NV38wt	unc-54p::Q40::YFP
cyp35A5	Pcyp-35A5::GFP		SD1444	unc-119(ed3); gaIs237 [cyp-25A2p::his-24::mCherry + unc-119(+)]
cyp33E2	Pcyp-33E2::GFP		TU3311	uIs60[Punc119::YFP; Punc119::sid-1]
CZ2485	ahr-1(ju145)		TU3401	sid-1(pk3321); uIs69[myo-2p::mCherry + unc-119p::sid-1]
N2	wild-type		VP303	rde-1(ne300); neIs9 [myo-3::HA::RDE-1+ rol-6(su1006)]
NL2098	rrf-1(pk1417)		WM118	rde-1(ne219); kbIs7 [nhx-2p::rde-1 + rol-6(su1006)]

For maintenance, animals were kept synchronized by egg lay at 20 °C on Nematode Growth Media (NGM) plates and fed with *E. coli* OP50 according to methods described in [190]. For the experiments, worms were synchronized on plates supplemented with *E. coli* HT115(L4440), OP50(L4440) or OP50 according to the condition of interest. Unless stated otherwise, plates were supplemented with 1 mM IPTG, but not antibiotics when using HT115(L4440) or OP50(L4440).

Crossing CZ2485 with transgenic strains carrying the GFP

The *ahr-1* loss of function strain CZ2485 was crossed with transgenic strains carrying a fluorophore according to the protocol described below.

1. **Generation of males**

CZ2485 males were generated by heat stress. Briefly, 5 hermaphrodites in the L4 larval stage were incubated for 4 h at 30 °C. After the heat stress, they were kept at 25 °C to lay eggs. The male progeny of these worms was maintained at 20 °C. To secure a male containing populating adult males were frequently mated with L4 hermaphrodites.

2. **Mating**

One hermaphrodite L3/L4 larvae of the strain to be crossed with CZ2485 was put on a plate with 10 adult CZ2485 males. 5 L3 larvae of the F1 generation were then placed on plates (1 worm/plate) to produce progeny. After 2 - 3 days, the adult F1 worms were collected for genotyping. Only animals, which were heterozygote for the *ju145* allele, were used for further steps. If the GFP was visible under the fluorescence stereoscope, at least 32 GFP positive progeny (F2) of one *ju145* heterozygote F1 worm was put on fresh NGM plates (1 worm/plate) and collected for genotyping as soon as they had laid more than 50 eggs. After the genotyping of the F2, GFP positive progeny of *ju145* homozygote animals were kept, and again single animals were transferred to fresh plates. The progeny of these animals was again checked for the expression of GFP until an animal was found which had only GFP positive progeny, to

ensure that it is homozygote for the GFP transgene. In addition to the *ju145* homozygote animals, also animals being homozygote for wild-type *ahr-1* were segregated as a control.

3. Genotyping by single worm PCR and enzymatic restriction

For the genotyping, individual worms were collected in 2 – 5 µl of a mixture of 95 % worm lysis buffer and 5 % proteinase K (20 mg/ml in H_2O) and stored at -80 °C for at least 30 min. Afterward, the suspension was heated to 60 °C for 1.5 h and for 15 min at 95 °C. The lysed worms were kept on ice or at -20 °C for further processing.

Worm Lysis buffer

10 mM TRIS HCl, pH 8.3
50 mM KCl
2.5 mM $MgCl_2$
0.45 % NP40
0.45 % TWEEN 20
0.01 % Gelatine

The *ju145* allele contains a point mutation. To analyze whether the collected worms carry the *ju145* allele, I designed a primer pair, amplifying a 500-base pair fragment around the location of the point mutation (ahr-1 1 CGGAAAGTTGATGTCTCTAC, ahr-1 2 TGCTGACTAGACGATATACC). 20 - 23 µl of PCR mix was added to the lysed worms and the below-listed program was used for the amplification of the 500-base pair fragment.

PCR mix (for 1 reaction)

5.0 µl	5xPCR Buffer (New England Biolabs)
0.5 µl	dNTP mix (10mM)
0.15 µl	primer Forward (ahr-1 1)
0.15 µl	primer Reverse (ahr-1 2)
0.125 µl	Taq polymerase HotStar (New England Biolabs, M0815)
17.075 µl	H_2O (sterile)

PCR program for *ahr-1* primer

94 °C	30 s	1 cycle
94 °C	20 s	35 cycles
55 °C	30 s	
68 °C	30 s	
68 °C	5 min	1 cycle
10 °C	∞	

The PCR amplicon was further enzymatically cut, to explicitly check for the *ju145* point mutation. In the region of the point mutation, the wild-type *ahr-1* has the nucleotide sequence GGATC, which is a restriction site for enzymatic digestion by *AlwI* (cutting sequence: GGATC). The C to T nucleotide transition in the *ju145* allele instead results in a sequence of GGATT (Figure 11).

>wild-type *ahr-1* fragment

...CGGAAAGTTGATGTCTCTACATGGATTACCATCATCGTATGTAATGGGAAGAACTGCCTCGGGTCCAGTGCTCGGAATG
ATTTGCGTTTGCACgttagttgtttcaaactttgcgttcaggacttaaaaaaaaaatacttcagACCTTTTGTGCCGCCTTCAACATCCGATTTA
GCATCCGAAGACATGATTTTGAAAACAAAACATCAGTTGGATGGAGCTTTAGTATCTATGGATCAAAAgtgagttttattaggta
aaaataacttttctactgataattattaattacagGGTTTATGAAATGTTAGAAATTGATGAAACTGATCTACCAATGCCACTCTATAATC
TAGTCCACGTGGAAGATGCAGTCTGCATGGCTGAAGCTCATAAAGAAGgtgtcaatatttgatttctcgagcaatttgtaaataactacaa
tgaaatttcagCTATCAAAAACGGGTCATCTGGTCTTCTGGTATATCGTCTAGTCAGCA...

>*ju145 ahr-1* fragment

....CGGAAAGTTGATGTCTCTACATGGATTACCATCATCGTATGTAATGGGAAGAACTGCCTCGGGTCCAGTGCTCGGAATG
ATTTGCGTTTGCACgttagttgtttcaaactttgcgttcaggacttaaaaaaaaaatacttcagACCTTTTGTGCCGCCTTCAACATCCGATTTA
GCATCCGAAGACATGATTTTGAAAACAAAACATCAGTTGGATGGAGCTTTAGTATCTATGGATTAAAAgtgagttttattaggta
aaaataacttttctactgataattattaattacagGGTTTATGAAATGTTAGAAATTGATGAAACTGATCTACCAATGCCACTCTATAATC
TAGTCCACGTGGAAGATGCAGTCTGCATGGCTGAAGCTCATAAAGAAGgtgtcaatatttgatttctcgagcaatttgtaaataactacaa
tgaaatttcagCTATCAAAAACGGGTCATCTGGTCTTCTGGTATATCGTCTAGTCAGCA...

ahr-1 primer

AlwI restriction site

ju145 point mutation

Figure 11 Nucleotide sequence and characteristics of the *ahr-1* fragment amplified by PCR. In both, wild-type and *ahr-1(ju145)*, the designed primer pair amplifies a 500 bp sequence. While the wild-type sequence possesses a restriction site for *AlwI,* this restriction site is lost in the *ju145* allele.

For the enzymatic restriction, 10 µl of the *ahr-1* amplicon was mixed with 1.5 µl of CutSmart buffer, 0.3 µl of *AlwI* (New England Biolabs, R0513S) and 3.2 µl of nuclease-free water and incubated for 1.5 h at 37 °C. The restriction product was then loaded on a 2 % agarose gel for gel electrophoresis and genotypic analysis. The enzymatic restriction of the PCR amplicon results in the following bands on an agarose gel: wild-type – 250 bp, *ahr-1(ju145)* – 500 bp, heterozygote – 500 bp and 250 bp (Figure 12).

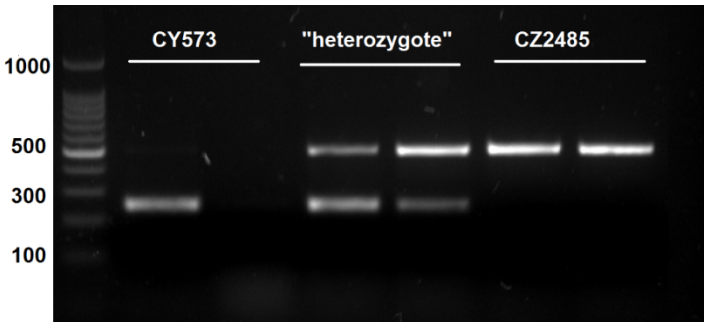

Figure 12 Visualization of fragments created by PCR for *ahr-1* and enzymatic restriction with *AlwI* on a 2 % agarose gel. CY573 possesses a wild-type *ahr-1* and was used as an example for a wild-type *ahr-1.* After enzymatic restriction with *AlwI*, a 250 bp fragment can be detected. CZ2485 carries a point mutation in the *ahr-1* gene at the position where *AlwI* cuts the fragment. The inability of *AlwI* to cut the fragment results in a 500 bp band. The "heterozygote" was created by mixing the PCR products of CY573 and CZ2428 and shows a 250 bp band and a 500 bp band. Ladder: Quick-Load 100 bp DNA Ladder (NEB, N0467).

Methods for Aim 1: Treatment with AhR modulators

Benzo(a)pyrene (BaP) treatment

Benzo(a)pyrene (Sigma Aldrich, B1760) was dissolved in DMSO (Carl Roth, 4720) in concentrations 1000 times higher than the desired concentration in the NGM. After autoclaving the NGM, BaP or DMSO were added to the media. According to the performed experiment the final concentrations of BaP in the media ranged between 0.1 µM and 10 µM. Control plates contained only 0.1 % DMSO.

Development on BaP

Starting from a synchronized population of eggs the development was examined 8, 24, 32, 48, 56 and 72 h after egg-lay, to cover most developmental stages. For each time point, the fraction of animals for each developmental stage was noted. From this, the mean developmental at each time point was calculated. Additionally, the time point at which the animals reached adulthood was counted on day 3, 4, and 5.

Curcumin treatment

Curcumin (Sigma Aldrich, C7727) was dissolved in DMSO (Carl Roth, 4720) in a concentration of 100 mM and supplied to the NGM after autoclaving. The final concentration of curcumin in the media was 100 µM (0.1 % DMSO). Control plates contained 0.1 % DMSO. If not stated otherwise, worms were treated continuously starting from hatching.

Reproduction on curcumin

The reproductive rate of curcumin and DMSO treated worms was measured during the main fertile period. Two days after egg-lay single L4 larvae were transferred to NGM plates and from then transferred to fresh NGM plates every 24 h until the 8th day after hatching. The number of eggs laid during this period was counted and the number of eggs laid per worm in one hour was calculated. Two days later the progeny hatched on each day were counted. Further, the total number of eggs and progeny of each worm were scored at the end of the experiment.

Quercetin treatment

Quercetin (Sigma Aldrich, Q4951) was dissolved in DMSO (Carl Roth, 4720) in a concentration of 100 mM and supplied to the NGM after autoclaving. The final concentration of curcumin in the media was 100 µM (0.1 % DMSO). Control plates contained 0.1 % DMSO.

UVB irradiation

Ultraviolet B (UVB) radiation is part of the light spectrum with wavelengths between 280 – 315 nm. To expose worms to UVB, a Waldmann UV 236 B (UV6) lamp with an emission maximum of 320 nm was used (Figure 13). During the exposure time, worms were kept on a bacteria-

free NGM plate. To achieve 600 J/m² the worms were exposed for 53 s with 18 cm between lamp and plate.

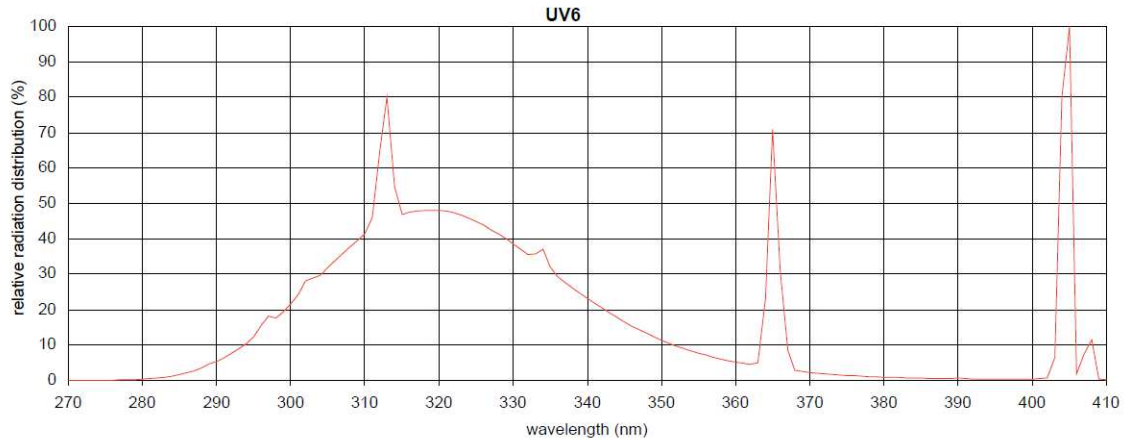

Figure 13 Emission spectrum of the Waldmann UV 236 B (UV6) lamp. Main emission spectrum: 280 – 360 nm, emission maximum: 320 nm.

Fertility of UVB irradiated and curcumin-treated worms

Worms were kept on curcumin or DMSO plates from eggs as described above. On the third day after hatching, the worms were irradiated with UVB on bacteria-free DMSO plates. 1 h after the irradiation, the worms were again transferred to either curcumin or DMSO plates containing bacteria. The number of eggs laid was counted 24 h post-irradiation using 3 times 3 worms per plate for 4 h. Two days afterward the number of progeny hatched was counted. To avoid potential effects of curcumin on the laid eggs, the fertility was assessed on DMSO plates.

UVB-induced Apoptosis

To investigate UVB-induced apoptosis, L4 larvae were treated with 600 J/m² UVB and the apoptotic corpses were counted 24 h post irradiation in the gonad loop region (Figure 14, death region). The apoptotic corpses were identified based on their shape. The apoptotic corpses were counted by Anjumara Shaik.

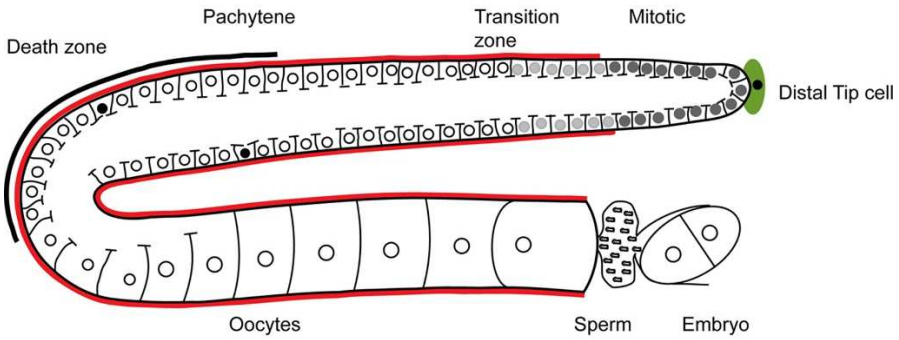

Figure 14 Schematic representation of one of the two gonad arms of an adult hermaphrodite. Germ cell apoptosis occurs mainly within the gonad loop region (black line). Solid black nuclei represent apoptotic nuclei [195].

Analysis of bacterial metabolites through Mass Spectrometry

1. Liquid NGM

Liquid NGM was prepared like solid NGM but without agar to prevent that the medium becomes solid. Like the solid NGM, the medium was poured into petri dishes (7 ml NGM/ 6 cm petri dish) and seeded with bacteria (200 µl, OD_{595} = 0.9) the next day. Control NGM plates were seeded with LB-medium. The medium was incubated for two days at room temperature to allow the bacteria to grow. Then, the bacteria were removed by centrifugation (4500 rpm, 10 min) and the medium was filtered (22 µm filter, Carl Roth P666.1) before using it for further processing.

2. Mass Spectrometry

Electrospray ionization mass spectrometry (ESI-MS) was used. It is a 'soft ionization' technique, causing only a low rate of fragmentation. Therefore, it is very well suited for the analysis of biological macromolecules. The mass spectrometer is composed of 3 central units: the ion source, the mass analyzer and the detector (Figure 15). An electrospray is used as an ion source to produce molecular ions of the intact (macro-) molecules. In the positive mode, the analyte is positively charged by protonation, while it is negatively charged by deprotonation in the negative mode. In the mass analyzer, these ions are separated according to their mass to charge ratio (m/z value). Finally, the ions are detected by the detector, and a mass spectrum is created [198].

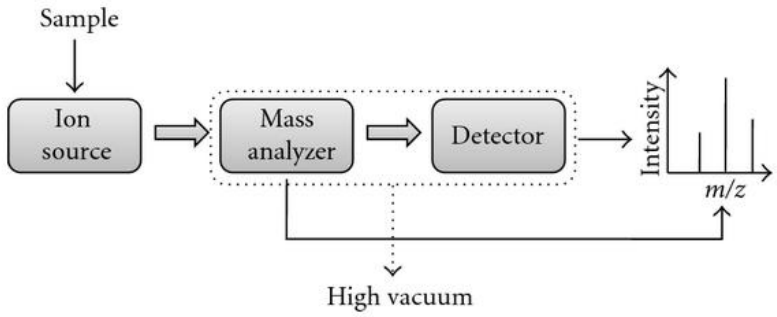

Figure 15 Basic components of a mass spectrometer [198].

For the LC-MS measurements, the liquid NGM samples were diluted 1:20 with methanol before injection of 10 µl sample volumes. Triterpenes were separated on a Dionex HPG 3200 HPLC system (Thermo Scientific) equipped with a 150 x 2.1 mm, 2.7 µm, C18-CSH column (Waters) with a binary gradient system. Mobile phase A consisted of water + 0.1% formic acid (FA), and mobile phase B consisted of methanol + 0.1% FA. The mobile phase gradient was as follows: Starting conditions were 5% mobile phase B, increased to 95% B within 10 min, the plateau was held for 4 min, and the system was returned to starting conditions within 1 min and held for another 4.5 min. The flow rate was 0.5 mL/min. The MS and MS/MS analysis were performed with a quadrupole-time-of-flight instrument (maXis 4G, Bruker Daltonics, Bremen,

Germany) equipped with an ESI source. The device was operated in positive-ion and negative-ion mode and the operating conditions were as follows: dry gas (nitrogen): 8.0 L/min, dry heater: 220 °C, nebulizer pressure: 1.8 bar, capillary voltage: 4500 V. Data analysis were performed using the software data analysis 4.2 and Metabolite detect 2.1 (Bruker daltonics, Bremen, Germany). Mass spectrometry was performed by Sabine Metzger (CEPLAS MS-Platform, University of Cologne and MS core unit IUF - Leibniz Institute for environmental Medicine, Düsseldorf).

Methods for Aim 2: Assessing aging

Lifespan

The lifespan analysis was started from a synchronized population of worms, which was transferred to fresh NGM plates daily during the fertile period. After the fertile phase, the animals were transferred every alternate day. Dead, alive and censored animals were scored during the transferring process. Animals were counted as dead when they did show neither movement, nor response to a manual stimulus with a platinum wire, nor pharyngeal pumping activity. Animals with internal hatching (bags), an exploded vulva or which died desiccated on the wall were censored. The number of dead and censored animals was used for survival analysis in OASIS [191] or OASIS 2 [192]. For the calculation of the mean lifespan and the survival curve in OASIS and OASIS 2, the Kaplan Meier estimator was used, and the p-values were calculated using the log-rank test between pooled populations of animals.

Movement/Healthspan

The movement was set as a parameter for healthy aging, and the phase of active movement is referred to as healthspan. It was assessed in the populations used for the lifespan assay. Animals, which were either crawling spontaneously or after a manual stimulus, were considered as moving while dead animals or animals without crawling behavior were considered as not moving. Statistical analysis was done as described for lifespan.

Quantification of polyQ aggregates

polyQ$_{40}$ aggregates were visualized in NV38b and NV38wt by fluorescence microscopy. The number and the size of the aggregates were quantified in Fiji [193]. To assess the number of aggregates, images were stitched using the Fiji pairwise stitching plugin [194] to create whole worms. The average size of the aggregates was instead measured in the non-stitched images. The number and the size of aggregates were counted using the plugin “Analyze Particles”. Aggregates were defined as a particle with a size between 0.002 and 1000 pixels and a fluorescence intensity between 25 and 255. The procedure was automatized using the following macro written by Alfonso Schiavi:

```
macro "Poly q40 whole worm [6]"
{original = getTitle();
rename("_"+original);
run("Duplicate...", "title=&original");
run("Subtract Background...", "rolling=50");
run("8-bit");
setThreshold(25, 255);
run("Convert to Mask");
run("Fill Holes");
run("Convert to Mask");
run("Open");
run("Watershed");
setTool("freehand");
waitForUser("please, select the ROI");
run("Analyze Particles...", "size=0.002-1000 show=Masks summarize in_situ");
run("Select None");
close();}
```

Pharyngeal pumping

Pharyngeal pumping was quantified by counting the grinder movements in the terminal bulb of the pharynx using a stereo-microscope. For this, a synchronized population of 20 worms was maintained by transferring to fresh NGM daily or every other day. On day 3, 7, 10 and 14, the pumping of 10 animals was counted twice per individuum for a 20 s interval. Only worms, which were crawling on the bacteria, were counted. The relative pharyngeal pumping activity was calculated using the pumping activity of day 3 for each strain/condition.

Heat stress

The resistance to heat stress was tested with 20 animals/condition per experiment at 35 °C on 3 cm plates wrapped with parafilm in an incubator (Intrafors HT Multitron). When using animals older than 3 days, animals were transferred to fresh NGM plates daily during the fertile phase. The number of dead animals was scored hourly by gently touching the worms with a platinum wire and analysis was performed as described for the lifespan assay.

Food race

The food attraction of *C. elegans* was used to study the functional neuronal decline during aging. The food race was performed as described in [196]. 50 µl of bacteria (either HT115(L4440) or OP50(L4440), according to the culture conditions of the worms) were seeded on a 9 cm NGM plate and grown for 2 days. Shortly before the assay, 25 µl of 15mM NaN_3 was spread on top of the bacteria to paralyze the worms as soon as they reached the food. Synchronized worms were collected in S-basal and washed 3 times. Then they were placed 45 mm away from the food spot, and the S-basal was removed. Afterward, the assay was started, and the number of worms which did and did not reach the food was counted after 1 and 2 h. A schematic representation of the assay is shown in Figure 16.

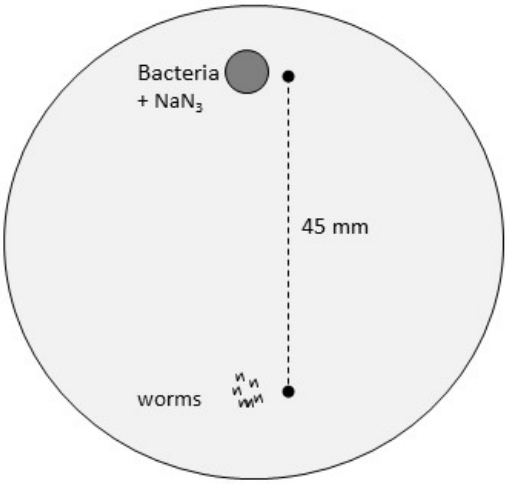

Figure 16 Scheme of food race experiments. Worms were placed in a distance of 45 mm from the attractant (bacteria). NaN_3 was supplemented on top of the bacterial lawn to paralyze worms reaching the food.

Pharyngeal pumping using the NemaMetrix ScreenChip System

The NemaMetrix ScreenChip System (https://nemametrix.com/products/screenchip-system/) is a worm screening platform developed to measure parameters related to pharyngeal pumping in real time. Using electrodes placed on microfluid chips, it detects the voltage changes caused by the contraction of the pharynx. This measurement is called electropharyngeogram (EPG) [197]. The NemaMetrix ScreenChip System allows measuring the following parameters: pump frequency, pump waveform shape, spike amplitude ratios, pump duration, and interpump interval. One pump is composed of two spikes, the excitation spike (E spike) and the relaxation spike (R spike). The pump frequency is identified as the average pumping rate during the time of recording. The pump amplitude is the amplitude between the E and the R spike of a pump. Figure 17 shows the characteristics of the EPG.

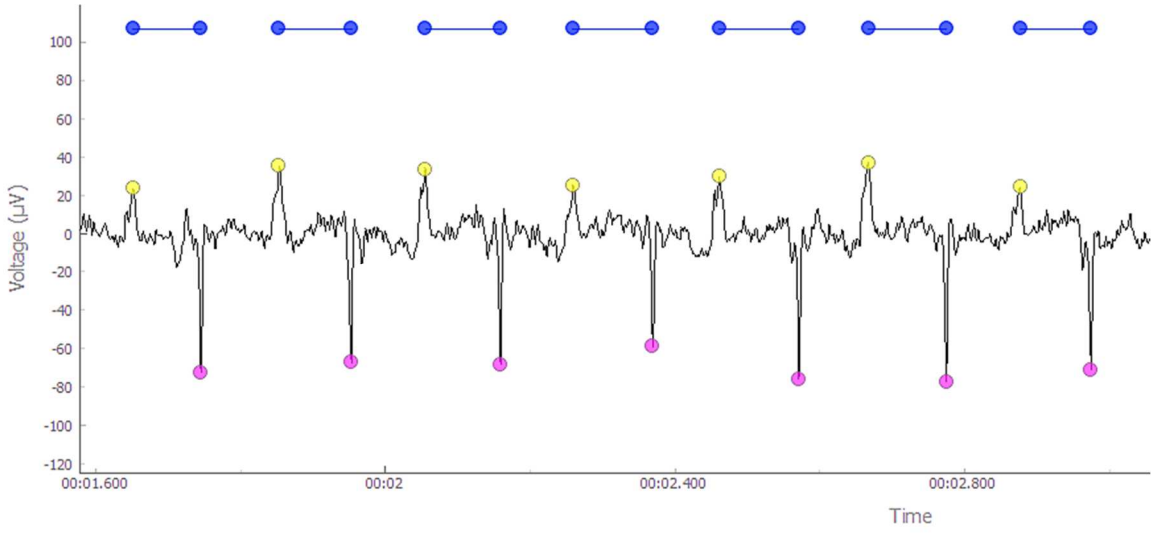

Figure 17 EPG of a 3-days old worm. The voltage change is plotted against the time. Upon contraction of the pharynx, a positive voltage change can be observed as an excitatory spike (E spike, shown as yellow dots). The relaxation of the pharynx muscle results in an adverse voltage change, the relaxation spike (R spike, shown as pink dots). The horizontal blue line represents the pump duration.

To measure the pharyngeal pumping rate with the NemaMetrix ScreenChip, worms were washed off the plates with S-basal and collected in a reaction tube. Then, the worms were washed twice with S-basal and twice with 10 mM serotonin (Sigma Aldrich, 14927) and incubated in 10 mM serotonin for 30 min. Worms were loaded on the ScreenChip SC40 with a syringe (0.01 ml – 1 ml). The EPG of single worms was recorded for a duration of approx. 2 min. Only worms which showed pumping activity were recorded, while those with no pumping activity were not considered. The following software was used: NemAcquire-2.1, and NemAnalysis-0.2 (https://nemametrix.com/products/software/).

Nile Red *in vivo* staining

Worms were kept on Nile Red plates (Nile Red concentration: 50 nM) from eggs. On day 3, day 7 and day 10, the worms were washed, collected in S-basal, and anesthetized with 15 mM NaN_3. The stained lipid droplets were visualized by fluorescence microscopy using the channel DS Red. Pictures were analyzed in Image J as grey intensities in the red channel in two defined areas (each 35 x 35 pixel) in the anterior part of the intestine. The quantified intensities were normalized to the mean fluorescence of the wild-type on HT115 at each time point.

Tryptophan supplementation

The concentration of tryptophan and the supplementation procedure was taken from [128] with minor changes. Tryptophan (Carl Roth 4858.2) was dissolved in water at a concentration of 12.5 mg/ml and incubated shaking at 30°C for 45 min. Afterward, the solution was filtered (pore size: 0.22 µm, Carl Roth P666.1). For a 6 cm diameter plate 200 µl of 12.5 mg/ml tryptophan was spotted on the bacterial lawn of an NGM plate, which was kept at room temperature for overnight. After the supplementation, the dish was kept at room temperature for another day.

Assessment of age-associated features at 25 °C

Lifespan, movement, and polyQ aggregation analysis were performed as described above. N2 and CZ2485 were grown at 25 °C from the time point of birth. The polyQ-expressing worms instead are temperature sensitive, and therefore they were kept at 20 °C until reaching the L4 stage and were afterward kept at 25 °C for the rest of their lifespan.

Methods for Aim 3: Identification of AHR-1 target gene expression

Quantification of transgene expression

The expression of fluorescently-tagged genes was investigated by using fluorescence microscopy. For this, worms expressing fluorescently tagged genes were paralyzed with 15 mM – 70 mM NaN_3 and pictures were taken with identical exposure times and settings. The pictures were then analyzed in either Image J or Fiji [193]. For the analysis of the mean expression in the whole worm the following macro, written by Alfonso Schiavi, was used:

```
macro "whole worm [w]"
{nome = getImageID();
run("Duplicate...", "title=red-1");
run("Enhance Contrast", "saturated=0.4");
run("Invert LUT");
run("Remove Outliers...", "radius=20 threshold=50 which=Dark");
run("Gaussian Blur...", "sigma=3");
setAutoThreshold();
setThreshold(5, 255);
run("Smooth");
run("Smooth");
run("Convert to Mask");
run("Despeckle");
run("Create Selection");
run("Enlarge...", "enlarge=-0.8");
roiManager("Add");
wait(1000);
run("Close");
wait(1000);
close();
wait(1000);
run("Restore Selection");
roiManager("Add") }
```

For the analysis of the mean expression in specific regions of the worm, the expression was measured in a circular area (50 x 50 pixels) in the region of interest. The quantified intensities were normalized to the mean fluorescence of the wild-type in each experiment. Statistical analysis was performed with the pooled data.

Measurement of Pcyp-35B1::GFP intensity

The relative intensity of Pcyp-35B1::GFP was measured in 4-days old worms following different exposures of BaP or DMSO. Fluorescence images were analyzed using Fiji [193] and the following macro created by Alfonso Schiavi:

```
macro " whole worm [8]"
{original = getTitle();
rename("_"+original);
run("Duplicate...", "title=&original");
setThreshold(220, 65535);
run("Convert to Mask");
run("Fill Holes");
run("Convert to Mask");
run("Create Selection");
roiManager("Add");
setTool("freehand");
wait(1000);
run("Close");
run("Close");
run("Restore Selection");
waitForUser("please, select the ROI");
run("Set Measurements...", "area mean standard min shape integrated area_fraction display
redirect=None decimal=3");
run("Measure");
run("Select None");}
```

The integrated density was chosen as parameter for the expression. The quantified intensities were normalized to the mean of untreated wild-type in each experiment. Statistical analysis was performed with the pooled data.

Fluorescence Microscopy

For the fluorescence microscopy, a ZEISS Imager M2 with an Axiocam MRm camera was used.

Quantitative Real-time PCR (qPCR)

To assess the expression of *cyp* genes, I used quantitative Real-time PCR (qPCR). This technique uses fluorescent DNA-binding dyes. Due to the replication of DNA during the amplification process, the increase of the fluorescence can be detected and used as a measurement of gene expression.

1. **Sample collection, mRNA extraction, and cDNA synthesis**

For qPCR, approximately 1000 3-days old worms per condition were washed with S-basal 3 times and then collected in H_2O. The mRNA was extracted using the RNeasy-/Shredder Kit (Qiagen, 74104 and 79654). First, the worms were lysed in RLT buffer and DTT using a TissueLyser (Qiagen). Afterward, the lysate was poured on the Shredder column to remove genomic DNA. After providing optimal binding conditions for the RNA by adding ethanol to the supernatant, the samples were poured into RNeasy columns to bind the RNA. An additional step of DNase treatment (RNase-free DNase Set (Qiagen, 79254)) was added to remove possible remaining DNA. After washing and elution steps the RNA content was quantified by spectrophotometry, and 1.2 µg of mRNA was used for the cDNA synthesis (Omniscript RT Kit (Qiagen, 205111)). Briefly, the RNA was thawed on ice and mixed with RT buffer, dNTP mix, oligo-dT primer, RNase inhibitor, and Omniscript RT reverse transcriptase. The mixture was incubated at 37 °C for 1 h. Afterward, the cDNA was stored at - 20 °C.

2. **Primer design**

Primers were designed using NCBI Primer BLAST (https://www.ncbi.nlm.nih.gov/tools/primer-blast/ [199]). Each primer pair was designed to span an exon-exon junction to ensure that only cDNA and not genomic DNA is amplified. Ralph Menzel kindly provided some primer pairs; the other primers were purchased from Sigma Aldrich. Primer pairs and their features are listed in Table S 10.

3. **PCR conditions**

For the Real-time qPCR, the cDNA was diluted 1:20 in 10 mM TRIS (pH 8.0). For the reaction, the qPCR Green Core kit (Jena Biosciences, PCR-333L) was used. This kit contains the fluorescent DNA stain EvaGreen®, which binds to DNA and becomes fluorescent upon DNA binding. A master mix composed of the following components was made, and 18 µl of master mix was mixed with 2 µl of cDNA.

qPCR master mix (for 1 reaction)

		Final concentration
15.2 µl	water	
2 µl	qPCR Green buffer (10x)	1x
0.4 µl	dNTP mix (10 mM)	200 µM
0.15 µl	primer F (50 µM)	375 nM
0.15 µl	primer R (50 µM)	375 nM
0.1 µl	qPCR polymerase (5 units/µl)	0.025 units/µl

The samples were run in a MyiQ2 cycler (BioRad), and the expression of each sample was measured in duplicate on the same multi-well plate. The following PCR program was used.

PCR program for qPCR

Initial denaturation	95°C	2 min	
Denaturation	95 °C	20 s	35 cycles
Annealing	T °C	20 s	
Elongation	72 °C	30 s	
Final denaturation	95 °C	1 min	
Melting curve	55 °C	1 min	
	Temperature increase 0.5°C/10s		

The annealing temperature (T) was adjusted to each primer pair in an initial step (Optimization of primer efficiency). After the PCR, the product was melted (melting curve) by increasing the temperature by 0.5 °C every 10 s. The melting curve was analyzed afterward to ensure that only one product got amplified. *cdc-42* and *act-1* were used as reference genes.

4. Optimization of primer efficiency

To test the efficiency of the primer pairs and to optimize the PCR conditions, the following cDNA concentrations were used: 1:20, 1:100, 1:500, and 1:2500 (in 10 mM TRIS, pH 8.0). The efficiency was calculated by the BioRad iQ5 software installed on the device. This software uses the logarithmic starting quantity of the sample (*e.g.*, -1.301 for the 1:20 dilution) and the mean Ct to for linear regression. The efficiency is defined as $E = 10^{-1/m} - 1$ with m being the slope of the regression curve. It is a measure of how much of the product is produced in each cycle. The primer efficiency was used as a marker for quality, and only primer pairs with an efficiency higher than 75 % and smaller than 125 % were used. As an additional marker for the quality of the primer pairs, the melting curve was analyzed. The peaks of the melting curve can give a hint, whether the primer pair is specific and only one PCR product got amplified (only one peak observable), or whether there might be other products being amplified (more than one peak). To ensure that the right product was amplified, the PCR product was checked for its size by gel electrophoresis. If the efficiency was higher than 125 % or two PCR products were amplified, a higher annealing temperature was tested. In cases where the efficiency was lower than 75 % or no PCR product was amplified, a lower annealing temperature was tested.

Each primer pair was tested at least in duplicate, and only primer pairs which passed all three quality control criteria were used for qPCR. Primer pairs which could be optimized in this study are listed in Table S 11 along with their efficiency and the conditions used.

5. Analysis

After optimization of the PCR conditions for each primer pair, qPCR was run. To minimize the technical error, the samples for each primer pair were run in duplicate on the same plate according to the scheme in Figure 18.

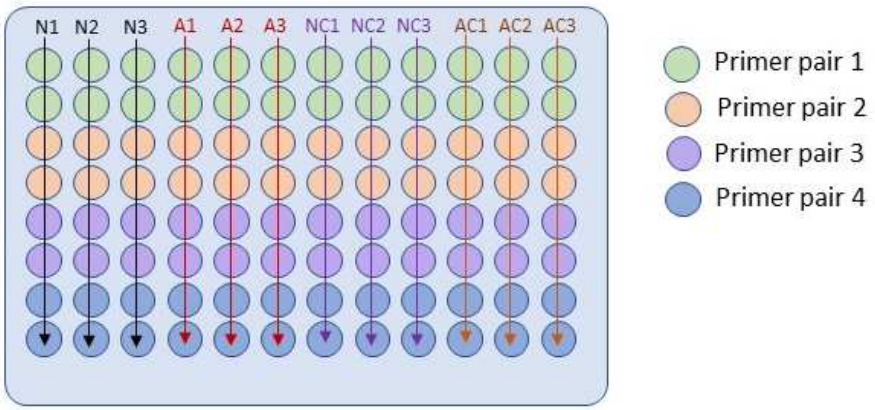

Figure 18 Example of plate design. The cDNA samples were and the mixes containing the primer pairs horizontal. Letter code: N = wild-type DMSO, A = *ahr-1(ju145)* DMSO, NC = wild-type curcumin, AC = *ahr-1(ju145)* curcumin; numbers show the biological replicate.

The expression of the *cyp*s was calculated relative to the reference genes *act-1* and *cdc-42* using the iQ5 software. All data collected were enabled for gene study according to the BioRad user instructions, and the expression was calculated using the normalized expression (ddC_T). The efficiency of each primer pair reaction was added for correct quantification of the normalized expression. More detailed information on how the software calculates the gene expression can be found in the iQ5 Optical System Software Instruction Manual (http://www.bio-rad.com/webroot/web/pdf/lsr/literature/Bulletin_10005604.pdf). From these normalized expression values, the fold-change compared to wild-type DMSO was calculated for each replicate.

Microarray

For the analysis of gene expression by microarray, samples from 5 independent replicates were collected as described above for the qPCR and the RNA was extracted. The samples were further processed, and the microarray was performed by René Deenen from the Genomics & Transcriptomics Laboratory (GTL) of the Biological and Medical Research Center (BMFZ) at the Heinrich Heine University Düsseldorf. For the microarray, an Affymetrix Chip was used. The microarray raw data in the format of CEL was analyzed by Alfonso Schiavi using the software R (version 3.4.2) and Bioconductor [200]. Background correction,

normalization, and expression calculation of all the array were performed with the oligo package [201] and the RMA method. Then, quality control of the array was run using the package arrayQualityMetrics_3.34.0 [202]. Because of the quality measures, sample ahr-1C5 was excluded from further analysis (Figure S 7). The differentially expressed genes were identified using the limma package and a linear model and moderated t-statistic with FDR to test for multiple comparisons [203]. A p-value of 0.1 was applied. The differentially expressed genes were analyzed for GeneOntology term enrichment using Cytoscape (version 3.6.0) [204] with the plugin ClueGo (version 2.5.0) [205].

Gene silencing by RNA-mediated interference (RNAi)

Gene silencing was achieved through feeding bacteria expressing plasmids with dsRNA against specific genes [206]. All plasmids used were derived from the vector L4440, a 2790 bp vector, containing a multicloning site between two IPTG-inducible T7 polymerase promoters and amp resistance as selection marker [206]. To silence a specific gene in *C. elegans*, dsRNA targeted against the mRNA of this gene is cloned inside the multicloning site of the L4440 vector. Upon IPTG feeding, the bacteria produce dsRNA, which is processed into short interfering RNAs (si-RNAs) and in turn degrade the mRNA of the specific gene in *C. elegans* [207]. For RNAi, either *E. coli* HT115(DE3) or *E. coli* OP50(xu363) [122] were used. Both bacterial strains have a disruption of the *rnc* gene, which encodes for an RNaseIII, and carry an IPTG-inducible T7 polymerase cassette [122, 208]. These two characteristics are crucial for the performance of RNAi experiments since the IPTG-inducible T7 polymerase cassette is required to produce dsRNA from plasmids and the disruption of *rnc* ensures that this dsRNA is not cleaved by the RNaseIII. If not stated otherwise, RNAi feeding applied continuously from birth to death.

Box plots

Box plots were created in GraphPad Prism 6 and show the median (line), the mean (+), the 25th to 75th percentile (box). The whiskers and outliers (represented as dots) were calculated by the Tukey method.

Statistical analysis

If not stated, statistical analysis was performed in GraphPad Prism 6. For life-/healthspan assays, statistical analysis was done in OASIS [191, 192]. Statistical analysis of the microarray was performed in R.

4. Results

Benzo(a)pyrene (BaP) affects development and lifespan in an AHR-1-dependent manner, under specific conditions

To determine, whether *C. elegans* is a good model to study evolutionarily conserved AhR functions, I specifically investigated if known mammalian AhR modulators affect *C. elegans* life traits in an AHR-1-dependent manner. In mammals, some of the toxic effects of BaP are mediated by AhR-induction of *cyps* [131] and in *C. elegans* BaP induces *cyp* gene expression [209]. I, therefore, investigated whether AHR-1 also mediates toxic effects of BaP in *C. elegans.* In an initial experiment, I tested the effect of different concentrations of BaP on the development of the wild-type and *ahr-1(ju145).* A concentration of 0.1 µM did not significantly affect the larval development of the wild-type and *ahr-1(ju145)*, while concentrations of 1 µM and 10 µM resulted in a slower development in both genetic backgrounds. The development was affected starting around the L2 to L3 larval stage, while the early development from eggs to L2 larvae was not affected by BaP (Figure 19A - B). Interestingly, loss of *ahr-1* significantly increased resistance to 1 µM of BaP: in 3 days only 65 % of the wild-type reached adulthood versus 94 % in *ahr-1(ju145)* (Figure 19C). 10 µM of BaP instead had a similar detrimental effect on wild-type and *ahr-1(ju145):* after 3 days 31 % of the wild-type and 25 % of *ahr-1(ju145)* reached adulthood; another 27 % of wild-type and 38 % of *ahr-1(ju145)* needed 4 days; while 39 % of the wild-type and 30 % of *ahr-1(ju145)* still did not reach adulthood after 5 days. These data indicate that BaP affects development in an AHR-1-dependent manner only under specific conditions. Since 1 µM BaP showed AHR-1-dependent effects on the development, I investigated the effect on this concentration on the lifespan. When supplemented from adulthood, a concentration of 1 µM BaP significantly shortened the lifespan of the wild-type but not of *ahr-1(ju145)* (Figure 19 D), suggesting that at least some concentrations of BaP affect aging of *C. elegans* in an AHR-1-dependent manner.

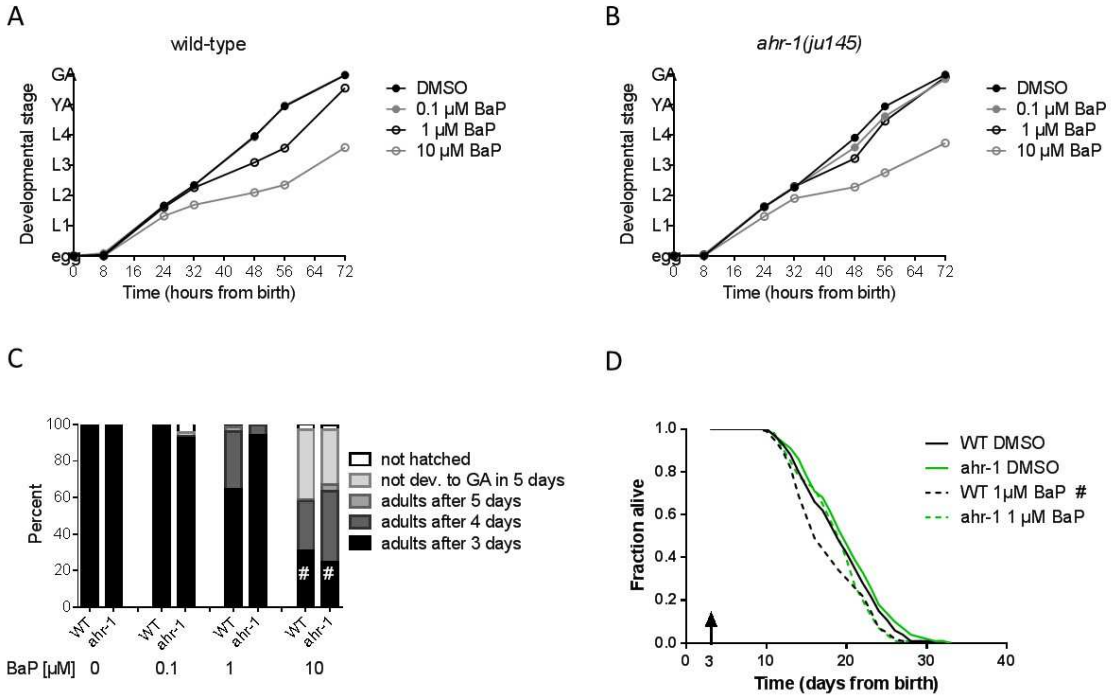

Figure 19 BaP affects the development and lifespan of worms in a concentration-dependent manner. A - B) Curves showing the mean developmental stage of BaP- or DMSO-treated wild-type and *ahr-1(ju145)* in the first 72 h after egg-lay in 3 pooled independent experiments. The curve for WT 0.1 µM BaP is hidden behind the curve of WT DMSO. C) Percentage of worms reaching adulthood between 3 and 5 days after egg-lay in 3 pooled independent experiments. No. of worms: 60 – 127, # p-value < 0.05 *vs.* DMSO, statistical test: Two-way ANOVA with Tukey's multiple comparisons test D) Kaplan Meier survival curve of wild-type and *ahr-1(ju145)* treated with DMSO or BaP from day 3 (indicated by arrow head). Curves show the pooled data of 2 independent experiments. # p-value < 0.05 *vs.* DMSO, statistical test: Log-rank test. See Table S 1 for mean survival times and statistical analysis.

Curcumin extends *C.elegans* healthspan in an AHR-1-dependent manner

Curcumin and quercetin extend lifespan in *C. elegans* and suppress AhR signaling in mammals [101, 102, 106, 107, 152, 210]. To investigate, whether the lifespan-extending effects of quercetin and curcumin are also dependent on the AhR in *C. elegans*, I treated wild-type and *ahr-1(ju145)* with lifespan-extending concentrations of both compounds. As expected from our previous findings [173], *ahr-1(ju145)* mutants are long-lived compared to wild-type animals: loss of AHR-1 function specifically prolonged lifespan and movement period by 13 and 17 % respectively. The time in which the animals are actively moving was defined the time as healthspan. Both quercetin and curcumin were dissolved in DMSO and supplemented to the medium after autoclaving, however, while curcumin dissolved nicely in the NGM, plates containing quercetin showed many precipitates. Quercetin strongly extended the lifespan and healthspan in the first replica by 37 % (Figure S 1) in an AHR-1-dependent manner but for reasons which are still not clear (*e.g.*, poor solubility, different batch), quercetin was without effect in the other replicates (Figure S 1). Curcumin instead showed a very reproducible lifespan and healthspan extension in the wild-type but did not affect the lifespan of *ahr-1(ju145)* (Figure 20A - B). Lifespan and healthspan were increased by 14 and 17 % respectively in curcumin-treated wild-type. During the lifespan analysis, I noticed an increased amount of

sterile eggs in curcumin fed wild-type at day 7 and day 8, when the DMSO treated wild-type were not laying eggs anymore. On *ahr-1(ju145)* I observed a similar, but even stronger phenotype on both, DMSO and curcumin. I, therefore, checked whether loss of AHR-1 function and curcumin treatment have any effect on *C. elegans* fertility. However, wild-type and *ahr-1(ju145)* produced the same amount of eggs and progeny if treated with curcumin or DMSO (Figure 20 C - E). Comparing the total brood size, DMSO treated *ahr-1(ju145)* had slightly less progeny compared to DMSO treated wild-type (Figure 20 E). Besides the animals' ability to move, pharyngeal pumping activity also declines during physiological aging. I thus assessed the pharyngeal pumping activity of curcumin and DMSO treated wild-type and *ahr-1(ju145)*. For this, I calculated the relative pumping rate of each worm relative to the pumping frequency on day 3 of the same strain. As expected pharyngeal pumping linearly declined during aging. However, neither curcumin nor loss of *ahr-1* ameliorated the age-dependent decline in pharyngeal pumping (Figure 20E).

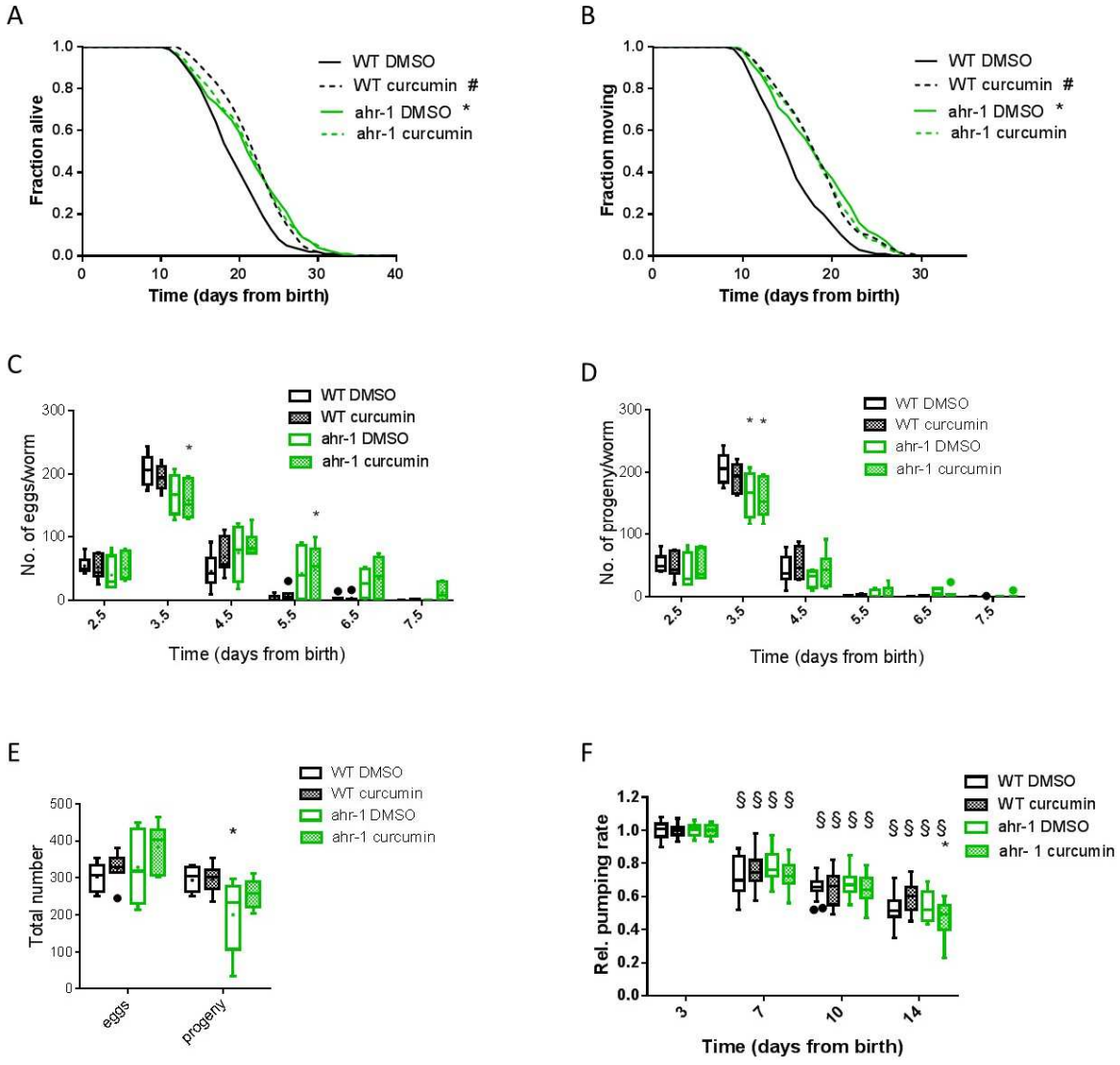

Figure 20 Curcumin extends lifespan and healthspan in wild-type but not in *ahr-1(ju145)* without affecting fertility and pharyngeal pumping. A – B) Kaplan Meier survival curves of wild-type and *ahr-1(ju145)* supplemented with

100 µM curcumin or DMSO from birth. Pooled data from 5 independent experiments are shown. * p-value < 0.05 *vs.* WT, # p-value < 0.05 *vs.* DMSO, statistical test: Log-rank test. Mean life- and healthspans and statistical analysis are listed in Table S 2. C - E) Curcumin does not influence the fertility. Number of eggs (C) and progeny (D) produced per worm in a 24-h time frame starting from 2 days after hatching. E) The total number of eggs and progeny produced in the fertile phase of 5 – 8 worm in 2 independent experiments, * p-value < 0.05 *vs.* WT, statistical test: Two-way ANOVA with Tukey's multiple comparisons test. F) Pharyngeal pumping activity is not affected by curcumin. The relative pharyngeal pumping activity compared to day 3 of 12 – 20 worms in 2 independent experiments is shown. * p-value < 0.05 *vs.* WT, § p-value < 0.05 *vs.* day 3, statistical test: Two-way ANOVA with Tukey's multiple comparisons test.

Accumulation of muscle polyglutamine (polyQ) aggregates and a faster decline in locomotion ability (compared to wild-type animals) are classical age-associated features observable in *C. elegans* models of neurodegenerative disease. For my experiments, I used the strain AM141 [63], which carries 40 polyQ repeats ($polyQ_{40}$) coupled to a fluorophore in the muscle cells. It is a worm model for polyQ disorders, which is a commonly used model for neurodegenerative diseases. While the expression is evenly in young animals due to the soluble character of the polyQ aggregating proteins, they get insoluble during aging and aggregate. To investigate whether AHR-1 and curcumin are involved in the aggregation of insoluble polyQ, I initially crossed the $polyQ_{40}$ carrying AM141 in the background of the *ju145* allele. For this, I crossed AM141 with CZ2485, which carries the *ju145* allele. I called the homozygote strains arising from this cross NV38wt and NV38b. NV38wt (in the following polyQ;wt) carries the $polyQ_{40}$ and a wild-type *ahr-1* allele, while NV38b (in the following polyQ;ahr-1) carries the $polyQ_{40}$ and the *ju145 ahr-1* allele. To understand, whether curcumin and loss of *ahr-1* affect polyQ aggregation and toxicity, I treated polyQ;wt and polyQ;ahr-1 worms with curcumin and investigated lifespan, movement, and polyQ aggregation. Similar to previous experiments, loss of AHR-1 extended the lifespan and healthspan of the $polyQ_{40}$ strain by 13 and 17 % respectively. However, contrary to the effect on wild-type animals, curcumin supplementation significantly extended the lifespan of polyQ;wt and polyQ;ahr-1 (Figure 21A): in both strains, curcumin extended the lifespan by 14 % and because of the additive effect of curcumin and loss of AHR-1 function, polyQ;ahr-1 worms treated with curcumin had the longest lifespan, which was 29 % increased compared to untreated polyQ;wt. Also, the healthspan was extended by curcumin in both strains, although lower in *ahr-1* loss of function worms (Figure 21B): while curcumin extended the healthspan by 19 % in polyQ;wt, the increase in healthspan was only 8 % in *ahr-1* loss of functions worms. Unexpectedly, both, loss of *ahr-1* function and curcumin, increased the number of polyQ aggregates in 10-days old worms to a similar extent (Figure 21C), but they did not affect the aggregate size (Figure 21 D). Of note, despite the synergistic effect of curcumin and *ahr-1* loss of function on lifespan and movement in the polyQ-expressing worms, their combined effect on the number of polyQ aggregates was not additive while it was slightly additive on the size of the aggregates. These data indicate that while the pro-longevity effect of curcumin on polyQ expressing worms is independent of the AHR-1, its pro-aggregation effect appears to be AHR-1 dependent. Interestingly, my results also suggest that, at least in this experimental context and opposed to the current view, the number of aggregates does not

directly correlate with their toxic effects; rather the higher the number of aggregates, the longer the lifespan (thus implying a protective effect of polyQ aggregation).

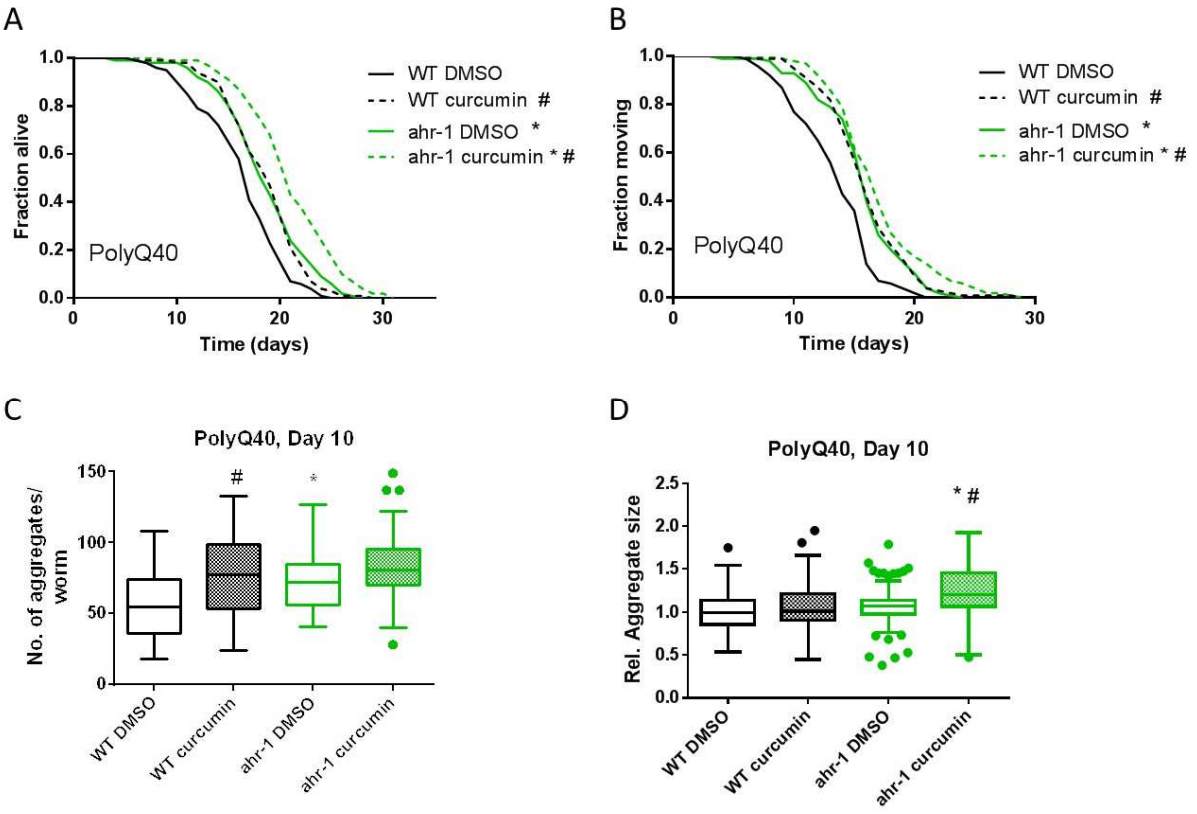

Figure 21 Curcumin affects aggregation and extends the lifespan and healthspan of polyQ40-expressing polyQ;wt and polyQ;ahr-1. A - B) Kaplan Meier curves of polyQ;wt and polyQ;ahr-1 supplemented with 100 µM curcumin from birth. The curve shows the pooled data from 3 independent experiments. * p-value < 0.05 *vs.* WT, # p-value < 0.05 *vs.* DMSO, statistical test: Log-rank test. Detailed information in Table S 2. C - D) Effect of curcumin on the number (C) and size (D) of polyQ$_{40}$ aggregates in polyQ;wt and polyQ;ahr-1 in 3 independent experiments. No. of worms 59 – 68, * p-value < 0.05 *vs.* WT, # p-value < 0.05 *vs.* DMSO, statistical test: Two-way ANOVA with Tukey's multiple comparisons test.

AHR-1 protects against UVB-induced apoptosis in the germline

Previous experiments of my Master's thesis project revealed that *ahr-1* loss of function worms are more sensitive towards the UVB-induced reduction in fertility. Specifically, the hatching rate of eggs laid 8 - 24 h after irradiation was significantly reduced in *ahr-1(ju145)* compared to wild-type. In mice, the AhR inhibitor resveratrol has protective effects against UVB-induced cancer formation [211]. To understand, whether also curcumin protects against UVB-induced damage in *C. elegans*, I irradiated curcumin-treated, and DMSO treated wild-type and *ahr-1(ju145)* with 600 J/m² UVB and assessed the effect on animals' fecundity and fertility. UVB irradiation affected the number of eggs laid to a similar extent regardless of the genetic background or curcumin treatment (Figure 22A). There was a tendency of a reduced number of eggs in UVB treated worms, but despite curcumin-treated *ahr-1(ju145)*, the effect was not statistically significant. Instead, as noticed previously, UVB significantly affected the egg viability in the *ahr-1(ju145)* mutants (Figure 22B). Only 66 and 62 % of the laid eggs hatched

in UVB treated *ahr-1(ju145)* grown on DMSO and curcumin respectively. However, curcumin did not have any effect on the egg viability after UVB treatment neither in wild-type nor *ahr-1(ju145).*

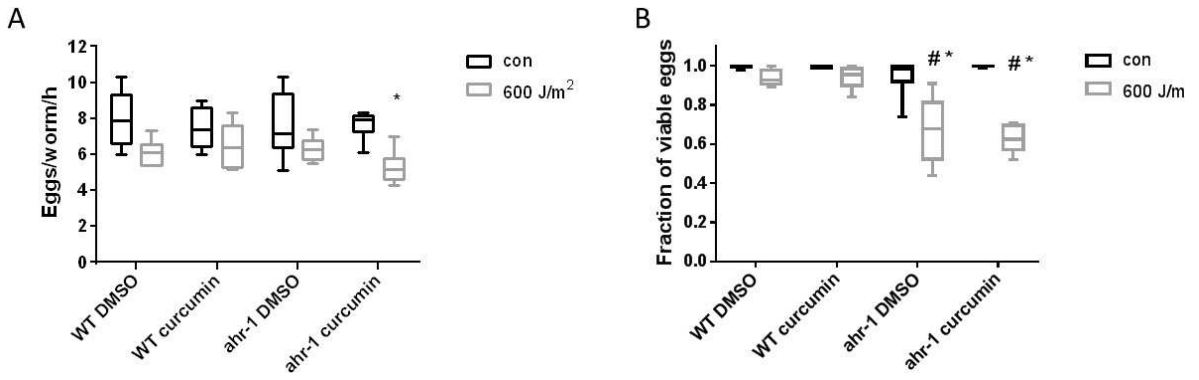

Figure 22 Curcumin does not affect the fertility of UVB-treated worms. Wild-type and *ahr-1(ju145)*, grown on either DMSO or curcumin containing plates were either irradiated with 600 J/m² UVB or left untreated. A) Number of eggs laid per worm per hour 24 h after irradiation. B) Fraction of eggs hatched from A). Pooled data of 2 independent experiments are shown. No. of worms: 6, * p-value < 0.05 *vs.* con, # p-value < 0.05 *vs.* WT, statistical test: Two-way ANOVA with Tukey's multiple comparisons test.

The reduced egg viability 24 h after UVB indicates an increased sensitivity of *ahr-1* mutant meiotic germ cells to radiation. UVB irradiation results in the induction of apoptosis in the meiotic compartment of the germline [212] and in mammalian cells loss of AhR sensitizes cells to UVB-induced apoptosis [213]. Thus, to understand whether apoptosis might be responsible for the reduced hatching rate in *ahr-1(ju145)*, I investigated apoptosis in irradiated wild-type and *ahr-1(ju145)* 24 h after irradiation with 600 J/m² UVB. As expected, the number of apoptotic corpses was significantly increased by UVB compared to untreated worms in the wild-type strain and, similar to mammalian cells, even more in the absence of *ahr-1*. Interestingly, I also observed an increased number of apoptotic corpses in the *ahr-1* mutant compared to wild-type in basal conditions (Figure 23A). Thus, when comparing the induction of apoptosis by UVB, wild-type showed a stronger increase in apoptosis than *ahr-1(ju145)* (Figure 23B): while apoptosis was increased 6.7-fold in wild-type, it was only increased 2.6-fold in *ahr-1(ju145).* The smaller induction of apoptosis in *ahr-1(ju145)* indicates that UVB increases apoptosis at least partially through AHR-1.

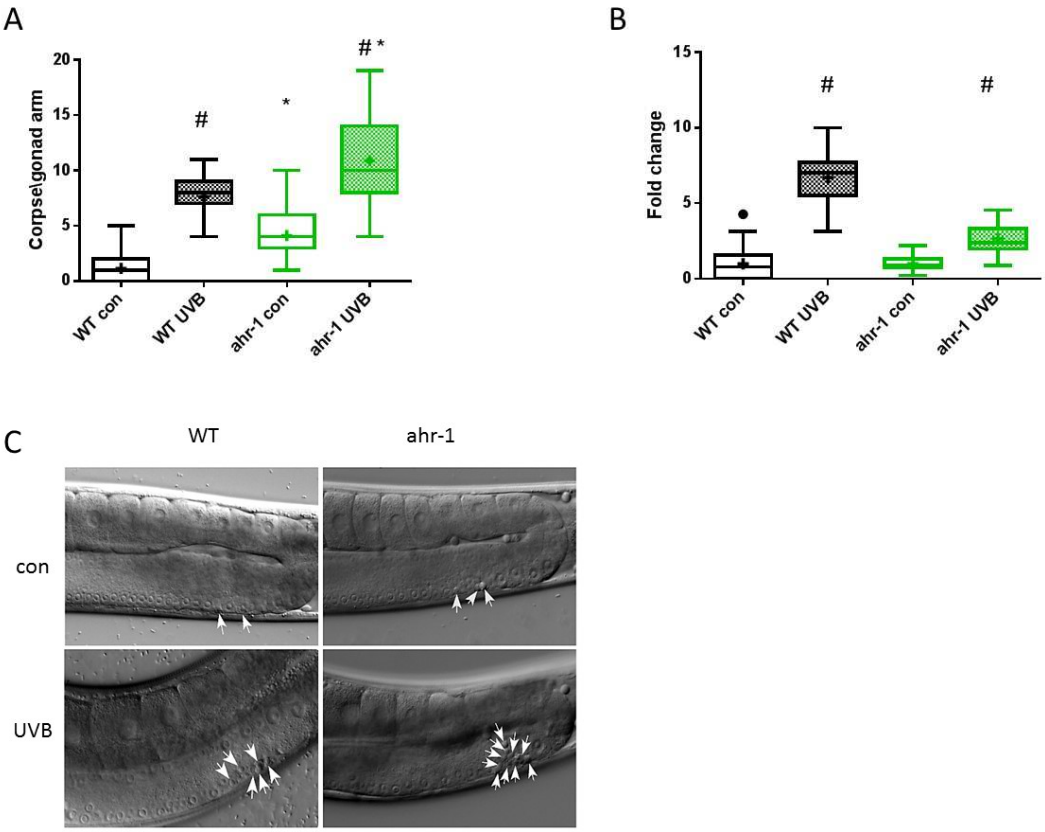

Figure 23 UVB irradiation and AHR-1 loss of function induce apoptosis. Number of apoptotic corpses per gonad arm (A) and fold change of apoptosic corpses in UVB treated worms in relation to control worms of the same strain (B). Worms were either irradiated with 600 J/m² UVB or left untreated as L4 larvae, and apoptotic corpses were counted in the meiotic compartment of the gonad 24 h after irradiation. Pooled data of 3 independent replicates are shown. No. of worms 38 - 39; * p-value < 0.05 *vs.* con, # p-value < 0.05 *vs.* WT, statistical test: One-way ANOVA with Sidak's multiple comparisons test. C) Representative pictures of germlines of control and UVB irradiated wild-type and *ahr-1(ju145)*. White arrowheads indicate apoptotic corpses.

Loss of AHR-1 function extends lifespan and healthspan on an *E. coli* HT115 diet

Preliminary data of my Master's thesis revealed that loss of AHR-1 extends lifespan in a food-dependent manner. More specifically, AHR-1 loss of function extends the lifespan, when *C. elegans* is cultured on plates containing *E. coli* HT115(L4440) on NGM supplemented with IPTG and antibiotics but not on *E. coli* OP50 on NGM alone. The antibiotics ampicillin and tetracycline are often used in combination with HT115(DE3) as a selection marker and to avoid bacterial contamination of the experiments. To investigate, whether the effect of *ahr-1* loss of function on lifespan is due to the supplementation of antibiotics, I compared the lifespan of wild-type and *ahr-1(ju145)* on an HT115(L4440) diet, either supplemented with or without antibiotics. I found that antibiotics did not have any effect on the lifespan in neither wild-type nor *ahr-1(ju145)*. In both conditions, *ahr-1(j145)* worms had a slightly longer lifespan than the wild-type (Figure 24A): the mean lifespan extension was 6 % on an HT115 diet containing antibiotics and 10 % on a diet without antibiotics. Coherent with the lifespan extension, *ahr-1(ju145)* animals showed a slower decline in movement, leading to an extension of 11 % in the mean healthspan on a diet containing antibiotics and 13 % on a diet without antibiotics (Figure

24B). I also assessed the pharyngeal pumping activity, and found that in both genetic backgrounds, wild-type, and *ahr-1(ju145)*, the pumping frequency declined during aging (Figure 24C, D). This decline was slightly slower in *ahr-1(ju145)* when supplemented with antibiotics. The effect was more pronounced in the absence of antibiotics and statistically significant for day 10: while old wild-type worms had a relative pumping frequency of 0.62, *ahr-1(ju145)* had a relative pumping frequency of 0.71. As the last parameter for healthy aging, I studied the heat shock resistance of wild-type and *ahr-1(ju145)* during aging. For this, I counted the survival to strong heat stress (35 °C). Interestingly, the resistance to heat stress was decreased in 7-days old wild-type compared to day 3 wild-type (Figure 24E). Very surprisingly, the heat stress resistance did not decrease but increase in 7-days old compared to 3-days old *ahr-1(ju145)*. While there was no difference between the heat stress resistance in 3-days old wild-type and *ahr-1(ju145)*, from day 7 onwards, *ahr-1(ju145)* animals were more resistant than wild-type. This difference was strongest visible at day 7 (Figure 24F). From these experiments, I concluded that the supplementation of antibiotics is not the cause of the differences in lifespan between wild-type and *ahr-1(ju145)* on *E. coli* HT115(L4440).

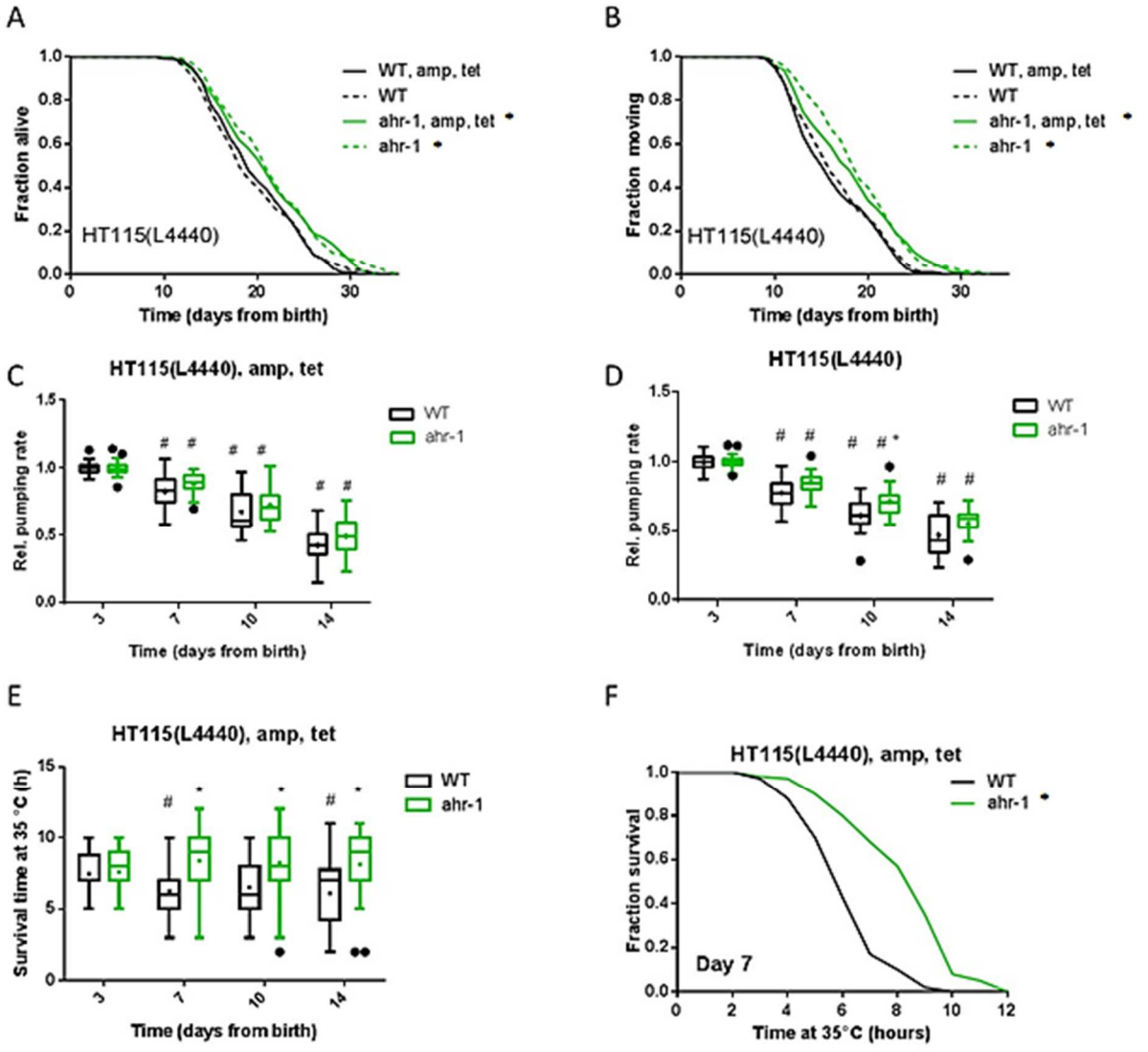

Figure 24 *ahr-1* loss of functions extends healthy aging independent of antibiotic supplementation. A – B) Kaplan Meier curves of wild-type and *ahr-1(ju145)* on HT115(L4440) either supplemented with antibiotics (amp, tet) or not. Pooled data of 3 independent experiments are shown. # p-value < 0.05 *vs.* WT, statistical test: Log-rank test. C – D) The pharyngeal pumping activity is declining slower in *ahr-1(ju145).* The relative pharyngeal pumping on HT115(L4440) supplemented with antibiotics (C) or without antibiotics (D) is shown for 11 – 30 worms in 3 independent experiments, * p-value <0.05 *vs.* WT, # p-value <0.05 *vs.* day 3. Statistical test: Two-way ANOVA with Sidak's multiple comparisons test. E – F) Aged *ahr-1(ju145)* worms are more resistant to heat stress than aged wild-type worms. E) Survival times of wild-type and *ahr-1(ju145)* to heat stress (35 °C). Pooled data of 60 worms in 3 independent experiments are shown, * p-value < 0.05 *vs.* WT, # p-value < 0.05 *vs.* day, statistical test: Two-way ANOVA with Sidak's multiple comparisons test. F) Kaplan-Meier survival curve of 7-days old wild-type and *ahr-1(ju145)* at 35°C. Pooled data of 3 independent experiments are shown. * p-value < 0.05 *vs.* WT, statistical test: Log-rank test. Detailed information in Table S 3.

Loss of AHR-1 function affects lifespan and healthspan in a diet-dependent manner

Previous experiments revealed that the lifespan extension of *ahr-1(ju145)* is increased compared to wild-type on an HT115(L4440) diet independently of the supplementation of antibiotics. Therefore, the mentioned differences in the lifespan extension of *ahr-1(ju145)* on an OP50 diet are most likely associated with the different bacteria. During my studies, an RNAi compatible OP50 strain with similar features as HT115(DE3) was created [122]. I thus used this RNAi compatible strain, OP50(xu363), to better compare the effects of different *E. coli* diets on the lifespan of wild-type and *ahr-1(ju145)* worms. In an initial step, I transformed OP50(xu363) with the empty vector L4440 and named the corresponding strain OP50(L4440) (Figure S 2). I then performed life- and healthspan analysis of wild-type and *ahr-1(ju145)* on HT115(L4440) and OP50(L4440), which I will refer to as HT115 and OP50 for brevity. While the wild-type had a similar lifespan and healthspan feeding on HT115 or OP50, *ahr-1(ju145)* lived longer on HT115 than on OP50 (Figure 25A). Similar to previous experiments, on HT115, AHR-1 loss of function worms showed a 14 % increase in the mean lifespan compared to wild-type, while there was no difference between wild-type and *ahr-1(ju145)* on OP50. Similar results could be observed in the healthspan, which was increased by 20 % in *ahr-1(ju145)* compared to wild-type on an HT115 diet only (Figure 25B). Given that the improved healthspan of *ahr-1* mutants is diet-dependent, I decided to investigate the role of bacterial diet in mediating other age-dependent features such as the decline of neuromuscular functions. To this extent, I assessed the ability of *C. elegans* to sense food and move towards it at different ages. In a food race assay, I compared the ability of wild-type and *ahr-1(ju145)* to reach the corresponding food source. Most of the young (day 3) animals reached the food source regardless of the genotype or the diet. After 1 h between 64 and 82 % of the worms reached the food source (Figure 25C), while it were between 89 and 97 % after 2 h (Figure 25D). The ability to reach the food significantly declined on day 7 in wild-type and *ahr-1(ju145)* feeding on HT115 but not on OP50, suggesting that the diet influences the neuro-muscular functions. Comparing the different conditions at day 7, neither loss of *ahr-1* function nor the food source had a robust effect on the food attraction.

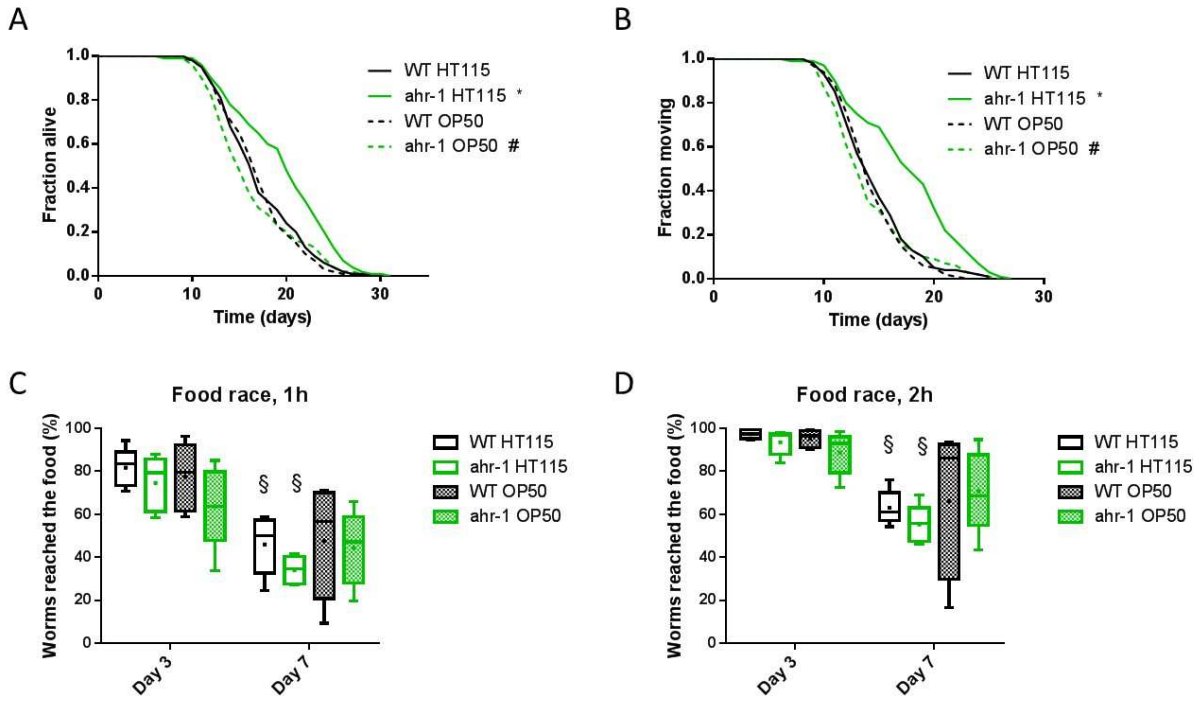

Figure 25 *ahr-1* loss of functions extends healthy aging in a diet-dependent manner. A - B) Kaplan Meier curves of wild-type and *ahr-1(ju145)* feeding on HT115 compared to OP50. Pooled data of 3 independent experiments are shown. * p-value < 0.05 *vs.* WT, # p-value < 0.05 *vs.* HT115, statistical test: Log-rank test. Detailed information in Table S4. C – D) Decline of neuro-muscular function during aging in wild-type and *ahr-1(ju145)* feeding on HT115 or OP50 in a food attraction assay. Pooled data of 5 independent experiments are shown. § p-value < 0.05 *vs.* day 3; Statistical test: Two-way ANOVA with Tukey's multiple comparisons test.

An increased lifespan is often accompanied by an increase in heat stress resistance [70]. Thus, I investigated the heat stress resistance of HT115 and OP50 fed wild-type and *ahr-1(ju145)*. In line with previous experiments, there was no difference between the heat stress resistance of young (day 3) wild-type and *ahr-1(ju145)* on HT115 and OP50 (Figure 26A, B). Middle-aged (day 7) and aged (day 14) *ahr-1(ju145)* instead were more resistant to heat stress than wild-type on HT115, but, interestingly, more sensitive on OP50 (Figure 26A, C, D). The increase in heat stress resistance was 36 and 30 % for *ahr-1(ju145)* on HT115 at day 7 and day 14 respectively. On an OP50 diet, the heat stress resistance was reduced by 20 and 15 % in 7- and 14-days old *ahr-1(ju145)* respectively. Surprisingly, although lifespan and healthspan were not affected by the different diets in the wild-type, middle-aged wild-type showed a 40 % greater heat resistance on OP50 than on HT115 (Figure 26C). On day 14, instead, an OP50 did not have any beneficial effect on heat stress survival anymore.

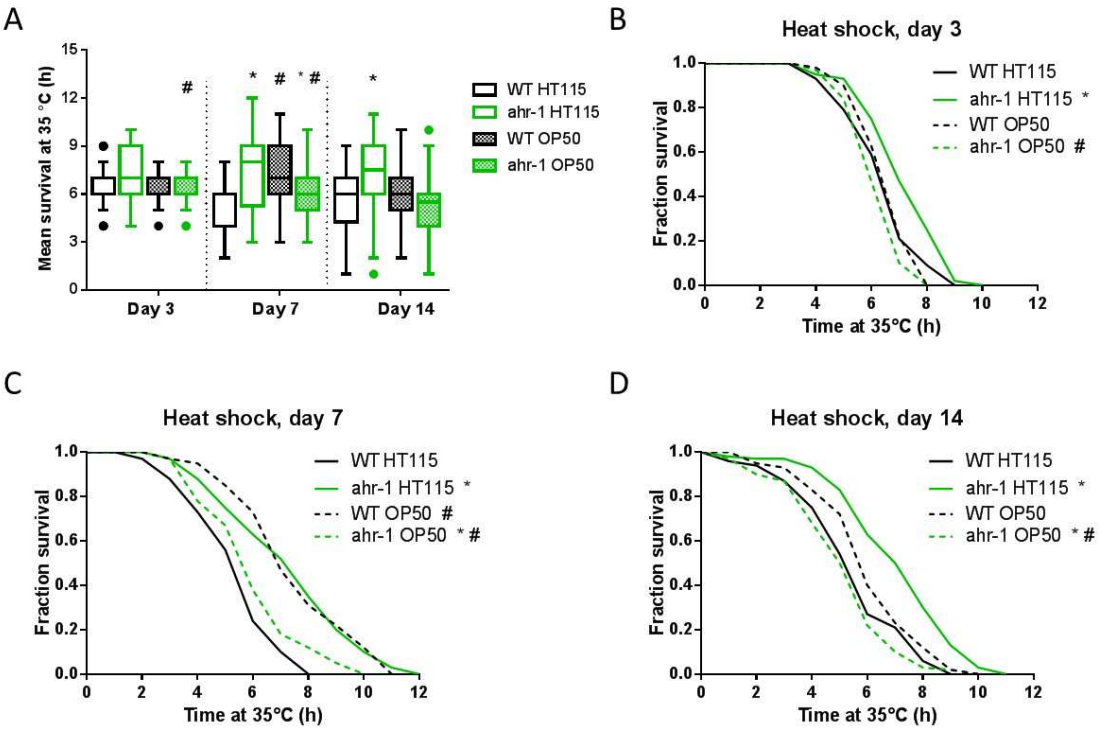

Figure 26 Loss of *ahr*-1 increases heat stress resistance in middle-aged and aged worms. A) Survival upon heat stress of wild-type and *ahr-1(ju145)* feeding on HT115 compared to OP50. Pooled data of 3 independent experiments are shown. No. of worms: 52 – 60. * p-value < 0.05 *vs.* WT, # p-value < 0.05 *vs.* HT115, statistical test: Sidak's multiple comparisons test. B - D) Kaplan-Meier survival curves of wild-type and *ahr-1(ju145)* on HT115 or OP50 at 35°C. Pooled data of 3 independent experiments are shown. * p-value < 0.05 *vs.* WT, # p-value < 0.05 *vs.* HT115, statistical test: Log-rank test. Mean survival times and statistical analysis are shown in Table S 4.

A complex neuromuscular behavior, which declines during aging is pharyngeal pumping. Previously, I have noticed an increased relative pharyngeal pumping rate of *ahr-1(ju145)* on HT115. During my studies, the company NemaMetrix developed an automatic screening device, which can characterize different parameters of pharyngeal pumping. I used this technique, to study various aspects of pharynx activity during aging. To stimulate pharyngeal pumping, I treated the worms with the neurotransmitter serotonin, which induces pharyngeal pumping in *C. elegans* [214]. I quantified the pumping frequency, amplitude, duration, and the inter-pump interval. In young wild-type, but not AHR-1 loss of function worms, the diet influenced the pumping frequency, and they exhibited a higher frequency on an OP50 diet (Figure 27A). During aging, the pumping frequency significantly decreased in all conditions. With the exception for *ahr-1(ju145)* feeding on HT115, the decline was already observable at day 7. On day 7, *ahr-1(ju145)* had a significantly higher pumping frequency than wild-type on an HT115 diet. At 10-days of age, a decline of pumping frequency was also observable in *ahr-1(j145)* on HT115. Nevertheless, on HT115 *ahr-1(ju145)* had still an increased pumping frequency compared to wild-type, while there were no differences between the diets. Besides the frequency, aging affected the amplitude of the pumps. Comparing 3-days old worms to 7-days old worms, the amplitude of the pumps significantly increased in all conditions (Figure 27B) independently of the diet and AHR-1 function. Aging also marginally affected the pump duration (Figure 27C), but not the inter-pump interval (Figure 27D). The analysis of the EPG

shapes did not reveal any striking differences between the strains, suggesting that there are no significant defects in neurons regulating pumping (Figure S 4).

All in all, the data from the pharyngeal pumping suggest that loss of AHR-1 function has a beneficial effect on the pumping frequency of aging worms, while not affecting other parameters of pharyngeal pumping.

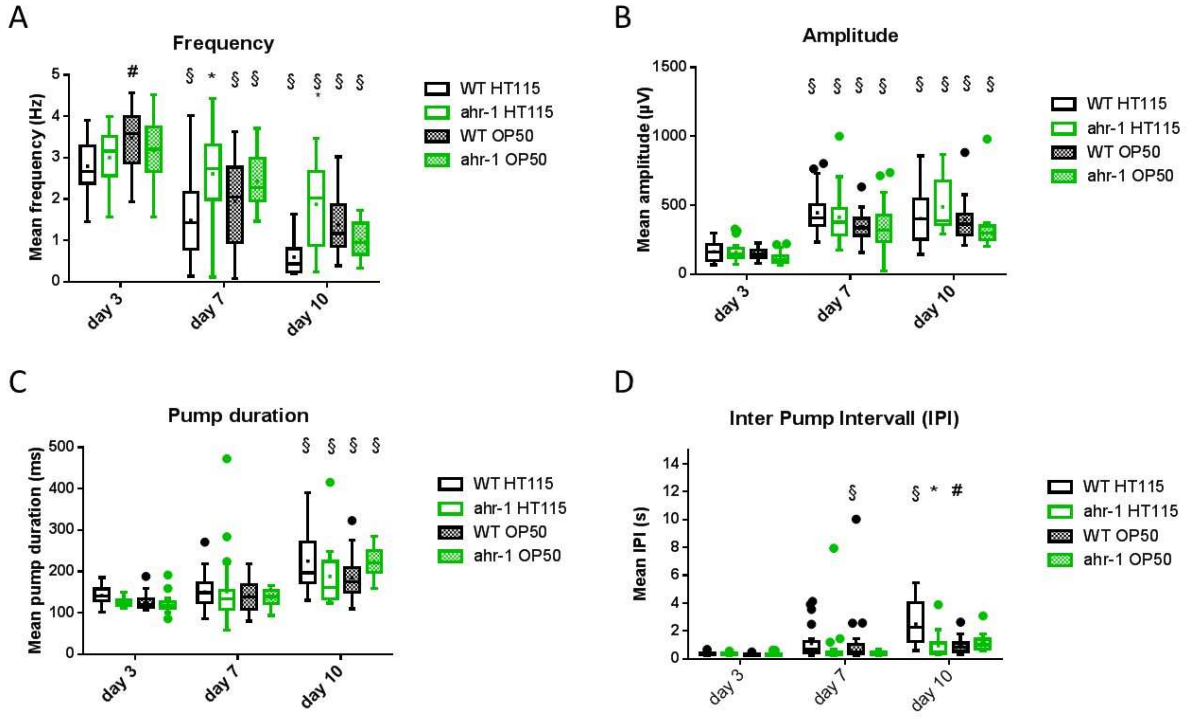

Figure 27 Decline of pharyngeal pumping activity during aging in wild-type and *ahr-1(ju145)* feeding on HT115 or OP50. A – D) Quantification of different pharyngeal pumping parameters during aging. Pooled data of 10 – 36 worms in 3 independent experiments are shown. * p-value < 0.05 *vs.* WT, # p-value < 0.05 *vs.* HT115, § p-value < 0.05 *vs.* day 3, statistical test: Two-way ANOVA with Tukey's multiple comparisons test.

Changes in the pharyngeal pumping activity influence the food intake and might influence the accumulation of fat. Moreover, different food sources often lead to differences in the fat storage of the animals [118]. Therefore, I tested whether feeding on HT115 and OP50 might alter the accumulation of lipid droplets in wild-type and *ahr-1(ju145)*. *In vivo* Nile Red staining showed an increased accumulation of lipid droplets in middle-aged animals (day 7) compared to young animals (day 3) in all conditions (Figure 28A). From day 7 to day 10, the intensity of Nile Red staining was decreased (Figure 28A). The comparison of wild-type and *ahr-1(ju145)* revealed a slight but significant increased accumulation of lipid droplets in young (3-days old) *ahr-1(ju145)* compared to wild-type (Figure 28B) on both bacterial food sources, but the differences disappeared during aging (Figure 28C – D). On the contrary, there was no difference in lipid droplet levels between 3-days old animals of the same strain on different food sources, but aged animals showed significantly reduced accumulation of lipid droplets on OP50 compared to HT115. The minor changes in lipid droplet accumulation between wild-type and *ahr-1(ju145)*

indicate that changes in the lipid accumulation might not be the driving force of the differences in lifespan.

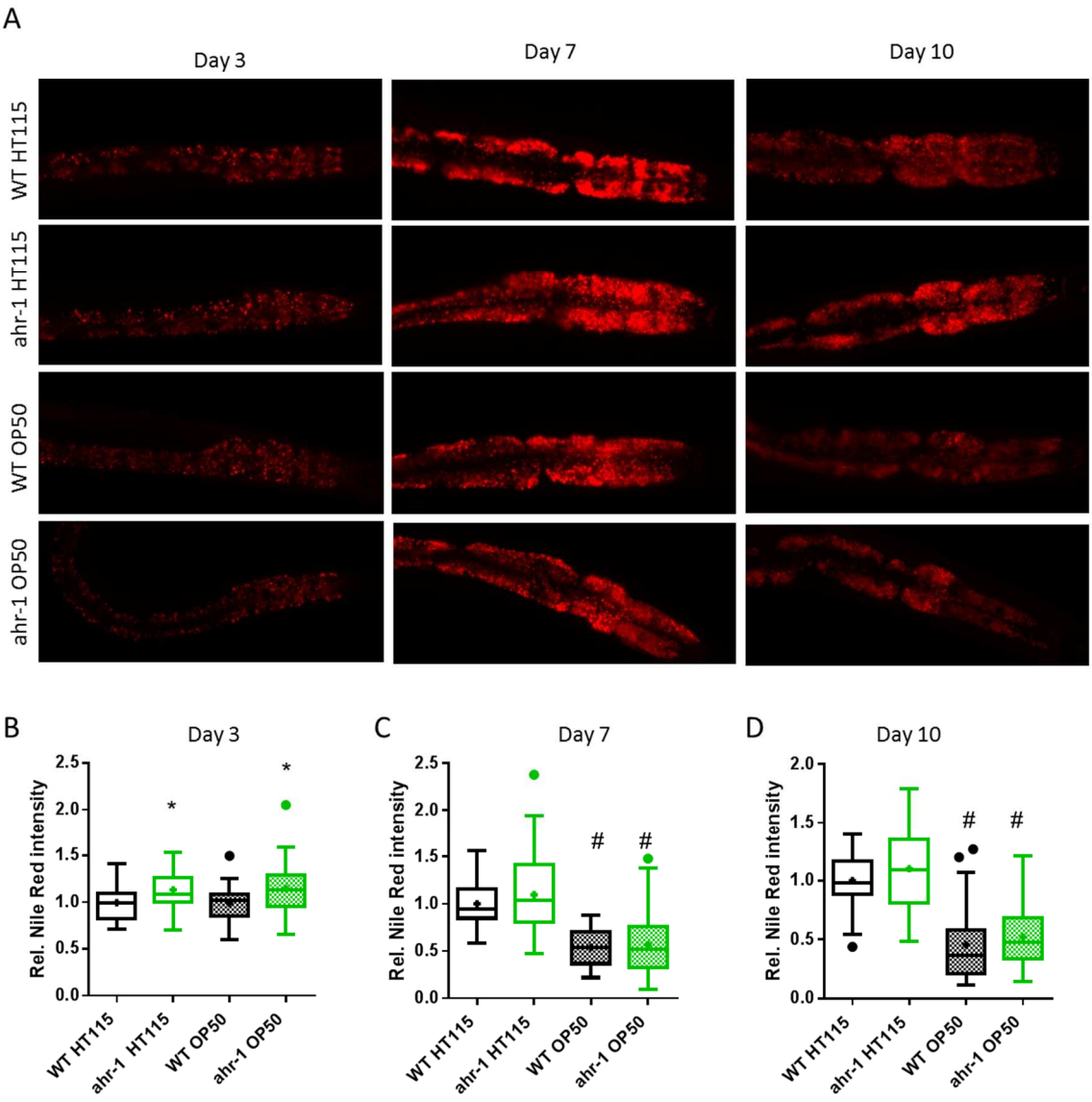

Figure 28 Nile Red *in vivo* staining of wild-type and *ahr-1(ju145)*. A) Representative pictures of the intestines of wild-type and *ahr-1(ju145)* grown on OP50 or HT115 after Nile Red staining. Worms are orientated with the anterior on the right. B – D) Relative Nile Red intensity in relation to the mean intensity of WT HT115. The Nile Red intensity was measured in a circular area at the anterior part of the intestine. Pooled data of 36 – 42 worm in 2 independent experiments are shown. * p-value < 0.05 *vs.* WT, # p-value < 0.05 *vs.* HT115, statistical test: One-way ANOVA with Tukey's multiple comparisons test,

After seeing that loss of *ahr-1* and curcumin affect the aggregation of polyQ$_{40}$ in previous experiments, I wanted to understand the influence of bacterial diet on polyQ$_{40}$ aggregation. I quantified the polyQ$_{40}$ aggregates in animals of different ages feeding on different *E. coli* diets. In young animals (day 4), the number of aggregates was similar in both strains and on both diets (Figure 29B). Also, the aggregate size was identical in polyQ;wt on both diets, while polyQ;ahr-1 had larger aggregates than polyQ;wt on HT115 (Figure 29E). In middle-aged worms (day 7) differences in the aggregation number and size appeared: on an OP50 diet

polyQ;ahr-1 had a higher amount (19 %) of aggregates than polyQ;wt (Figure 29C) and on both diets, the size of the aggregates was bigger in polyQ;ahr-1 than in polyQ;wt (Figure 29F). The most substantial diet- and genotype-dependent differences in polyQ were observed in aged animals. At day 10 of age, polyQ;wt showed a 38 % increased aggregation on an OP50 diet compared to an HT115 diet (Figure 29A - B). On both bacterial foods, the accumulation of polyQ was higher in polyQ;ahr-1 (Figure 29A, D). The increase was 66 % on HT115 and 31 % on OP50. Similar to the number of aggregates, also the size of the aggregates was affected by the diet and loss of AHR-1 function. PolyQ;wt had bigger aggregates on OP50 than on HT115, while the opposite was true for polyQ;ahr-1 (Figure 29A, G). On both diets, the aggregates were bigger in polyQ;ahr-1 than in polyQ;wt. In conclusion, loss of AHR-1 function leads to an age-dependent increase in polyQ number and size, which, consistent with previous findings, is partially suppressed by the OP50 diet. Besides AHR-1 loss of function, the bacterial diet influences the number and the size of the aggregates.

The aggregation of polyQ impairs the movement and shortens the lifespan of worms [63, 215]. I, therefore, checked life- and healthspan of $polyQ_{40}$ worms. A comparison of the life-/healthspans of polyQ;wt and polyQ;ahr-1 with wild-type and *ahr-1(ju145)* respectively showed that the lifespan of polyQ;wt was slightly shortened compared to wild-type on both bacterial food sources (Figure S 3A), while there was no polyQ-mediated shortening of the lifespan in *ahr-1* loss of function worms (Figure S 3B). Whereas the lifespan was only marginally affected by the $polyQ_{40}$ expression, the effects on healthspan were stronger (Figure S 3C, D), and the healthspan was also reduced in polyQ;ahr-1 compared to *ahr-1(ju145)*. Interestingly, although the loss of AHR-1 function led to a greater amount of $polyQ_{40}$ aggregates in the neurodegenerative disease models, the lifespan of these worms was strongly increased by loss of AHR-1 function. On an HT115 diet, polyQ;ahr-1 had an increase in lifespan of 27 % (Figure 29H). This is a much greater lifespan extension than *ahr-1(ju145)* compared to wild-type (N2). Surprisingly, loss of AHR-1 function increased the lifespan of $polyQ_{40}$ expressing worms also on an OP50 diet, although to a lesser extent than on HT115. Similar to wild-type (N2), the lifespan of polyQ;wt was not affected by the different *E. coli* diets, while polyQ;ahr-1 lived significantly shorter on an OP50 diet than on HT115. The healthspan was influenced similarly: polyQ;ahr-1 had an increased healthspan on both diets and diet did not influence the healthspan of polyQ;wt (Figure 29I).

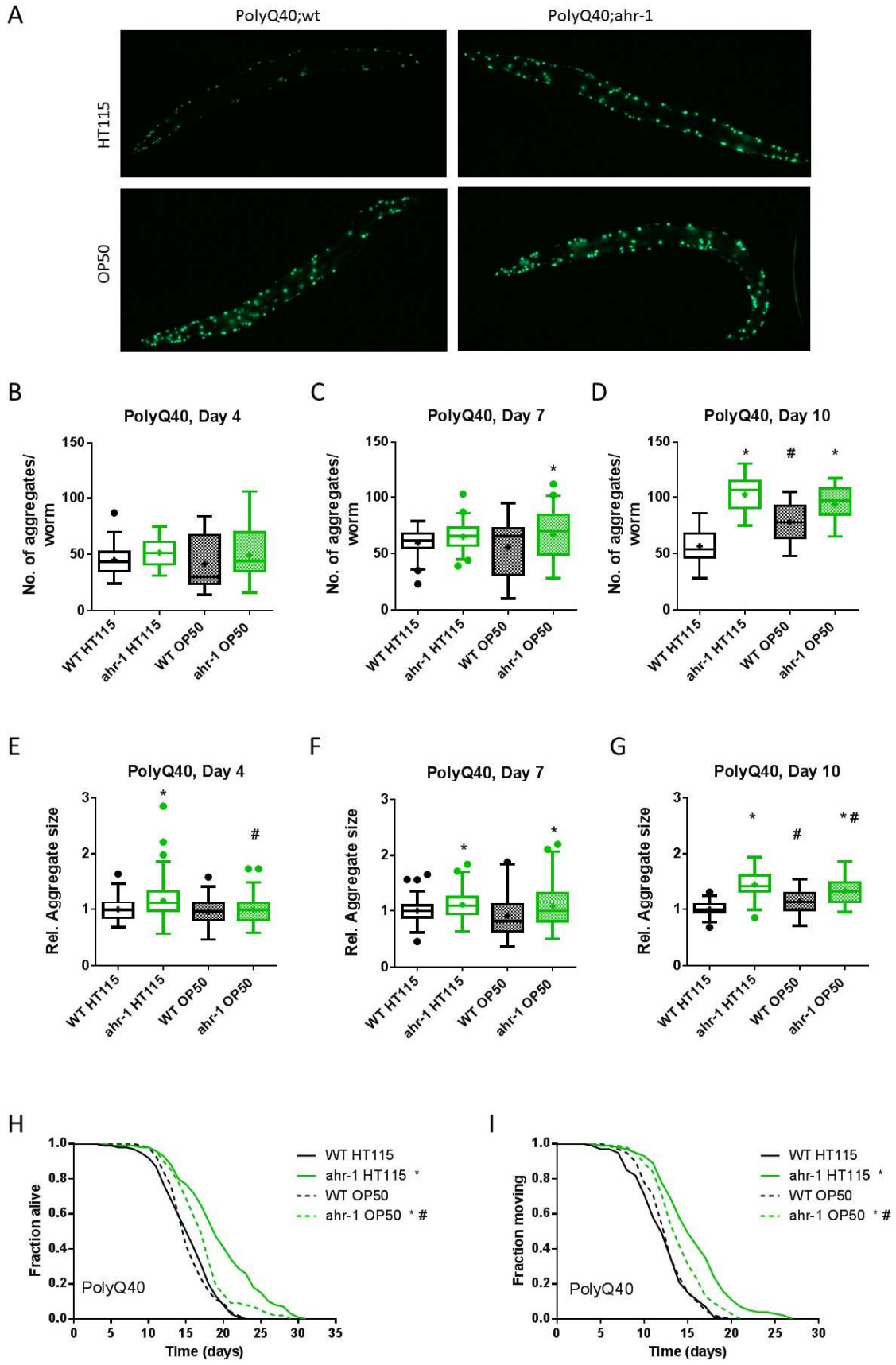

Figure 29 AHR-1 loss of function worms accumulate more polyQ$_{40}$ but live longer. A) Representative fluorescence images of 10-days old polyQ;wt and polyQ;ahr-1 on HT115 and OP50. B – G) Quantification of aggregates in polyQ;wt and polyQ;ahr-1 at different ages in 3 independent replicates. Statistical test: One-way ANOVA with Tukey's multiple comparisons test, * p-value < 0.05 *vs.* polyQ;wt, # p-value < 0.05 *vs.* HT115. No. of worms 26 - 64.

H – I) Kaplan Meier curves of polyQ;wt and polyQ;ahr-1 in 3 independent experiments. * p-value < 0.05 *vs.* WT, # p-value < 0.05 *vs.* HT115, statistical test: Log-rank test. Detailed information in Table S 5.

Loss of AHR-1 function influences lifespan and healthspan in a temperature-dependent manner

Life- and healthspan of worms are temperature-dependent, often in a genotype-dependent manner [216], and higher temperatures accelerate aggregation in the polyQ strain [217]. Therefore, to understand whether the healthy aging phenotype of *ahr-1(ju145)* is also temperature dependent, I performed life- and healthspan analysis at 25 °C. Surprisingly, compared to wild-type, *ahr-1(ju145)* feeding on HT115 showed a substantial reduction in life- and healthspan at 25 °C (Figure 30A, B). Lifespan and healthspan were reduced by 13 and 10 % respectively. On an OP50 diet instead, only the healthspan but not the lifespan of *ahr-1(ju145)* was reduced compared to wild-type. Compared to HT115 feeding, an OP50 diet significantly reduced the lifespan of both, wild-type and *ahr-1(ju145)* by 19 and 12 % respectively. Also, the healthspan was decreased by 17 % in wild-type and 16 % in *ahr-1(ju145)* on an OP50 diet. In worms expressing $polyQ_{40}$::YFP instead, there were only minor differences in lifespan and healthspan between worms feeding on HT115 and OP50 as well as between worms with a wild-type *ahr-1* allele and the *ju145* allele (Figure 30C, D). Most strikingly, although *ahr-1(ju45)* was short-lived compared to wild-type at 25 °C on an HT115 diet, polyQ;ahr-1 worms were slightly long-lived compared to polyQ;wt. This extension in mean lifespan was 9 % and therefore much smaller than the lifespan extension at 20 °C. Also, the differences in polyQ aggregation were less pronounced at 25 °C, although 10-days old polyQ;ahr-1 still had a slightly higher number of aggregates compared to polyQ;wt on both bacterial diets (Figure 30E, F). This data is consistent with the higher number of aggregates observed in polyQ;ahr-1 at 20 °C. Overall, it seems that the higher temperature suppresses the beneficial diet-dependent effects of loss of *ahr-1* on life- and healthspan (in both wild-type and polyQ strain).

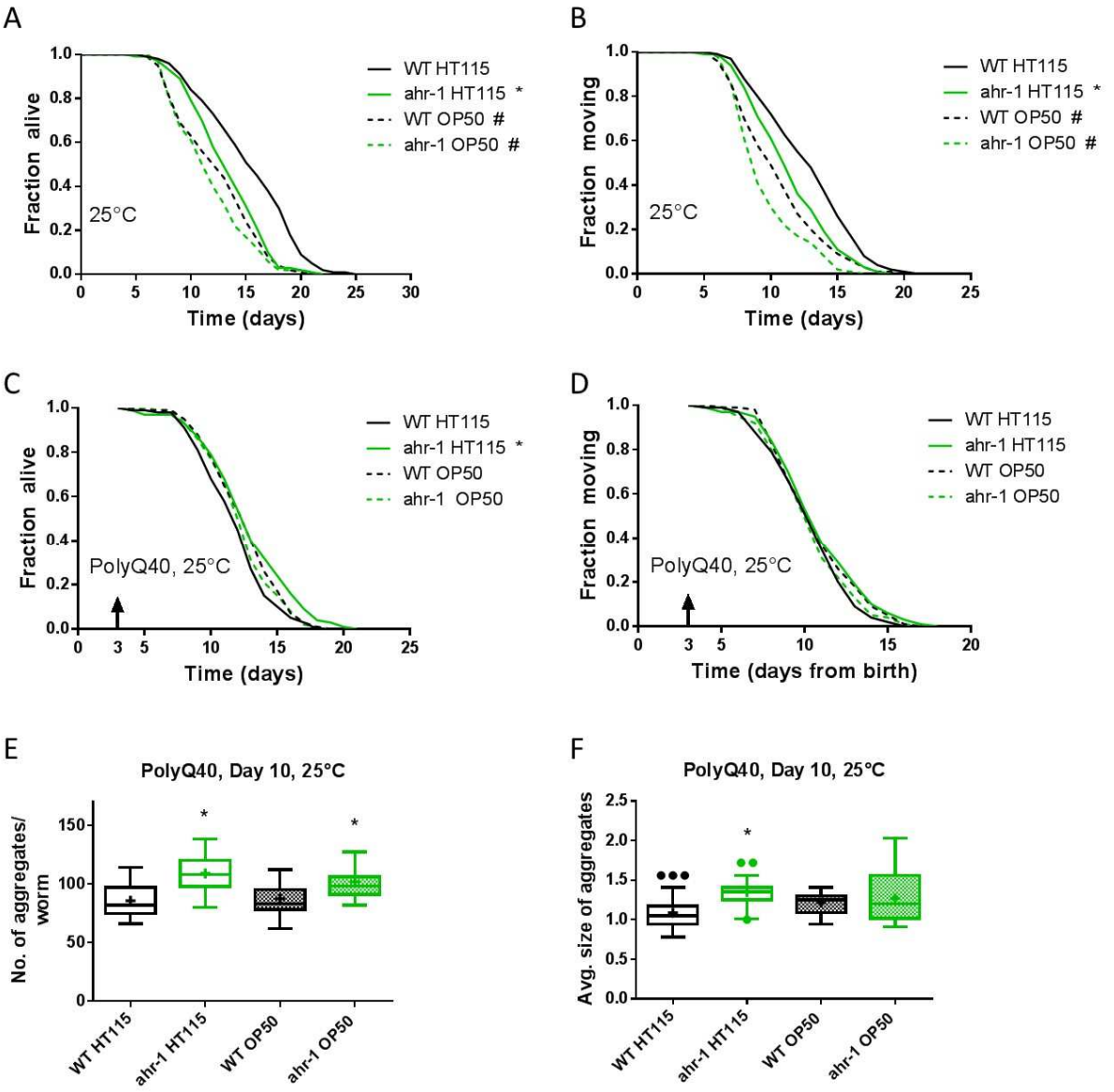

Figure 30 At 25 °C, *ahr-1(ju145)* is short-lived compared to wild-type and loses its protection against the toxicity of polyQ$_{40}$ aggregates. A – B) Kaplan Meier curves of wild-type and *ahr-1(ju145)* grown at 25 °C. Pooled data of 3 independent replicates are shown. * p-value < 0.05 *vs.* WT, # p-value < 0.05 *vs.* HT115, statistical test: Log-rank test. C – D) Kaplan Meier curves of polyQ;wt and polyQ;ahr-1. Worms were grown at 25 °C from day 3 (indicated by arrowhead). Pooled data of 3 independent replicates are shown. * p-value < 0.05 *vs.* WT, # p-value < 0.05 *vs.* HT115, statistical test: Log-rank test. Mean survival times and statistical analysis of panels A – D are shown in Table S 6. E – F) Quantification of aggregates in 10-days old polyQ;wt and polyQ;ahr-1 grown at 25 °C from day 3. Pooled data of 2 independent replicates are shown. No of worms: 19 - 21, * p-value < 0.05 *vs.* WT, statistical test: One-way ANOVA with Tukey's multiple comparisons test.

Loss of AHR-1 function does not affect lifespan, healthspan, and heat stress resistance on killed bacteria

To understand why aging is differentially affected by the bacterial diet in the *ahr-1* mutant, I tested whether the nutritional value of the bacteria or bacterial metabolites might be responsible for the differences in lifespan. The main known difference in the nutritional composition of the different *E. coli* diets is that HT115 has a higher carbohydrate content than OP50 [118]. This or other unknown differences in the composition of the bacteria might affect

aging and stress resistance of *C. elegans*. If the nutritional value of the bacteria is responsible for the difference, it should be not changed by killing the bacteria. To test this hypothesis, I used bacteria which had been killed by UVB irradiation and dissolved in fresh medium prior to seeding them to the NGM plates to remove as many metabolites as possible. I decided to use heat stress resistance of 7-days old worms as a screening parameter since it was the parameter with the most potent effect. Killing the bacteria before seeding abolished the differences between wild-type and *ahr-1(ju145)* on both diets (Figure 31A): *ahr-1(ju145)* was no longer long-lived on HT115 and no longer short-lived on OP50. Interestingly, the difference in heat shock resistance between the bacterial diet persisted and wild-type and *ahr-1(ju145)* survived for a longer time when feeding on OP50 than on HT115. This experiment indicates that it is not the nutritional components of the different *E. coli* strains but instead possible produced metabolites, which have AhR-mediated effects on stress resistance and potentially on lifespan. If this was true, the difference in stress resistance observed on living bacteria should be persistent when the bacteria are killed after they had grown on the NGM for 2 days. Indeed, when grown on bacteria which had been killed on the NGM plate after a period of 2 days, *ahr-1(ju145*) had a higher heat stress resistance than wild-type on HT115 (Figure 31B). On killed OP50 instead, *ahr-1(ju145)* and wild-type did not show any difference in heat stress survival. To further investigate whether the potential metabolites of the bacteria are sufficient to cause *ahr-1*-dependent differences in heat stress resistance, I used dead bacteria in combination with the LB-medium in which either the same bacterial strain or the other one had grown. In these switched media experiments, I found that wild-type and *ahr-1(ju145)* had equal heat stress resistances in any of the bacteria/media combinations. Also, the differences between the survival times on killed HT115 and OP50 were not affected by the media. Worms remained long-lived on OP50 supplemented with HT115 media compared to HT115 augmented with HT115 media (Figure 31C) and on OP50 supplemented with OP50 media compared to HT115 with OP50 media (Figure 31D). This indicates that, if bacterial metabolites cause the differences between wild-type and *ahr-1(ju145),* these metabolites are likely produced on the NGM plates rather than in the LB-medium.

In mammals, bacterial metabolites of tryptophan like indole, tryptamine and indole-3-acetate act as AhR ligands [161]. Also, in *C. elegans* a study indicates that tryptophan metabolites might cause an essential difference between *E. coli* strains HT115 and OP50 [128]. Specifically, a loss of *nhr-114* strain is sterile on OP50, but not on HT115 and that this sterility can be restored by addition of tryptophan [128]. I, therefore, investigated whether supplementation of tryptophan abolished the differences between wild-type and *ahr-1(ju145)* and between HT115 and OP50. When using living bacteria and supplementing the bacterial lawn with either 1.25 or 2.5 mg of L-tryptophan, wild-type, and *ahr-1(ju145)* had a similar heat stress resistance on HT115 (Figure 31E - F). On OP50 instead, *ahr-1(ju145)* was still short-

lived compared to wild-type. But surprisingly both strains had significantly shorter survival times on OP50 compared to HT115, when supplemented with tryptophan. This is in so far surprising that wild-type worms had a higher heat stress resistance on living OP50 without tryptophan (Figure 31E). Under tryptophan supplementation, the survival times were shortened by 21 and 34 % respectively in wild-type and *ahr-1(ju145),* when using 1.25 mg of tryptophan and 26 and 41 %, when using 2.5 mg of tryptophan.

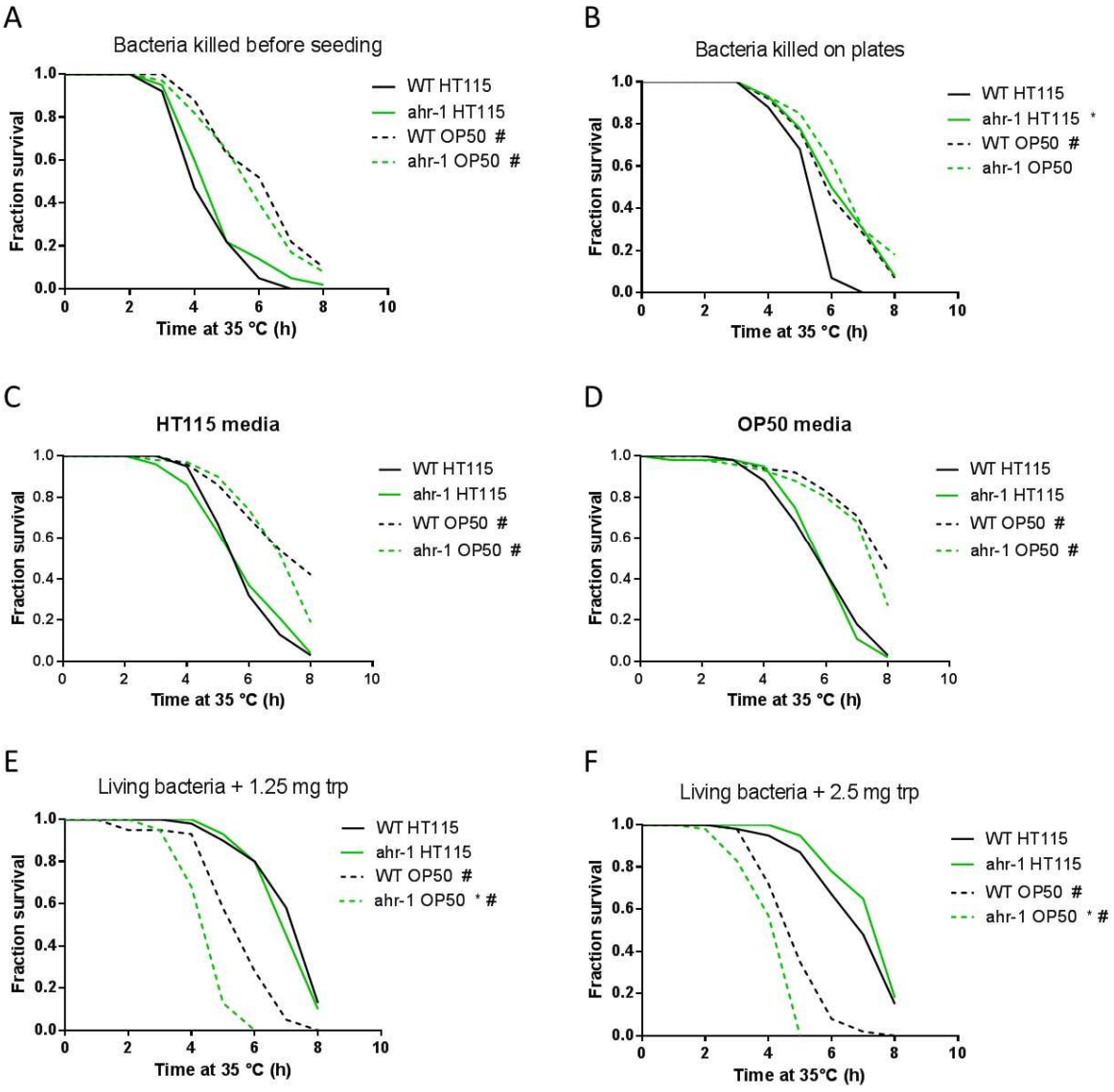

Figure 31 Survival upon heat stress in 7-days old wild-type and *ahr-1(ju145)* feeding on either HT115 or OP50. A) Kaplan Meier survival curves on bacteria killed before seeding to the NGM. B) Kaplan Meier survival curves on bacteria which had grown on the NGM for 2 days before being killed. C) Survival on killed bacteria, which had been supplemented with the LB-medium, in which HT115 had grown. D) Survival on killed bacteria, which had been supplemented with the LB-medium, in which OP50 had grown. E - F) Survival curves on living bacteria supplemented with 1.25 mg (E) or 2.5 mg (F) of L-tryptophan. In all the panels pooled data of 2 – 3 independent experiments are shown. * p-value < 0.05 *vs.* WT, # p-value < 0.05 *vs.* HT115, statistical test: Log-rank test. Detailed information in Table S 7.

The experiments on the heat stress survival revealed that killing the bacteria by UVB irradiation before seeding them to the NGM was the only method to abolish the differences between wild-

type and *ahr-1(ju145)* on both diets. I, therefore, checked whether killing the bacteria also eliminates the difference between the lifespans of wild-type and *ahr-1(ju145).* Indeed, on both diets, wild-type, and *ahr-1(ju145)* had similar life- and healthspans (Figure 32). Like in the heat stress resistance, killing the bacteria resulted in a significantly extended lifespan on OP50 compared to HT115. The increase in lifespan was 35 and 30 % in wild-type and *ahr-1(ju145)* respectively. The data described so far are indicating that bacterial metabolites might cause differences in the lifespans of wild-type and *ahr-1(ju145)*.

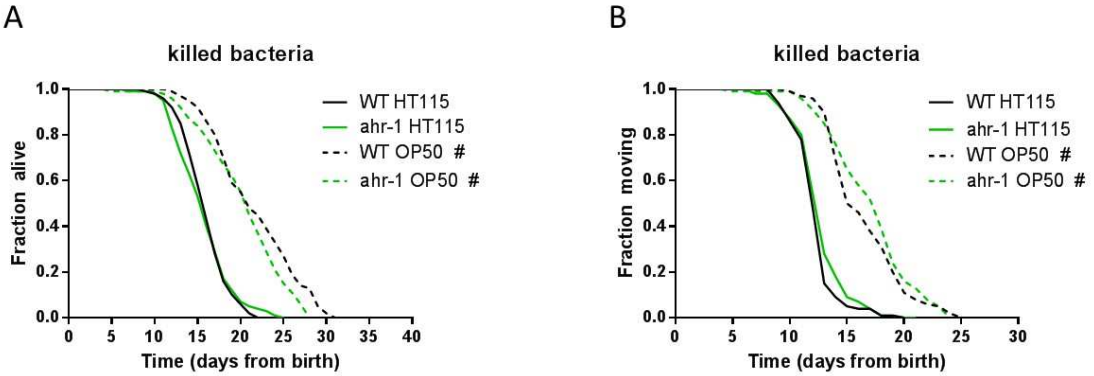

Figure 32 On killed bacteria, wild-type and *ahr-1(ju145)* have similar lifespans. A – B) Kaplan Meier curves of WT and *ahr-1* grown on HT115 and OP50 which had been killed prior to seeding. Pooled data of 2 independent expeiments are shown. * p-value < 0.05 *vs.* WT, # p-value < 0.05 *vs.* HT115, statistical test: Log-rank test. Detailed information in Table S 8.

Mass spectrometry analysis reveals that HT115 might produce higher levels of tryptophan and indole-containing compounds

In the next step, I wanted to identify metabolites produced by the bacteria to understand, which potential metabolites might be responsible for the differences between the lifespan of wild-type and *ahr-1(ju145)* observed on living bacteria. For this, I grew HT115 and OP50 for 2 days in liquid NGM. After removal of the bacteria, I analyzed the medium by mass spectrometry. The spectra of 3 replicates were highly reproducible (Figure S 5). The samples were analyzed in the positive and negative mode to identify positively and negatively charged metabolites. In the positive mode, one major peak was found in NGM of both HT115 and OP50, but not in control NGM (Figure 33A), while a smaller peak was only found in the NGM, in which OP50 was grown. This unique peak for OP50 had the retention time of 11.5 min (Figure 33A). A closer analysis of this peak showed that it was mainly composed of products with a mass to charge ratio (m/z) of 611 and 553. While there was an intensity of $2.5*10^5$ of m/z 611 in the OP50 sample, the HT115 sample had only an intensity of $2.5*10^4$. For m/z 553, the intensities of HT115 and OP50 were similar ($2.5*10^4$ and $2.0*10^4$). Therefore, the main difference in this peak is probably caused by m/z 611. Further degradation of m/z 611 showed that it is composed of m/z 317.1029. The analysis of m/z 317 revealed that the identified molecule might have one of the following formulas $C_{17}H_{16}O_6$ or $C_{18}H_{12}N_4O_2$. The compounds associated

with these formulas are listed in Table 2. There was no evidence that bacteria produce any of these compounds. Also, on the *E. coli* Metabolome Database (http://ecmdb.ca), there were no metabolites with the suggested formulas [218, 219]. In the negative mode, both bacteria samples showed a peak with a retention time of approx. 8 min, which was not visible in the control (Figure 33B, arrowheads). Additionally, the OP50 sample showed a peak at approx. 9.5 min (Figure 33B). The same peak was also observable in the HT115 sample, but with a much smaller amplitude.

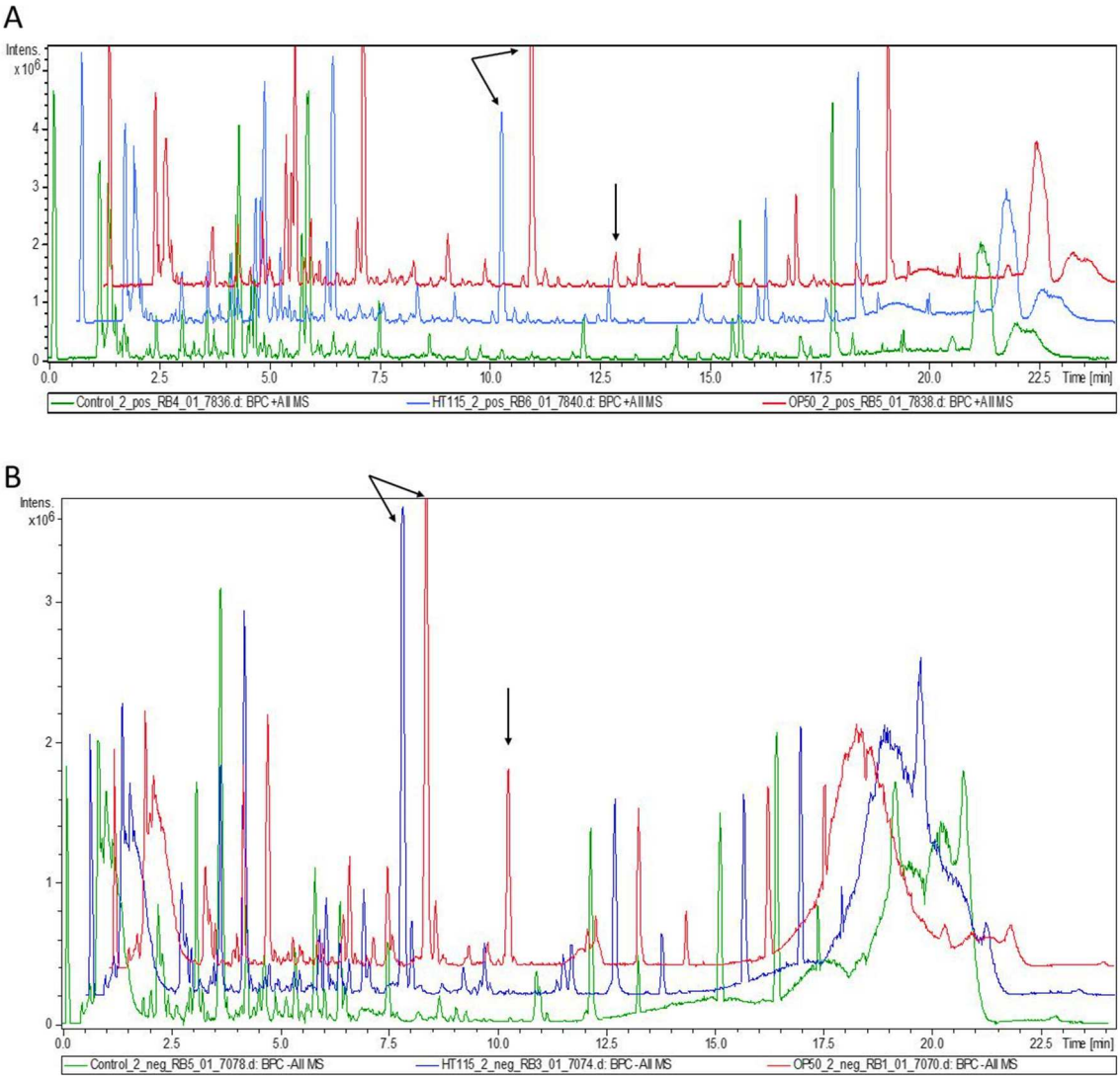

Figure 33 Representative base peak chromatograms (BPC) of NGM control (green), NGM in which HT115 had grown (blue) and NGM in which OP50 had grown (red). The arrows point out peaks, which were found only in the spectra of the NGM, in which bacteria were grown. (A) Positive BPC, (B) Negative BPC.

Table 2 Analysis of the peak unique for OP50 in the positive mode at a retention time of 11.5 min (indicated by a vertical arrowhead in Figure 33A).

Retention time	**m/z**	**Formula**	**Compound name (according to http://www.chemspider.com)**
11.5 min	317	$C_{17}H_{16}O_6$	3,3'-Methylenebis(6-hydroxy-5-methylbenzoic acid) Ethyl 4-[2-(2,4-dihydroxyphenyl)-2-oxoethoxy]benzoate

			Dimethyl 4-hydroxy-4'-methoxy-2,3-biphenyldicarboxylate 2-(3,4-Dihydro-2H-1,5-benzodioxepin-7-yl)-1-(2,3,4-trihydroxyphenyl)ethanone Ethyl (1R)-1-(2-hydroxy-1,3-dioxo-2,3-dihydro-1H-inden-2-yl)-2-oxocyclopentanecarboxylate 3,3'-Methylenebis(2-hydroxy-5-methylbenzoic acid)
11.5 min	317	$C_{18}H_{12}N_4O_2$	N-[4-([1,3]Oxazolo[4,5-b]pyridin-2-yl)phenyl]nicotinamide 1-Phenyl-5,5a-dihydro-1H-pyrazolo[4',3':5,6]pyrimido[2,1-a]isoindole-4,10-dione 3-(1H-Benzimidazol-2-yl)pyrrolo[1,2-a]quinazoline-2,5(1H,4H)-dione N-[3-(1,3-Benzoxazol-2-yl)phenyl]-2-pyrazinecarboxamide 9,10-Dimethyl-3-nitrobenzimidazo[1,2-a]quinoline-6-carbonitrile 4H-pyrano[3,2-c]quinoline-3-carbonitrile, 2-amino-5-hydroxy-4-(3-pyridinyl)-
11.5 min	611		dimer of 317 minus the sodium adduct

I then compared the chemical structure of these compounds to the structure of known AhR modulators, but I could not find any indication that one of these compounds has a similar structure to the different classes of AhR modulators (Figure 34).

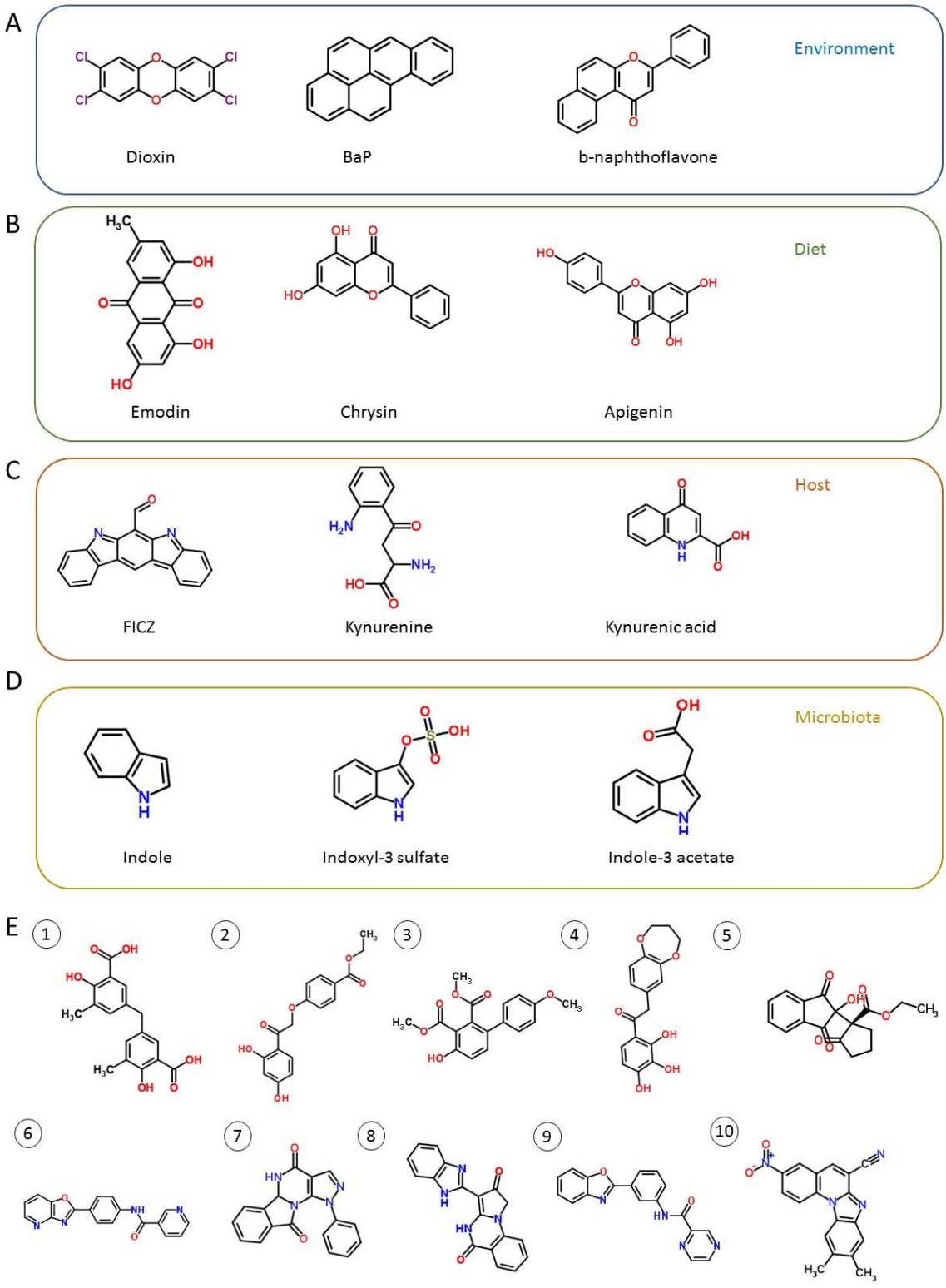

Figure 34 Chemical structure of known AhR ligands and the potential compounds enriched in the OP50 medium compared to the HT115 medium. A - D) Chemical structure mammalian AhR ligands: environmental ligands (A), dietary ligands (B), endogenous produced ligands (C) and ligands produced by microbiota (D). E) Chemical structure of the potential compounds associated with m/z 317 (Table 2). (1) 3,3'-Methylenebis(6-hydroxy-5-methylbenzoic acid), (2) Ethyl 4-[2-(2,4-dihydroxyphenyl)-2-oxoethoxy]benzoate, (3) Dimethyl 4-hydroxy-4'-methoxy-2,3-biphenyldicarboxylate, (4) 2-(3,4-Dihydro-2H-1,5-benzodioxepin-7-yl)-1-(2,3,4-trihydroxy-phenyl)ethanone, (5) Ethyl (1R)-1-(2-hydroxy-1,3-dioxo-2,3-dihydro-1H-inden-2-yl)-2-oxocyclo-pentane-carboxylate, (6) N-[4-([1,3]Oxazolo[4,5-b]pyridin-2-yl)phenyl]nicotinamide, (7) 1-Phenyl-5,5a-dihydro-1H-pyrazolo[4',3':5,6]pyrimido[2,1-a]isoindole-4,10-dione, (8) 3-(1H-Benzimidazol-2-yl)pyrrolo[1,2-a]quinazoline-

2,5(1H,4H)-dione, (9) N-[3-(1,3-Benzoxazol-2-yl)phenyl]-2-pyrazinecarboxamide, (10) 9,10-Dimethyl-3-nitrobenzimidazo[1,2-a]quinoline-6-carbonitrile.

To identify more compounds with different occurrences in HT115 and OP50, the spectra were subtracted from each other. After subtraction of the HT115 spectrum from OP50 in the positive mode, one main peak with a retention time of 8.8 min remained (Figure 35A, peak 22). This peak was further analyzed and was composed of 4 big peaks with m/z 219, m/z 317, m/z 379, and m/z 611. M/z 219 has likely the formula $C_8H_{14}N_2O_5$, and according to the ChemSpider webpage (http://www.chemspider.com [220]), it is probably an alanine-glutamate dipeptide (Ala-Glu), and therefore a compound which is likely to be produced by bacteria (Table 3). On the *E. coli* Metabolome Database, there is evidence that Ala-Glu is produced by *E. coli* K12 [218, 219]. The comparison between the chemical structure of Ala-Glu and known AhR ligands shows no similarities making it quite unlikely that Ala-Glu might act as a ligand for AHR-1 (Figure 36A). In total there were 420 results for the formula $C_8H_{14}N_2O_5$. For m/z 317, m/z 379, and m/z 611 the following chemical formulas were suggested respectively: $C_8H_{18}N_6O_6$, $C_{16}H_{10}N_8O_4$, $C_{16}H_{36}N_{12}O_{12}$. According to the formula, I found 7 potential compounds for m/z 379 (Table 3), but none of these is associated with bacterial metabolism, and none of the compounds has structural similarities to known AhR ligands (Figure 36B). As seen before, the fragment spectra of m/z 611 showed that m/z 611 is mainly composed of 317, but with the calculated formulas, I could not find any compounds for m/z 317 and m/z 611.

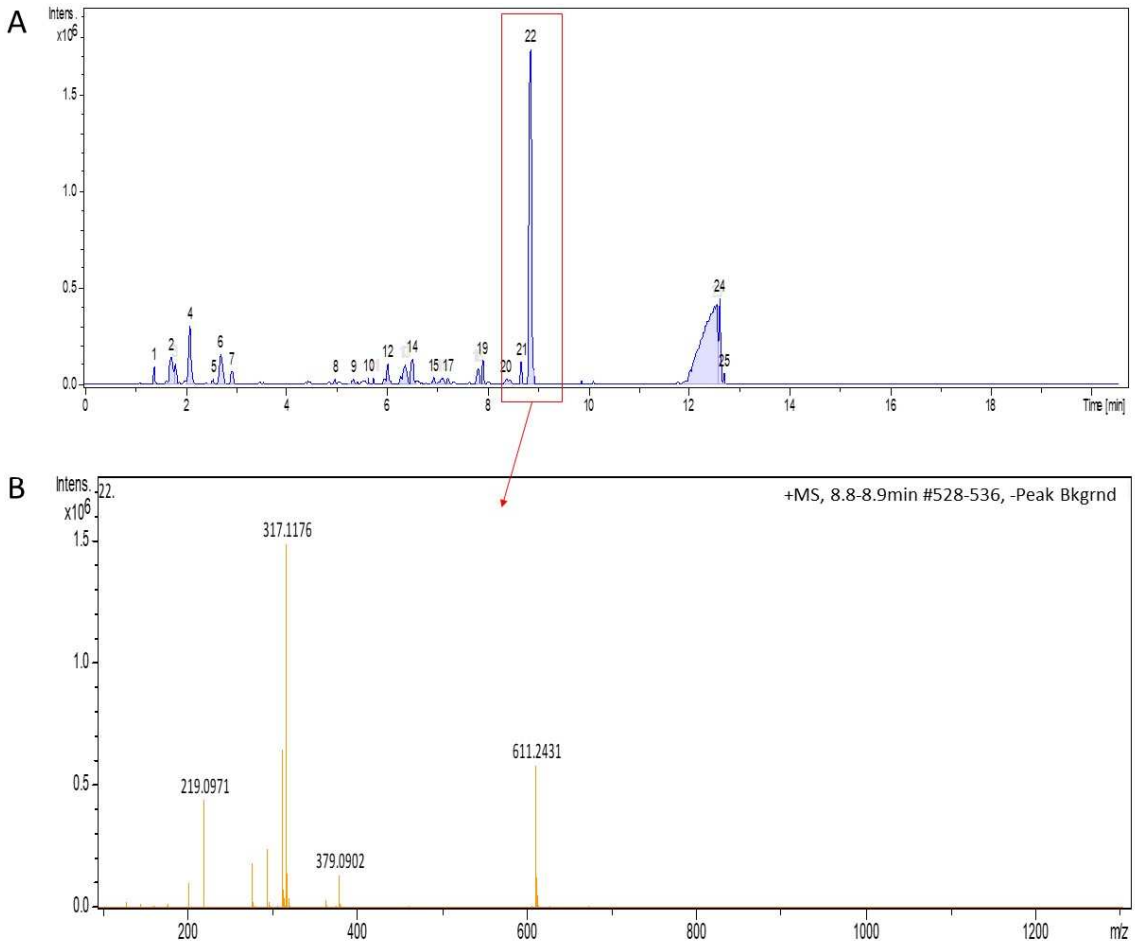

Figure 35 ESI MS analysis in positive mode. A) BPC of OP50 medium after subtraction of the HT115 BPC. B) Masses in peak 22 of panel A. Further analysis of the formulas and the possible compounds are listed in Table 4.

Table 3 Analysis of compounds in peak 22 in the ESI-mass spectrum in positive mode (Figure 35). The hits were evaluated according to the number of PubMed entries. If no PubMed entry was found, compounds were sorted according to the number of References. The best 6 hits are listed.

Retention time	m/z	Formula	Compound name (according to http://www.chemspider.com)
8.8 min	219	$C_8H_{14}N_2O_5$	Alanylglutamic acid Glutamylalanine γ-Glutamylalanine N-[2-(Hydroxycarbamoyl)-3-methylbutanoyl]glycine acetylalanylserine N-(2-Acetoxyethyl)-D-α-asparagine
	317	$C_8H_{18}N_6O_6$	None found
	379	$C_{16}H_{10}N_8O_4$	9-(2-Furyl)-8-(4-nitrophenyl)-4,9-dihydrotetrazolo[1',5':1,2]pyrimido[4,5-d]pyridazin-5-ol 8-(2-Furyl)-9-(4-nitrophenyl)-1,9-dihydrotetrazolo[1',5':1,2]pyrimido[4,5-d]pyridazin-5(6H)-one 8-(2-Furyl)-9-(3-nitrophenyl)-1,9-dihydrotetrazolo[1',5':1,2]pyrimido[4,5-d]pyridazin-5(6H)-one

			6-(1H-Benzotriazol-1-yl)-5-nitro-N-(3-nitrophenyl)pyrimidin-4-amine (2E)-[2-(4-Nitrophenyl)hydrazino](3-oxo-2(3H)-quinoxalinylidene)acetyl azide 6-Nitro-2-[(2Z)-2-(6-nitro-2(1H)-quinoxalinylidene)hydrazino]quinoxaline
	611	$C_{16}H_{36}N_{12}O_{12}$	None found

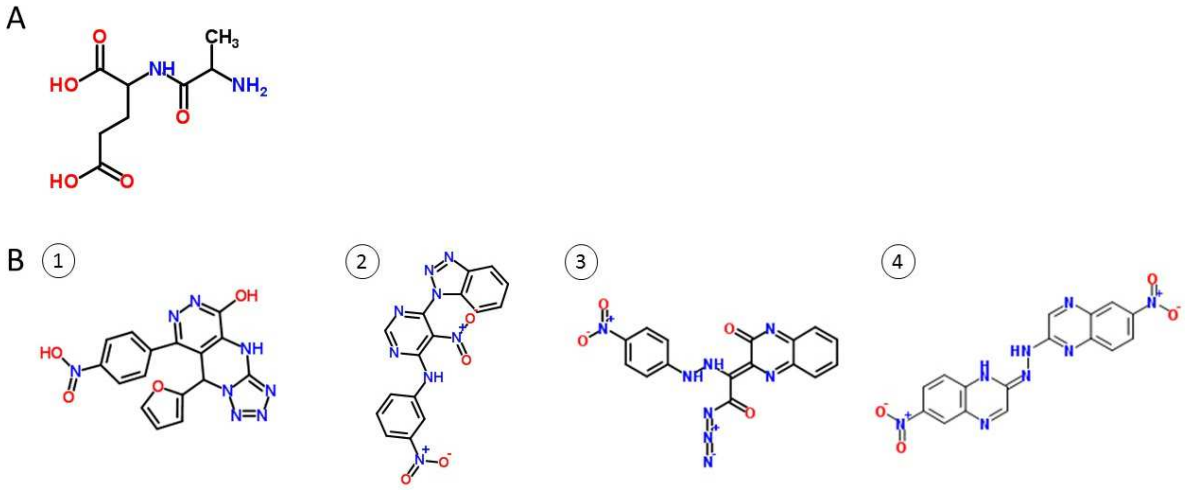

Figure 36 Chemical structures of potential compounds in peak 22 (Figure 35). A) Alanylglutamic acid (Ala-Glu). B) (1) 9-(2-Furyl)-8-(4-nitrophenyl)-4,9-dihydrotetrazolo[1',5':1,2]pyrimido[4,5-d]pyridazin-5-ol, (2) 6-(1H-Benzotriazol-1-yl)-5-nitro-N-(3-nitrophenyl)pyrimidin-4-amine, (3) (2E)-[2-(4-Nitrophenyl)hydrazino](3-oxo-2(3H)-quinoxalinylidene)acetyl azide, (4) 6-Nitro-2-[(2Z)-2-(6-nitro-2(1H)-quinoxalinylidene)hydrazino]quinoxaline.

In the negative mode, the comparison between the OP50 and HT115 media showed one main peak with a retention time of 8.8 min (Figure 37A, peak 33). This peak was further analyzed and was composed of m/z 339. The fragmentation of this peak showed that it is composed of m/z 134, m/z 161, and m/z 337. There were no chemical formulas suggested for these masses.

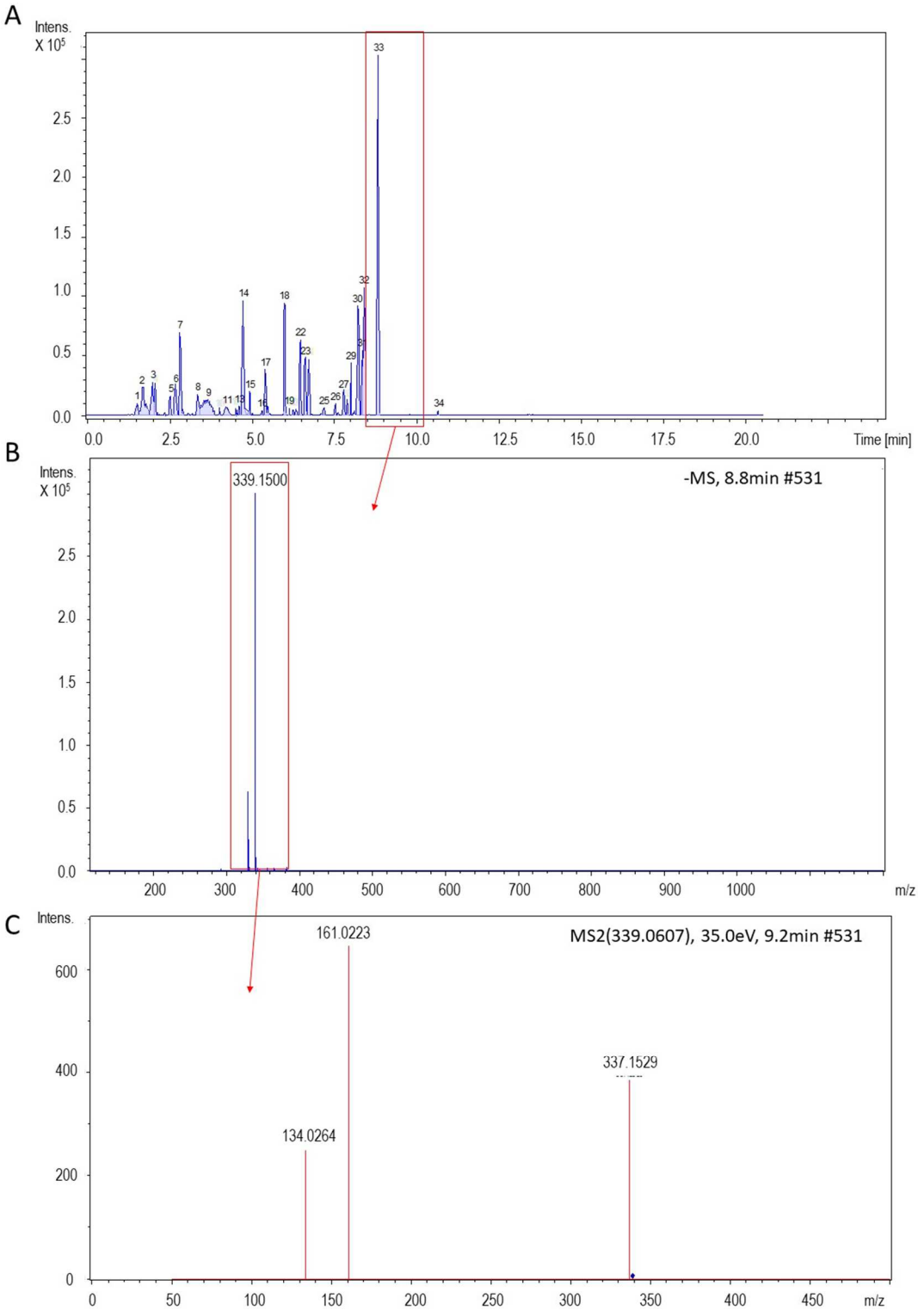

Figure 37 ESI MS analysis in negative mode. A) BPC of OP50 after subtraction of the HT115 BPC. B) Masses in the peak 33 of panel A. C) Fragment spectra of m/z 339.

When comparing HT115 to OP50, the subtracted spectrum showed 3 prominent peaks (Figure 38A, Peak 2, 3, and 27) with retention times of 1.5, 1.8, and 7.3 min in the positive mode. In peak 2 m/z 148 and m/z 361, with the respective formulas $C_4H_{10}N_3O_3$ and $C_{17}H_{25}N_6O_3$ were found. M/z 148 is most likely asparagine amide (Table 4, Figure 39A), which is similar to the amino acid L-asparagine, an amino acid produced by *E. coli* [218, 219]. For m/z 361, 7 different

compounds were found, one of them was an arginine-tryptophan dipeptide (Table 4). This is of particular interest since arginine and tryptophan are metabolites of *E. coli* and tryptophan derivatives are AhR modulators [136, 218, 219]. Peak 3 was composed of m/z 216 and m/z 432. The chemical formula for m/z 432 was $C_{10}H_{26}N_{17}O_{3,}$ for which I could not find any compound on ChemSpider. Peak 27 contained only m/z 385, for which the chemical formula $C_{22}H_{32}N_4O_2$ was suggested. Searching for $C_{22}H_{32}N_4O_2$ I found 4 potential compounds in ChemSpider, The chemical structures of compounds found for m/z 148, m/z 361, and m/z 385 are shown in Figure 39.

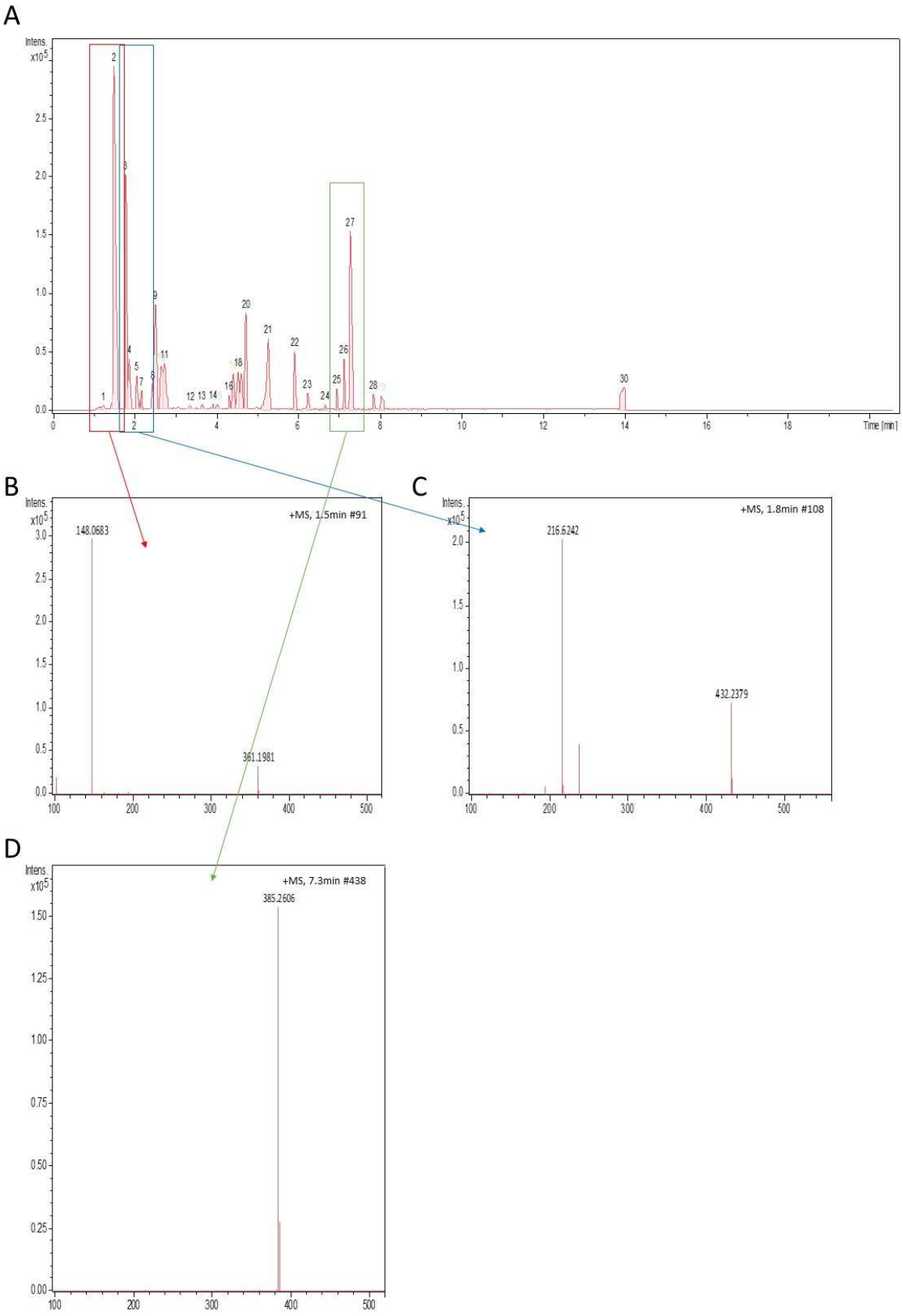

Figure 38 Positive ESI MS analysis. A) HT115 BPC after subtraction of the OP50 BPC. B) Masses in peak 2 of panel A. C) Masses in peak 3 of panel A. D) Masses in peak 27 of panel A. A further analysis of the formulas and the possible compounds are listed in Table 4.

Table 4 Analysis of compounds in peak 2, 3, and 27 of the positive ESI-mass spectrum (Figure 38). The best 6 hits are listed. The hits were evaluated according to the number of PubMed entries. If no PubMed entry was found, compounds were sorted according to the number of References.

Retention time	**m/z**	**Formula**	**Compound name (according to http://www.chemspider.com)**
1.5 min	148	$C_4H_{10}N_3O_3$	asparagine amide
	361	$C_{17}H_{24}N_6O_3$	Arginine Tryptophan dipeptide 2-{[4-(Ethylamino)-6-(isopropylamino)-1,3,5-triazin-2-yl]oxy}ethyl phenylcarbamate 2-(9-Cyclohexyl-1-methyl-2,4-dioxo-1,4,6,7,8,9-hexahydropyrimido[2,1-f]purin-3(2H)-yl)acetamide N4-(4-Ethoxyphenyl)-N2-(3-methylbutyl)-5-nitro-2,4,6-pyrimidinetriamine 2-[(3-Benzyl-6-oxo-1,2,5,6-tetrahydro-1,2,4-triazin-5-yl)acetyl]-N-butylhydrazinecarboxamide 2-[4-(2-Methyl-2H-tetrazol-5-yl)phenoxy]-N-[3-(4-morpholinyl)propyl]acetamide
1.8 min	432	$C_{10}H_{26}N_{17}O_3$	none found
7.3 min	385	$C_{22}H_{32}N_4O_2$	8-Butyl-3,3-dimethyl-6-(4-propionyl-1-piperazinyl)-3,4-dihydro-1H-pyrano[3,4-c]pyridine-5-carbonitrile 2-(4-Benzyl-1-piperazinyl)-6-(methoxymethyl)-5-(3-methylbutyl)-4(1H)-pyrimidinone 2-[3-(4-Methoxyphenyl)-5-methyl-1H-pyrazol-4-yl]-N-(2,2,6,6-tetramethyl-4-piperidinyl)acetamide 1-Isobutyl-N-[3-(1-isopropyl-1H-benzimidazol-2-yl)propyl]-5-oxo-3-pyrrolidinecarboxamide

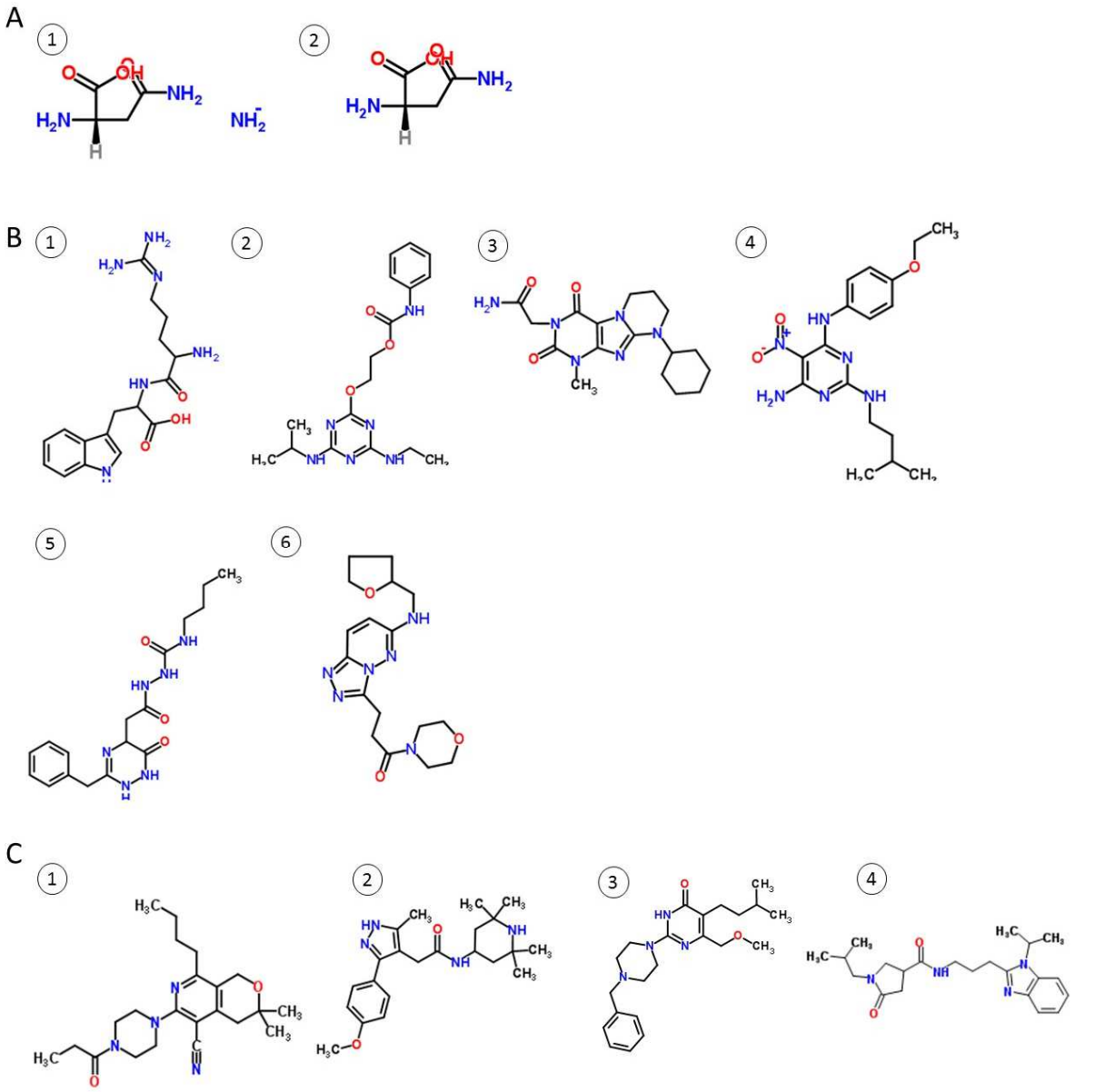

Figure 39 Chemical structures of potential compounds in peaks 2, and 27 (Figure 38). A) (1) asparagine amide, (2) asparagine. B) (1) Arginine Tryptophan dipeptide, (2) 2-{[4-(Ethylamino)-6-(isopropylamino)-1,3,5-triazin-2-yl]oxy}ethyl phenylcarbamate, (3) 2-(9-Cyclohexyl-1-methyl-2,4-dioxo-1,4,6,7,8,9-hexahydropyrimido[2,1-f]purin-3(2H)-yl)acetamide, (4) N4-(4-Ethoxyphenyl)-N2-(3-methylbutyl)-5-nitro-2,4,6-pyrimidinetriamine, (5) 2-[(3-Benzyl-6-oxo-1,2,5,6-tetrahydro-1,2,4-triazine-5-yl)acetyl]-N-butylhydrazinecarboxamide, (6) 2-[4-(2-Methyl-2H-tetrazole-5-yl)phenoxy]-N-[3-(4-morpholinyl)propyl]acetamide. C) (1) 8-Butyl-3,3-dimethyl-6-(4-propionyl-1-piperazinyl)-3,4-dihydro-1H-pyrano[3,4-c]pyridine-5-carbonitrile, (2) 2-(4-Benzyl-1-piperazinyl)-6-(methoxymethyl)-5-(3-methylbutyl)-4(1H)-pyrimidinone, (3) 2-[3-(4-Methoxyphenyl)-5-methyl-1H-pyrazol-4-yl]-N-(2,2,6,6-tetramethyl-4-piperidinyl)acetamide, (4) 1-Isobutyl-N-[3-(1-isopropyl-1H-benzimidazole-2-yl)propyl]-5-oxo-3-pyrrolidinecarboxamide

In the negative mode, there were 2 main peaks in the spectrum of HT115 after subtraction of the OP50 spectrum (Figure 40A). One peak, peak 19, with a retention time of 5.8 min was further analyzed. The masses in peak 19 were m/z 164, m/z 283, and m/z 402 (Figure 40B). The following formulas were suggested for these masses respectively: $C_5H_{11}N_5$, $C_{11}H_{12}N_{10}$, and $C_{22}H_{25}N_7O$. For m/z 164 I found 2 compounds on ChemSpider, N-(1-Methyl-1H-1,2,4-triazole-5-yl)-1,2-ethanediamine and 1H-Tetrazole-5-ethanamine, N, N-dimethyl- (Table 5).

None of these compounds have been found as bacterial metabolites so far. For m/z 283 I found 18 potential compounds, and for m/z 402 seven, of which the 6 best hits are listed in Table 5. According to the formula, m/z 283 might be 7-methyladenine–adenine, which is a mixture of 7-methyladenine and adenine, a purine base found in DNA and RNA. M/z 402 contains probably an indole group or a group similar to indole and could, therefore, be an AHR-1 modulator (Figure 41C).

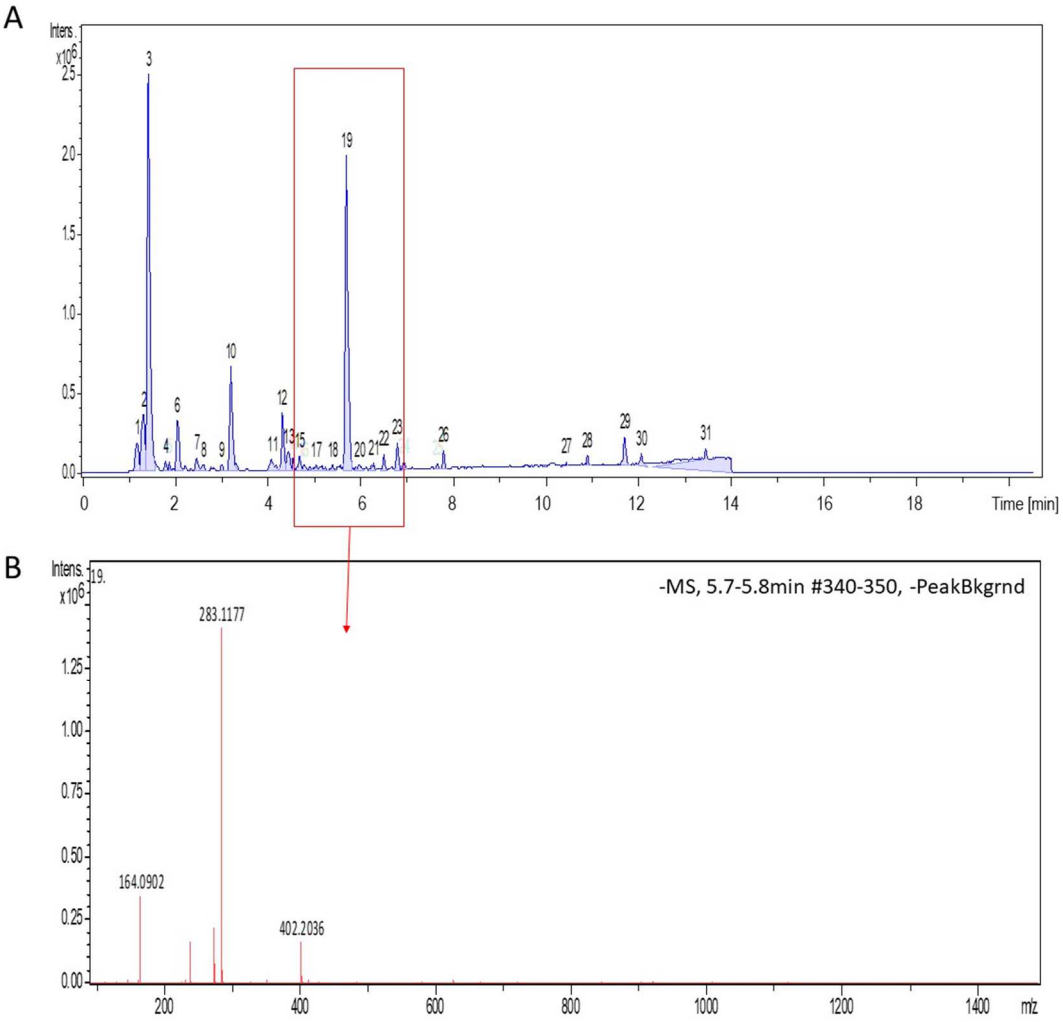

Figure 40 ESI MS analysis in negative mode. A) HT115 BPC after subtraction of the OP50 BPC. B) Masses in peak 19 of panel A. A further analysis of the formulas and the possible compounds are listed in Table 5.

Table 5 Analysis of compound in peak 19 in the negative ESI-mass spectrum (Figure 40B). The best 6 hits are listed. The hits were evaluated according to the number of PubMed entries. If no PubMed entry was found, compounds were sorted according to the number of References.

Retention time	**m/z**	**Formula**	**Compound name (First hits on http://www.chemspider.com)**
5.8 min	164	$C_5H_{11}N_5$	N-(1-Methyl-1H-1,2,4-triazol-5-yl)-1,2-ethanediamine
			1H-Tetrazole-5-ethanamine, N, N-dimethyl-
	283	$C_{11}H_{12}N_{10}$	5-Amino-3-[3-(tetrazolo[1,5-b]pyridazin-6-ylamino)propyl]-1H-pyrazole-4-carbonitrile
			7-methyl-adenine–adenine

		2,2'-{[4-(Ethylamino)-6-(1H-1,2,4-triazol-1-yl)-1,3,5-triazin-2-yl]imino}diacetonitrile N-[(2-Methyl-4-pyrimidinyl)methyl]-6-(1H-1,2,4-triazol-1-yl)-1,3,5-triazine-2,4-diamine N-[(5-Methyl-2-pyrazinyl)methyl]-6-(1H-1,2,4-triazol-1-yl)-1,3,5-triazine-2,4-diamine 4-(5,6-Dihydroimidazo[1,2-a]pyrazin-7(8H)-yl)-6-(1H-1,2,4-triazol-1-yl)-1,3,5-triazin-2-amine
402	$C_{22}H_{25}N_7O$	N-[2-(1H-Indol-3-yl)ethyl]-1-(3-methyl[1,2,4]triazolo[4,3-b]pyridazin-6-yl)-4-piperidinecarboxamide N-[1-(1H-Indol-3-yl)-2-propanyl]-1-(7H-purin-6-yl)-3-piperidinecarboxamide N-[1-(1H-Indol-3-yl)-2-propanyl]-1-(7H-purin-6-yl)-4-piperidinecarboxamide N-[3-(1-Isobutyl-1H-benzimidazol-2-yl)propyl]-4-(1H-tetrazol-1-yl)benzamide N-[(1S)-1-(1H-Benzimidazol-2-yl)-2-methylpropyl]-4-(2-isopropyl-2H-tetrazol-5-yl)benzamide N-[2-(1-Isopropyl-1H-benzimidazol-2-yl)ethyl]-3-phenyl-2-(1H-tetrazol-1-yl)propanamide

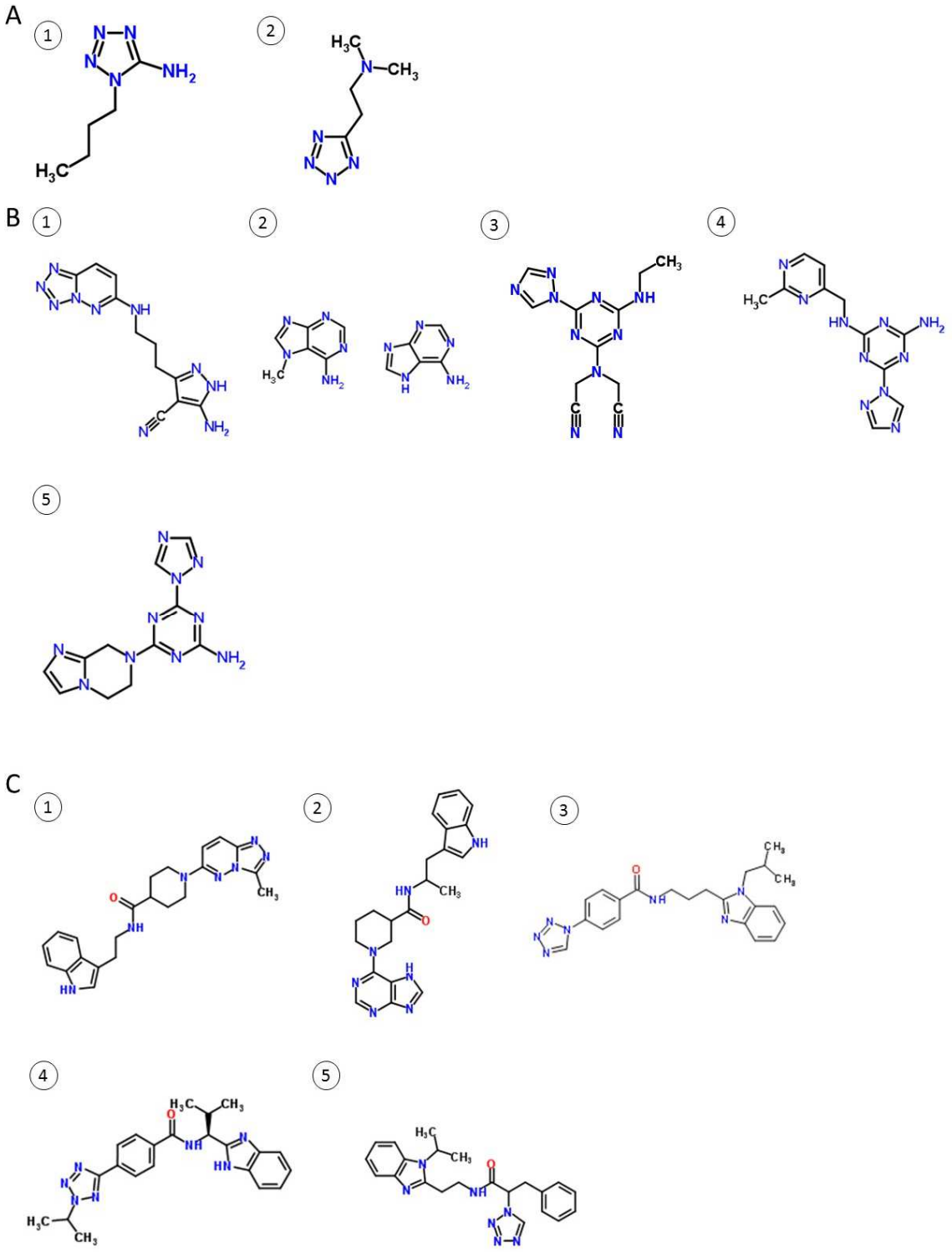

Figure 41 Chemical structures of potential compounds in peak 19 (Figure 40). A) (1) N-(1-Methyl-1H-1,2,4-triazol-5-yl)-1,2-ethanediamine, (2) 1H-Tetrazole-5-ethanamine, N, N-dimethyl-. B) (1) 5-Amino-3-[3-(tetrazolo[1,5-b]pyridazin-6-ylamino)propyl]-1H-pyrazole-4-carbonitrile, (2) 7-methyl-adenine–adenine, (3) 2,2'-{[4-(Ethylamino)-6-(1H-1,2,4-triazol-1-yl)-1,3,5-triazin-2-yl]imino}diacetonitrile, (4) N-[(2-Methyl-4-pyrimidinyl)methyl]-6-(1H-1,2,4-triazol-1-yl)-1,3,5-triazine-2,4-diamine, (5) 4-(5,6-Dihydroimidazo[1,2-a]pyrazin-7(8H)-yl)-6-(1H-1,2,4-triazol-1-yl)-1,3,5-triazin-2-amine. C) (1) N-[2-(1H-Indol-3-yl)ethyl]-1-(3-methyl[1,2,4]triazolo[4,3-b]pyridazin-6-yl)-4-piperidinecarboxamide, (2) N-[1-(1H-Indol-3-yl)-2-propanyl]-1-(7H-purin-6-yl)-3-piperidinecarboxamide, (3) N-[3-(1-Isobutyl-1H-benzimidazol-2-yl)propyl]-4-(1H-tetrazol-1-yl)benzamide, (4) N-[(1S)-1-(1H-Benzimidazol-2-yl)-2-methylpropyl]-4-(2-isopropyl-2H-tetrazol-5-yl)benzamide, (5) N-[2-(1-Isopropyl-1H-benzimidazol-2-yl)ethyl]-3-phenyl-2-(1H-tetrazol-1-yl)propanamide.

Indole is a bacterial metabolite and AhR ligand in mammals [161, 162]. Moreover, lifespan-extending effects of indole have been found to require AHR-1 in *C. elegans* [221]. Therefore, I was specifically interested in whether OP50 and HT115 might produce different amounts of indole, but I could not find any differences in the media of HT115 and OP50 for molecules with the mass of indole (molecular weight: 117.15 g/mol).

AHR-1 regulates genes responsible for the detoxification response

To further understand how the potential AHR-1 modulators affect gene expression, I used transgenic strains expressing the GFP or mcherry under the promoter of potential AHR-1 target genes. In a first approach, I wanted to identify genes differentially expressed upon loss of AHR-1, to later check the expression of these genes in response to the potential AHR-1 modulators. I, therefore, measured the GFP/mcherry expression of the following reporter strains either in control RNAi (L4440) or *ahr-1* RNAi-treated worms: *cyp-14A3*, *cyp-25A2*, *cyp-29A2*, *cyp-35A2*, *cyp-35A3*, *cyp-35B1*, and *cyp-37A1*, *gst-4,* and *ins-35.* Out of the tested genes, *cyp-35A2, cyp-35B1,* and *gst-4* were significantly increased while *cyp-37A1 was* significantly decreased by *ahr-1* RNAi compared to control RNAi with a magnitude of more than 10 % in at least 2 replicates (Figure 42, Table 6).

Table 6 Relative expression of transgenes in control or *ahr-1* RNAi-treated reporter strains. The relative expression was measured in worms on their first day of adulthood and normalized to control RNAi treated worms in each replicate. Statistical test: student's t-test.

Strain name	Gene	Rel. expression (mean ± SD)	No. experiments	No. worms	p-value
BC14926	***cyp-14A3***	anterior: 0.97 posterior: 1.05	3	35 - 38	0.544 0.333
SD1444	***cyp-25A2***	1.07 ± 0.16	2	38	0.067
BC20334	***cyp-29A2***	0.85 ± 0.60	2	42	0.377
cyp-35A2	***cyp-35A2***	anterior: 8.43 ± 11.96 posterior: 1.99 ± 2.14	3	42 - 43	< 0.001 0.005
cyp-35A3	***cyp-35A3***	1.08 ± 0.09	2	26 - 28	0.02
CY573	***cyp-35B1***	anterior: 2.60 ± 1.97 posterior: 2.90 ± 2.40	2 3	27 - 36, 40 - 60	< 0.001 < 0.001
BC15044	***cyp-37A***	0.66 ± 0.14	2	26 - 38	< 0.001
NV6	***gst-4***	1.58 ± 0.37	2	27 - 29	< 0.001
HT1798	***ins-35***	anterior: 0.93 ± 0.22 posterior: 0.60 ± 0.16	1 1	9 - 11	0.481 < 0.001

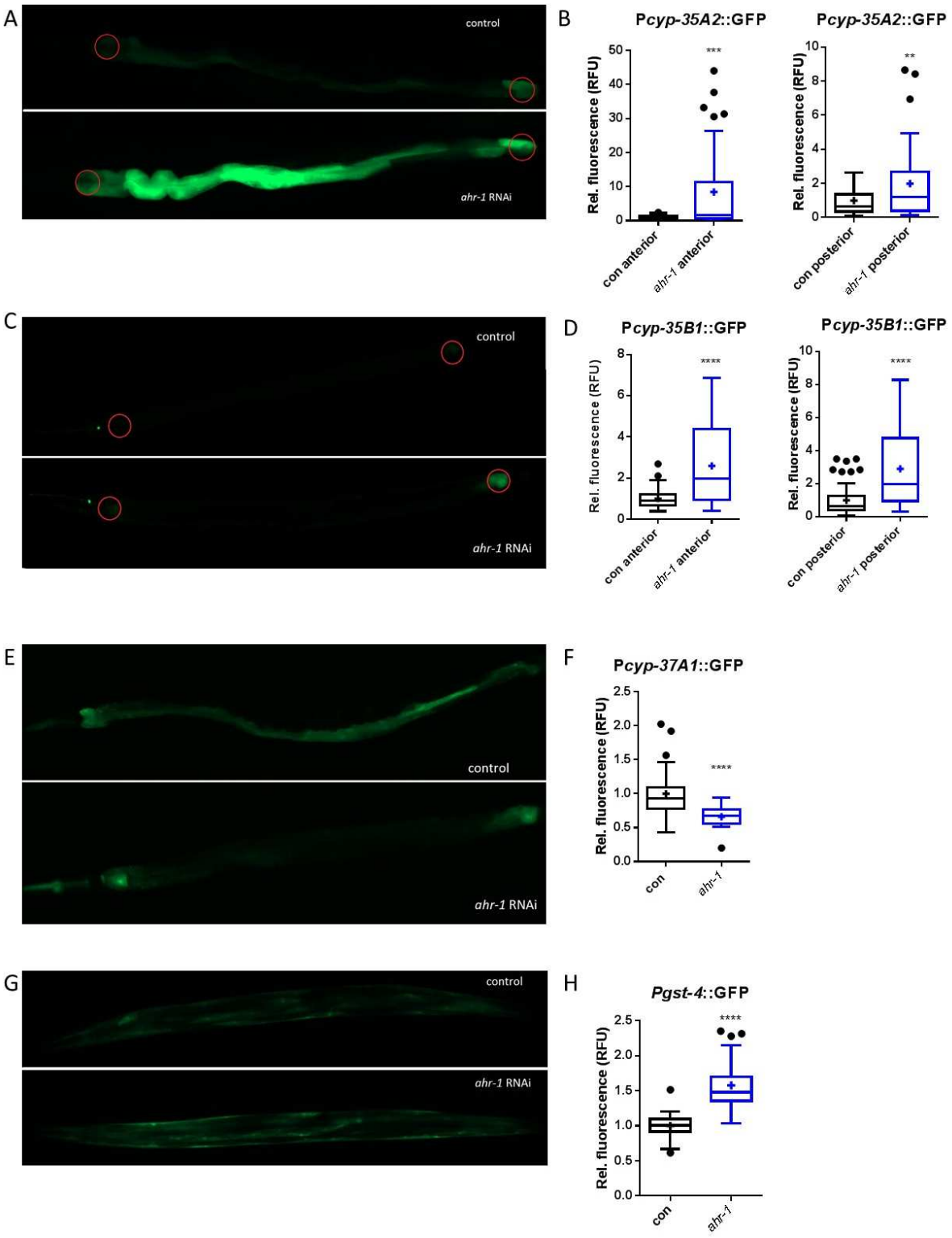

Figure 42 *cyp-35A2*, *cyp-35B1*, *cyp-37A1* and *gst-4* are potential target genes of AHR-1. A – G) Representative pictures of control and *ahr-1* RNAi treated cyp-35A2::GFP (A), CY573 (cyp-35B1::GFP) (C), BC15044 (cyp-37A1::GFP) (E), and NV6 (gst-4::GFP) (G). The region of interest (ROI) is marked by a red circle. If no ROI is indicated, fluorescence was measured in the whole worm. Worms are orientated with the anterior on the left. B - H) Quantification of the relative cyp-35A2::GFP (B), cyp-35B1::GFP (D) cyp-37A1::GFP (F), and gst-4::GFP (H) expression in control and *ahr-1* RNAi treated worms. * p-value <0.05, ** p-value <0.01, *** p-value < 0.001, **** p-value <0.0001, statistical test: student's t-test. Mean RFUs and p-values are listed in Table 6.

Because the changes in expression upon *ahr-1* RNAi were strongest for *gst-4*, *cyp-35A2,* and *cyp-35B1,* I decided to cross the *ju145* allele inside the transgenic strains for these genes.

While crossing for *cyp-35A2* was not possible for some undisclosed reasons (most likely associated with the integration site of the transgene), I successfully crossed the *ahr-1(ju145)* with CY573 (Pcyp-35B1::GFP) and NV6 (Pgst-4::GFP). The strains resulting from this cross were called NV33 and NV35, respectively. Surprisingly, and contrary to the data obtained with *ahr-1* RNAi, *ahr-1* loss of function animals had a lower expression of *cyp-35B1* than control animals on both bacterial food sources (Figure 43A - B). The reduction in *cyp-35B1* was stronger on HT115 (52 %) than on OP50 (29 %). There was no difference in the expression of *cyp-35B1* between an HT115 diet and an OP50 diet in worms with wild-type AHR-1 and mutant AHR-1 (Figure 43C). In contrast to *cyp-35B1*, *gst-4* expression was unaltered in *ahr-1* loss-of-function animals on HT115 and OP50 (Figure 43D). Therefore, *cyp-35B1* was used as potential AHR-1 target genes for further experiments.

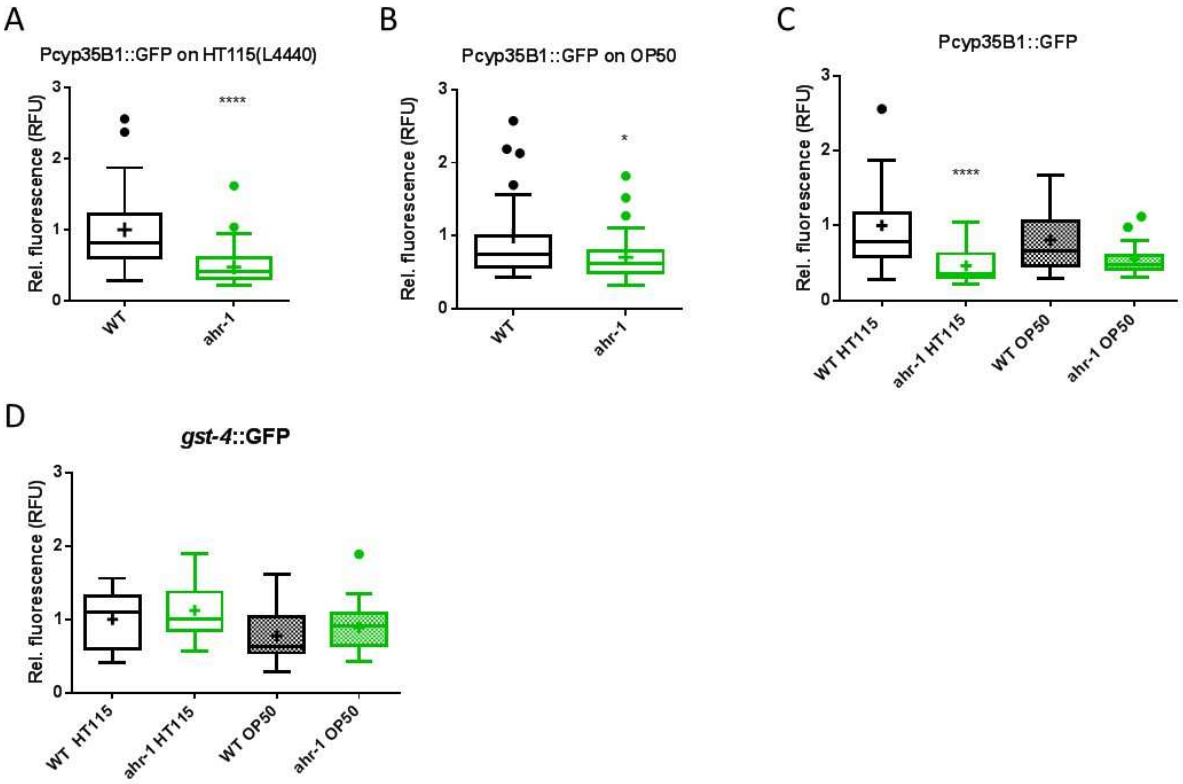

Figure 43 *cyp-35B1* but not *gst-4* is down-regulated in *ahr-1* loss of function worms. A – C) Expression of transgenic GFP in the posterior intestine of 3-days old CY573 (WT) and NV33 (ahr-1). A) Rel. *cyp-35B1* expression in WT and *ahr-1* on HT115. Pooled data of 52 - 63 worms in 3 independent experiments are shown. p-value < 0.0001; statistical test: student's t-test. B) Rel. *cyp-35B1* expression in WT and *ahr-1* on OP50. Pooled data of 42 - 43 worms in 3 independent experiments are shown. p-value=0.017; statistical test: student's t-test. C) Rel. *cyp-35B1* expression in WT and *ahr-1* on HT115 and OP50. Pooled data of 19 - 44 worms in 2 independent experiments are shown. **** p-value < 0.0001 *vs.* WT, statistical test: Tukey's multiple comparison's test. D) Rel. *gst-4* expression in NV35wt (WT) and NV35a (ahr-1) on HT115 and OP50. The expression of *gst-4*::GFP was measured in 3 regions (front, middle, back of the worm). Pooled data of 19 – 30 worms in 2 independent experiments are shown.

Thus, I tested if the potential AHR-1 modulators led to a differential expression of *cyp-35B1*. In a first approach, I tried a chronic treatment with BaP starting from eggs and measured the *cyp-35B1* expression in 4-days old worms. Chronic exposure to BaP did not induce *cyp-35B1* in worms with the wild-type *ahr-1* allele (Figure S 6A). Acute BaP exposure for 24 h starting

from adults instead increased the *cyp-35B1* expression (Figure S 6B). The induction of *cyp-35B1* was even higher when measured after 18 h (Figure S 6C) and I, therefore, decided to use 18 h of exposure. Exposure to 1 µM of BaP induced the expression of *cyp-35B1* 6-fold in NV33wt and 7-fold in NV33a (Figure 44A - B). The induction was not further increased when using 5 µM of BaP. Together with the data on the development, this indicates, that BaP affects *C. elegans* likely independent of AHR-1. Next, I wanted to assess the expression of *cyp-35B1* on curcumin-treated animals, but because curcumin showed fluorescence in the GFP channel, I could not use this transgenic strain for the investigation of *cyp-35B1* expression upon curcumin treatment. Since also UVB appears to have AHR-1-dependent effects, I measured the expression of *cyp-35B1* in response to UVB irradiation. 18 h after UVB irradiation, *cyp-35B1* was not significantly induced in animals with or without *ahr-1* (Figure 44C - D).

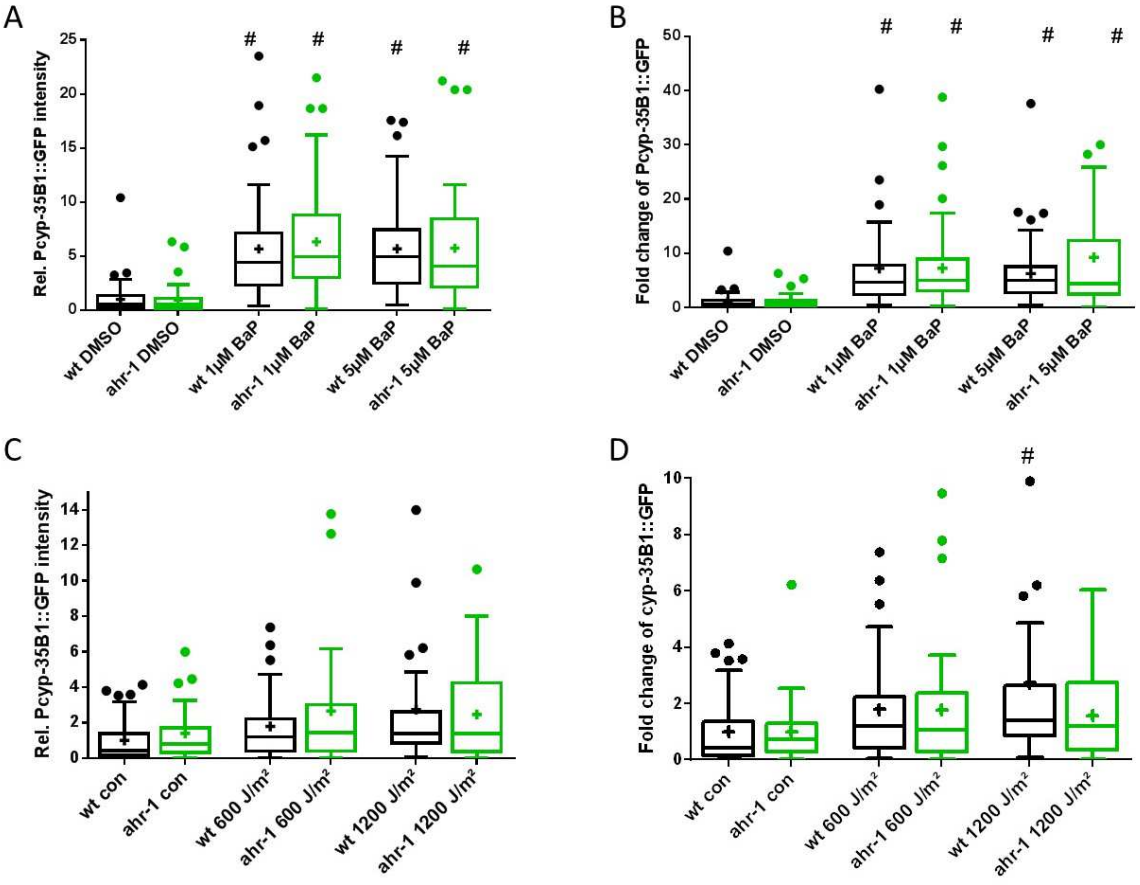

Figure 44 BaP, but not UVB induces transgenic *cyp-35B1*. A - B) BaP induces *cyp-35B1* in NV33wt and NV33a. Fluorescence was measured 18 h after exposure in adults. Pooled data of 51 – 65 worms in 3 independent experiments are shown. # p-value < 0.05 *vs.* DMSO, statistical test: One-way ANOVA with Sidak's multiple comparisons test. A) *Pcyp-35B1*::GFP intensity normalized to NV33wt DMSO. B) *Pcyp-35B1*::GFP intensity normalized to DMSO of each strain. C – D) *cyp-35B1* is only marginally induced by UVB in NV33wt and NV33a. Fluorescence was measured 18 h after UVB exposure in adults. Pooled data of 28 – 37 worms in 2 independent experiments are shown, # p-value < 0.05 *vs.* control, statistical test: One-way ANOVA with Sidak's multiple comparisons test.

AHR-1 is required in the nervous system to regulate lifespan

The differences in *cyp-35B1*::GFP expression upon *ahr-1* RNAi (Figure 42) and in the *ahr-1(ju145)* (Figure 43) were striking. Therefore, I wanted to understand whether the partial absence of AHR-1 by RNAi is sufficient for the changes in life- and healthspan. Moreover, given that the different AHR-1 modulators could affect its activity through different tissues, I used tissue-specific RNAi to investigate whether the absence of AHR-1 in specific tissues is sufficient to modulate animals' lifespans. For this, I applied *ahr-1* RNAi on different *C. elegans* strains (Table 7), in which RNAi is effective only or mainly in specific tissues: in the hypodermis [222], in the germline [223, 224], in somatic tissues [225], in the muscles [226], in the intestine [227], and in the nervous system [228, 229]. For these experiments, I used the *E. coli* HT115(DE3) strain, which is commonly used for RNAi experiments. Surprisingly, but consistent with the differential effect between RNAi knockdown and knockout, loss of AHR-1 by RNAi did not have any impact on the lifespan of the wild-type strain (Table 7, Figure 45A) but slightly shortened the healthspan by 4 % (Table 8, Figure 45B). Also, *ahr-1* RNAi did neither affect life- nor healthspan, when only applied in the hypodermis, in the germline, in somatic tissues, in the muscles or the intestine (Table 7 and Table 8). To test the effect of *ahr-1* RNAi in the nervous system, I used 3 different strains: TU3401, in which RNAi is effective exclusively in the nervous system [228], TU3311, which shows increased RNAi efficiency in neurons, while RNAi is still effective in other tissues as well [228] and CL6114, which is in general RNAi hypersensitive with specific sensitivity in the nervous system [229]. While *ahr-1* RNAi did not have any effect on the lifespan of TU3401 and CL6114, it significantly shortened life- and healthspan of TU3311 by 11 % (Table 7, Table 8, and Figure 45C - D).

Table 7 Effect of *ahr-1* RNAi on lifespan. The L4440 plasmid was used as negative control.

Condition	Genotype	Description	Lifespan (days)	No. of worms	No. of experiments	P-value
N2 Control	wild-type	wild-type	19.88 ± 0.29	280	5	0.14
N2 *ahr-1* RNAi			19.46 ± 0.29	264	5	
NR222 Control	rde-1(ne219); kzIs9 [lin-26p::nls::GFP + lin-26p::rde-1) + rol-6(su1006)]	Hypodermis-specific RNAi	19.07 ± 0.34	120	2	0.23
NR222 *ahr-1* RNAi			18.78 ± 0.30	120	2	
NL2098 Control	rrf-1(pk1417)	germline-specific RNAi	18.26 ± 0.45	120	2	0.83
NL2098 *ahr-1* RNAi			18.24 ± 0.43	120	2	
NL2550 Control	ppw-1(pk2505)	RNAi only in somatic tissues	19.51 ± 0.59	120	2	0.11
NL2550 *ahr-1* RNAi			18.78 ± 0.46	120	2	
WM118 Control	rde-1(ne300); neIs9 [myo-3::HA::RDE-1+ pRF4(rol-6(su1006)]	muscle-specific RNAi	15.49 ± 0.45	120	2	0.92
WM118 *ahr-1* RNAi			15.40 ± 0.45	120	2	
VP303 Control		intestine-specific RNAi	18.68 ± 0.41	120	2	0.47

VP303 *ahr-1* RNAi	rde-1(ne219); kbIs7 [nhx-2p::rde-1 + rol-6(su1006)]		18.50 ± 0.37	120	2	
TU3401 Control	sid-1(pk3321); uIs69[myo-2p::mCherry + unc-119p::sid-1]	nervous system specific RNAi	16.48 ± 0.31	180	3	0.09
TU3401 *ahr-1* RNAi			17.23 ± 0.32	180	3	
TU3311 Control	uIs60[Punc119::YFP; Punc119::sid-1]	RNAi enhanced in the nervous system	19.99 ± 0.44	180	3	0.001
TU3311 *ahr-1* RNAi			17.50 ± 0.43	180	3	
CL6114 Control	nre-1(hd20) lin-15b(hd126)	RNAi hypersensitive, effective RNAi in the nervous system	16.35 ± 0.26	120	2	0.45
CL6114 *ahr-1* RNAi			16.27 ± 0.21	112	2	

Table 8 Effect of loss of AHR-1 loss of function on healthspan. The L4440 plasmid was used as negative control.

Condition	Genotype	Description	Healthpan (days)	No. of worms	No. of ex-periments	P-value
N2 Control	wild-type	wild-type	16.00 ± 0.25	280	5	0.04
N2 *ahr-1* RNAi			15.33 ± 0.25	264	5	
NR222 Control	rde-1(ne219); kzIs9 [lin-26p::nls::GFP + lin-26p::rde-1) + rol-6(su1006)]	Hypodermis-specific RNAi	15.12 ± 0.26	120	2	0.65
NR222 *ahr-1* RNAi			15.21± 0.29	120	2	
NL2098 Control	rrf-1(pk1417)	germline-specific RNAi	14.16 ± 0.34	120	2	0.89
NL2098 *ahr-1* RNAi			13.98 ± 0.34	120	2	
NL2550 Control	ppw-1(pk2505)	RNAi only in somatic tissues	15.92 ± 0.53	120	2	0.19
NL2550 *ahr-1* RNAi			15.25 ± 0.40	120	2	
WM118 Control	rde-1(ne300); neIs9 [myo-3::HA::RDE-1+ pRF4(rol-6(su1006)]	muscle-specific RNAi	11.91 ± 0.29	120	2	0.27
WM118 *ahr-1* RNAi			11.44 ± 0.29	120	2	
VP303 Control	rde-1(ne219); kbIs7 [nhx-2p::rde-1 + rol-6(su1006)]	intestine-specific RNAi	16.52 ± 0.33	120	2	0.72
VP303 *ahr-1* RNAi			16.78 ± 0.32	120	2	
TU3401 Control	sid-1(pk3321); uIs69[pCFJ99(myo-2p::mCherry + unc-119p::sid-1]	nervous system specific RNAi	12.47 ± 0.23	180	3	0.11
TU3401 *ahr-1* RNAi			13.03 ± 0.24	180	3	
TU3311 Control	uIs60[Punc119::YFP; Punc119::sid-1]	RNAi enhanced in the nervous system	15.87 ± 0.37	180	3	0.003
TU3311 *ahr-1* RNAi			14.11 ± 0.37	180	3	
CL6114 Control	nre-1(hd20) lin-15b(hd126)	RNAi hypersensitive, effective RNAi in the nervous system	12.78 ± 0.22	120	2	0.80
CL6114 *ahr-1* RNAi			12.94 ± 0.20	112	2	

To test, whether *ahr-1* RNAi has a similar effect when using OP50, I transformed OP50(xu363) [122] with *ahr-1* isolated from HT115(*ahr-1*) (Figure S 2). I then fed wild-type worms and TU3311 with OP50(L4440) and OP50(*ahr-1*) and analyzed life- and healthspan. Very surprisingly, using *ahr-1* RNAi in an OP50 background strongly extended lifespan and

healthspan of wild-type animals (Figure 45E - F) but it did not affect lifespan and healthspan in TU3311 (Figure 45G - H). TU3311 animals had problems with internal hatching on OP50(L4440) resulting in 47 % of the animals to be censored because of internal hatching. Moreover, TU3311 worms feeding on OP50(L4440) were much smaller than TU3311 feeding on HT115(L4440). Both phenotypes, the internal hatching, and the smaller body size were lost on OP50(*ahr-1*) and TU3311 on OP50(*ahr-1*) looked like TU3311 on an HT115 diet. The internal hatching on OP50(L4440) was also observed in the wild-type but to a lesser extent. The survival analysis with the *ahr-1* RNAi is in agreement with the gene expression data in the previous chapter and indicate inverse functions of *ahr-1* knock-down versus knock-out possibly due to residual AHR-1 activity in the silenced animals or to gain-of-function alleles of the *ahr-1* mutant. These and other potential explanation are currently being investigated.

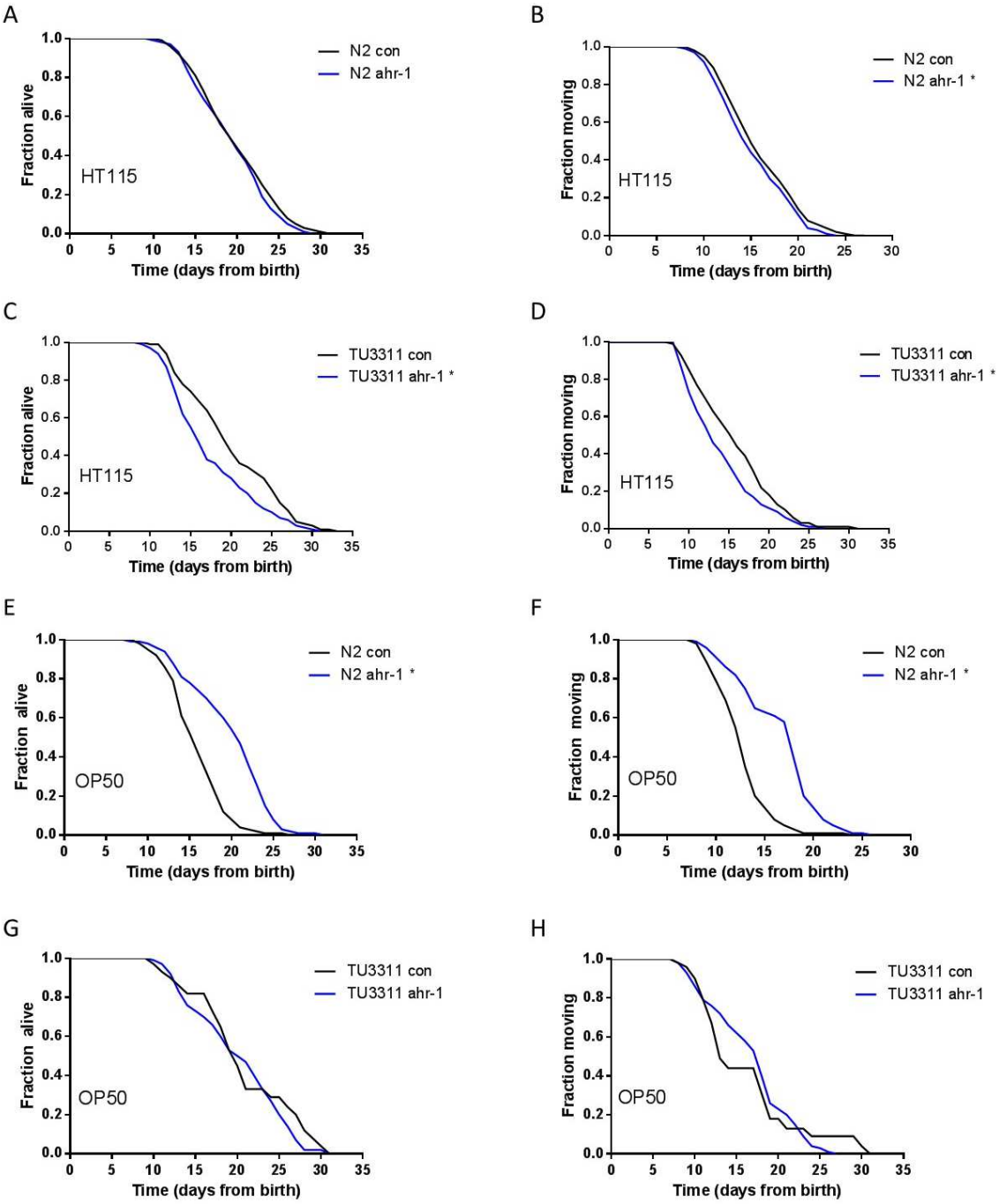

Figure 45 *ahr-1* RNAi in the nervous system affects healthy aging with opposite effects depending on the bacterial diet. A – B) Kaplan Meier curves of wild-type worms treated with control or *ahr-1* RNAi on an HT115 diet. Pooled data of 5 independent experiments are shown. * p-value < 0.05 *vs.* con, statistical test: Log-rank test. C – D) Kaplan Meier curves of worms with enhanced RNAi efficiency in the nervous system treated with control or *ahr-1* RNAi on an HT115 diet. Pooled data of 3 independent experiments are shown. * p-value < 0.05 vs. con, statistical test: Log-rank test. E – F) Kaplan Meier curves of wild-type worms treated with control or *ahr-1* RNAi from eggs on an OP50 diet. Pooled data of 2 independent replicates are shown. * p-value < 0.05 vs. con, statistical test: Log-rank test. G – H) Kaplan Meier curves of worms with enhanced RNAi efficiency in the nervous system treated with control or *ahr-1* RNAi on an OP50 diet. Pooled data of 2 independent replicates are shown. * p-value < 0.05 vs. con, statistical test: Log-rank test. See Table S 9 for detailed information.

Curcumin treatment leads to the differential expression of cytochrome P450 genes in an AHR-1-dependent manner

In the next step, since *cyps* are primary targets of mammalian AHR, but I could not investigate their expression in response to curcumin due to its intrinsic fluorescence activity, I wanted to understand whether curcumin affects the expression profile of *cyp*s in an AHR-1-dependent manner. I thus assessed the expression of *cyp*s using qPCR. I performed qPCR for genes of the CYP family, using 3-days old worms either grown on DMSO or curcumin. *C. elegans* possesses a total of 83 *cyp* genes, out of which 10 are pseudogenes. I tried to optimize the conditions for all remaining 73 genes but could only find suitable conditions for 47 genes. Out of these 47 *cyp*s, only *cyp-13*B1, a homolog of human *Cyp3a4,* showed statistically significant changes in the mRNA expression. The mRNA levels of *cyp-13B1* were increased 14-fold in curcumin-treated wild-type and 36-fold in control treated *ahr-1(ju145)* compared to control treated wild-type (Figure 46A). Also, *cyp-13B1* levels were strongly reduced in *ahr-1(ju145)* treated with curcumin compared to control *ahr-1(ju145)* and wild-type on curcumin. Interestingly, Pietsch *et al.* [109] also found *cyp-13B1* to be induced by quercetin, which is an AhR inhibitor in mammals.

Curcumin had the tendency to induce also other genes of the *cyp* family, although the changes were not statistically significant. Of particular interest might be *cyp-13A1*, *cyp-14A2*, *cyp-31A3*, *cyp-33C8*, *cyp-33E2*, *cyp-36A1* and *cyp-43A1.* In the wild-type, curcumin treatment increased the mRNA expression of *cyp-13A1* 4-fold, while there was no change in *cyp-13A1* on *ahr-1(ju145)* in response to curcumin (Figure 46A). The mRNA expression of *cyp-14A2* was increased 6-fold by curcumin in the wild-type, and 8-fold in *ahr-1(ju145)* compared to wild-type, while there was no change in *cyp-14A2* expression upon curcumin treatment in *ahr-1(ju145)* (Figure 46B). These data suggest that *cyp-14A2* is modulated in the same way by curcumin and AHR-1 loss of function and that the increase in *cyp-14A2* expression upon curcumin treatment might be dependent on AHR-1. I obtained very similar results for the expression of *cyp-31A3* with a 4-fold increase in expression in curcumin-treated wild-type and a 6-fold increase in control treated *ahr-1(ju145)* (Figure 46C). Also, *cyp-33C8* was induced in *ahr-1(ju145)* and curcumin-treated wild-type, but in contrast to *cyp-14A2* and *cyp-31A3,* it remained to be slightly inducible by curcumin in *ahr-1(ju145)* (Figure 46D). *Cyp-33E2* and *cyp-36A1* instead were, similar to *cyp-13A1*, only increased in curcumin-treated wild-type, but there was no difference between wild-type and *ahr-1(ju145)* (Figure 46D and F). Since there was no difference between *ahr-1(ju145)* on control conditions and curcumin, these genes might be regulated by AHR-1 in response to curcumin. *Cyp-43A1* was increased in wild-type treated with curcumin and to a lesser extent on *ahr-1(ju145)* control, while curcumin treatment of *ahr-1(ju145)* reduced the levels of mRNA to wild-type control levels. The only *cyps* with a tendency of being reduced after curcumin treatment were of the *cyp-35* class. Genes of this class have

been shown previously to be induced by xenobiotics [209]. Curcumin treatment reduced the expression of *cyp-35A2*, *cyp-35A4*, and *cyp-35C1* with relative expression levels of 0.48, 0.19 and 0.44 respectively (Figure 46F). Loss of AHR-1 function instead did not have any effect on their expression and the reduction of these genes by curcumin was independent of AHR-1.

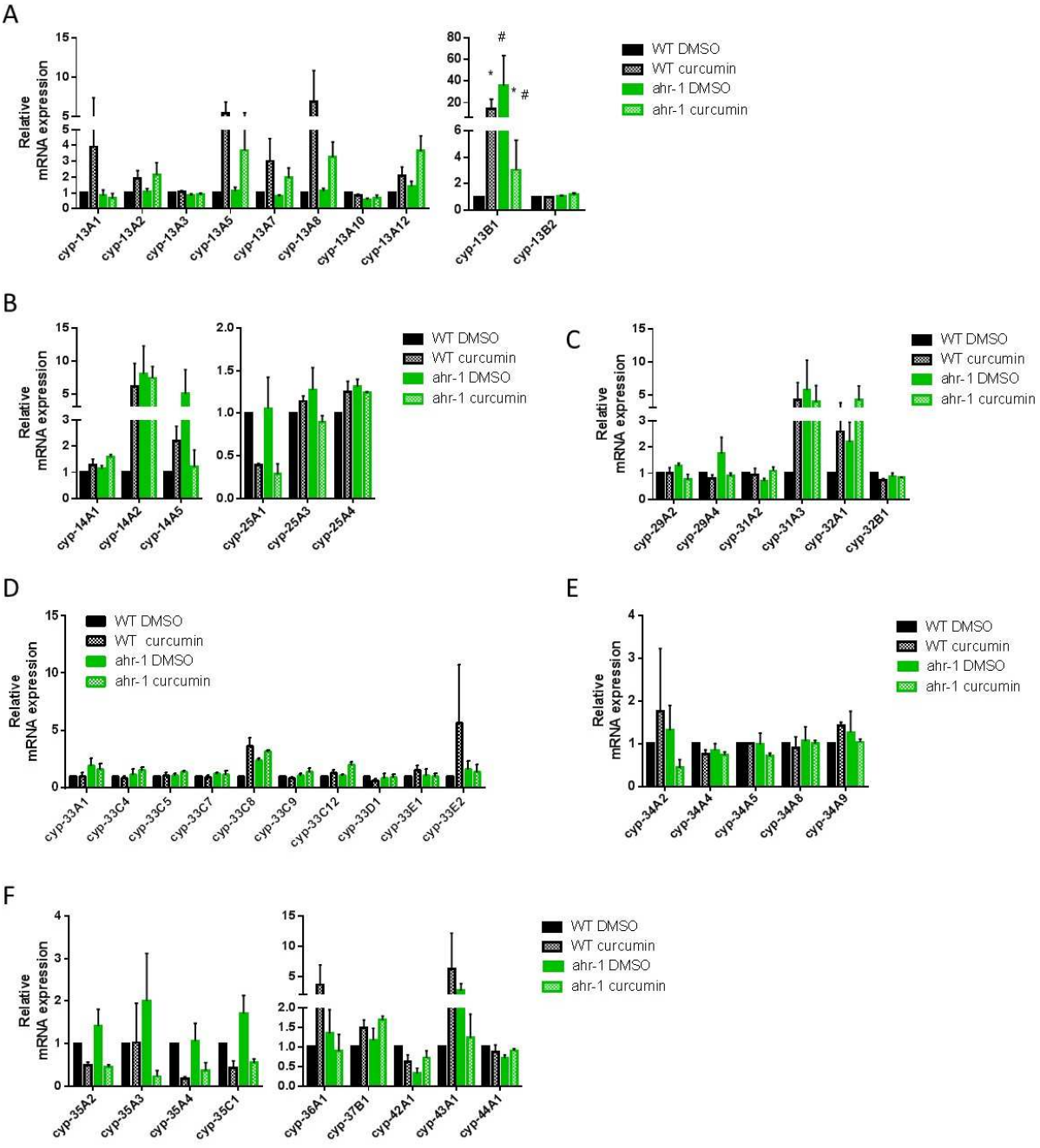

Figure 46 Relative mRNA expression of *cyps* in wild-type and *ahr-1(ju145)* treated with DMSO or curcumin. A) *cyp-13*, B) *cyp-14* and *cyp-25*, C) *cyp-29*, *cyp-31*, and *cyp-32*, D) *cyp-33*, E) *cyp-34*, and F) cyp-35, *cyp-36*, *cyp-37*, *cyp-43*, and *cyp-44*. Bars show mean ± SEM of the relative expression normalized to WT DMSO of each replica. Pooled data of 3 independent experiments are shown. * p-value < 0.05 *vs.* DMSO, # p-value < 0.05 *vs.* WT, statistical test: Two-way ANOVA with Tukey's multiple comparisons test.

Genes induced by curcumin are mainly AHR-1-dependent

Finally, to understand, whether also genes other than *cyp*s are differentially expressed by curcumin in an AHR-1-dependent manner, I performed a microarray analysis as an unbiased approach. I collected 5 replicates of wild-type and *ahr-1(ju145)* either supplemented with curcumin or DMSO. The microarray analysis revealed that out of the roughly 30.000 genes investigated, 80 genes were up- and 281 down-regulated in *ahr-1(ju145)* compared to wild-type on DMSO (Figure 47). The change in gene expression was low for all the tested conditions and rarely genes were differentially expressed more than 2-fold. Among the 10 strongest up-regulated genes were genes involved in carbohydrate binding, while there were mainly transcription factors among the top 10 down-regulated genes (Table 9). The strongest overexpressed gene was *irld-35*, a gene coding for an Insulin/EGF-Receptor L Domain protein. While the strongest under-expressed gene was R02F11.1 which is expressed in the pharynx and neurons and is affected by different compounds including D-glucose, neurotoxins, and resveratrol [230]. Also the transcription factor ATF-2, which negatively regulates the transcription of the autophagy genes *lgg-1* and *bec-1* were among the strongest under-expressed genes. Although not among the strongest differentially expressed genes, another autophagy-related gene, *pha-4*, was downregulated in *ahr-1(ju145)* (logFC - 0.60), suggesting that autophagy might be one of the molecular mechanisms affected by AHR-1.

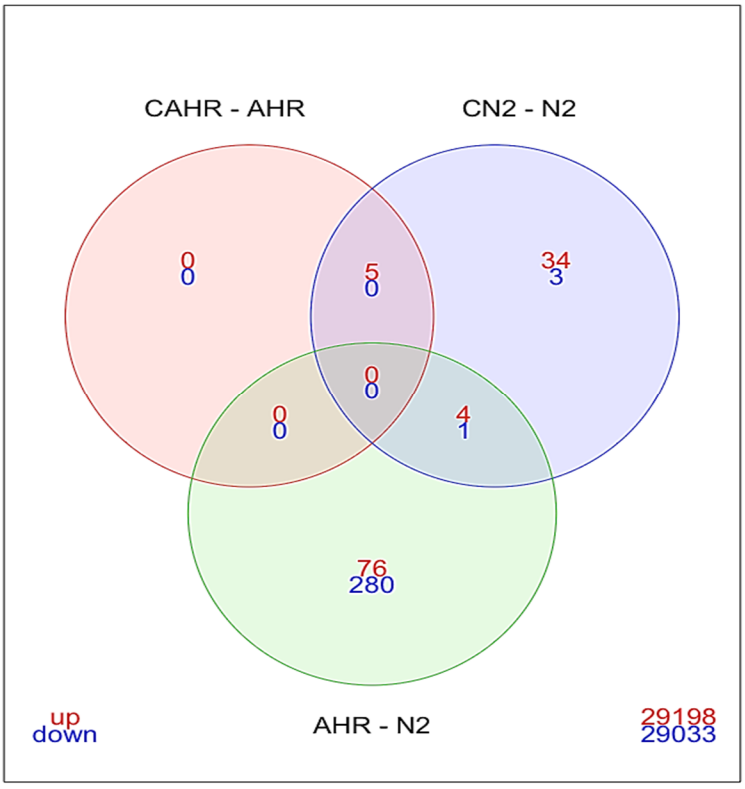

Figure 47 Venn diagram of differentially expressed genes in the microarray. To increase the number of genes, a p-value of 0.10 was chosen for significance. The value in the right lower corner: genes on the array, which were not differentially expressed. CAHR = *ahr-1(ju145)* on curcumin, AHR *ahr-1(ju145)* on DMSO, CN2 = wild-type on curcumin, N2 = wild-type on DMSO.

Table 9 List of the most robust over-/under-expressed genes in *ahr-1 vs.* WT on DMSO. See Table S 12 for a full list of differentially expressed.

Gene Name	***Gene class***	***Molecular function***	***logFC***	***adj.P.Value***
irld-35	Insulin/EGF-Receptor L Domain protein	unknown	1.968	0.0019
clec-209	C-type Lectin	carbohydrate binding	1.882	0.0182
F56A4.2	unknown	unknown	1.882	0.0182
C01B4.6	unknown	catalytic activity, isomerase activity, carbohydrate binding	1.671	$9.3 * 10^{-9}$
Y19D10A.16	unknown	catalytic activity, aldose-1-epimerase activity, isomerase activity, carbohydrate binding	1.671	$9.3 * 10^{-9}$
F56A4.3	unknown	unknown	1.660	0.0013
srd-61	Serpentine Receptor, class D	unknown	1.614	0.0001
srd-75	Serpentine Receptor, class D	unknown	1.614	0.0001
C01B4.7	unknown	unknown	1.605	0.0028
Y19D10A.4	unknown	transmembrane transporter activity	1.605	0.0028
R02F11.1	unknown	unknown	-2.308	0.0312
hbl-1	HunchBack Like	RNA polymerase II regulatory region sequence-specific DNA binding, RNA polymerase II transcription factor activity, sequence-specific DNA binding, transcription factor activity, metal ion binding	-2.013	0.0171
atf-2	cAMP-dependent transcription factor	RNA polymerase II regulatory region DNA binding, transcriptional repressor activity, RNA polymerase II core promoter proximal region sequence-specific binding, transcription factor activity, protein binding	-1.958	0.0227
lpr-4	Lipocalin-related protein	unknown	-1.834	0.0227
K04H4.2	unknown	chitin binding	-1.831	0.0248
egl-46	Egg-laying defective	RNA polymerase II transcription factor activity, sequence-specific DNA binding, RNA polymerase II transcription factor binding	-1.823	0.0406
T20F5.4	unknown	unknown	-1.803	0.0400
ptr-4	Patched related family	unknown	-1.766	0.0162
lpr-5	Lipocalin-related protein	unknown	-1.752	0.0227
dyf-7	Abnormal dye filling	protein self-association	-1.743	0.0227

The comparison between curcumin- and DMSO-treated wild-type worms showed 43 up- and 4 down-regulated genes (Figure 47). Of these in 47 genes, only 5 genes were also differentially expressed between curcumin- and DMSO-treated *ahr-1(ju145)*, indicating that most of the genes were regulated by curcumin in an AHR-1-dependent manner. Genes up-regulated in an AHR-1-dependent manner had mainly transferase activities. The gene with the most robust AHR-1-dependent induction was H43E16.1 (Table 10), which is expressed in the intestine and neurons and is affected by different compounds including rotenone and quercetin [230]. In line with the qPCR studies, *cyp-13A5* was overexpressed in curcumin-treated wild-type in the microarray. The gene with the strongest AHR-1-dependent suppression was instead *lys-7*, which encodes for a lysozyme required for the innate immune response [230]. Together with *lys-7, cyp-35A3* and C14A4.9 were suppressed by curcumin in an AHR-1-dependent manner. Interestingly, *cyp-35A5* is inducible by different xenobiotics while indole and quercetin affect C14A4.9 expression [230], and these compounds are all known to affect AhR activity in mammals.

Table 10 List of the strongest over-/under-expressed genes in WT DMSO *vs.* WT curcumin, but not in *ahr-1 vs. ahr-1* curcumin. Gene class and molecular function were extracted from wormbase. A full list of differentially expressed genes can be found in Table S 13.

Gene name	***Gene class***	***Molecular function***	***logFC***	***adj.P.Value***
H43E16.1	unknown	unknown	1.533	0.0215
numr-1	Nuclear localized metal responsive	unknown	1.423	0.0339
mul-1	Mucin-like	unknown	1.341	0.0293
oac-14	O-acyltransferase homolog	transferase activity, transferring acyl groups other than amino-acyl groups	1.239	0.0852
F58B4.5	unknown	unknown	1.214	0.0297
comt-4	Catechol-O-methyl-transferase	O-methyltransferase activity	1.171	0.0289
F09C8.1	unknown	hydrolase activity, acting on ester bonds	1.078	0.0293
ugt-48	UDP-glucuronosyl-transferase	calmodulin binding, glucuronosyltransferase activity, UDP-glycosyltransferase activity, transferase activity, transferring hexosyl and glycosyl groups	1.069	0.0339
cyp-13A5	Cytochrome P450	monooxygenase activity, metal ion binding, heme binding, oxidoreductase activity	1.055	0.0568
T19C9.8	unknown	unknown	0.964	0.0838
lys-7	Lysozyme	unknown	-1.538	0.0838
cyp-35A5	Cytochrome P450	monooxygenase activity, metal ion binding, heme binding, oxidoreductase activity, steroid hydroxylase activity	-1.082	0.0866
C14A4.9	unknown	unknown	-0.546	0.0787

Curcumin treatment induced 5 genes in the wild-type and *ahr-1(ju145)*: *pgp-1*, *clec-169*, ZK742.3, C40H1.8, and *clec-57* (Table 11). The P-glycoprotein PGP-1 is involved in the transport of xenobiotics, and toxic bacterial metabolites [230]. The c-type lectins *clec-169* and *clec-57*, as well as C40H1.8, are affected by different compounds of which tryptophan, indole, and bisphenol A are in common [230]. Interestingly, most of the genes induced by curcumin in both wild-type and *ahr-1(ju145)* were stronger induced than the genes only induced in the wild-type, but not in *ahr-1(ju145)*.

Table 11 List of genes differentially expressed between WT control vs. WT curcumin and AHR control vs. AHR curcumin. Gene class and molecular function were extracted from wormbase.

Gene name	***Gene class***	***Molecular function***	***log FC***	***adj.P.Value***
pgp-1	P-glycoprotein related	nucleotide binding, ATP binding, xenobiotic-transporting ATPase activity, ATPase activity, efflux transmembrane transporter activity, hydrolase activity	2.735	3.1E-08
clec-169	C-type lectin	carbohydrate binding	2.170	1.1E-04
ZK742.3	unknown	catalytic activity, FMN binding, oxidoreductase activity	2.056	7.5E-07
C40H1.8	unknown	Hydrolase activity	2.032	1.8E-02
clec-57	C-type lectin	carbohydrate binding	0.958	3.8E-03

Remarkably, other 5 genes were regulated similarly in curcumin-treated wild-type compared to DMSO-treated wild-type and *ahr-1(ju145)* on DMSO compared to wild-type on DMSO, suggesting that curcumin might act similar to *ahr-1* suppression. These genes were: *slc-17.5*, *ugt-9*, *nhr-239*, *ugt-29*, and C14A4.9 (Table 12). Of these especially the *ugt*s are of special interest since, similar to *cyp*s, they are detoxification enzymes. Besides the 2 above-mentioned *ugt*s, *ugt-57* was repressed in *ahr-1(ju145)* compared to wild-type, and *ugt-48* was induced in curcumin-treated wild-type.

Table 12 List of genes regulated in the same way on WT control vs. WT curcumin and WT control vs. *ahr-1* control. Gene class and molecular function were extracted from wormbase.

Gene name	***Gene class***	***Molecular function***	***LogFC WT con vs. WT cur***	***LogFC WT con vs. AHR con***
slc-17.5	Solute carrier homolog	transmembrane transporter activity	0.639	0.456
ugt-9	UDP-glucuronosyl-transferase	glucuronosyltransferase activity, transferase activity, transferring hexosyl groups	0.573	0.409
nhr-239	Nuclear hormone receptor	metal ion binding, zinc ion binding, transcription factor activity, sequence-specific DNA binding	0.426	0.392
ugt-29	UDP-glucuronosyl-transferase	glucuronosyltransferase activity, transferase activity, transferring hexosyl and glycosyl groups	0.357	0.340
C14A4.9	unknown	unknown	-0.546	-0.629

I also used the data from the microarray to understand in which biological processes AHR-1 might be involved. For this, I analyzed the list of differentially expressed genes for the enrichment of specific Gene-ontology (GO) terms. To reduce the redundancy of GO terms, I used fused GO terms [205]. The full list of enriched GO terms with the associated genes before and after fusion can be found in Table S 14 and Table S 15. Analysis of the GO terms showed that genes differentially expressed in *ahr-1(ju145)* compared to wild-type were enriched in terms for the following biological processes: cell differentiation, regulation of transcription by RNA polymerase II, cuticle development, axogenesis, sex differentiation, homophilic cell adhesion via plasma membrane adhesion molecules, interneuron axon guidance, nucleosome assembly, neuron fate specification, and cell-matrix adhesion. Cell differentiation had the strongest enrichment with more than half of the differentially expressed genes between *ahr-1(ju145)* and wild-type, which are associated with a GO term belonging to this term (Figure 48A). Interestingly, 60 % of the genes associated to interneuron axon guidance were differentially expressed in *ahr-1(ju145)* compared wild-type, pointing out the role of AHR-1 in the nervous system (Figure 48B), as also supported by changes in genes involved in neuron fate specification. Another essential function of AHR-1 might be cell-cell interaction since 50 % of the genes associated with homophilic cell adhesion via plasma membrane adhesion molecules were altered in *ahr-1(ju145)*. In general, the GO terms enriched in *ahr-1(ju145)* support a role for AHR-1 in development and differentiation rather than detoxification as in mammals, thus possibly revealing novel and more ancestral role for this evolutionarily conserved transcription factor.

The analysis of GO term enrichment for the molecular function showed that AHR-1 mainly controls the expression of other transcription factors, with the GO term transcription regulatory region DNA binding, accounting for half of the molecular functions (Figure 49). The other half was shared by the GO terms protein heterodimerization activity and peptidase inhibitor activity. Transcription factor genes regulated by AHR-1 were *atf-2*, *atf-8*, *blmp-1*, *ceh-30, ces-1*, *ces-2*, *cfi-1*, *egl-46*, *hbl-1*, *pha-4*, *pros-1*, *sox-2, ttx-1*, and *unc-86* (Table S 16). Many of these transcription factors are expressed or have functions in the nervous system. Overall, the GO term enrichment for molecular functions is in agreement with the complexity of action of the AHR in response to different factors and may reveal novel molecular mechanisms underlying its differential activities via regulation of other transcription factors or proteins.

A

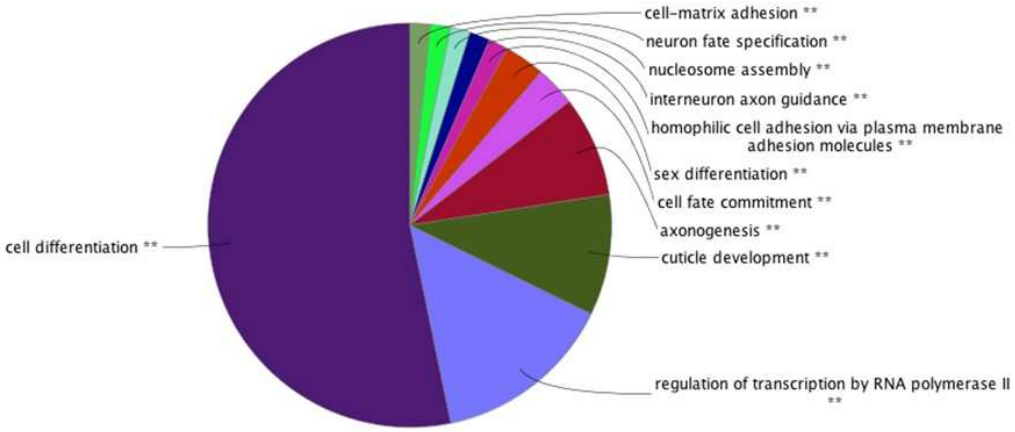

B

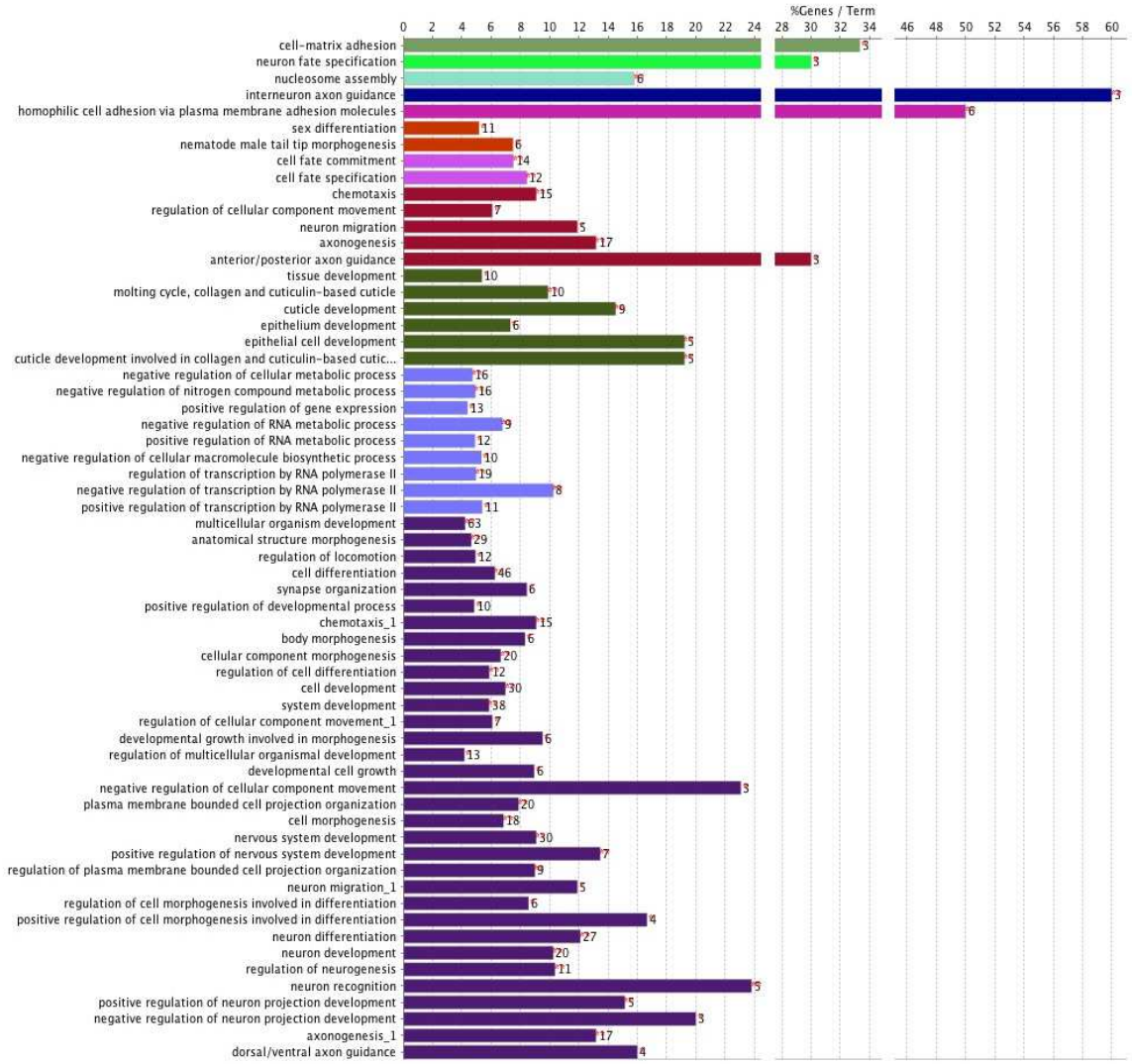

Figure 48 Gene Ontology (GO) enrichment for biological processes after GO term fusion. A) Pie chart of fused enriched GO terms in *ahr-1(ju145) vs*. wild-type. B) Chart showing the percentage of genes enriched compared to genes associated with this GO term. Colors of the bars represent the colors in the pie chart of the fused GO terms. The number of genes differentially expressed for each GO term is shown beside the bars.

A

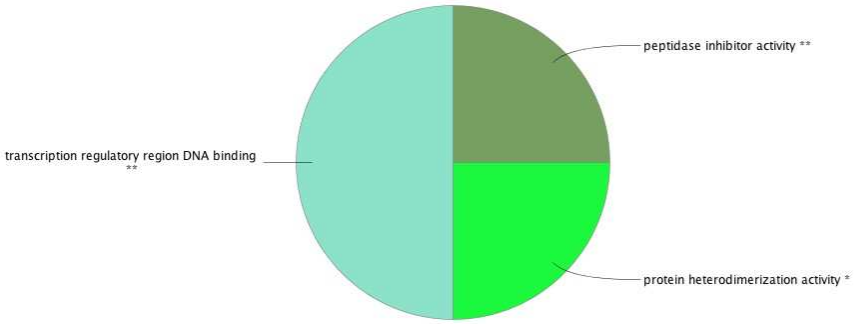

B

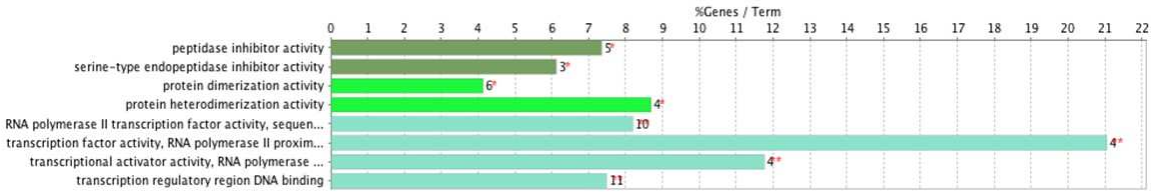

Figure 49 Gene Ontology (GO) enrichment for molecular functions after GO term fusion. A) Pie chart of fused enriched GO terms in *ahr-1(ju145)* vs. wild-type. B) Diagram showing the percentage of genes enriched compared to genes associated with this GO term. Colors of the bars represent the colors in the pie chart of the fused GO terms. The number of genes differentially expressed for each GO term is shown beside the bars.

5. Discussion

Aim 1 Identification of potential AHR-1 modulators

The first aim of this study was to determine whether different classes of mammalian AhR modulators affect life traits of *C. elegans* in an AHR-1-dependent fashion. I therefore systematically tested environmental factors (BaP), dietary factors (curcumin), host-mediated factors (UVB) and factors produced by microbes (different *E. coli* diets).

Benzo(a)pyrene (BaP) affects development and lifespan in an AHR-1-dependent manner, under specific conditions

In my studies, I used the PAH benzo(a)pyrene as a classical AhR ligand to test whether it affects life traits of *C. elegans* depending on AHR-1. BaP is an environmental pollutant produced by incineration processes, cigarette smoke, and charcoal grilled meat. Exposure to BaP causes a variety of cancers as well as neurotoxicity in rodents and humans [231]. Further, BaP exposure negatively influences the lifespan in mice [150]. The toxic effects of BaP are known to be mediated by the AhR in vertebrates, but the exact mechanisms of AhR-mediated BaP toxicity remain elusive. The neurodegenerative effects of BaP are conserved in vertebrate species since also zebrafish develop symptoms similar to AD and PD when chronically exposed to low doses of BaP [151]. A recent study showed moreover, that BaP has AhR-mediated transgenerational effects on neurobehavioral and physiological functions, leading to hyper locomotor activity, a lower heartbeat rate and decreased mitochondrial function [232]. While the toxic effects of BaP are well-studied in vertebrates, few is known in invertebrate model organisms. Only a couple of studies describing the impact of BaP in *C. elegans* exist. These studies revealed that exposure to BaP causes oxidative stress [233], while there is conflicting evidence about the genotoxicity of BaP [234, 235]. Further, BaP exposure induces the expression of specific CYP genes in *C. elegans* [209, 236].

Here, I showed that BaP affects the development of *C. elegans* in a concentration-dependent manner. The developmental toxicity was mainly independent on AHR-1 function since wild-type and *ahr-1(ju145)* were modified in a similar way on most concentrations. In line with that, also the induction of *cyp-35B1* was independent on AHR-1. The BaP-dependent induction of *cyp-35B1* has also been previously described [209]. Moreover, the results are coherent with the studies of Jones and co-workers, who found that *ahr-1* RNAi does not prevent the induction of phase I and II detoxification genes (*cyp, gst,* and *ugt*) by different xenobiotics [181]. Together with previous studies showing that classical AhR ligands like dioxin do not bind to the *C. elegans* AhR homolog [174, 175, 237], the data on BaP suggest that xenobiotics might not be ligands of AHR-1. This supports the hypothesis of Powell-Coffman and colleagues that the

ancestral function of the AhR is not the metabolism of xenobiotics [174]. On the other hand, a concentration of 1 µM BaP had *ahr-1*-dependent effects on the development and the lifespan of worms, suggesting that at least some concentrations have *ahr-1*-dependent effects. Since BaP has neurodegenerative effects, and loss of *ahr-1* function affected the aggregation and toxicity of polyQ in a model for neurodegenerative diseases in my studies, it would be interesting to investigate the effect of BaP on polyQ aggregation in *ahr-1* proficient and *ahr-1* deficient worms.

Curcumin extends healthy lifespan in an AHR-1-dependent manner

Besides the xenobiotic ligands, other classes of AhR ligands/modulators had not been studied for their dependency on AHR-1 in *C. elegans*. Here, I used curcumin to investigate, whether dietary AhR modulators also affect aging in *C. elegans* in an AHR-1-dependent manner. Curcumin is a well-described polyphenolic nutritional AhR modulator. It is the primary component of turmeric, a spice frequently used in the Indian and Asian cuisine. Although it has been used in traditional medicine for thousands of years, its health-promoting effects have been first scientifically proven as late as the 1970s [238]. Up to date, several studies exist, describing the effect of curcumin on the aging process and the progression of age-associated diseases. Its health-promoting effects are described in different species including invertebrate species like *C. elegans* and *Drosophila*, in rodent species like mice and rats, as well as in humans [239]. Especially the protective effects of curcumin in age-related neurodegenerative diseases seem to be well-conserved in other species since curcumin reduces the pathology in models of AD in nematodes, flies, and mice [101, 153, 154]. It shows as well protective effects in animal models for PD in flies and mice [240, 241]. While the effects of curcumin on the AhR are well-studied in mammalian model systems, there is no firm evidence so far that curcumin might have similar effects in other species. Only a single study in *Drosophila* showed that curcumin and quercetin ameliorated the genotoxic impact of monocyclic aromatic hydrocarbons [242].

In this study, I found that curcumin increases lifespan and healthspan depending on AHR-1 without affecting the brood size. Interestingly, curcumin and AHR-1 loss of function lead to a similar extent of lifespan extension compared to untreated wild-type, suggesting that curcumin might act as an AHR-1 inhibitor. In fact, some *cyp* genes, namely *cyp-13B1*, *cyp-14A2*, *cyp-31A1*, *cyp-32A1*, *cyp-33C8*, and *cyp-43A1* had a similar increase in expression on curcumin and *ahr-1(ju145).* Moreover, microarray studies showed that most of the genes differentially regulated between wild-type on DMSO and wild-type on curcumin were not altered upon curcumin treatment in *ahr-1(ju145)*. Altogether, this indicates a strong dependency of lifespan-extending effects of curcumin on AHR-1. In further studies it has to be clarified, which of the differentially expressed genes contributes to the lifespan extension of curcumin.

Surprisingly, in my experiments, curcumin increased the number of polyQ aggregates in aged worms, while, at the same time, it extended the lifespan and healthspan of polyQ-expressing worms. This somehow uncouples the correlation between aggregation and lifespan shortening of polyQ aggregates. The increase in aggregation was dependent on AHR-1 since there was no increase in the number of aggregates in curcumin-treated *ahr-1* loss of function animals. As both, *ahr-1* loss of function and curcumin treatment increased the number of aggregates to the same extent, also here an AHR-1 inhibitory function of curcumin is likely. In the literature, the effect of curcumin on the number of polyQ aggregates is conflicting, while it increased the aggregation of GFP labeled polyQ-expanded huntingtin [243], it showed a preventative effect against polyQ aggregation in yeast [244]. Although the increase in aggregates was AHR-1 dependent, curcumin increased the lifespan and healthspan of polyQ-expressing animals independent of AHR-1. This further shows that aggregation and lifespan extension might be uncoupled and work through different pathways. In fact, besides being an AhR ligand, several other signaling pathways and molecular targets are influenced by curcumin (*e.g.*, Nrf2, β-catenin, NF-κB, p38 MAPK). Especially a study in PD mice suggests that the beneficial effects of curcumin are dependent on the JNK pathway, an evolutionary conserved mitogen-activated protein kinase (MAPK) pathway [241]. It would be therefore interesting to test whether the *C. elegans* JNK homolog JNK-1 is required for the lifespan extension of curcumin-treated polyQ-expressing worms and whether there might be a crosstalk between AHR-1 and JNK-1.

AHR-1 protects against UVB stress

UV light is ubiquitously in the environment and can be considered an environmental factor affecting human health and aging. UVB light has a wavelength of 280 – 315 nm and can penetrate human skin, where it causes the formation of the tryptophan photoproduct FICZ. The reactions leading to the creation of FICZ are quite well understood and require the presence of tryptophan and its conversion to the FICZ precursor indole-3-acetaldehyde (I3A) [156]. FICZ, in turn, activates the AhR signaling pathway, which leads to the dissociation of AhR co-factors, the nuclear localization of the AhR and eventually AhR target gene expression. Target genes of the UVB activated AhR signaling pathway are *Cyp1a1* and *Cox-2*, a cyclooxygenase [139]. Interestingly, both genes do not have direct orthologs in *C. elegans* [245, 246]. Upon UVB stress, a crosstalk between the EGFR signaling pathway and the AhR can be observed in mammals [139]. The activation of the AhR pathway in response to UVB is evolutionarily conserved in vertebrates since UVB light and FICZ induce CYP expression also in zebrafish [247, 248]. Despite the evolutionary function of the AhR pathway in UVB response in vertebrates, few is known about the effect of UVB in invertebrate model organisms. Studies in *C. elegans* have mainly focused on the effect of UVC on germline apoptosis and DNA damage,

while only very few groups used UVB radiation. They found that in *C. elegans*, UVB irradiation leads to a dose-dependent increase in larval mortality and germ cell apoptosis [212].

Here, I used UVB to test, whether host-mediated factors, which activate AhR in mammals, might have AHR-1-dependent effects on *C. elegans* as well. In previous studies I had shown that *ahr-1(ju145)* is more sensitive to the UVB-induced reduction of fertility, suggesting a protective role of AHR-1 against UVB stress. I hypothesized that the reduced fertility might be due to the increased apoptosis in UVB-irradiated *ahr-1(ju145)*. Indeed, I found that AHR-1 loss of function increased apoptosis under basal condition and upon UVB irradiation. Similar findings have been previously discovered in human keratinocytes and mice [213], suggesting a potentially conserved AHR-dependent UVB response between *C. elegans* and humans. Comparing the fold-induction of apoptosis between wild-type and *ahr-1(ju145)*, I found that UVB induces apoptosis to a greater extent in wild-type than in *ahr-1(ju145),* indicating that the increase in apoptosis might be partially dependent on AHR-1. Interestingly, also the data from the microarray support the observed increase in apoptosis since genes responsible for apoptosis are enriched in *ahr-1(ju145)* (Table S 14). Specifically, *ceh-30*, *cst-1*, *dre-1*, *rpm-1*, and *unc-129* were differentially expressed between wild-type and *ahr-1(ju145).* In mice, inhibition of AhR using resveratrol has chemopreventative effects upon UVB irradiation by inducing apoptosis [211]. I, therefore, hypothesized that curcumin supplementation might impact the fertility of UVB treated wild-type to a similar extent of AHR-1 loss of function. In my hands, the treatment with curcumin did not affect the fertility of UVB treated wild-type and *ahr-1(ju145)*. Whether it does instead affect apoptosis in *C. elegans* is not known and will be part of my further investigations.

AHR-1 influences lifespan in a diet-dependent manner

C. elegans and its gut microbes form an ecological unit, the holobiont. It is just recently that the interaction between bacterial diet and *C. elegans* has been the focus of studies. In this context, bacterial metabolites (folate, nitric oxide, and tryptophan, indole and vitamin B12) have been identified as critical modulators of the *C. elegans* biology [121, 128, 221, 249, 250]. As shown in this study and by other groups, already a slight difference in the bacterial diet by feeding the *E. coli* K-12 strain HT115 instead of the *E. coli* B strain OP50 can cause variations in the lifespan, stress resistance and age-associated diseases of worms [119, 121, 126].

In this study, I showed that AHR-1 influences the lifespan, healthspan, and heat stress resistance of *C. elegans* in a diet-dependent manner: Loss of AHR-1 function extended lifespan and healthspan on HT115, but not on OP50. The increase in lifespan on HT115 was accompanied by an increase in heat stress resistance in middle-aged and aged animals, but not in young animals. Also, on OP50 the heat stress resistance of *ahr-1(ju145)* was only

affected in middle-aged and aged worms, but in contrast to HT115, *ahr-1(ju145)* was more sensitive compared to wild-type. The age-dependent effect of AHR-1 loss of function is interesting and points out, that especially during aging the abundance of AHR-1 has a growing impact on the survival. This is supported by data from Sonowal *et al.*, who found that the expression of *ahr-1* is increased during aging [221].

Although AHR-1 is expressed in the nervous system and RNAi studies of this work showed that *ahr-1* RNAi in the nervous system influences aging, *ahr-1(ju145)* worms did not display any differences in the food race experiments. This indicates that sensory functions are probably not targeted by AHR-1. The pharyngeal pumping activity instead was increased in middle-aged and aged *ahr-1(ju145)* on HT115, but not on OP50. The analysis of the EPGs showed that only the pumping frequency, but not the amplitude, the pump duration, and the interpump interval (IPI) was altered in *ahr-1(ju145)* on HT115. In line with studies of Russell *et al.*, I found that the pharyngeal pumping frequency declines, while the pump duration and amplitude increase with aging [251]. The increased pumping activity of aged *ahr-1(ju145)* is likely due to a slower degeneration of the pharyngeal muscles [19-21]. Therefore, pumping and healthspan show together that muscle aging, but not aging of the nervous system might be affected by AHR-1. This data is somehow conflicting with my RNAi studies, which revealed that *ahr-1* RNAi in the nervous system, but not in other tissues (including muscles) affects aging.

To understand, whether bacterial metabolites might cause the differences in age-associated features of *ahr-1(ju145)*, I performed heat stress resistance tests on killed bacteria, and living bacteria supplemented with tryptophan. Experiments with killed bacteria indicated that in fact, bacterial metabolites might be responsible for the lifespan extension of *ahr-1(ju145)* on HT115 since wild-type and *ahr-1(ju145)* did not show any differences in heat stress resistance and lifespan on killed bacteria. Comparing the mean survival times from the different heat shock experiments, it appears that killing HT115 before seeding adjusts the heat stress resistance by decreasing the survival time of *ahr-1(ju145)* and not by increasing the survival time of wild-type. Since I did not see any beneficial effect of killed HT115 on the wild-type, I suppose that whatever is improving the survival time of *ahr-1(ju145)* on HT115 is not toxic. It might be a metabolite, which when degraded by AHR-1 or downstream AHR-1 target genes loses its beneficial effects. Interestingly, the comparison between the heat stress resistance of *ahr-1(ju145)* on killed versus living OP50 seems to be not altered. This suggests that whatever increases the survival of *ahr-1(ju145)* on HT115 is not (or only in low amounts) produced by OP50. Further, the unaltered heat shock resistance of *ahr-1(ju145)* on killed and living OP50 might indicate that OP50 does not produce any harmful metabolite that reduces the survival time of *ahr-1(ju145)*. Instead, a metabolite produced by OP50 might increase its survival in the

wild-type, since the survival of wild-type seems to be shortened on killed bacteria. This effect is likely dependent on the activity of AHR-1.

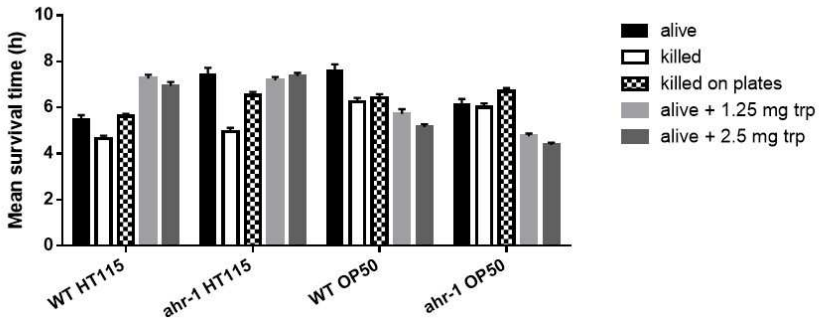

Figure 50 Overview of survival times of wild-type and *ahr-1(ju145)* on alive, killed, and tryptophan supplemented bacteria. Bars show the mean survival times with standard error of different heat shock experiments. No statistical evaluation was performed because the experiments were not performed simultaneously.

Also, the supplementation of tryptophan to living bacteria showed exciting results. Tryptophan is seemingly increasing the survival of wild-type on HT115 but shortening its survival on OP50 (Figure 50). Therefore, tryptophan supplementation has similar effects to *ahr-1* loss of function. Interestingly, it seems that tryptophan supplementation does not affect the survival time of *ahr-1(ju145)* on HT115, but further shortens it on OP50. The findings on HT115 are in agreement with a recent study, which shows that AHR-1 is required for the lifespan-extending effect of the tryptophan metabolite indole from the commensal gut bacterium *E. coli* MG1655* [221]. Moreover, an increased heat stress resistance and lifespan of tryptophan supplemented worms feeding on HT115 have been previously observed [252]. Interestingly, Gracida *et al.* found that on OP50 diet tryptophan results in an increased expression of *cyps*, *ugts*, and *gsts*, which I identified as potential AHR-1 target genes [128]. Altogether, there is evidence that bacterial tryptophan metabolites influence aging in an AHR-1 dependent, but since tryptophan supplementation did not abolish the differences in heat stress resistance between worms on the different diets, tryptophan metabolites are likely not the cause of the differences.

Mass spectrometry analysis reveals that HT115 might produce higher levels of tryptophan and indole-containing compounds

The data from the Mass spectrometry showed that there are differences in the metabolites produced by HT115 and OP50. The analysis of the compounds found in the media revealed differences in the amino acids/dipeptides Ala-Glu, Trp-Arg, and asparagine. While there is potentially a higher concentration of Ala-Glu in OP50 medium, HT115 might produce higher levels of Trp-Arg, and asparagine. The higher amount of Ala-Glu produced by OP50 is somehow surprising because worms feeding on OP50 have been found to have a much lower concentration of glutamate than on HT115 [123]. Interestingly, both amino acids extend lifespan when supplemented to HT115 [252]. Based on the experiments with killed bacteria, I

hypothesized that an OP50 metabolite might act as an AHR-1 modulator. The analysis of the chemical structure of Ala-Glu did not show similarities to known AHR-1 modulators, and Ala-Glu is thus probably not a direct ligand of AHR-1. Instead it might modulate the same pathway responsible for the lifespan-extending effects of *ahr-1* loss of function. Also, modifications of the Ala-Glu dipeptide by the digestive system of *C. elegans* are to be considered. Although Ala-Glu might not be a direct AHR-1 modulator, it would be interesting to study if Ala-Glu affects the lifespan of nematodes on HT115 and OP50 and whether this is mediated by AHR-1, *e.g.,* by crosstalk with another pathway.

From the mass spectrometry analysis, it became evident that HT115 might be producing compounds with similarities to AHR-1 modulators. In this context especially the production of Trp-Arg and indole-containing compounds, which could serve as AHR-1 ligands are of note. Supplementation of tryptophan, as well as arginine to HT115, extend the lifespan of *C. elegans* [252], and my experiments showed that tryptophan might cause as well an AHR-dependent increase in heat stress resistance (Figure 50). Therefore, it would be interesting to understand, whether the Trp-Ala dipeptide influences lifespan and gene expression of *cyps* and *ugts* in an AHR-1-dependent manner. Also, the influence of the indole containing compound on lifespan and gene expression would be an interesting topic, but further clarification by advanced MS analysis would be required to clearly identify that one of the indole-containing molecules is produced.

All in all, the experiments using different classes of mammalian AhR ligands in *C. elegans* have shown that many of the mammalian AhR modulators also affect *C. elegans* AHR-1. Although, it is not yet clear, whether these compounds act as direct AHR-1 ligands. Moreover, the existence of a functional ligand binding domain (LBD) of AHR-1 has not been shown yet. In collaboration with the laboratory of Laura Bonati (University of Milan) we did an *in silico* analysis of the AHR-1 PAS B domain, which, in principle, should carry the LBD. They found that the 3D structure and arrangement of the secondary structures of the PAS B domain are similar to those of AhR in mice, but there were differences in the size, shape, and amino acid composition of the cavities within the domain, and thus, in the property of the LBD (Figure 51). The cavity of the LBD was found to be very small and the binding of curcumin to the LBD could be excluded due to the size. It is therefore likely that the identified modulators influence AHR-1 signalling downstream of AHR-1 or by other mechanisms. It will be of further investigation to elucidate how UVB, curcumin and bacteria influence aging through AHR-1 if not by ligand binding. Interestingly, a ligand-independent but oxidative stress dependent activation of AhR has been also found in human keratinocytes [253]. Therefore, using *C. elegans* as a model

organism for AhR research could contribute to the better understanding of the (ligand-independent) functions of the AhR.

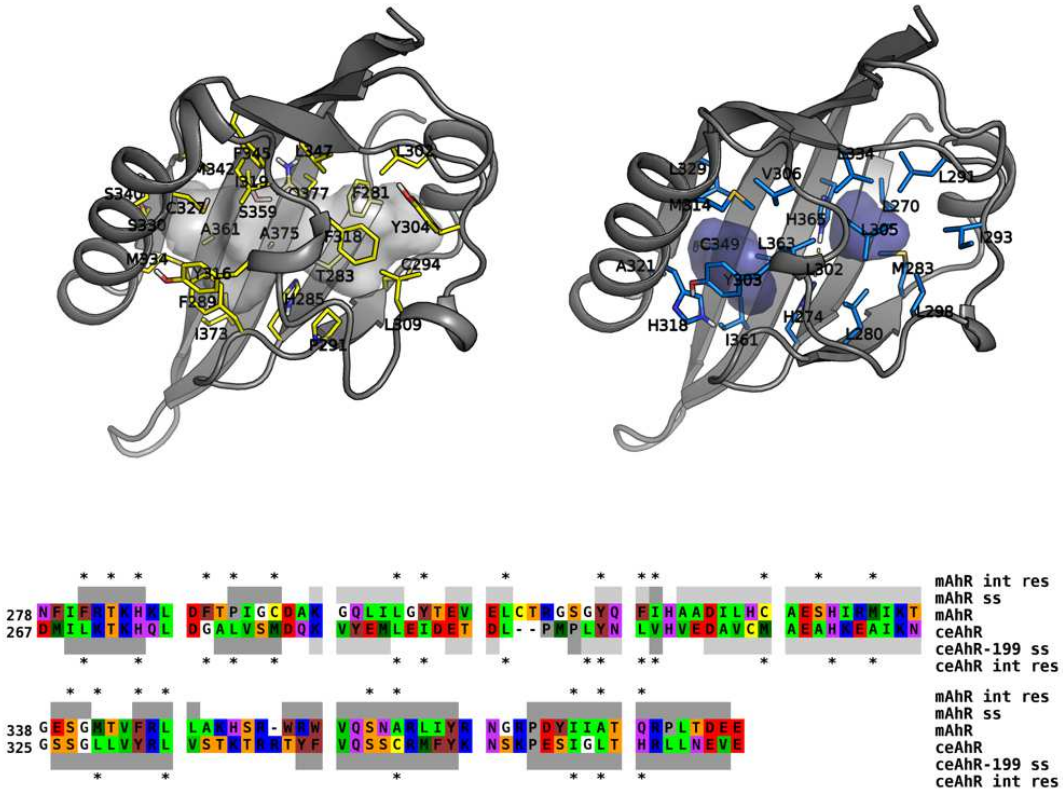

Figure 51 Models for homology and alignment of the PAS B domains of *C. elegans* AHR-1 (ceAhR) and murine AhR (mAhR). In the 3D structures, internal residues are shown as sticks and cavities as solvent-accessible surfaces. In the alignment, the secondary structures (obtained with DSSPcont) are shown in gray (helices in light gray and sheets in dark gray). Asterisks indicate the residues whose sidechains are inside the cavity (calculated with CASTp). Figure from Laura Bonati, University of Milan.

Aim 2 Impact of AHR-1 deficiency on aging and age-associated phenotypes

AHR-1 influences polyQ accumulation and toxicity independent of the diet

Although there have not been any studies directly showing a link between AhR and neurodegenerative diseases, it has been proposed that the interaction between ligands produced by the microbiota and the host AhR might be involved in the progression of neurodevelopmental and neurodegenerative diseases [164]. In *C. elegans* different *E. coli* diets influence the accumulation of misfolded proteins in models for AD, PD and polyQ disorders [126]. Therefore, I investigated whether diet has AHR-1-dependent effects in polyQ-expressing worms. I found that aged *ahr-1* mutant worms have an increased number of aggregates on both diets. Moreover, the size of the aggregates was increased in *ahr-1* loss of function worms. Interestingly, the differences in the number and the size of the aggregates were age-dependent and appeared only in aged worms. While the bacterial diet did not have any influence on the aggregate number in *polyQ;ahr-1*, in polyQ;wt an OP50 diet increased the number of aggregates in aged animals. An increase in aggregation on OP50 was also

noticed by Munos-Lonato et al. [126]. Although the increased aggregation was accompanied by an earlier onset of paralysis of polyQ worms in their hands [126], this effect was absent in my experiments and aggregation and paralysis were not correlated. Instead, the higher number of aggregates in *ahr-1* loss of function worms was accompanied by an increase in lifespan. On the one hand, this could mean that rather the degradation than the accumulation of polyQ causes toxicity and that loss of *ahr-1* leads to a lower toxicity of polyQ aggregates. Although, commonly the opposite is assumed protective effects of inclusions have been also observed in neuronal cells [254]. On the other hand, the increased aggregation could be also an artifact caused by the design of the transgenic $polyQ_{40}$ model. The used strain expressed fluorescently tagged $polyQ_{40}$ in the body wall muscles of the worms by using the *unc-54* promotor [63]. A recent study showed that *unc-54* and other muscle-specific genes show a decreased expression with age, starting as early as the first day of adulthood [255]. Of note, they found that the decrease in *unc-54* expression is slowed down in long-lived *daf-2* mutants. Therefore, it could be possible that *ahr-1* loss of function simply slows down the reduction of *unc-54* and cause a higher aggregation phenotype because of the stronger activity of the *unc-54* promotor. This is particularly interesting in the background of the age-dependent differences in $polyQ_{40}$ aggregation. To exclude this, experiments using the polyQ expressed under a different promoter (*e.g.,* using AM101, which expresses the polyQ in the neurons under the promotor *rgef-1* [66]) could be performed. Moreover, with regard to the increase in motility of *ahr-1(ju145)*, it would be interesting to investigate the activity of the *unc-54* promotor comparing wild-type and *ahr-1(ju145)* at different ages.

All in all, the potential influence of the AhR on polyQ aggregation and toxicity is a novel and relevant topic with regard to human neurodegenerative processes. After further proof of the meaningfulness with respect to the transgenic model, it would be an interesting topic for further investigation in other model organisms.

AHR-1 affects aging in a temperature-depending manner

The lifespan of *C. elegans* is dependent on the temperature and worms live shorter at higher temperatures and longer at colder temperatures [216]. While the interplay between genetics and temperature is still not very much investigated, a recent study showed that it is more the rule than the exception [216]. They specifically tested the lifespan at temperatures of 15, 20, and 25 °C and found that while some mutations robustly increase/decrease the lifespan at all temperatures, two third of the investigated strains showed an interplay between temperature and genetics.

In this study, I tested the lifespan of *ahr-1(ju145)* at 20 and 25 °C and found that while *ahr-1(ju145)* is long-lived compared to wild-type at 20 °C on an HT115, it lives shorter than wild-

type at 25 °C. Also, an OP50 diet shortened the lifespan of wild-type and *ahr-1(ju145)* at 25 °C. Miller *et al*. [216] found that protein quality control and heat stress mechanisms are essential for longevity at higher temperatures (25 °C), while immunity is important for lifespan extension at lower temperatures (15 °C). The shortened lifespan of *ahr-1(ju145)* and an OP50 diet might, therefore, be because of a decrease in protein quality control, which is suggested by the increased number of $polyQ_{40}$ aggregates. Interestingly, the difference in the number of polyQ aggregates between worms with wild-type and mutant *ahr-1* was reduced at 25 °C.

One of the major and most confusing questions in this context might be why *ahr-1* loss of function and an OP50 diet shorten lifespan at 25 °C although they increase heat stress resistance of worms cultured at 20 °C. One possible explanation might be that loss of AHR-1 function and an OP50 diet protect against acute but not chronic heat stress, because the mechanisms that protect against chronic heat stress might be different from the mechanisms required for acute heat stress. The difference in the mechanisms to acute versus chronic stress was also found to be involved in proteostasis [256].

ahr-1 RNAi and *ahr-1(ju145)* have opposing effects on lifespan

Experiments with *ahr-1* RNAi showed that *ahr-1* RNAi reduced the lifespan in a strain with enhanced RNAi efficiency in the nervous system, when feeding on HT115(DE3). On OP50(xu363), instead, *ahr-1* RNAi did not affect the lifespan when enhanced in the nervous system. This is somehow coherent with the finding that the lifespan of *ahr-1(ju145)* is only affected on HT115, but not on OP50. But, the fact that *ahr-1* RNAi decreases the lifespan, while the *ahr-1* loss of function allele *ju145* increases lifespan was what surprised me. It suggests that *ahr-1* RNAi and *ahr-1(ju145)* might affect aging in an opposing way. Also, the lifespan data of the wild-type on *ahr-1* RNAi either in HT115(DE3) or OP50(xu363), give exactly the opposite outcome of *ahr-1(ju145).* While aging was not affected on OP50(L4440) in *ahr-1(ju145)*, the lifespan of the wild-type was increased on OP50(*ahr-1*). Vice versa, *ahr-1(ju145)* increased the lifespan on HT115, while there was no effect on the lifespan of *ahr-1* RNAi-treated wild-type on HT115(DE3). The hypothesis of the opposing effects is further strengthened by the observation that *ahr-1* RNAi strongly increased the expression of *cyp-35B1*, while it was decreased in *ahr-1(ju145).* One of the most interesting questions about this observation is why RNAi and *ju145* act in opposing ways. One hypothesis is that *ju145* is actually a gain-of-function allele. Considering the experiments on the different AhR modulators tested in this study, this hypothesis is unlikely because *ahr-1(ju145)* the gene expression of *cyps* between *ahr-1(ju145)* and curcumin, which is considered to be an AhR inhibitor, were similar for many genes. On the other hand, the data might be explained by the hypothesis that *ahr-1* RNAi acts as an AHR-1 activator. The observation that *ahr-1* RNAi increases the expression of *cyp-35B1*, which is also activated by the mammalian AhR activator BaP might

argue for this hypothesis. It would be therefore interesting to study the localization of AHR-1 in response to *ahr-1* RNAi treatment, to understand whether *ahr-1* RNAi causes the nuclear translocation of AHR-1 and might be therefore an AHR-1 activator. Also, to really understand, whether there is the possibility that *ahr-1(ju145)* is a gain-of-function strain, it would be crucial to know whether a truncated form of AHR-1 is expressed in *ahr-1(ju145)* and if so, whether it translocates to the nucleus.

Aim 3 Identification of AHR-1 target genes in response to AHR-1 modulators

AHR-1 regulates genes responsible for the detoxification response

In mammals target genes of AhR include genes for detoxification like cyps, ugts and gst [130, 135, 136]. I found that similar target genes are also regulated by AHR-1 in *C. elegans*. In initial experiments, using *ahr-1* RNAi on transgenic reporter strains, I discovered that *cyp-35B1* was strongly induced on *ahr-1* RNAi. It was therefore surprising that *cyp-35B1* was slightly reduced in the background of the *ju145* allele. Experiments on BaP, UVB and different bacteria showed no AHR-1-dependent effects on the *cyp-35B1* expression. Also, the microarray analysis did not show any significant differences of *cyp-35B1* expression in curcumin-treated wild-types. Therefore, it would be essential to find other target genes, which are responsive to the potential AHR-1 modulators.

Indeed, unpublished studies of our lab showed that the UDP-glucuronosyl transferase gene *ugt-45* might be a better suited AHR-1 target gene. In these experiments, *ugt-45* was induced by curcumin treatment, but reduced by UVB irradiation, both in an AHR-1-dependent manner. Moreover, *ugt-45* RNAi prevented the lifespan extension of *ahr-1(ju145)*. It would be therefore interesting to investigate, whether *ugt-45* is also differentially expressed on an OP50 compared to an HT115 diet. Further, also the *cyp* genes identified by qPCR would be good potential candidates. Especially *cyp-13B1*, which was induced by curcumin in the wild-type and by *ahr-1* loss of function. Studies have shown that *cyp-13B1* is suppressed by SKN-1 and induced by quercetin, an AhR inhibitor in mammals [109, 257]. Surprisingly, *cyp-13B1* was none of the genes differentially expressed in curcumin-treated worms in the microarray. Instead, *cyp-13A5* was the only gene, differentially expressed in curcumin-treated wild-type with both methods, qPRC, and microarray. Interestingly, the genes differentially expressed between wild-type and wild-type curcumin but not between *ahr-1(ju145)* and *ahr-1(ju145)* curcumin, were often also responsive to other phytochemicals known as mammalian AhR and support the hypothesis that AHR-1 responds to dietary AhR ligands (Table 13).

Table 13 Regulation of genes differentially expressed in wild-type curcumin versus wild-type DMSO by other potential AHR-1 ligands.

Gene name	***Gene class***	***responsible to AhR ligands (according to WormBase)***
H43E16.1	unknown	quercetin
numr-1	Nuclear localized metal responsive	quercetin
mul-1	Mucin-like	indole
oac-14	O-acyltransferase homolog	quercetin, tryptophan
F58B4.5	unknown	tryptophan, indole, quercetin, resveratrol
comt-4	Catechol-O-methyl-transferase	regulated by ahr-1, indole
F09C8.1	unknown	regulated by ahr-1, quercetin
ugt-48	UDP-glucuronosyl-transferase	
cyp-13A5	Cytochrome P450	quercetin, tryptophan, indole
T19C9.8	unknown	tryptophan, quercetin
lys-7	Lysozyme	resveratrol
cyp-35A5	Cytochrome P450	PCBs, PAHs
C14A4.9	unknown	indole, quercetin

AHR-1 is required in the nervous system to regulate lifespan

Among the genes differentially expressed between *ahr-1(ju145)* and wild-type in the microarray studies were many genes with functions in the nervous system. This is not surprising since AHR-1 is solely expressed in the nervous system and several functions of AHR-1 in the nervous system are reported [175, 176, 179, 182]. Using *ahr-1* RNAi in strains with RNAi sensitivity in different tissues showed that AHR-1 is in fact required in the nervous system to regulate lifespan. In this context, it would be interesting to examine, whether a neuro-specific rescue of AHR-1 in the *ahr-1(ju145)* strain would prevent the lifespan extension. A role of AHR-1 in the nervous system would be further of interest in the background of its potential involvement in the progression of neurodegenerative diseases.

Potential crosstalk between AHR-1 and other pathways

The data on diet and temperature show that environmental factors like diet and temperature together shape the lifespan of *ahr-1(ju145)* and point towards a crosstalk between AHR-1 and the TOR pathway or mitochondria. The hypothesis of a crosstalk between the TOR pathway and AHR-1 in mediating diet- and temperature-dependent effects on aging is supported by findings that a *rict-1* mutant is long-lived at 25 °C, but short-lived at 20 °C [125], and by this

shows basically the opposite effect of *ahr-1(ju145)*. Also, the lifespan of *rict-1* depends on the bacterial diet [79, 125]. On the other hand, studies showing that diet affects mitochondrial function [121] together with unpublished data of our laboratory showing that lowering mitochondrial function has beneficial effects on the lifespan at 20 °C, but not at 25 °C support the hypothesis of a crosstalk between mitochondria and AHR-1.

Studies have shown, that compared to an HT115 diet an OP50 diet lowers the oxygen consumption and the ATP production, decreases the mitochondrial copy number, and disturbs mitochondrial function [121-123]. Studies of the Kirienko laboratory showed that feeding on OP50 causes a vitamin B12 deficiency, which disrupts mitochondrial function and sensitizes worms to stress without influencing lifespan [121]. I noticed that on an OP50 diet, wild-type worms are rather more stress resistant, but his might be solely due to the fact that they performed heat shock at a different temperature and in young worms. Interestingly, also tryptophan supplementation, which I found might have similar effects to loss of AHR-1 function, activates the UPR^{mit} [252].

Besides mitochondria, also the TORC2 pathway is relevant for the lifespan altering effects of the different *E. coli* diets. Loss of function of the main TORC2 component, RICT-1, leads to a normal lifespan on HT115, but a shortened lifespan on OP50 at 25 °C [79]. Remarkably, the diet-dependent effect of *rict-1* on lifespan is as well temperature-dependent [125]. This somehow connects the findings between *ahr-1* and *rict-1* because both mutants show diet and temperature-dependent effects on aging. Also, my microarray studies showed that *ahr-1* mutants show altered expression of the FOXA homolog *pha-4,* which is a downstream target of the TOR pathway. Moreover, the finding that tryptophan extents lifespan and heat stress resistance on an HT115 diet by inhibition of the TOR pathway further supports the hypothesis of a connection between AHR-1 and the TOR pathway [252].

Because of the involvement of mitochondria and TORC2, it would be of great interest to investigate whether crosstalk between AHR-1 and mitochondria or TORC2 exists, and how this influences aging.

6. Summary

The aryl-hydrocarbon receptor (AhR) is a highly conserved transcription factor of the bHLH/PAS protein family and mediates the hazardous effects of many environmental toxicants. Its activity is modulated by environmental, dietary, host-mediated, and microbial factors. While the classical AhR ligand, dioxin, does not bind the *C. elegans* AhR homolog AHR-1, no other potential ligands have been tested for their ability to influence *C. elegans* life traits through AHR-1. Therefore, the rationale of this project was to understand whether AHR-1 influences aging in response to known mammalian AhR modulators in *C. elegans*.

In the first part of the project, I investigated whether AHR-1 mediates responses to different classes of mammalian AhR modulators. I used benzo(a)pyrene, curcumin, UVB and different *E. coli* diets (HT115 *vs.* OP50) as representatives of environmental, dietary, host-mediated, and microbial AhR modulators. While curcumin, UVB, and bacteria showed *ahr-1*-dependent effects, benzo(a)pyrene acted mainly in an *ahr-1*-independent manner. Next, I characterized the role of AHR-1 in the aging process and found that AHR-1 influenced aging in a diet- and temperature-dependent manner: *ahr-1* loss of function increased lifespan on HT115, but not OP50 at 20°C, while it shortened lifespan on both diets at 25 °C. Instead, *ahr-1* mutants were protected against polyglutamine toxicity regardless of the diet, suggesting a role of the AHR-1 in polyglutamine disorders. I narrowed down the differential effect between HT115 and OP50 in the *ahr-1* mutant to potential bacterial metabolites and therefore, I compared the composition of the bacterial secretome and found differences in tryptophan and indole-containing compounds. In the last part, I identified detoxification enzymes as potential targets of AHR-1 signaling in *C. elegans*. I tested the expression of the most promising candidate in *ahr-1* proficient and *ahr-1* deficient worms in response to benzo(a)pyrene, UVB and on the different bacteria, but was left without any striking *ahr-1*-dependent differences. A microarray study instead showed that genes regulated in response to curcumin are mainly regulated in an *ahr-1*-dependent manner.

Based on my findings, in the future I would like to specifically investigate how AHR-1 is modulated by the different compounds found to influence aging in an *ahr-1* dependent manner. A major interest will be the sub-cellular localization of AHR-1 as well as the expression of AHR-1 target genes. Also, the identification and influence of *E. coli* metabolites on the lifespan will be a part of future work. Finally, the interaction between AHR-1 and mitochondria and the TOR signaling pathway will investigated.

7. Zusammenfassung

Der Aryl-Hydrocarbon-Rezeptor (AhR) ist ein hochkonservierter Transkriptionsfaktor der bHLH / PAS-Proteinfamilie und vermittelt die schädlichen Effekte vieler Umweltgifte. Seine Aktivität wird durch Umwelteinflüsse, Ernährung, Wirt-vermittelte und mikrobielle Faktoren beeinflusst. Der klassische AhR-Ligand, Dioxin, bindet nicht an das *C. elegans* AhR-Homolog AHR-1 und es wurden keine anderen potentiellen Liganden auf ihren AHR-1-abhängigen Einfluss auf *C. elegans* getestet. Das Ziel dieses Projekts war es daher, zu verstehen, ob AHR-1 die Alterung in Reaktion auf bekannte Säuger-AhR-Modulatoren in *C. elegans* beeinflusst.

Im ersten Teil des Projekts habe ich untersucht, ob AHR-1 auf verschiedene Klassen von Säugetier-AhR-Modulatoren reagiert. Ich habe Benzo(a)pyren, Curcumin, UVB und verschiedene *E.-coli* Stämme (HT115 *vs.* OP50) als Vertreter für Umwelt-, Ernährungs-, Wirts-vermittelte und mikrobielle AhR-Modulatoren verwendet. Während Curcumin, UVB und Bakterien *ahr-1*-abhängige Effekte zeigten, wirkte Benzo(a)pyren hauptsächlich *ahr-1*-unabhängig. Als nächstes habe ich die Rolle von AHR-1 im Alterungsprozess charakterisiert und herausgefunden, dass AHR-1 die Alterung in Abhängigkeit von der bakteriellen Futterquelle und der Temperatur beeinflusst: bei 20 °C hatten *ahr-1* Mutanten eine höhere Lebenserwartung auf HT115, aber nicht auf OP50, während sie bei 25 °C auf beiden Bakterien eine verkürzte Lebensspanne hatten. Unabhängig von der Futterquelle schützte der Funktionsverlust von AHR-1 gegen Polyglutamin-Toxizität, was auf eine Rolle des AHR-1 bei Polyglutamin-Störungen hindeutet. Der unterschiedliche Effekt von HT115 und OP50 auf die Lebensspanne der *ahr-1* Mutante konnte auf baterielle Metaboliten zurückgeführt werden und ich habe daher die Komposition des bakteriellen Sekretoms untersucht und Unterschiede in der Konzentration von Tryptophan und Idol-Verbindungen gefunden. Im letzten Teil habe ich Entgiftungsenzyme als potenzielle Ziele des AHR-1-Signalweges in *C. elegans* identifiziert. Daraufhin habe ich die Expression des vielversprechendsten Gens in *ahr-1*-kompetenten und *ahr-1*-defizienten Würmern unter dem Einfluss von Benzo(a)pyren, UVB und den verschiedenen Bakterien untersucht, konnte jedoch keine auffälligen *ahr-1*-abhängigen Unterschiede feststellen. Eine Microarray-Studie zeigte stattdessen, dass Gene, die in Reaktion auf Curcumin reguliert werden, hauptsächlich in Abhängigkeit von AHR-1 reguliert werden.

Basierend auf meinen Ergebnissen, möchte ich in zukünftigen Studien untersuchen wie AHR-1 durch die verschiedenen Substanzen, die Altern in Abhängigkeit von AHR-1 beeinflussen, moduliert wird. Dabei sollen besonders die sub-zelluläre Lokalisation von AHR-1 und die Expression von AHR-1 Zielgenen im Fokus stehen. Außerdem wird die Identifizierung der *E. coli* Metaboliten und dessen Einfluss auf die Lebensspanne eine zentrale Rolle spielen.

Schlussendlich soll die Interaktion von AHR-1 mit Mitochondrien und dem TOR Signalweg untersucht werden.

8. Bibliography

1. Kaeberlein, M., *The Biology of Aging: Citizen Scientists and Their Pets as a Bridge Between Research on Model Organisms and Human Subjects.* Vet Pathol, 2016. **53**(2): p. 291-8.
2. Lopez-Otin, C., et al., *The hallmarks of aging.* Cell, 2013. **153**(6): p. 1194-217.
3. Jin, K., *Modern Biological Theories of Aging.* Aging Dis, 2010. **1**(2): p. 72-74.
4. Kenyon, C., *The genetics of ageing.* Nature, 2010. **464**(7288): p. 504-12.
5. Dato, S., et al., *The genetics of human longevity: an intricacy of genes, environment, culture and microbiome.* Mech Ageing Dev, 2017. **165**(Pt B): p. 147-155.
6. Kaeberlein, M., *Longevity and aging.* F1000Prime Rep, 2013. **5**: p. 5.
7. Brenner, S., *The genetics of Caenorhabditis elegans.* Genetics, 1974. **77**(1): p. 71-94.
8. Corsi, A.K., B. Wightman, and M. Chalfie, *A Transparent window into biology: A primer on Caenorhabditis elegans.* WormBook, 2015: p. 1-31.
9. Riddle, D.L., et al., *Introduction to C. elegans*, in *C. elegans II*, D.L. Riddle, et al., Editors. 1997: Cold Spring Harbor (NY).
10. Lints, R. and D. Hall, *Male introduction*, in *WormAtlas*. 2009.
11. Hubbard, E.J. and D. Greenstein, *Introduction to the germ line.* WormBook, 2005: p. 1-4.
12. Sulston, J.E. and H.R. Horvitz, *Post-embryonic cell lineages of the nematode, Caenorhabditis elegans.* Dev Biol, 1977. **56**(1): p. 110-56.
13. Riddle, D., et al., *Section I, The Biological Model*, in *C. elegans II. 2nd edition.*, Riddle DL, et al., Editors. 1997, Cold Spring Harbor (NY): Cold Spring Harbor Laboratory Press.
14. Sulston, J. and J. Hodgkin, *Methods*, in *The nematode Caenorhabditis elegans*, W. Wood, Editor. 1988, Cold Spring Harbor, New York: Cold Spring Harbor Laboratory. p. 587–606.
15. Olsen, A. and M. Gill, *Introduction*, in *Ageing: Lessons from C. elegans*, A. Olsen and M. Gill, Editors. 2017, Springer International Publishing. p. 1 - 7.
16. Collins, J.J., et al., *The measurement and analysis of age-related changes in Caenorhabditis elegans.* WormBook, 2008: p. 1-21.
17. Riddle, D.L., et al., *Section I Introduction: the Neural Circuit For Locomotion*, in *C. elegans II. 2nd edition.*, Riddle DL, et al., Editors. 1997, Cold Spring Harbor (NY): Cold Spring Harbor Laboratory Press.
18. Liu, J., et al., *Functional aging in the nervous system contributes to age-dependent motor activity decline in C. elegans.* Cell Metab, 2013. **18**(3): p. 392-402.
19. Herndon, L.A., et al., *Stochastic and genetic factors influence tissue-specific decline in ageing C. elegans.* Nature, 2002. **419**(6909): p. 808-14.
20. Huang, C., C. Xiong, and K. Kornfeld, *Measurements of age-related changes of physiological processes that predict lifespan of Caenorhabditis elegans.* Proc Natl Acad Sci U S A, 2004. **101**(21): p. 8084-9.
21. Herndon, L.A., et al., *Effects of Ageing on the Basic Biology and Anatomy of C. elegans*, in *Ageing: Lessons from C. elegans*, A. Olsen and M.S. Gill, Editors. 2017, Springer International Publishing. p. 9 - 39.
22. Avery, L. and H.R. Horvitz, *Pharyngeal pumping continues after laser killing of the pharyngeal nervous system of C. elegans.* Neuron, 1989. **3**(4): p. 473-85.
23. Bansal, A., et al., *Uncoupling lifespan and healthspan in Caenorhabditis elegans longevity mutants.* Proc Natl Acad Sci U S A, 2015. **112**(3): p. E277-86.
24. Rollins, J.A., et al., *Assessing Health Span in Caenorhabditis elegans: Lessons From Short-Lived Mutants.* J Gerontol A Biol Sci Med Sci, 2017. **72**(4): p. 473-480.
25. Mango, S.E., *The C. elegans pharynx: a model for organogenesis.* WormBook, 2007: p. 1-26.
26. Glenn, C.F., et al., *Behavioral deficits during early stages of aging in Caenorhabditis elegans result from locomotory deficits possibly linked to muscle frailty.* J Gerontol A Biol Sci Med Sci, 2004. **59**(12): p. 1251-60.
27. Hosono, R., *Age dependent changes in the behavior of Caenorhabditis elegans on attraction to Escherichia coli.* Exp Gerontol, 1978. **13**(1-2): p. 31-6.

28. Maglioni, S., et al., *Mitochondrial stress extends lifespan in C. elegans through neuronal hormesis.* Exp Gerontol, 2014. **56**: p. 89-98.
29. Stein, G.M. and C.T. Murphy, *The Intersection of Aging, Longevity Pathways, and Learning and Memory in C. elegans.* Front Genet, 2012. **3**: p. 259.
30. Pan, C.L., et al., *Genetic analysis of age-dependent defects of the Caenorhabditis elegans touch receptor neurons.* Proc Natl Acad Sci U S A, 2011. **108**(22): p. 9274-9.
31. Altun, Z.F. and D.H. Hall, *Muscle system, somatic muscle*, in *WormAtlas*. 2009.
32. Regmi, S.G., S.G. Rolland, and B. Conradt, *Age-dependent changes in mitochondrial morphology and volume are not predictors of lifespan.* Aging (Albany NY), 2014. **6**(2): p. 118-30.
33. Altun, Z.F. and D.H. Hall, *Nervous system, general description*, in *WormAtlas*. 2011.
34. Chew, Y.L., et al., *Aging in the nervous system of Caenorhabditis elegans.* Commun Integr Biol, 2013. **6**(5): p. e25288.
35. Toth, M.L., et al., *Neurite sprouting and synapse deterioration in the aging Caenorhabditis elegans nervous system.* J Neurosci, 2012. **32**(26): p. 8778-90.
36. Tank, E.M., K.E. Rodgers, and C. Kenyon, *Spontaneous age-related neurite branching in Caenorhabditis elegans.* J Neurosci, 2011. **31**(25): p. 9279-88.
37. Wolkow, C.A., et al., *Regulation of C. elegans life-span by insulinlike signaling in the nervous system.* Science, 2000. **290**(5489): p. 147-50.
38. Torgovnick, A., et al., *Healthy aging: what can we learn from Caenorhabditis elegans?* Z Gerontol Geriatr, 2013. **46**(7): p. 623-8.
39. Altun, Z.F. and D.H. Hall, *Alimentary system, intestine*, in *Wormatlas*. 2009.
40. McGhee, J.D., *The C. elegans intestine.* WormBook, 2007: p. 1-36.
41. Cabreiro, F. and D. Gems, *Worms need microbes too: microbiota, health and aging in Caenorhabditis elegans.* EMBO Mol Med, 2013. **5**(9): p. 1300-10.
42. Garigan, D., et al., *Genetic analysis of tissue aging in Caenorhabditis elegans: a role for heat-shock factor and bacterial proliferation.* Genetics, 2002. **161**(3): p. 1101-12.
43. Portal-Celhay, C., E.R. Bradley, and M.J. Blaser, *Control of intestinal bacterial proliferation in regulation of lifespan in Caenorhabditis elegans.* BMC Microbiol, 2012. **12**: p. 49.
44. McGee, M.D., et al., *Loss of intestinal nuclei and intestinal integrity in aging C. elegans.* Aging Cell, 2011. **10**(4): p. 699-710.
45. Lints, R. and D.H. Hall, *Reproductive system, overview*, in *WormAtlas*. 2009.
46. Shi, C. and C.T. Murphy, *Reproductive Ageing*, in *Ageing: Lessons from C. elegans*, A. Olsen and M. Gill, Editors. 2017, Springer International Publishing. p. 137 - 162.
47. Luo, S. and C.T. Murphy, *Caenorhabditis elegans reproductive aging: Regulation and underlying mechanisms.* Genesis, 2011. **49**(2): p. 53-65.
48. Prince, M., et al., *World Alzheimer Report 2015. The Global Impact of Dementia. An Analysis of Prevalence, Incidence, Cost and Trends.* 2015.
49. Alzheimer's Association. 2017; Available from: http://www.alz.org.
50. Mucke, L. and D.J. Selkoe, *Neurotoxicity of amyloid beta-protein: synaptic and network dysfunction.* Cold Spring Harb Perspect Med, 2012. **2**(7): p. a006338.
51. Link, C.D., *Expression of human beta-amyloid peptide in transgenic Caenorhabditis elegans.* Proc Natl Acad Sci U S A, 1995. **92**(20): p. 9368-72.
52. Wu, Y., et al., *Amyloid-beta-induced pathological behaviors are suppressed by Ginkgo biloba extract EGb 761 and ginkgolides in transgenic Caenorhabditis elegans.* J Neurosci, 2006. **26**(50): p. 13102-13.
53. Fong, S., et al., *Energy crisis precedes global metabolic failure in a novel Caenorhabditis elegans Alzheimer Disease model.* Sci Rep, 2016. **6**: p. 33781.
54. Parkinson's Disease Foundation. 2017; Available from: http://www.pdf.org.
55. Wolozin, B., et al., *Watching worms whither: modeling neurodegeneration in C. elegans.* Prog Mol Biol Transl Sci, 2011. **100**: p. 499-514.

56. Saha, S., et al., *LRRK2 modulates vulnerability to mitochondrial dysfunction in Caenorhabditis elegans.* J Neurosci, 2009. **29**(29): p. 9210-8.
57. Gitler, A.D., et al., *The Parkinson's disease protein alpha-synuclein disrupts cellular Rab homeostasis.* Proc Natl Acad Sci U S A, 2008. **105**(1): p. 145-50.
58. Nass, R., D.M. Miller, and R.D. Blakely, *C. elegans: a novel pharmacogenetic model to study Parkinson's disease.* Parkinsonism Relat Disord, 2001. **7**(3): p. 185-191.
59. van Ham, T.J., et al., *C. elegans model identifies genetic modifiers of alpha-synuclein inclusion formation during aging.* PLoS Genet, 2008. **4**(3): p. e1000027.
60. Hamamichi, S., et al., *Hypothesis-based RNAi screening identifies neuroprotective genes in a Parkinson's disease model.* Proc Natl Acad Sci U S A, 2008. **105**(2): p. 728-33.
61. Lakso, M., et al., *Dopaminergic neuronal loss and motor deficits in Caenorhabditis elegans overexpressing human alpha-synuclein.* J Neurochem, 2003. **86**(1): p. 165-72.
62. The Huntington's Disease Collaborative Research Group, *A novel gene containing a trinucleotide repeat that is expanded and unstable on Huntington's disease chromosomes. The Huntington's Disease Collaborative Research Group.* Cell, 1993. **72**(6): p. 971-83.
63. Morley, J.F., et al., *The threshold for polyglutamine-expansion protein aggregation and cellular toxicity is dynamic and influenced by aging in Caenorhabditis elegans.* Proc Natl Acad Sci U S A, 2002. **99**(16): p. 10417-22.
64. Satyal, S.H., et al., *Polyglutamine aggregates alter protein folding homeostasis in Caenorhabditis elegans.* Proc Natl Acad Sci U S A, 2000. **97**(11): p. 5750-5.
65. Brignull, H.R., et al., *Polyglutamine proteins at the pathogenic threshold display neuron-specific aggregation in a pan-neuronal Caenorhabditis elegans model.* J Neurosci, 2006. **26**(29): p. 7597-606.
66. Gidalevitz, T., et al., *Progressive disruption of cellular protein folding in models of polyglutamine diseases.* Science, 2006. **311**(5766): p. 1471-4.
67. Chen, X., et al., *Using C. elegans to discover therapeutic compounds for ageing-associated neurodegenerative diseases.* Chem Cent J, 2015. **9**: p. 65.
68. Schiavi, A. and N. Ventura, *The interplay between mitochondria and autophagy and its role in the aging process.* Exp Gerontol, 2014. **56**: p. 147-53.
69. Fontana, L., L. Partridge, and V.D. Longo, *Extending healthy life span--from yeast to humans.* Science, 2010. **328**(5976): p. 321-6.
70. Shore, D.E. and G. Ruvkun, *A cytoprotective perspective on longevity regulation.* Trends Cell Biol, 2013. **23**(9): p. 409-20.
71. Kenyon, C., et al., *A C. elegans mutant that lives twice as long as wild type.* Nature, 1993. **366**(6454): p. 461-4.
72. An, S.W.A., et al., *Longevity Regulation by Insulin/IGF-1 Signalling*, in *Ageing: Lessons from C. elegans*, A. Olsen and M. Gill, Editors. 2017, Springer International Publishing. p. 63-81.
73. Antikainen, H., et al., *TOR-mediated regulation of metabolism in aging.* Aging Cell, 2017. **16**(6): p. 1219-1233.
74. Long, X., et al., *TOR deficiency in C. elegans causes developmental arrest and intestinal atrophy by inhibition of mRNA translation.* Curr Biol, 2002. **12**(17): p. 1448-61.
75. Kaeberlein, M. and S. Shamieh, *The Role of TOR Signaling in Aging*, in *Comparative Biology of Aging*, N.S. Wolf, Editor. 2010, Springer Science & Business Media. p. 147 - 161.
76. Robida-Stubbs, S., et al., *TOR signaling and rapamycin influence longevity by regulating SKN-1/Nrf and DAF-16/FoxO.* Cell Metab, 2012. **15**(5): p. 713-24.
77. Jia, K., D. Chen, and D.L. Riddle, *The TOR pathway interacts with the insulin signaling pathway to regulate C. elegans larval development, metabolism and life span.* Development, 2004. **131**(16): p. 3897-906.
78. Sheaffer, K.L., D.L. Updike, and S.E. Mango, *The Target of Rapamycin pathway antagonizes pha-4/FoxA to control development and aging.* Curr Biol, 2008. **18**(18): p. 1355-64.
79. Soukas, A.A., et al., *Rictor/TORC2 regulates fat metabolism, feeding, growth, and life span in Caenorhabditis elegans.* Genes Dev, 2009. **23**(4): p. 496-511.

80. Lapierre, L.R. and M. Hansen, *Lessons from C. elegans: signaling pathways for longevity.* Trends Endocrinol Metab, 2012. **23**(12): p. 637-44.
81. Cristina, D., et al., *A regulated response to impaired respiration slows behavioral rates and increases lifespan in Caenorhabditis elegans.* PLoS Genet, 2009. **5**(4): p. e1000450.
82. Schiavi, A., et al., *Autophagy induction extends lifespan and reduces lipid content in response to frataxin silencing in C. elegans.* Exp Gerontol, 2013. **48**(2): p. 191-201.
83. Schiavi, A., et al., *Iron-Starvation-Induced Mitophagy Mediates Lifespan Extension upon Mitochondrial Stress in C. elegans.* Curr Biol, 2015. **25**(14): p. 1810-22.
84. Palikaras, K., E. Lionaki, and N. Tavernarakis, *Coordination of mitophagy and mitochondrial biogenesis during ageing in C. elegans.* Nature, 2015. **521**(7553): p. 525-8.
85. Amrit, F.R.G. and A. Ghazi, *Influences of Germline Cells on Organismal Lifespan and Healthspan*, in *Ageing: Lessons from C. elegans*, A. Olsen and M. Gill, Editors. 2017, Springer International Publishing. p. 109 - 135.
86. Antebi, A., *Regulation of longevity by the reproductive system.* Exp Gerontol, 2013. **48**(7): p. 596-602.
87. Kenyon, C., *A pathway that links reproductive status to lifespan in Caenorhabditis elegans.* Ann N Y Acad Sci, 2010. **1204**: p. 156-62.
88. Cargill, S.L., et al., *Age of ovary determines remaining life expectancy in old ovariectomized mice.* Aging Cell, 2003. **2**(3): p. 185-90.
89. Mason, J.B., et al., *Transplantation of young ovaries to old mice increased life span in transplant recipients.* J Gerontol A Biol Sci Med Sci, 2009. **64**(12): p. 1207-11.
90. Hansen, M., *Autophagy and Ageing*, in *Ageing: Lessons from C. elegans*, A. Olsen and M. Gill, Editors. 2017, Springer International Publishing. p. 331 - 354.
91. Chang, J.T., et al., *Spatiotemporal regulation of autophagy during Caenorhabditis elegans aging.* Elife, 2017. **6**.
92. Alavez, S., *Protein Homeostasis and Ageing in C. elegans*, in *Ageing: Lessons from C. elegans*, A. Olsen and M. Gill, Editors. 2017, Springer International Publishing. p. 265 - 283.
93. Miller, D.L., J. Horsman, and F.I. Heinis, *Stress Response Pathways*, in *Ageing: Lessons from C. elegans*, A. Olsen and M. Gill, Editors. 2017, Springer International Publishing. p. 191 - 217.
94. Kevei, E., W. Pokrzywa, and T. Hoppe, *Repair or destruction-an intimate liaison between ubiquitin ligases and molecular chaperones in proteostasis.* FEBS Lett, 2017. **591**(17): p. 2616-2635.
95. Jia, K., A.C. Hart, and B. Levine, *Autophagy genes protect against disease caused by polyglutamine expansion proteins in Caenorhabditis elegans.* Autophagy, 2007. **3**(1): p. 21-5.
96. Florez-McClure, M.L., et al., *Decreased insulin-receptor signaling promotes the autophagic degradation of beta-amyloid peptide in C. elegans.* Autophagy, 2007. **3**(6): p. 569-80.
97. Kapahi, P., M. Kaeberlein, and M. Hansen, *Dietary restriction and lifespan: Lessons from invertebrate models.* Ageing Res Rev, 2017. **39**: p. 3-14.
98. Mattison, J.A., et al., *Caloric restriction improves health and survival of rhesus monkeys.* Nat Commun, 2017. **8**: p. 14063.
99. Colman, R.J., et al., *Caloric restriction delays disease onset and mortality in rhesus monkeys.* Science, 2009. **325**(5937): p. 201-4.
100. Zhang, Y. and W.B. Mair, *Dietary restriction in C. elegans*, in *Ageing: Lessons from C. elegans*, A. Olsen and M. Gill, Editors. 2017, Springer International Publishing. p. 355 - 391.
101. Alavez, S., et al., *Amyloid-binding compounds maintain protein homeostasis during ageing and extend lifespan.* Nature, 2011. **472**(7342): p. 226-9.
102. Liao, V.H., et al., *Curcumin-mediated lifespan extension in Caenorhabditis elegans.* Mech Ageing Dev, 2011. **132**(10): p. 480-7.
103. Eng, S.A. and S. Nathan, *Curcumin rescues Caenorhabditis elegans from a Burkholderia pseudomallei infection.* Front Microbiol, 2015. **6**: p. 290.

104. Rudrappa, T. and H.P. Bais, *Curcumin, a known phenolic from Curcuma longa, attenuates the virulence of Pseudomonas aeruginosa PAO1 in whole plant and animal pathogenicity models.* J Agric Food Chem, 2008. **56**(6): p. 1955-62.
105. Regitz, C., L.M. Dussling, and U. Wenzel, *Amyloid-beta (Abeta(1)(-)(4)(2))-induced paralysis in Caenorhabditis elegans is inhibited by the polyphenol quercetin through activation of protein degradation pathways.* Mol Nutr Food Res, 2014. **58**(10): p. 1931-40.
106. Kampkotter, A., et al., *Investigations of protective effects of the flavonoids quercetin and rutin on stress resistance in the model organism Caenorhabditis elegans.* Toxicology, 2007. **234**(1-2): p. 113-23.
107. Kampkotter, A., et al., *Increase of stress resistance and lifespan of Caenorhabditis elegans by quercetin.* Comp Biochem Physiol B Biochem Mol Biol, 2008. **149**(2): p. 314-23.
108. Pietsch, K., et al., *Hormetins, antioxidants and prooxidants: defining quercetin-, caffeic acid- and rosmarinic acid-mediated life extension in C. elegans.* Biogerontology, 2011. **12**(4): p. 329-47.
109. Pietsch, K., et al., *Meta-Analysis of Global Transcriptomics Suggests that Conserved Genetic Pathways are Responsible for Quercetin and Tannic Acid Mediated Longevity in C. elegans.* Front Genet, 2012. **3**: p. 48.
110. Wood, J.G., et al., *Sirtuin activators mimic caloric restriction and delay ageing in metazoans.* Nature, 2004. **430**(7000): p. 686-9.
111. Regitz, C., et al., *Resveratrol reduces amyloid-beta (Abeta(1)(-)(4)(2))-induced paralysis through targeting proteostasis in an Alzheimer model of Caenorhabditis elegans.* Eur J Nutr, 2016. **55**(2): p. 741-747.
112. Guo, H., Y.Q. Dong, and B.P. Ye, *Cranberry extract supplementation exerts preventive effects through alleviating Abeta toxicity in Caenorhabditis elegans model of Alzheimer's disease.* Chin J Nat Med, 2016. **14**(6): p. 427-33.
113. Guha, S., et al., *The longevity effect of cranberry extract in Caenorhabditis elegans is modulated by daf-16 and osr-1.* Age (Dordr), 2013. **35**(5): p. 1559-74.
114. Wu, Z., et al., *Ginkgo biloba extract EGb 761 increases stress resistance and extends life span of Caenorhabditis elegans.* Cell Mol Biol (Noisy-le-grand), 2002. **48**(6): p. 725-31.
115. Wilson, M.A., et al., *Blueberry polyphenols increase lifespan and thermotolerance in Caenorhabditis elegans.* Aging Cell, 2006. **5**(1): p. 59-68.
116. Eisenberg, T., et al., *Induction of autophagy by spermidine promotes longevity.* Nat Cell Biol, 2009. **11**(11): p. 1305-14.
117. Dong, Y., et al., *Nutraceutical interventions for promoting healthy aging in invertebrate models.* Oxid Med Cell Longev, 2012. **2012**: p. 718491.
118. Brooks, K.K., B. Liang, and J.L. Watts, *The influence of bacterial diet on fat storage in C. elegans.* PLoS One, 2009. **4**(10): p. e7545.
119. Maier, W., et al., *A neuromedin U receptor acts with the sensory system to modulate food type-dependent effects on C. elegans lifespan.* PLoS Biol, 2010. **8**(5): p. e1000376.
120. Han, B., et al., *Microbial Genetic Composition Tunes Host Longevity.* Cell, 2017. **169**(7): p. 1249-1262 e13.
121. Revtovich, A., R. Lee, and N. Kirienko, *Interplay between mitochondria and diet mediates pathogen and stress resistance in C. elegans.* bioRxiv, 2017.
122. Xiao, R., et al., *RNAi Interrogation of Dietary Modulation of Development, Metabolism, Behavior, and Aging in C. elegans.* Cell Rep, 2015. **11**(7): p. 1123-33.
123. Reinke, S.N., et al., *Caenorhabditis elegans diet significantly affects metabolic profile, mitochondrial DNA levels, lifespan and brood size.* Mol Genet Metab, 2010. **100**(3): p. 274-82.
124. Pang, S. and S.P. Curran, *Adaptive capacity to bacterial diet modulates aging in C. elegans.* Cell Metab, 2014. **19**(2): p. 221-31.
125. Mizunuma, M., et al., *mTORC2-SGK-1 acts in two environmentally responsive pathways with opposing effects on longevity.* Aging Cell, 2014. **13**(5): p. 869-78.

126. Munoz-Lobato, F., et al., *Protective role of DNJ-27/ERdj5 in Caenorhabditis elegans models of human neurodegenerative diseases.* Antioxid Redox Signal, 2014. **20**(2): p. 217-35.
127. Grants, J.M. and S. Taubert, *Bacterial diet affects vulval organogenesis in Caenorhabditis elegans Mediator kinase module mutants.* Matters, 2016.
128. Gracida, X. and C.R. Eckmann, *Fertility and germline stem cell maintenance under different diets requires nhr-114/HNF4 in C. elegans.* Curr Biol, 2013. **23**(7): p. 607-13.
129. Poland, A., E. Glover, and A.S. Kende, *Stereospecific, high affinity binding of 2,3,7,8-tetrachlorodibenzo-p-dioxin by hepatic cytosol. Evidence that the binding species is receptor for induction of aryl hydrocarbon hydroxylase.* J Biol Chem, 1976. **251**(16): p. 4936-46.
130. Ashida, H., S. Nishiumi, and I. Fukuda, *An update on the dietary ligands of the AhR.* Expert Opin Drug Metab Toxicol, 2008. **4**(11): p. 1429-47.
131. Abel, J. and T. Haarmann-Stemmann, *An introduction to the molecular basics of aryl hydrocarbon receptor biology.* Biol Chem, 2010. **391**(11): p. 1235-48.
132. Ikuta, T., et al., *Nuclear localization and export signals of the human aryl hydrocarbon receptor.* J Biol Chem, 1998. **273**(5): p. 2895-904.
133. Enan, E. and F. Matsumura, *Identification of c-Src as the integral component of the cytosolic Ah receptor complex, transducing the signal of 2,3,7,8-tetrachlorodibenzo-p-dioxin (TCDD) through the protein phosphorylation pathway.* Biochem Pharmacol, 1996. **52**(10): p. 1599-612.
134. Ikuta, T., Y. Kobayashi, and K. Kawajiri, *Phosphorylation of nuclear localization signal inhibits the ligand-dependent nuclear import of aryl hydrocarbon receptor.* Biochem Biophys Res Commun, 2004. **317**(2): p. 545-50.
135. Yueh, M.F., et al., *Involvement of the xenobiotic response element (XRE) in Ah receptor-mediated induction of human UDP-glucuronosyltransferase 1A1.* J Biol Chem, 2003. **278**(17): p. 15001-6.
136. Xue, Z., et al., *Mechanisms and therapeutic prospects of polyphenols as modulators of the aryl hydrocarbon receptor.* Food Funct, 2017. **8**(4): p. 1414-1437.
137. Mulero-Navarro, S. and P.M. Fernandez-Salguero, *New Trends in Aryl Hydrocarbon Receptor Biology.* Front Cell Dev Biol, 2016. **4**: p. 45.
138. Bersten, D.C., et al., *bHLH-PAS proteins in cancer.* Nat Rev Cancer, 2013. **13**(12): p. 827-41.
139. Fritsche, E., et al., *Lightening up the UV response by identification of the arylhydrocarbon receptor as a cytoplasmatic target for ultraviolet B radiation.* Proc Natl Acad Sci U S A, 2007. **104**(21): p. 8851-6.
140. Agostinis, P., M. Garmyn, and A. Van Laethem, *The Aryl hydrocarbon receptor: an illuminating effector of the UVB response.* Sci STKE, 2007. **2007**(403): p. pe49.
141. Tilstra, J.S., et al., *NF-kappaB in Aging and Disease.* Aging Dis, 2011. **2**(6): p. 449-65.
142. Vogel, C.F. and F. Matsumura, *A new cross-talk between the aryl hydrocarbon receptor and RelB, a member of the NF-kappaB family.* Biochem Pharmacol, 2009. **77**(4): p. 734-45.
143. Luecke, S., et al., *Cytochrome P450 1A1 gene regulation by UVB involves crosstalk between the aryl hydrocarbon receptor and nuclear factor kappaB.* Chem Biol Interact, 2010. **184**(3): p. 466-73.
144. Sykiotis, G.P., et al., *The role of the antioxidant and longevity-promoting Nrf2 pathway in metabolic regulation.* Curr Opin Clin Nutr Metab Care, 2011. **14**(1): p. 41-8.
145. Dietrich, C., *Antioxidant Functions of the Aryl Hydrocarbon Receptor.* Stem Cells Int, 2016. **2016**: p. 7943495.
146. Hwang, H.J., et al., *Mitochondrial-targeted aryl hydrocarbon receptor and the impact of 2,3,7,8-tetrachlorodibenzo-p-dioxin on cellular respiration and the mitochondrial proteome.* Toxicol Appl Pharmacol, 2016. **304**: p. 121-32.
147. Tappenden, D.M., et al., *The aryl hydrocarbon receptor interacts with ATP5alpha1, a subunit of the ATP synthase complex, and modulates mitochondrial function.* Toxicol Appl Pharmacol, 2011. **254**(3): p. 299-310.
148. Marinkovic, N., et al., *Dioxins and human toxicity.* Arh Hig Rada Toksikol, 2010. **61**(4): p. 445-53.

149. Mandal, P.K., *Dioxin: a review of its environmental effects and its aryl hydrocarbon receptor biology.* J Comp Physiol B, 2005. **175**(4): p. 221-30.
150. Sakakibara, H., et al., *Effects of Japanese kelp (kombu) on life span of benzo[a]pyrene-fed mice.* J Nutr Sci Vitaminol (Tokyo), 2005. **51**(5): p. 369-73.
151. Gao, D., et al., *Chronic exposure to low benzo[a]pyrene level causes neurodegenerative disease-like syndromes in zebrafish (Danio rerio).* Aquat Toxicol, 2015. **167**: p. 200-8.
152. Amakura, Y., et al., *Screening of the inhibitory effect of vegetable constituents on the aryl hydrocarbon receptor-mediated activity induced by 2,3,7,8-tetrachlorodibenzo-p-dioxin.* Biol Pharm Bull, 2003. **26**(12): p. 1754-60.
153. Caesar, I., et al., *Curcumin promotes A-beta fibrillation and reduces neurotoxicity in transgenic Drosophila.* PLoS One, 2012. **7**(2): p. e31424.
154. Lim, G.P., et al., *The curry spice curcumin reduces oxidative damage and amyloid pathology in an Alzheimer transgenic mouse.* J Neurosci, 2001. **21**(21): p. 8370-7.
155. Rannug, A., et al., *Certain photooxidized derivatives of tryptophan bind with very high affinity to the Ah receptor and are likely to be endogenous signal substances.* J Biol Chem, 1987. **262**(32): p. 15422-7.
156. Smirnova, A., et al., *Evidence for New Light-Independent Pathways for Generation of the Endogenous Aryl Hydrocarbon Receptor Agonist FICZ.* Chem Res Toxicol, 2016. **29**(1): p. 75-86.
157. Opitz, C.A., et al., *An endogenous tumour-promoting ligand of the human aryl hydrocarbon receptor.* Nature, 2011. **478**(7368): p. 197-203.
158. DiNatale, B.C., et al., *Kynurenic acid is a potent endogenous aryl hydrocarbon receptor ligand that synergistically induces interleukin-6 in the presence of inflammatory signaling.* Toxicol Sci, 2010. **115**(1): p. 89-97.
159. Song, J., et al., *A ligand for the aryl hydrocarbon receptor isolated from lung.* Proc Natl Acad Sci U S A, 2002. **99**(23): p. 14694-9.
160. Lowe, M.M., et al., *Identification of cinnabarinic acid as a novel endogenous aryl hydrocarbon receptor ligand that drives IL-22 production.* PLoS One, 2014. **9**(2): p. e87877.
161. Jin, U.H., et al., *Microbiome-derived tryptophan metabolites and their aryl hydrocarbon receptor-dependent agonist and antagonist activities.* Mol Pharmacol, 2014. **85**(5): p. 777-88.
162. Rothhammer, V., et al., *Type I interferons and microbial metabolites of tryptophan modulate astrocyte activity and central nervous system inflammation via the aryl hydrocarbon receptor.* Nat Med, 2016. **22**(6): p. 586-97.
163. Moura-Alves, P., et al., *AhR sensing of bacterial pigments regulates antibacterial defence.* Nature, 2014. **512**(7515): p. 387-92.
164. Lee, H.U., et al., *Host-microbiome interactions: the aryl hydrocarbon receptor and the central nervous system.* J Mol Med (Berl), 2017. **95**(1): p. 29-39.
165. Gao, W., et al., *Genetic variants associated with skin aging in the Chinese Han population.* J Dermatol Sci, 2017. **86**(1): p. 21-29.
166. Singh, K.P., et al., *Loss of aryl hydrocarbon receptor promotes gene changes associated with premature hematopoietic stem cell exhaustion and development of a myeloproliferative disorder in aging mice.* Stem Cells Dev, 2014. **23**(2): p. 95-106.
167. Hu, P., et al., *Aryl hydrocarbon receptor deficiency causes dysregulated cellular matrix metabolism and age-related macular degeneration-like pathology.* Proc Natl Acad Sci U S A, 2013. **110**(43): p. E4069-78.
168. Biljes, D., et al., *Impaired glucose and lipid metabolism in ageing aryl hydrocarbon receptor deficient mice.* EXCLI J, 2015. **14**: p. 1153-63.
169. Qiao, Y., et al., *Airborne polycyclic aromatic hydrocarbons trigger human skin cells aging through aryl hydrocarbon receptor.* Biochem Biophys Res Commun, 2017. **488**(3): p. 445-452.
170. Ono, Y., et al., *Role of the aryl hydrocarbon receptor in tobacco smoke extract-induced matrix metalloproteinase-1 expression.* Exp Dermatol, 2013. **22**(5): p. 349-53.
171. Dziubanek, G., et al., *Long-term exposure to urban air pollution and the relationship with life expectancy in cohort of 3.5 million people in Silesia.* Sci Total Environ, 2017. **580**: p. 1-8.

172. Lim, M.A., et al., *Increased Th17 differentiation in aged mice is significantly associated with high IL-1beta level and low IL-2 expression.* Exp Gerontol, 2014. **49**: p. 55-62.
173. Eckers, A., et al., *The aryl hydrocarbon receptor promotes aging phenotypes across species.* Sci Rep, 2016. **6**: p. 19618.
174. Powell-Coffman, J.A., C.A. Bradfield, and W.B. Wood, *Caenorhabditis elegans orthologs of the aryl hydrocarbon receptor and its heterodimerization partner the aryl hydrocarbon receptor nuclear translocator.* Proc Natl Acad Sci U S A, 1998. **95**(6): p. 2844-9.
175. Qin, H. and J.A. Powell-Coffman, *The Caenorhabditis elegans aryl hydrocarbon receptor, AHR-1, regulates neuronal development.* Dev Biol, 2004. **270**(1): p. 64-75.
176. Huang, X., J.A. Powell-Coffman, and Y. Jin, *The AHR-1 aryl hydrocarbon receptor and its co-factor the AHA-1 aryl hydrocarbon receptor nuclear translocator specify GABAergic neuron cell fate in C. elegans.* Development, 2004. **131**(4): p. 819-28.
177. Aarnio, V., et al., *Transcriptional profiling reveals differential expression of a neuropeptide-like protein and pseudogenes in aryl hydrocarbon receptor-1 mutant Caenorhabditis elegans.* Comp Biochem Physiol Part D Genomics Proteomics, 2014. **9**: p. 40-8.
178. Aarnio, V., et al., *Fatty acid composition and gene expression profiles are altered in aryl hydrocarbon receptor-1 mutant Caenorhabditis elegans.* Comp Biochem Physiol C Toxicol Pharmacol, 2010. **151**(3): p. 318-24.
179. Qin, H., Z. Zhai, and J.A. Powell-Coffman, *The Caenorhabditis elegans AHR-1 transcription complex controls expression of soluble guanylate cyclase genes in the URX neurons and regulates aggregation behavior.* Dev Biol, 2006. **298**(2): p. 606-15.
180. Bell, D.R. and A. Poland, *Binding of aryl hydrocarbon receptor (AhR) to AhR-interacting protein. The role of hsp90.* J Biol Chem, 2000. **275**(46): p. 36407-14.
181. Jones, L.M., et al., *Adaptive and specialised transcriptional responses to xenobiotic stress in Caenorhabditis elegans are regulated by nuclear hormone receptors.* PLoS One, 2013. **8**(7): p. e69956.
182. Smith, C.J., et al., *Sensory Neuron Fates Are Distinguished by a Transcriptional Switch that Regulates Dendrite Branch Stabilization.* Neuron, 2013. **79**(2): p. 266-80.
183. Chamoli, M., et al., *A novel kinase regulates dietary restriction-mediated longevity in Caenorhabditis elegans.* Aging Cell, 2014. **13**(4): p. 641-55.
184. Zhang, J., et al., *Neuronal target identification requires AHA-1-mediated fine-tuning of Wnt signaling in C. elegans.* PLoS Genet, 2013. **9**(6): p. e1003618.
185. Prochazkova, J., et al., *The Interplay of the Aryl Hydrocarbon Receptor and beta-Catenin Alters Both AhR-Dependent Transcription and Wnt/beta-Catenin Signaling in Liver Progenitors.* Toxicological Sciences, 2011. **122**(2): p. 349-360.
186. Zhao, S., et al., *Activation of the aryl hydrocarbon receptor represses mammosphere formation in MCF-7 cells.* Cancer Letters, 2012. **317**(2): p. 192-198.
187. Williams, E.G., et al., *An evolutionarily conserved role for the aryl hydrocarbon receptor in the regulation of movement.* PLoS Genet, 2014. **10**(9): p. e1004673.
188. Kamath, R.S. and J. Ahringer, *Genome-wide RNAi screening in Caenorhabditis elegans.* Methods, 2003. **30**(4): p. 313-21.
189. Chung, C.T. and R.H. Miller, *A rapid and convenient method for the preparation and storage of competent bacterial cells.* Nucleic Acids Res, 1988. **16**(8): p. 3580.
190. Stiernagle, T., *Maintenance of C. elegans.* WormBook, 2006: p. 1-11.
191. Yang, J.S., et al., *OASIS: online application for the survival analysis of lifespan assays performed in aging research.* PLoS One, 2011. **6**(8): p. e23525.
192. Han, S.K., et al., *OASIS 2: online application for survival analysis 2 with features for the analysis of maximal lifespan and healthspan in aging research.* Oncotarget, 2016. **7**(35): p. 56147-56152.
193. Schindelin, J., et al., *Fiji: an open-source platform for biological-image analysis.* Nat Methods, 2012. **9**(7): p. 676-82.

194. Preibisch, S., S. Saalfeld, and P. Tomancak, *Globally optimal stitching of tiled 3D microscopic image acquisitions.* Bioinformatics, 2009. **25**(11): p. 1463-5.
195. Gartner, A., P.R. Boag, and T.K. Blackwell, *Germline survival and apoptosis.* WormBook, 2008: p. 1-20.
196. Nyamsuren, O., et al., *A mutation in CHN-1/CHIP suppresses muscle degeneration in Caenorhabditis elegans.* Dev Biol, 2007. **312**(1): p. 193-202.
197. Lockery, S.R., et al., *A microfluidic device for whole-animal drug screening using electrophysiological measures in the nematode C. elegans.* Lab Chip, 2012. **12**(12): p. 2211-20.
198. Banerjee, S. and S. Mazumdar, *Electrospray ionization mass spectrometry: a technique to access the information beyond the molecular weight of the analyte.* Int J Anal Chem, 2012. **2012**: p. 282574.
199. Ye, J., et al. *Primer-BLAST: A tool to design target-specific primers for polymerase chain reaction.* 2012; Available from: https://www.ncbi.nlm.nih.gov/tools/primer-blast/.
200. Huber, W., et al., *Orchestrating high-throughput genomic analysis with Bioconductor.* Nat Methods, 2015. **12**(2): p. 115-21.
201. Carvalho, B.S. and R.A. Irizarry, *A framework for oligonucleotide microarray preprocessing.* Bioinformatics, 2010. **26**(19): p. 2363-7.
202. Kauffmann, A., R. Gentleman, and W. Huber, *arrayQualityMetrics--a bioconductor package for quality assessment of microarray data.* Bioinformatics, 2009. **25**(3): p. 415-6.
203. Ritchie, M.E., et al., *limma powers differential expression analyses for RNA-sequencing and microarray studies.* Nucleic Acids Res, 2015. **43**(7): p. e47.
204. Shannon, P., et al., *Cytoscape: a software environment for integrated models of biomolecular interaction networks.* Genome Res, 2003. **13**(11): p. 2498-504.
205. Bindea, G., et al., *ClueGO: a Cytoscape plug-in to decipher functionally grouped gene ontology and pathway annotation networks.* Bioinformatics, 2009. **25**(8): p. 1091-3.
206. Timmons, L. and A. Fire, *Specific interference by ingested dsRNA.* Nature, 1998. **395**(6705): p. 854.
207. Grishok, A., *RNAi mechanisms in Caenorhabditis elegans.* FEBS Lett, 2005. **579**(26): p. 5932-9.
208. Timmons, L., D.L. Court, and A. Fire, *Ingestion of bacterially expressed dsRNAs can produce specific and potent genetic interference in Caenorhabditis elegans.* Gene, 2001. **263**(1-2): p. 103-12.
209. Menzel, R., T. Bogaert, and R. Achazi, *A systematic gene expression screen of Caenorhabditis elegans cytochrome P450 genes reveals CYP35 as strongly xenobiotic inducible.* Arch Biochem Biophys, 2001. **395**(2): p. 158-68.
210. Nishiumi, S., K. Yoshida, and H. Ashida, *Curcumin suppresses the transformation of an aryl hydrocarbon receptor through its phosphorylation.* Arch Biochem Biophys, 2007. **466**(2): p. 267-73.
211. Aziz, M.H., et al., *Chemoprevention of skin cancer by grape constituent resveratrol: relevance to human disease?* FASEB J, 2005. **19**(9): p. 1193-5.
212. Lans, H., et al., *Involvement of global genome repair, transcription coupled repair, and chromatin remodeling in UV DNA damage response changes during development.* PLoS Genet, 2010. **6**(5): p. e1000941.
213. Frauenstein, K., et al., *Evidence for a novel anti-apoptotic pathway in human keratinocytes involving the aryl hydrocarbon receptor, E2F1, and checkpoint kinase 1.* Cell Death Differ, 2013. **20**(10): p. 1425-34.
214. Avery, L. and H.R. Horvitz, *Effects of starvation and neuroactive drugs on feeding in Caenorhabditis elegans.* J Exp Zool, 1990. **253**(3): p. 263-70.
215. Kim, D.K., et al., *Cell-to-cell Transmission of Polyglutamine Aggregates in C. elegans.* Exp Neurobiol, 2017. **26**(6): p. 321-328.
216. Miller, H., et al., *Genetic interaction with temperature is an important determinant of nematode longevity.* Aging Cell, 2017. **16**(6): p. 1425-1429.

217. Haldimann, P., et al., *The novel hydroxylamine derivative NG-094 suppresses polyglutamine protein toxicity in Caenorhabditis elegans.* J Biol Chem, 2011. **286**(21): p. 18784-94.
218. Sajed, T., et al., *ECMDB 2.0: A richer resource for understanding the biochemistry of E. coli.* Nucleic Acids Res, 2016. **44**(D1): p. D495-501.
219. Guo, A.C., et al. *ECMDB: The E. coli Metabolome Database*. 2012; ECMDB Version 2.0 [Available from: http://ecmdb.ca.
220. Royal Society of Chemistry. *ChemSpider*. Available from: http://www.chemspider.com.
221. Sonowal, R., et al., *Indoles from commensal bacteria extend healthspan.* Proc Natl Acad Sci U S A, 2017. **114**(36): p. E7506-E7515.
222. Qadota, H., et al., *Establishment of a tissue-specific RNAi system in C. elegans.* Gene, 2007. **400**(1-2): p. 166-73.
223. Sijen, T., et al., *On the role of RNA amplification in dsRNA-triggered gene silencing.* Cell, 2001. **107**(4): p. 465-76.
224. Kumsta, C. and M. Hansen, *C. elegans rrf-1 mutations maintain RNAi efficiency in the soma in addition to the germline.* PLoS One, 2012. **7**(5): p. e35428.
225. Tijsterman, M., et al., *PPW-1, a PAZ/PIWI protein required for efficient germline RNAi, is defective in a natural isolate of C. elegans.* Curr Biol, 2002. **12**(17): p. 1535-40.
226. Yigit, E., et al., *Analysis of the C. elegans Argonaute family reveals that distinct Argonautes act sequentially during RNAi.* Cell, 2006. **127**(4): p. 747-57.
227. Espelt, M.V., et al., *Oscillatory Ca2+ signaling in the isolated Caenorhabditis elegans intestine: role of the inositol-1,4,5-trisphosphate receptor and phospholipases C beta and gamma.* J Gen Physiol, 2005. **126**(4): p. 379-92.
228. Calixto, A., et al., *Enhanced neuronal RNAi in C. elegans using SID-1.* Nat Methods, 2010. **7**(7): p. 554-9.
229. Schmitz, C., P. Kinge, and H. Hutter, *Axon guidance genes identified in a large-scale RNAi screen using the RNAi-hypersensitive Caenorhabditis elegans strain nre-1(hd20) lin-15b(hd126).* Proc Natl Acad Sci U S A, 2007. **104**(3): p. 834-9.
230. WormBase. *WormBase*. 2018; WS263:[Available from: http://www.wormbase.org.
231. Chepelev, N.L., et al., *Neurotoxicity may be an overlooked consequence of benzo[a]pyrene exposure that is relevant to human health risk assessment.* Mutat Res Rev Mutat Res, 2015. **764**: p. 64-89.
232. Knecht, A.L., et al., *Transgenerational inheritance of neurobehavioral and physiological deficits from developmental exposure to benzo[a]pyrene in zebrafish.* Toxicol Appl Pharmacol, 2017. **329**: p. 148-157.
233. Wu, H., et al., *Benzo-alpha-pyrene induced oxidative stress in Caenorhabditis elegans and the potential involvements of microRNA.* Chemosphere, 2015. **139**: p. 496-503.
234. Leung, M.C., et al., *Caenorhabditis elegans generates biologically relevant levels of genotoxic metabolites from aflatoxin B1 but not benzo[a]pyrene in vivo.* Toxicol Sci, 2010. **118**(2): p. 444-53.
235. Imanikia, S., et al., *The application of the comet assay to assess the genotoxicity of environmental pollutants in the nematode Caenorhabditis elegans.* Environ Toxicol Pharmacol, 2016. **45**: p. 356-61.
236. Chakrapani, B.P., S. Kumar, and J.R. Subramaniam, *Development and evaluation of an in vivo assay in Caenorhabditis elegans for screening of compounds for their effect on cytochrome P450 expression.* J Biosci, 2008. **33**(2): p. 269-77.
237. Butler, R.A., et al., *An aryl hydrocarbon receptor (AHR) homologue from the soft-shell clam, Mya arenaria: evidence that invertebrate AHR homologues lack 2,3,7,8-tetrachlorodibenzo-p-dioxin and beta-naphthoflavone binding.* Gene, 2001. **278**(1-2): p. 223-34.
238. Srimal, R.C. and B.N. Dhawan, *Pharmacology of diferuloyl methane (curcumin), a non-steroidal anti-inflammatory agent.* J Pharm Pharmacol, 1973. **25**(6): p. 447-52.
239. Monroy, A., G.J. Lithgow, and S. Alavez, *Curcumin and neurodegenerative diseases.* Biofactors, 2013. **39**(1): p. 122-32.

240. Siddique, Y.H., F. Naz, and S. Jyoti, *Effect of curcumin on lifespan, activity pattern, oxidative stress, and apoptosis in the brains of transgenic Drosophila model of Parkinson's disease.* Biomed Res Int, 2014. **2014**: p. 606928.
241. Yu, S., et al., *Curcumin prevents dopaminergic neuronal death through inhibition of the c-Jun N-terminal kinase pathway.* Rejuvenation Res, 2010. **13**(1): p. 55-64.
242. Singh, M.P., et al., *Genotoxicity and apoptosis in Drosophila melanogaster exposed to benzene, toluene and xylene: attenuation by quercetin and curcumin.* Toxicol Appl Pharmacol, 2011. **253**(1): p. 14-30.
243. Dikshit, P., et al., *Curcumin enhances the polyglutamine-expanded truncated N-terminal huntingtin-induced cell death by promoting proteasomal malfunction.* Biochem Biophys Res Commun, 2006. **342**(4): p. 1323-8.
244. Verma, M., et al., *Curcumin prevents formation of polyglutamine aggregates by inhibiting Vps36, a component of the ESCRT-II complex.* PLoS One, 2012. **7**(8): p. e42923.
245. Huang, X.B., et al., *Aspirin increases metabolism through germline signalling to extend the lifespan of Caenorhabditis elegans.* PLoS One, 2017. **12**(9): p. e0184027.
246. Pan, S.T., et al., *Computational Identification of the Paralogs and Orthologs of Human Cytochrome P450 Superfamily and the Implication in Drug Discovery.* Int J Mol Sci, 2016. **17**(7).
247. Behrendt, L., et al., *Induction of cytochrome P450 1 genes and stress response genes in developing zebrafish exposed to ultraviolet radiation.* Aquat Toxicol, 2010. **98**(1): p. 74-82.
248. Jonsson, M.E., et al., *The tryptophan photoproduct 6-formylindolo[3,2-b]carbazole (FICZ) binds multiple AHRs and induces multiple CYP1 genes via AHR2 in zebrafish.* Chem Biol Interact, 2009. **181**(3): p. 447-54.
249. Gusarov, I., et al., *Bacterial nitric oxide extends the lifespan of C. elegans.* Cell, 2013. **152**(4): p. 818-30.
250. Virk, B., et al., *Excessive folate synthesis limits lifespan in the C. elegans: E. coli aging model.* BMC Biol, 2012. **10**: p. 67.
251. Russell, J.C., et al., *Electrophysiological measures of aging pharynx function in C. elegans reveal enhanced organ functionality in older, long-lived mutants.* J Gerontol A Biol Sci Med Sci, 2017.
252. Edwards, C., et al., *Mechanisms of amino acid-mediated lifespan extension in Caenorhabditis elegans.* BMC Genet, 2015. **16**: p. 8.
253. Xiao, W., et al., *Ligand-independent activation of aryl hydrocarbon receptor signaling in PCB3-quinone treated HaCaT human keratinocytes.* Toxicol Lett, 2015. **233**(3): p. 258-66.
254. Saudou, F., et al., *Huntingtin acts in the nucleus to induce apoptosis but death does not correlate with the formation of intranuclear inclusions.* Cell, 1998. **95**(1): p. 55-66.
255. Mergoud Dit Lamarche, A., et al., *UNC-120/SRF independently controls muscle aging and lifespan in Caenorhabditis elegans.* Aging Cell, 2018. **17**(2).
256. Kirstein-Miles, J. and R.I. Morimoto, *Ribosome-associated chaperones act as proteostasis sentinels.* Cell Cycle, 2013. **12**(15): p. 2335-6.
257. Oliveira, R.P., et al., *Condition-adapted stress and longevity gene regulation by Caenorhabditis elegans SKN-1/Nrf.* Aging Cell, 2009. **8**(5): p. 524-41.

Statutory Declaration

I declare that I have authored this thesis independently, that I have not used other than the declared sources / resources, and that I have explicitly marked all material which has been quoted either literally or by content from the used sources.

Düsseldorf, …… ……

(Vanessa Brinkmann)

Eidesstattliche Erklärung

Ich erkläre an Eides statt, dass ich die vorliegende Arbeit selbstständig verfasst, andere als die angegebenen Quellen/Hilfsmittel nicht benutzt, und die den benutzten Quellen wörtlich und inhaltlich entnommenen Stellen als solche kenntlich gemacht habe.

Düsseldorf, den …… ……

(Vanessa Brinkmann)

Contribution to scientific publications

Accepted manuscripts

1. Schiavi A, Maglioni S, Palikaras K, Shaik A, Strapazzon F, **Brinkmann V**, Torgovnick A, Castelein N, De Henau S, Braeckman BP, Cecconi F, Tavernarakis N, Ventura N. Iron-Starvation-Induced Mitophagy Mediates Lifespan Extension upon Mitochondrial Stress in C. elegans. **Curr Biol, 2015**

This study identied a conserved mitophagy pathway required for lifespan extension induced by mitochondrial stress in *C. elegans* and that mitophagy mediates an iron starvation response to cope with mitochondrial stress. I contributed to this study by investigating the influence of iron starvation on the development and fertility of *C. elegans* and found that mitochondrial stress increases sensitivity to high concentrations of the iron chelator 2,2'-dipyridyl. Moreover, I performed replicates for lifespan experiments with mutants for iron transport and storage (*smf-3, ftn-2*) and mitophagy (*pdr-1*, *pink-1*) in response to mitochondrial stress (*frh-1* interference). Further, I investigated the role of *glb-10* for the lifespan extension of frh-1 RNAi and iron starvation.

2. Eckers A, Jakob S, Heiss C, Haarmann-Stemmann T, Goy C, **Brinkmann V**, Cortese-Krott MM, Sansone R, Esser C, Ale-Agha N, Altschmied J, Ventura N, Haendeler J. The aryl hydrocarbon receptor promotes aging phenotypes across species. **Sci Rep, 2016**

This study shows that the AhR influences health parameters in mice, humans and *C. elegans*. I performed lifespan, healthspan, heat stress and pharyngeal pumping experiments in *C. elegans ahr-1* mutants and found that loss of AHR-1 function has a beneficial effect on these parameters.

Manuscripts in preparation

Brinkmann V, Schiavi A, Shaik A, Tschage L, Puchta D, Kleinjohann J, Menzel R, Ventura N. The Aryl-Hydrocarbon Receptor (AHR-1) has evolutionary conserved functions and influences healthy aging in *C. elegans*

This manuscript includes the major findings of my PhD studies.

Supplement

Table S 1 Mean life- and healthspans of worms supplemented with either DMSO (control) or 1 µM BaP from day 3 after hatching. Bonferroni p-values were calculated in OASIS, statistical test: log-rank test. Kaplan Meier curves are shown in Figure 19.

	Lifespan ± SEM (days)	**No. of worms**	**No. of experiments**	**P-value vs. WT**	**P-value vs. DMSO**
WT DMSO	19.30 ± 0.45	120	2	------	------
WT BaP	20.03 ± 0.47	120	2	------	0.046
ahr-1 DMSO	17.69 ± 0.43	120	2	0.714	------
ahr-1 BaP	18.87 ± 0.42	120	2	0.845	0.074

Table S 2 Mean life- and healthspans of worms supplemented with either DMSO (control) or 100 µM curcumin. Bonferroni p-values were calculated in OASIS, statistical test: log-rank test. Kaplan Meier curves are shown in Figure 20 and Figure 21.

	Lifespan ± SEM (days)	**No. of worms**	**No. of experiments**	**P-value vs. WT**	**P-value vs. DMSO**
WT DMSO	18.63 ± 0.29	290	5	------	------
WT curcumin	21.27 ± 0.29	300	5	------	< 0.001
ahr-1 DMSO	21.01 ± 0.37	300	5	< 0.001	------
ahr-1 curcumin	21.20 ± 0.37	300	5	1.000	1.000
	Healthspan ± SEM (days)	**No. of worms**	**No. of experiments**	**P-value *vs.* WT**	**P-value *vs.* OP50**
WT DMSO	15.79 ± 0.24	290	5	------	------
WT curcumin	18.46 ± 0.27	300	5	------	< 0.001
ahr-1 DMSO	18.42 ± 0.32	300	5	< 0.001	------
ahr-1 curcumin	18.40 ± 0.31	300	5	1.000	1.000
	Lifespan ± SEM (days)	**No. of worms**	**No. of experiments**	**P-value *vs.* WT**	**P-value *vs.* DMSO**
polyQ;wt DMSO	16.45 ± 0.36	180	3	------	------
polyQ;wt curcumin	18.72 ± 0.30	180	3	------	< 0.001
polyQ;ahr-1 DMSO	18.68 ± 0.35	180	3	< 0.001	------
polyQ;ahr-1 curcumin	21.23 ± 0.36	180	3	< 0.001	< 0.001
	Healthspan ± SEM (days)	**No. of worms**	**No. of experiments**	**P-value *vs.* WT**	**P-value *vs.* DMSO**
polyQ;wt DMSO	13.56 ± 0.29	180	3	------	------
polyQ;wt curcumin	16.10 ± 0.27	180	3	------	< 0.001
polyQ;ahr-1 DMSO	15.84 ± 0.28	180	3	< 0.001	------
polyQ;ahr-1 curcumin	17.17 ± 0.32	180	3	0.050	0.010

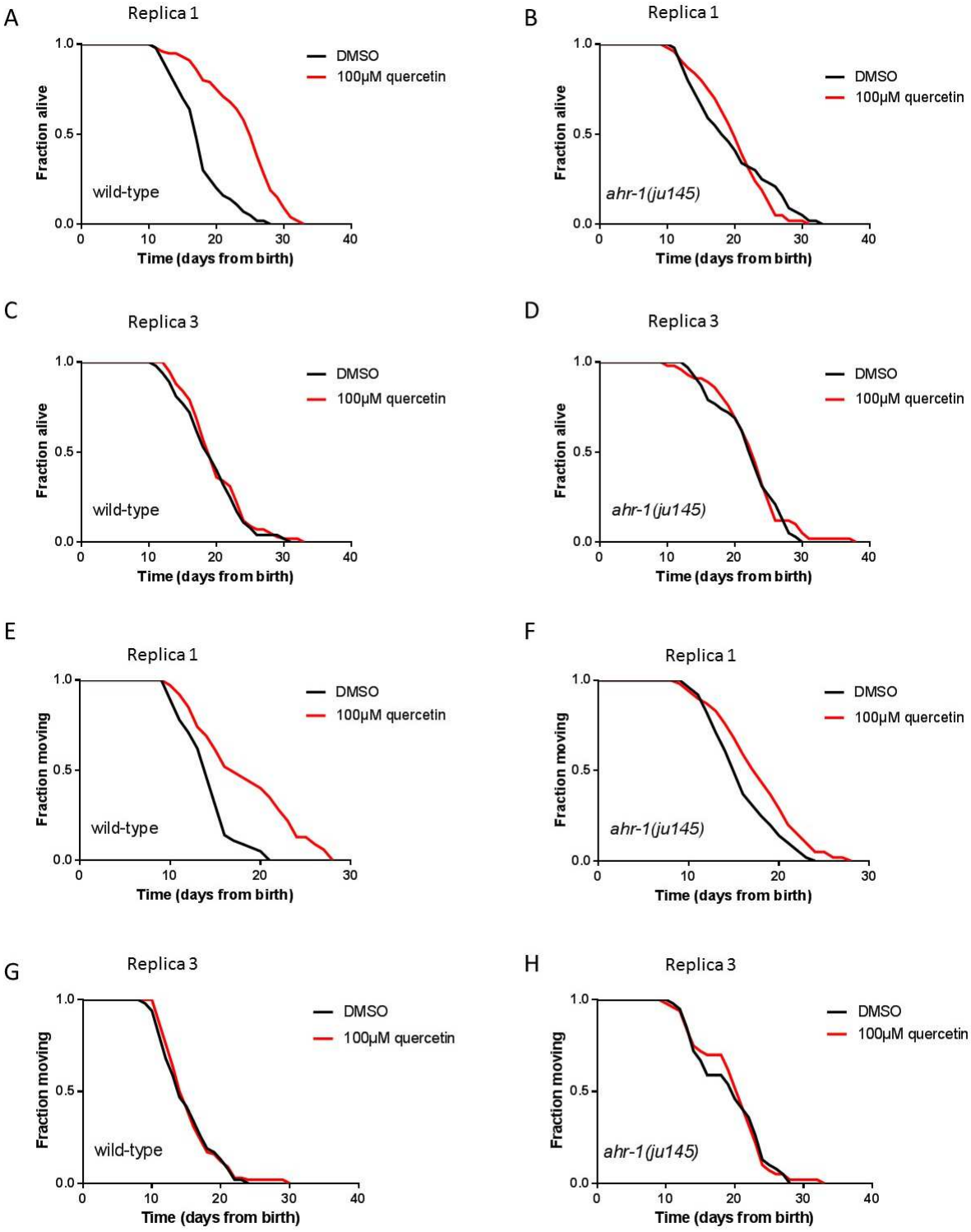

Figure S 1 Effects of quercetin on healthy aging. A - B) Quercetin extends lifespan in wild-type but not in *ahr-1(ju145)*. Mean lifespan ± SEM (in days): WT DMSO 17.64 ± 0.59, WT quercetin 24.13 ± 0.70, ahr-1 DMSO 19.64 ± 0.92, ahr-1 quercetin 19.91 ± 0.73; n=1, N= 50 - 60; Bonferroni p-values: WT DMSO vs. WT quercetin <0.001, WT DMSO vs. ahr-1 DMSO 0.135, ahr-1 DMSO vs. ahr-1 quercetin 1.000, statistical test: log-rank test. C – D) In other replicates quercetin has no effect on lifespan. Replica 3 is shown representative for replicates 2 – 5. Mean lifespan ± SEM (in days): WT DMSO 19.23 ± 0.62, WT quercetin 19.91 ± 0.58, ahr-1 DMSO 22.00 ± 0.74, ahr-1 quercetin 22.51 ± 0.80; n=1, N= 60; Bonferroni p-values: WT DMSO vs. WT quercetin 1.000, WT DMSO vs. ahr-1 DMSO 0.065, ahr-1 DMSO vs. ahr-1 quercetin 1.000, statistical test: log-rank test. E - F) Quercetin strongly extends healthspan in wild-type and to a lesser extent also in *ahr-1(ju145)*. Mean healthspan ± SEM (in days): WT DMSO 14.22 ± 0.43, WT quercetin 19.56 ± 0.65, ahr-1 DMSO 16.77 ± 0.80, ahr-1 quercetin 17.74 ± 0.67; n=1, N= 50 - 60; Bonferroni p-values: WT DMSO vs. WT quercetin <0.001, WT DMSO vs. ahr-1 DMSO 0.016, ahr-1 DMSO vs. ahr-1 quercetin 1.000, statistical test: log-rank test. In other replicates quercetin has no effect on lifespan. Replica 3 is

shown as a representation of replicate 2 – 5. Mean healthspan ± SEM (in days): WT DMSO 15.10 ± 0.51, WT quercetin 15.45 ± 0.50, ahr-1 DMSO 19.35 ± 0.79, ahr-1 quercetin 19.79 ± 0.77; n=1, N= 60; Bonferroni p-values: WT DMSO vs. WT quercetin 1.000, WT DMSO vs. ahr-1 DMSO <0.001, ahr-1 DMSO vs. ahr-1 quercetin 1.000, statistical test: log-rank test.

Table S 3 Mean life-, healthspans, and heat stress survival times of wild-type and *ahr-1(ju145)* feeding on HT115. Survival curves are shown in Figure 24. Bonferroni p-values were calculated in OASIS, statistical test: log-rank test.

	Lifespan ± SEM (days)	**No. of worms**	**No. of experiments**	**P-value *vs.* WT**	**P-value *vs.* amp, tet**
WT amp, tet	20.01± 0.38	180	3	------	------
WT	19.68 ± 0.39	180	3	------	1.000
ahr-1 amp, tet	21.25 ± 0.45	180	3	0.048	------
ahr-1	21.67 ± 0.46	180	3	0.011	1.000
	Healthspan ± SEM (days)	**No. of worms**	**No. of experiments**	**P-value *vs.* WT**	**P-value *vs.* amp, tet**
WT amp, tet	16.47 ± 0.37	180	3	------	------
WT	16.86 ± 0.35	180	3	------	1.000
ahr-1 amp, tet	18.33 ± 0.43	180	3	0.001	------
ahr-1	19.08 ± 0.41	180	3	< 0.001	1.000
	Survival ± SEM (h)	**No. of worms**	**No. of experiments**	**P-value vs. WT**	
WT amp, tet	6.27 ± 0.20	60	3	------	------
ahr-1 amp, tet	8.38 ± 0.26	60	3	< 0.001	------

Table S 4 Mean lifespans and healthspans and heat stress survival of wild-type and *ahr-1(ju145)* feeding on HT115 or OP50. Kaplan Meier curves are shown in Figure 25 and Figure 26. Bonferroni p-values were calculated in OASIS, statistical test: log-rank test.

	Lifespan ± SEM (h)	**No. of worms**	**No. of experiments**	**P-value *vs.* WT**	**P-value *vs.* HT115**
WT HT115	17.24 ± 0.33	180	3	------	------
ahr-1 HT115	19.69 ± 0.41	180	3	< 0.001	------
WT OP50	17.06 ± 0.35	170	3	------	1.000
ahr-1 OP50	16.43 ± 0.41	180	3	1.000	< 0.001
	Healthspan ± SEM (h)	**No. of worms**	**No. of experiments**	**P-value *vs.* WT**	**P-value *vs.* HT115**
WT HT115	14.78 ± 0.27	180	3	------	------
ahr-1 HT115	17.78 ± 0.37	180	3	< 0.001	------
WT OP50	14.55 ± 0.26	170	3	------	1.000
ahr-1 OP50	14.29 ± 0.34	180	3	1.000	< 0.001
	Survival ± SEM (h)	**No. of worms**	**No. of experiments**	**P-value *vs.* WT**	**P-value *vs.* HT115**
WT HT115 day 3	6.60 ± 0.17	58	3	------	------
ahr-1 HT115 day 3	7.37 ± 0.18	59	3	0.005	------
WT OP50 day 3	6.73 ± 0.12	59	3	------	1.000
ahr-1 OP50 day 3	6.38 ± 0.12	58	3	0.117	< 0.001
WT HT115 day 7	5.47 ± 0.20	59	3	------	------
ahr-1 HT115 day 7	7.43 ± 0.30	60	3	< 0.001	------
WT OP50 day 7	7.61 ± 0.27	59	3	------	< 0.001
ahr-1 OP50 day 7	6.15 ± 0.22	60	3	< 0.001	0.001
WT HT115 day 14	5.60 ± 0.27	52	3	------	------
ahr-1 HT115 day 14	7.28 ± 0.26	60	3	< 0.001	------

WT OP50 day 14	6.20 ± 0.23	60	3	------	0.326
ahr-1 OP50 day 14	5.28 ± 0.24	60	3	0.026	< 0.001

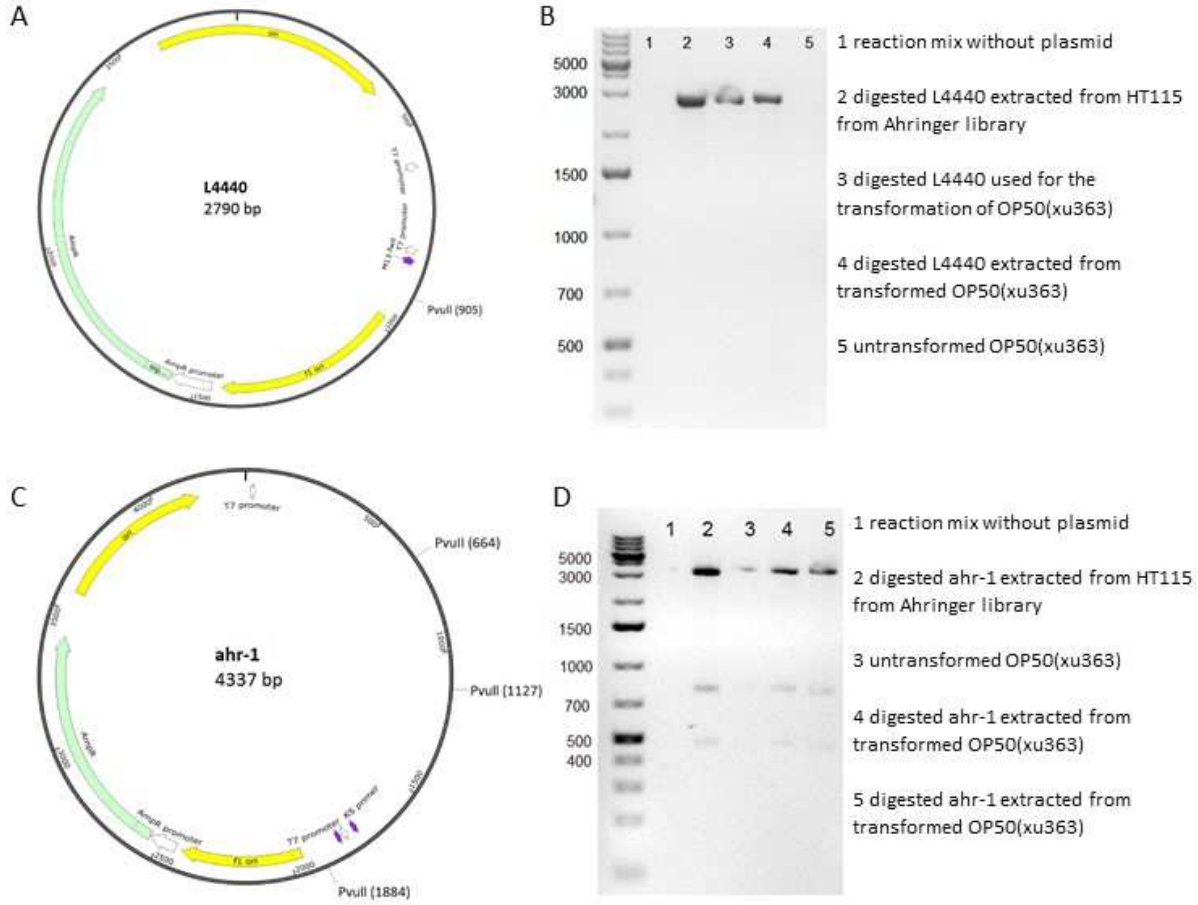

Figure S 2 A) L4440 plasmid map with *PvuII* cutting sites. *PvuII* cuts one time creating a 2790 bp fragment. B) Gel electrophoresis of *PvuII* digested L4440 plasmids extracted from either HT115(DE3) or OP50(xu363) transformed with the plasmid in panel A. Ladder: Thermo Scientific GeneRuler 1kb Plus DNA Ladder. C) ahr-1 plasmid map with *PvuII* cutting sites. *PvuII* cuts three times creating fragments of the following sizes: 3117 bp, 757 bp, and 463 bp. D) Gel electrophoresis of *PvuII* digested ahr-1 plasmids extracted from either HT115(DE3) or OP50(xu363) transformed with the plasmid in panel C. Ladder: Thermo Scientific GeneRuler 1kb Plus DNA Ladder.

Table S 5 Mean lifespans and healthspans of polyQ;wt and polyQ;ahr-1 feeding on HT115 or OP50. Kaplan Meier curves are shown in Figure 29**.** Bonferroni p-values were calculated in OASIS, statistical test: log-rank test.

	Lifespan ± SEM (days)	**No. of worms**	**No. of experiments**	**P-value *vs.* WT**	**P-value *vs.* OP50**
polyQ;wt HT115	15.37 ± 0.34	180	3	------	------
polyQ;wt OP50	15.48 ± 0.28	180	3	------	1.000
polyQ;ahr-1 HT115	19.57 ± 0.47	180	3	< 0.001	------
polyQ;ahr-1 OP50	17.30 ± 0.34	180	3	< 0.001	< 0.001
	Healthspan ± SEM (days)	**No. of worms**	**No. of experiments**	**P-value *vs.* WT**	**P-value *vs.* OP50**
polyQ;wt HT115	12.23 ± 0.29	180	3	------	------
polyQ;wt OP50	12.76 ± 0.24	180	3	------	1.000
polyQ;ahr-1 HT115	15.77 ± 0.36	180	3	< 0.001	------
polyQ;ahr-1 OP50	14.15 ± 0.26	180	3	< 0.001	< 0.001

Table S 6 Mean lifespans and healthspans of wild-type, *ahr-1(ju145),* polyQ;wt and polyQ;ahr-1 at 25 °C feeding on HT115 or OP50. Kaplan Meier curves are shown in Figure 30. Bonferroni p-values were calculated in OASIS, statistical test: log-rank test.

	Lifespan ± SEM (days)	**No. of worms**	**No. of experiments**	**P-value *vs.* WT**	**P-value *vs.* HT115**
WT HT115	15.44 ± 0.32	180	3	------	------
WT OP50	12.46 ± 0.31	180	3	------	< 0.001
ahr-1 HT115	13.43 ± 0.29	180	3	< 0.001	------
ahr-1 OP50	11.89 ± 0.29	180	3	0.544	0.007
polyQ;wt HT115	11.96 ± 0.24	150	3	------	------
polyQ;wt OP50	12.72 ± 0.23	150	3	------	0.119
polyQ;ahr-1 HT115	13.01 ± 0.30	150	3	0.005	------
polyQ;ahr-1 OP50	12.46 ± 0.23	150	3	1.000	0.106
	Healthspan ± SEM (days)	**No. of worms**	**No. of experiments**	**P-value *vs.* WT**	**P-value *vs.* HT115**
WT HT115	12.97 ± 0.26	180	3	------	------
WT OP50	10.78 ± 0.26	180	3	------	< 0.001
ahr-1 HT115	11.63 ± 0.26	180	3	0.001	------
ahr-1 OP50	9.80 ± 0.26	180	3	0.014	< 0.001
polyQ;wt HT115	10.50 ± 0.21	150	3	------	------
polyQ;wt OP50	10.93 ± 0.21	150	3	------	0.3621
polyQ;ahr-1 HT115	11.01 ± 0.24	150	3	0.171	------
polyQ;ahr-1 OP50	10.58 ± 0.22	150	3	0.942	0.436

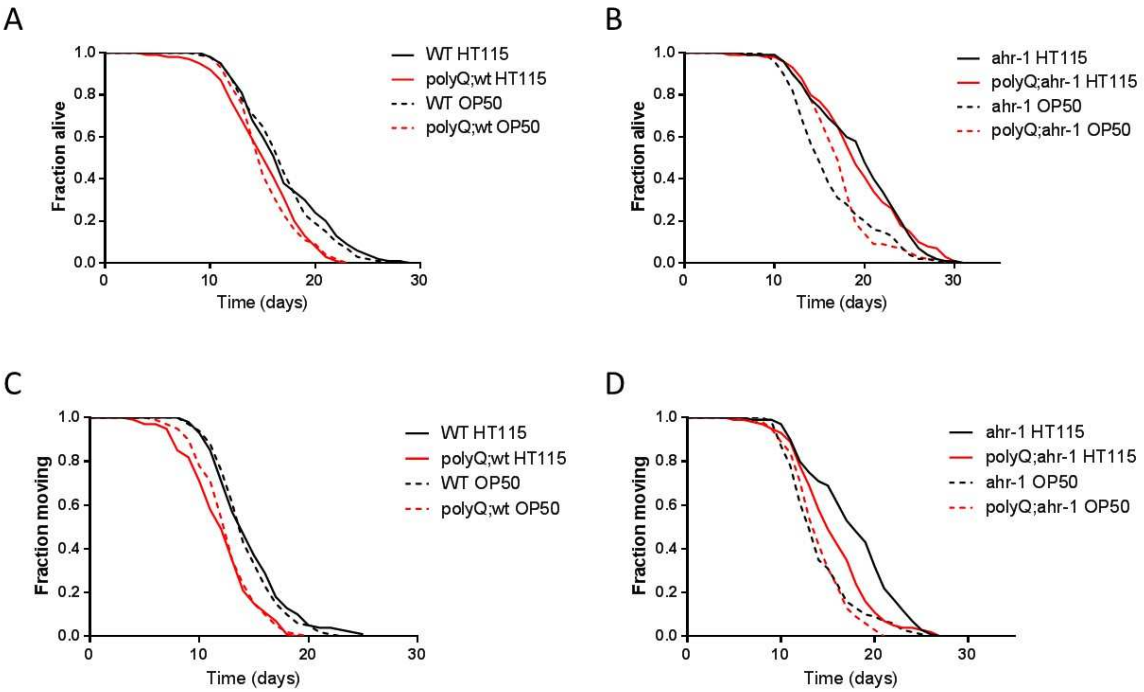

Figure S 3 Influence of polyQ$_{40}$ expression on life- and healthspan. A) Kaplan Meier survival curves for the lifespans of wild-type and polyQ;wt on HT115 and OP50. B) Kaplan Meier survival curves for the lifespans of *ahr-1(ju145*) and polyQ;ahr-1 on HT115 and OP50. C) Healthspan curves of wild-type and polyQ;wt on HT115 and OP50. D) Healthspan curves of *ahr-1(ju145)* and polyQ;ahr-1 on HT115 and OP50. The experiments were not performed at the same time. Therefore, no statistical analysis was performed.

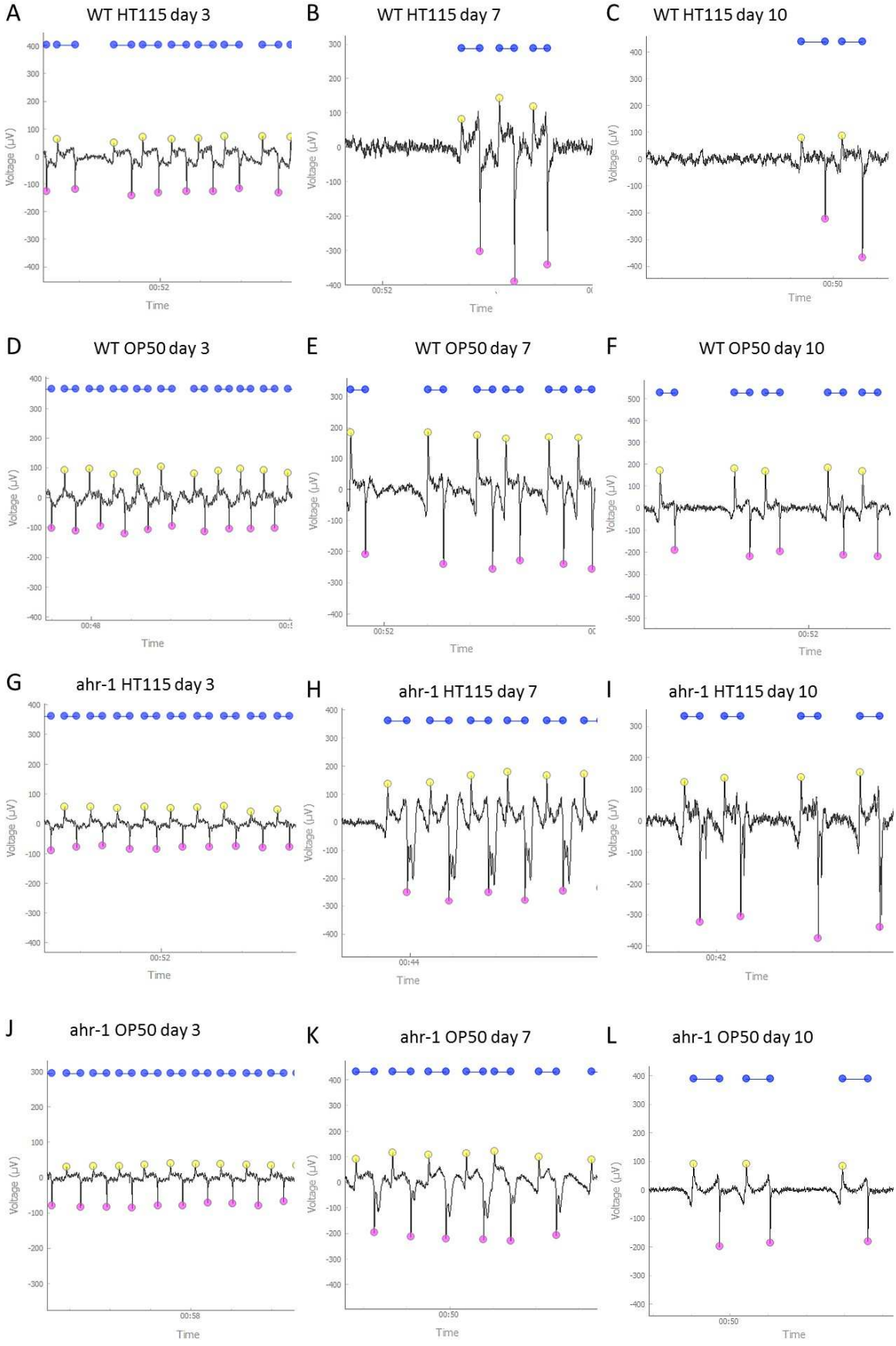

Figure S 4 Representative EPGs of wild-type and *ahr-1(ju145)* during aging. E-spikes are represented as yellow dots and R-spikes as magenta dots.

Table S 7 Mean survival times of wild-type and *ahr-1(ju145)* feeding on HT115 or OP50. A) Survival on bacteria, which have been killed prior to seeding. B) Survival on bacteria, which were grown on NGM for two days before killing. C) Survival on killed bacteria, which had been supplemented with the LB-medium, in which HT115 had grown overnight. D) Survival on killed bacteria, which had been supplemented with the LB-medium, in which OP50 had grown overnight. E - F) Survival curves on living bacteria supplemented with 1.25 mg (E) or 2.5 mg (F) of L-tryptophan. Kaplan Meier curves are shown in Figure 31. Bonferroni p-values were calculated in OASIS, statistical test: log-rank test.

		Survival ± SEM (h)	No. of worms	No. of experiments	P-value *vs.* WT	P-value *vs.* HT115
A	**WT HT115**	4.65 ± 0.13	60	3	------	------
	WT OP50	6.25 ± 0.17	60	3	------	< 0.001
	ahr-1 HT115	4.96 ± 0.16	60	3	0.303	------
	ahr-1 OP50	6.00 ± 0.18	60	3	1.000	< 0.001
B	**WT HT115**	5.63 ± 0.10	60	3	------	------
	WT OP50	6.42 ± 0.16	60	3	------	< 0.001
	ahr-1 HT115	6.52 ± 0.16	60	3	< 0.001	------
	ahr-1 OP50	6.70 ± 0.15	60	3	0.268	0.599
C	**WT HT115/HT115**	6.07 ± 0.14	60	3	------	------
	WT OP50/HT115	7.07 ± 0.16	57	3	------	< 0.001
	ahr-1 HT115/HT115	6.04 ± 0.19	57	3	1.000	------
	ahr-1 OP50/HT115	7.10 ± 0.15	58	3	0.645	< 0.001
D	**WT HT115/OP50**	6.17 ± 0.17	60	3	------	------
	WT OP50/OP50	7.37 ± 0.16	52	3	------	< 0.001
	ahr-1 HT115/OP50	6.18 ± 0.16	56	3	1.000	------
	ahr-1 OP50/OP50	7.21 ± 0.20	56	3	1.000	< 0.001
E	**WT HT115, 1.25 mg**	7.25 ± 0.17	40	2	------	------
	WT OP50, 1.25 mg	5.73 ± 0.20	40	2	------	< 0.001
	ahr-1 HT115, 1.25 mg	7.18 ± 0.15	40	2	1.000	------
	ahr-1 OP50, 1.25 mg	4.75 ± 0.12	40	2	< 0.001	< 0.001
F	**WT HT115, 2.5 mg**	6.95 ± 0.16	60	3	------	------
	WT OP50, 2.5 mg	5.15 ± 0.13	60	3	------	< 0.001
	ahr-1 HT115, 2.5 mg	7.38 ± 0.12	60	3	0.354	------
	ahr-1 OP50, 2.5 mg	4.38 ± 0.10	60	3	< 0.001	< 0.001

Table S 8 Mean life- and healthspans of wild-type and *ahr-1(ju145)* feeding on killed HT115 or OP50. Bonferroni p-values were calculated in OASIS using the Log-rank test. Kaplan Meier survival curves are shown in Figure 32.

	Lifespan ± SEM (days)	No. of worms	No. of experiments	P-value *vs.* WT	P-value *vs.* HT115
WT HT115	16.06 ± 0.29	120	2	------	------
WT OP50	21.77 ± 0.60	110	2	------	< 0.001
ahr-1 HT115	15.78 ± 0.37	120	2	1.000	------
ahr-1 OP50	20.54 ± 0.57	120	2	0.156	< 0.001
	Healthspan ± SEM (days)	**No. of worms**	**No. of experiments**	**P-value *vs.* WT**	**P-value *vs.* HT115**
WT HT115	12.44 ± 0.21	120	2	------	------
WT OP50	16.67 ± 0.40	110	2	------	< 0.001
ahr-1 HT115	12.78 ± 0.25	120	2	0.659	------
ahr-1 OP50	17.23 ± 0.43	120	2	1.000	< 0.001

Table S 9 Mean life- and healthspans of wild-type and TU3311 feeding on HT115 or OP50 either transformed with the empty vector (L4440) or ahr-1 RNAi. Kaplan Meier survival curves are shown in Figure 44. Statistical test: log-rank test.

	Lifespan ± SEM (days)	**No. of worms**	**No. of experiments**	**P-value**
N2 HT115(L4440)	19.88 ± 0.29	280	5	0.136
N2 HT115(ahr-1)	19.46 ± 0.29	264	5	
TU3311 HT115(L4440)	15.87 ± 0.37	180	3	0.001
TU3311 HT115(ahr-1)	14.11 ± 0.37	180	3	
N2 OP50(L4440)	15.93 ± 0.35	120	2	< 0.001
N2 OP50(ahr-1)	19.95 ± 0.46	115	2	
TU3311 OP50(L4440)	20.71 ± 1.15	112	2	0.375
TU3311 OP50(ahr-1)	20.13 ± 0.53	113	2	
	Healthspan ± SEM (days)	**No. of worms**	**No. of experiments**	**P-value**
N2 HT115(L4440)	16.00 ± 0.25	280	5	0.043
N2 HT115(ahr-1)	15.33 ± 0.25	264	5	
TU3311 HT115(L4440)	15.87 ± 0.37	180	3	0.003
TU3311 HT115(ahr-1)	14.11 ± 0.37	180	3	
N2 OP50(L4440)	12.80 ± 0.28	120	2	< 0.001
N2 OP50(ahr-1)	16.66 ± 0.39	115	2	
TU3311 OP50(L4440)	16.21 ± 1.19	112	2	0.885
TU3311 OP50(ahr-1)	16.85 ± 0.48	113	2	

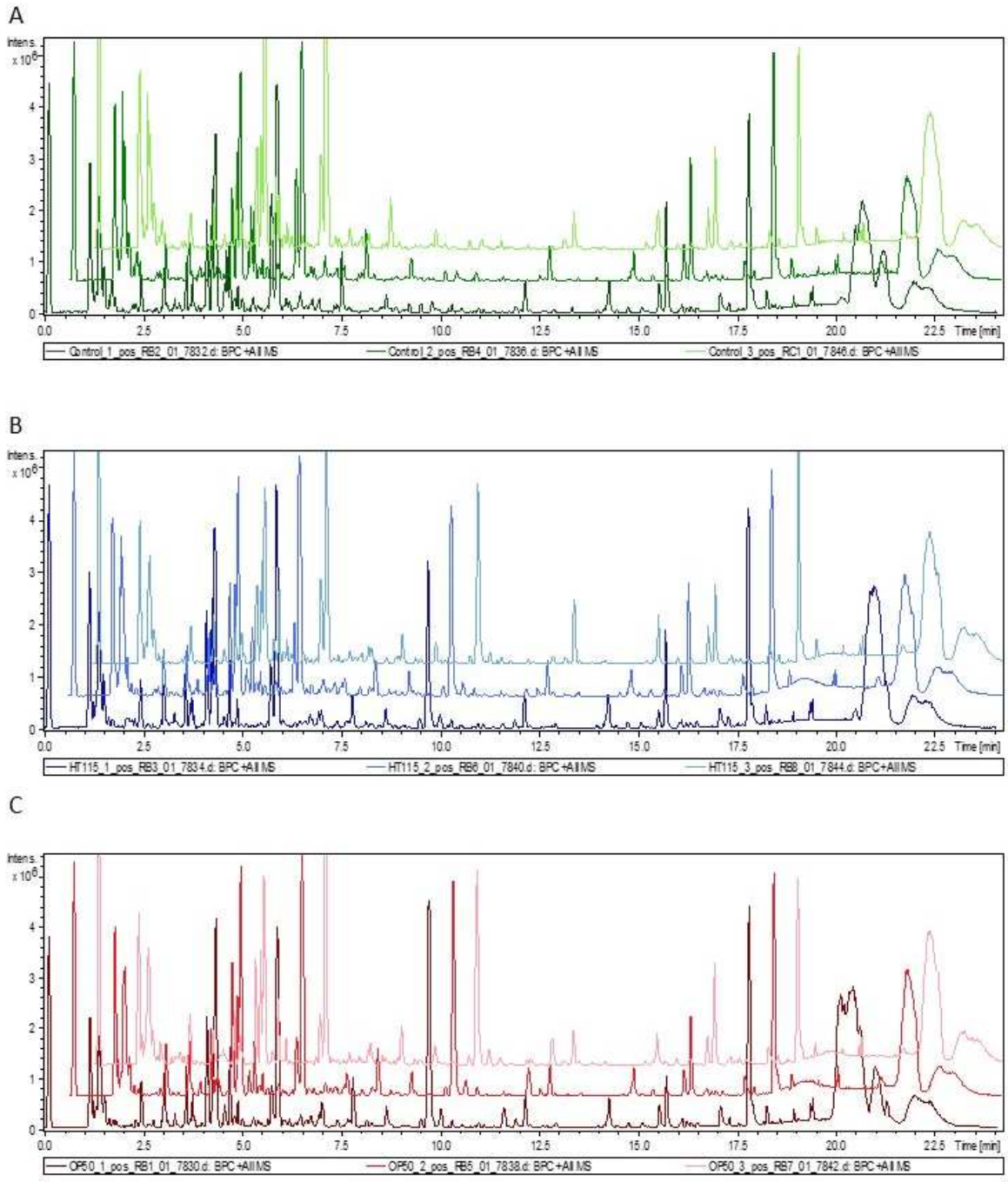

Figure S 5 overview ESI-LC-MS base peak chromatogram (BPC) of (A) control NGM, (B) NGM incubated with HT115, (C) NGM incubated with OP50 in 3 replicates.

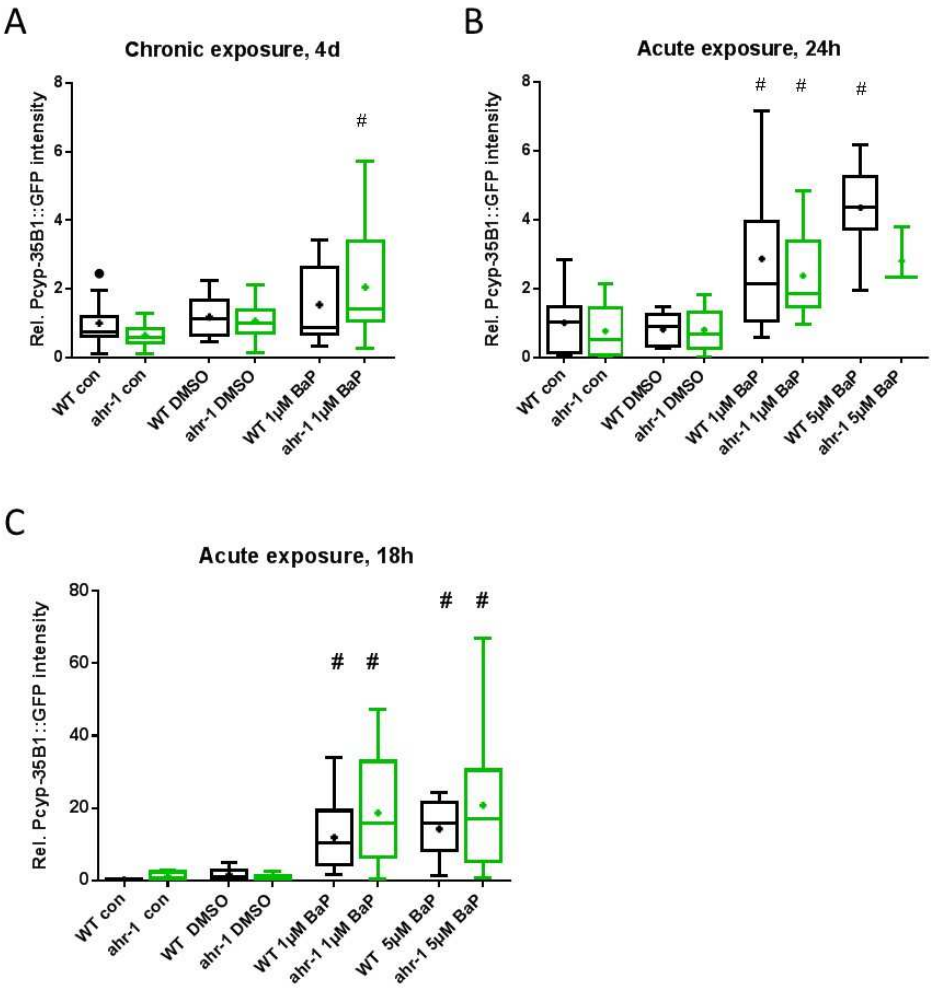

Figure S 6 Acute but not chronic BaP exposure induces *cyp-35B1* expression in NV33wt (WT) and NV33a (ahr-1). A) Worms were treated from eggs and the fluorescence was measured at day 4. N = 7 - 17, n = 1. B) Worms were treated from day 3 for 24 h. N = 3 - 11, n = 1. C) Worms were treated from day 3 for 18 h. N = 15 - 21, n = 1. # p-value < 0.05 BaP *vs.* DMSO, statistical test: One-Way ANOVA with Sidak's multiple comparisons test for all panels.

Table S 10 Primer pairs used for Real-time qPCR. The melting temperature was calculated from the length of the primers and the GC content.

Gene	Primer name	Sequence	Exon/ Exon	Length [bp]	%GC	Tm [°C]	Product length [bp]
cyp-13A1	13A1-1	GTACAACCTACACAAATCGC	Y	20	45	55.3	139
	13A1-2	TGAATCTCTGGATGAGTTGC	N	20	45	55.3	
cyp-13A2	13A2-1	GTGGACAAAGAAATATGGCAA	Y	21	38	53.9	176
	13A2-2	ACAAGTGAACTCGTTGTTCT	N	20	40	53.2	
cyp-13A3	13A3-1	GCCTGAAAGATGGGAATCTG	Y	20	50	57.3	127
	13A3-2	TGCCAGAAGCATCTTTTCTT	N	20	40	53.2	
cyp-13A4	13A4-1	AAGTGGATAAGCATCTGACA	N	20	40	53.2	274
	13A4-2	TTTCGGTTGTGAACTAAGGA	Y	20	40	53.2	
cyp-13A5	13A5-1	TGGACAAAAGAATACGGACC	Y	20	45	55.3	228
	13A5-2	CGTAGGTGATGACAGAGTTC	N	20	50	57.3	
cyp-13A6	13A6-1	GGATTGGACTAAACAATATGG	Y	21	38	53.9	646
	13A6-2	AGGTTCTCCTGGCTCAACTC	N	20	55	59.4	
	13A7-1	GACAAAGAAATACGGACCTG	Y	20	45	55.3	133

cyp-13A7	13A7-2	TGCAGTTAATTTTCTCCCGT	N	20	40	53.2	
cyp-13A8	13A8-1	AGCTCAAGGTTTTAGATGGA	Y	20	40	53.2	112
	13A8-2	CATAAGCTCCTGTGTGCTAT	N	20	45	55.3	
cyp-13A10	13A10-1	AAGACAGTGCGATGGAATTA	N	20	40	53.2	184
	13A10-2	TCTCCGAATATCGCTCTGA	Y	19	47	54.5	
cyp-13A11	13A11-1	GTAGTTGGAATTGTTAGTTAC	Y	21	33	51.9	474
	13A11-2	AATAGCTTTCCCGCCTGCTG	N	20	55	59.4	
cyp-13A12	cyp13A12-5	CTGGGAGCTTTAGCAAATTC	N	20	45	55.3	170
	cyp13A12-6	TCTCCTGATTCCCATCTTTC	Y	20	45	55.3	
cyp-13B1	cyp13B1-1	GGGCTGTTCCAGTGTTAGTC	N	20	55	59.4	236
	cyp13B1-4	AACATCGTGAACCTGCTTTA	Y	20	40	53.2	
cyp-13B2	13B2-1	TGAGAATGTATCCAGTTGCC	N	20	45	55.3	181
	13B2-2	GATTCGAGCCATCTTTCTGG	Y	20	50	57.3	
cyp-14A1	14A1-1	TTCACCAGTTCCCTCCAGAC	Y	20	55	59.4	176
	14A1-4	AGAACGGTGAGCTCGGTAAG	N	20	55	59.4	
cyp-14A2	14A2-3	AGTCCGGAAGGAAATACTTG	N	20	45	55.3	152
	14A2-2	CATCTCGGTTTGTATGAGTC	Y	20	45	55.3	
cyp-14A3	14A3-1	GCAGCAATGATGAAGTATCC	N	20	45	55.3	186
	14A3-2	TTCTTTGTTTGTGTGAGTTC	Y	20	35	51.2	
cyp-14A4	14A4-3	TTGGATGTTGTTGGCAACTC	N	20	45	55.3	143
	14A4-4	TTGGTATCCTTATTGCTTTG	Y	20	35	51.2	
cyp-14A5	14A5-3	ATAGGCACGGCGAGACTACC	N	20	45	55.3	286
	14A5-2	CAAGTACAGTCTTGTTCAAC	Y	20	40	53.2	
cyp-22A1	22A1-1	ATCTGTCACAGCCAACGAT	Y	19	47	54.4	160
	22A1-2	TGACGCATGGCAAGAATAAC	N	20	45	55.3	
cyp-23A1	23A1-1	ATTGGTTATGGTATCCGACT	Y	20	40	53.2	427
	23A1-2	AGGCTGCATAACTGTATGTG	N	20	45	55.3	
cyp-25A1	25A1-1	TGGCTCTCCTGATTTTAAGC	N	20	45	55.3	173
	25A1-2	AAGTTTTTCCTTGCGTTCTG	Y	20	40	53.2	
cyp-25A2	25A2-1	CTCTTCTGATTCTCACCTCAA	N	21	43	56.0	167
	25A2-2	TTTTTCTTTCCGGTCAACGA	Y	20	40	53.2	
cyp-25A3	25A3-1	AGCACTTCTTTCCTTTTCCC	Y	20	45	55.3	110
	25A3-2	TAAACATCTGCAAGTCCCTC	N	20	45	55.3	
cyp-25A4	25A4-3	CCAGTGTCTTTGATACTTCC	Y	20	45	55.3	135
	25A4-2	ACCCTCTCCAGCACGTCTTC	N	20	60	61.4	
cyp-29A2	29A2-7	TGCCATAATTCTGGCATATC	N	20	40	53.2	91
	29A2-4	AGGACCAGGTAGTTTACTTC	Y	20	45	55.3	
cyp-29A3	29A3-5	TGATTCTGCCCTGTTTATTG	N	20	40	53.2	107
	29A3-4	ACCGGGGAGCAAATCATC	Y	18	55	55.7	
cyp-29A4	29A4-7	TTCCAGTGGCTCTTGCATTG	N	20	50	57.3	95
	29A4-6	CATCTTTCCTCCATAAATCCAG	Y	22	40	56.2	
cyp-31A2	31A2-3	CCGCTGTACTTCTCGCTATG	N	20	55	59.4	485
	31A2-6	TTCTTCATCTGCTCCGAGGC	Y	20	55	59.4	
cyp-31A3	31A3-1	TACTCCGCCGATCTCGTG	N	18	61	58.2	249
	31A3-2	TTCTTCCTCTGCTCCGAGGG	Y	20	60	61.4	

cyp-32A1	32A-1	TCCTAGCTGATGCAGTCGAG	N	20	55	59.4	302
	32A1-2	CCGTTCTTGGATGACCTTTC	Y	20	50	57.3	
cyp-32B1	32B1-1	AGTTTTTGCATGTTCGGAAG	N	20	40	53.2	186
	32B1-2	ACCATAACTTCAACACACCA	Y	20	40	53.2	
cyp-33A1	33A1-1	GAAGTTAATATTCAGGAACAT	Y	21	28	49.8	161
	33A1-2	TACGCGAAGTAGACACGAAG	N	20	50	57.3	
cyp-33B1	33B1-5	TTTGCCAATGAAGCTCAACG	Y	20	45	55.3	172
	33B1-2	CGAAACGCTGACTGTCTTTG	N	20	50	57.3	
cyp-33C1	33C1-1	TGGTTTGCGGGCCTCAACAC	N	20	60	61.4	191
	33C1-4	CCTCGTTGTGATTCATTTATAGAC	Y	24	37	57.4	
cyp-33C2	33C2-1	GTTTATCAATGAAGCGCAAC	Y	20	40	53.2	158
	33C2-2	CCGGAAACACTTCCTCATTA	N	20	45	55.3	
cyp-33C3	33C3-1	GACTTCGACTCCCAGGAATC	N	20	55	59.4	457
	33C3-2	AGGGATCCGGGAAGACCTTC	Y	20	60	61.4	
cyp-33C4	33C4-1	AAAATCTTCCCAGACCCCT	N	19	47	54.5	191
	33C4-2	GAAGACGGTGAGATCTTGTATCTA	Y	24	42	59.3	
cyp-33C5	33C5-1	GTTTGTTTGTTCCTGTTCCA	N	20	40	53.2	187
	33C5-2	CATATGGAATGTTGCCCATC	Y	20	45	55.3	
cyp-33C6	33C6-1	TTGGATGGGTAACACTCCT	Y	19	48	54.8	187
	33C6-2	AAGTGCGAATTTTCGATGAG	N	20	40	53.2	
cyp-33C7	33C7-1	GAAGATTTGATGAAAGACTGGA	Y	22	36	54.5	206
	33C7-2	CAGAGGTCCAAGCAAGTATT	N	20	45	55.3	
cyp-33C8	33C8-1	GATGATGTGCTCAACTACTG	Y	20	45	55.3	151
	33C8-2	CTTGAGCCTTTTGCTTCTTC	N	20	45	55.3	
cyp-33C9	33C9-1	ATTTTCAAGCCGGAGAGATT	N	20	40	53.2	165
	33C9-2	CGGAACAACCCTGTATCTAT	Y	20	45	55.3	
cyp-33C11	33C11-1	TTTACCTTTTGGCTGGGAGA	Y	20	45	55.3	96
	33C11-2	ATCCTGATAAGTCTCTCCGT	N	20	45	55.3	
cyp-33C12	33C12-1	ATATTGTCCCGATCAACCAG	N	20	45	55.3	134
	33C12-2	TGGGTCTGGGAAAACCTTAT	Y	20	45	55.3	
cyp-33D1	33D1-1	CGTTTTGCAACAAACAACTC	Y	20	40	53.2	154
	33D1-2	CCAATGACTCTGTCTAGCTC	N	20	50	57.3	
cyp-33D3	33D3-1	ATTTTGGATGGCTAACAAGC	Y	20	40	53.2	229
	33D3-2	CATCAAATCTTTTCCCAGCC	N	20	45	55.3	
cyp-33E1	33E1-1	CAATGCAACTGTTAATGAATCT	Y	22	31	52.5	165
	33E1-2	TCAGGGAATATCTCTGGATC	Y	20	45	55.3	
cyp-33E2	33E2-5	ATGAATCACAACGTCTTGCC	N	20	45	55.3	151
	33E2-4	TCAGGGAAGATTTCTGGATT	Y	20	40	53.2	
cyp-34A1	34A1-1	AGAGATTTGAGCAGAACGAT	Y	20	40	53.2	139
	34A1-2	GTATCCTGCCTCCATTTCAA	N	20	45	55.3	
cyp-34A2	34A2-1	TGTGCGTGTCTTCTCAATAA	N	20	40	53.2	141
	34A2-2	TTGGACTTCACTAATCACGG	Y	20	45	55.3	
cyp-34A4	34A4-1	TGAACGATTTGAACAGGGTG	Y	20	45	55.3	197
	34A4-2	TTCTCTGCACATTTCTTTGC	N	20	40	53.2	

cyp-34A5	34A5-1	AGTTGTAGAGAAGCTGAGGA	N	20	45	55.3	113
	34A5-2	GAACCTCATTAACAACCGCA	Y	20	45	55.3	
cyp-34A6	34A6-3	ACACTGACGATGAGACTTTC	N	20	45	55.3	160
	34A6-2	TTTGCAATGATCAAATATAG	Y	20	25	47.1	
cyp-34A7	34A7-1	TCCGAATGGACCTACTCCTT	Y	20	50	57.3	435
	34A7-2	TTTACTTGAATTGCTCCGTC	N	20	40	53.2	
cyp-34A8	34A8-1	AGCTGTTTTTGATAACCGGAA	Y	21	38	53.9	94
	34A8-2	GGAGCAAATGGAGTAGTTGT	N	20	45	55.3	
cyp-34A9	34A9-3	GGCGCAACTATCAATGAAATCC	Y	22	45	58.2	278
	34A9-2	TCAGCTCTAGCCAGTGATTC	N	20	50	57.3	
cyp-34A10	34A10-3	GCTCCCAAAAGGACCTACTC	Y	20	55	59.4	186
	34A10-4	TCGTGTGCCACGTCATAATC	N	20	50	57.3	
cyp-35A1	35A1-1	TCTTGCGTTGTCATGCTGGT	N	20	50	57.3	448
	35A1-2	ATCAGCACATCTTGCATCCA	Y	20	45	55.3	
cyp-35A2	35A2-1	TTCTGTGCTTTTGGGATACC	N	20	45	55.3	173
	35A2-2	TATTACCGTACCTCTTTCTA	Y	20	35	51.2	
cyp-35A3	35A3-1	CGCTGCGTGTTTAAGTTGGC	N	20	55	59.4	173
	35A3-2	TGTTGCCGTATTTCTTTCTG	Y	20	40	53.2	
cyp-35A4	35A4-1	TCGGCAATTTTGAGTTGGTT	N	20	40	53.2	172
	35A4-2	TGTTGCCATATCTCTTTCTA	Y	20	35	51.2	
cyp-35A5	35A5-3	AGGAGTTCAGCCGTGGTGTC	Y	20	60	61.4	153
	35A5-2	CAGCGCATCTTGCATCCAGC	Y	20	60	61.4	
cyp-35B1	35B1-1	GAAGATTCTCATGTGCCGA	Y	19	47	54.4	229
	35B1-2	TTCAAAAACCAAACCGGAAC	N	20	40	53.2	
cyp-35B2	35B2-1	GGACTCGGCTTCAGACTTAT	N	20	50	57.3	770
	35B2-2	GCAATAGGTTTCCAGTCAGTAAAT	Y	24	37	57.4	
cyp-35B3	35B3-1	TATGACAGTGCCAGTTTGGG	N	20	50	57.3	728
	35B3-2	TTCCAATCATTAAATACAATTCAG	Y	24	25	52.5	
cyp-35C1	35C-5	GAGCCGAGCTGTATTTAATC	Y	20	45	55.3	127
	35C-2	ATGTCGAAGGCTTCGCATCT	N	20	50	57.3	
cyp-35D1	35D-1	GAGATTGCTGGTGGCCAACA	N	20	55	59.4	530
	35D-4	TTCCCGAAAACCAGGTAAAG	Y	20	45	55.3	
cyp-36A1	36A-3	GATCGATTCTTGAATAGTCGTG	Y	22	40	56.2	234
	36A-2	TCGTGATGCTCGGACTGTAA	N	20	50	57.3	
cyp-37A1	37A1-1	ATTATTTGTGAAACTGCAATGG	Y	22	31	52.5	416
	37AB-2	CACCACAGGGACCATCCAAT	N	20	55	59.4	
cyp-37B1	37B1-7	ATGTTTGAAGGCCACGACAC	Y	20	50	57.3	347
	37B1-2	TCCGGGTTGTACTGATTTGG	N	20	50	57.3	
cyp-42A1	42A1-3	TCTACAACAGGCACGGAAGG	N	20	55	59.4	503
	42A1-2	TGTGTCGTGGCCTTCAAATG	Y	20	50	57.3	
cyp-43A1	43A1-1	AGTCTGCTCGGATTCTTTTT	N	20	40	53.2	124
	43A1-2	GTGCCGTAATTTCCTCATAG	Y	20	45	55.3	
cyp-44A1	44A1-1	ATCGGGAACATTGGGTATTT	N	20	40	53.2	175
	44A1-2	CAGTTTGAACATCAGCAGGA	Y	20	45	55.3	

act-1 to 3	act1-3	TCCAAGAGAGGTATCCTTAC	Y	20	45	55.3	170
	act1-4	CGGTTAGCCTTTGGATTGAG	N	20	50	57.3	
cdc-42	cdc42-1	ATTACGCCGTCACAGTAATG	Y	20	45	55.3	248
	cdc42-2	ATCCCTGAGATCGACTTGAG	N	20	50	57.3	

Table S 11 PCR conditions for genes with optimized primer pairs.

Gene	Annealing temperature (°C)	Elongation time (s)	No. Of cycles	Primer efficiency (%)	Buffer concentration
cyp-13A1	55.5	20	45	91.2	2x
cyp-13A2	52.7	20	40	97.65	2x
cyp-13A3	52.7	20	45	100.5	2x
cyp-13A5	55.0	20	35	86.7	2x
cyp-13A7	52.7	20	40	93.17	2x
cyp-13A8	52.7	20	40	94.0	2x
cyp-13A10	52.0	30	45	103.7	2x
cyp-13A12	55.0	20	35	105.8	2x
cyp-13B1	52.7	20	40	96.2	2x
cyp-13B2	55.0	20	35	98.7	2x
cyp-14A1	59.0	30	45	94.40	2x
cyp-14A2	55.0	20	35	102.35	2x
cyp-14A5	52.7	20	40	100.15	2x
cyp-25A1	52.7	20	40	84.75	2x
cyp-25A2	53.0	20	40	93.1	1x
cyp-25A3	55.0	20	35	109.2	2x
cyp-25A4	55.0	20.0	35	106.4	2x
cyp-29A2	52.7	20.0	40	90.3	2x
cyp-29A4	55.5	20	40	107.4	2x
cyp-31A2	59	30	45	84.3	2x
cyp-31A3	57.5	20	45	81.85	2x
cyp-32A1	57.0	20	45	94.65	2x
cyp-32B1	51.5	50	45	97.85	2x
cyp-33A1	49.5	20	45	100.6	2x
cyp-33C4	54.0	20	35	107.25	2x
cyp-33C5	51.5	30	45	92.45	1x
cyp-33C7	54.0	20	35	97.35	2x
cyp-33C8	55.0	20	35	111.65	2x
cyp-33C9	53.5	40	40	111.0	2x
cyp-33C12	54.5	40	40	102.1	1x
cyp-33D1	53.5	40	50	106.07	2x
cyp-33E1	51.5	50	45	103.6	2x
cyp-33E2	52.7	20	50	100.25	2x
cyp-34A2	52.7	20	50	86.45	2x
cyp-34A4	51.5	50	45	81.45	2x
cyp-34A5	55.0	20	35	98.92	2x
cyp-34A8	53.5	40	50	109.3	2x

cyp-34A9	52.7	20	45	87.65	1x
cyp-35A2	48.5	20.0	40.0	79.6	1x
cyp-35A3	52.7	20	45	85.6	2x
cyp-35A4	49.5	20	45	107.73	2x
cyp-35C1	55.0	20	35	97.4	2x
cyp-36A1	55.5	20	40	79.85	2x
cyp-37B1	57.0	60	45	89.8	2x
cyp-42A1	54.5	40	40	122.2	1x
cyp-43A1	52.7	20	40	82.55	2x
cyp-44A1	52.7	20	40	81.55	2x
act-1 to 3	55.0	20.0	35.0	94.85	1x
				97.50	2x
cdc-42	55.0	20.0	35.0	88.00	1x
				80.80	2x

A

	array	sampleNames	*1	*2	*3	index	condition	batch
☐	1	77-ahr 1_(EleGene-1_0-st).CEL				1	Ahr1	1
☐	2	77-ahr 2_(EleGene-1_0-st).CEL				2	Ahr1	2
☐	3	77-ahr 3_(EleGene-1_0-st).CEL				3	Ahr1	3
☐	4	77-ahr 4_(EleGene-1_0-st).CEL				4	Ahr1	4
☐	5	77-ahr 5_(EleGene-1_0-st).CEL	x	x		5	Ahr1	5
☐	6	77-ahr C1_(EleGene-1_0-st).CEL				6	AhrC	1
☐	7	77-ahr C2_(EleGene-1_0-st).CEL				7	AhrC	2
☐	8	77-ahr C3_(EleGene-1_0-st).CEL				8	AhrC	3
☐	9	77-ahr C4_(EleGene-1_0-st).CEL				9	AhrC	4
☐	10	77-ahr C5_(EleGene-1_0-st).CEL				10	AhrC	5
☐	11	77-N2 1_(EleGene-1_0-st).CEL				11	N2	1
☐	12	77-N2 2_(EleGene-1_0-st).CEL				12	N2	2
☐	13	77-N2 3_(EleGene-1_0-st).CEL				13	N2	3
☐	14	77-N2 4_(EleGene-1_0-st).CEL				14	N2	4
☐	15	77-N2 5_(EleGene-1_0-st).CEL				15	N2	5
☐	16	77-N2 C1_(EleGene-1_0-st).CEL				16	N2C	1
☐	17	77-N2 C2_(EleGene-1_0-st).CEL				17	N2C	2
☐	18	77-N2 C3_(EleGene-1_0-st).CEL				18	N2C	3
☐	19	77-N2 C4_(EleGene-1_0-st).CEL				19	N2C	4
☐	20	77-N2 C5_(EleGene-1_0-st).CEL				20	N2C	5

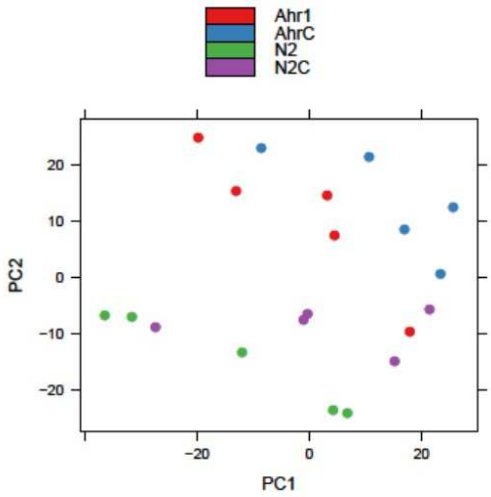

B

	array	sampleNames	*1	*2	*3	index	condition	batch
☐	1	77-ahr 1_(EleGene-1_0-st).CEL				1	ahr1	1
☐	2	77-ahr 2_(EleGene-1_0-st).CEL				2	ahr1	2
☐	3	77-ahr 3_(EleGene-1_0-st).CEL				3	ahr1	3
☐	4	77-ahr 4_(EleGene-1_0-st).CEL				4	ahr1	4
☐	5	77-ahr C1_(EleGene-1_0-st).CEL				5	AhrC	1
☐	6	77-ahr C2_(EleGene-1_0-st).CEL				6	AhrC	2
☐	7	77-ahr C3_(EleGene-1_0-st).CEL				7	AhrC	3
☐	8	77-ahr C4_(EleGene-1_0-st).CEL				8	AhrC	4
☐	9	77-ahr C5_(EleGene-1_0-st).CEL				9	AhrC	5
☐	10	77-N2 1_(EleGene-1_0-st).CEL				10	N2	1
☐	11	77-N2 2_(EleGene-1_0-st).CEL				11	N2	2
☐	12	77-N2 3_(EleGene-1_0-st).CEL				12	N2	3
☐	13	77-N2 4_(EleGene-1_0-st).CEL				13	N2	4
☐	14	77-N2 5_(EleGene-1_0-st).CEL				14	N2	5
☐	15	77-N2 C1_(EleGene-1_0-st).CEL				15	N2C	1
☐	16	77-N2 C2_(EleGene-1_0-st).CEL				16	N2C	2
☐	17	77-N2 C3_(EleGene-1_0-st).CEL				17	N2C	3
☐	18	77-N2 C4_(EleGene-1_0-st).CEL				18	N2C	4
☐	19	77-N2 C5_(EleGene-1_0-st).CEL				19	N2C	5

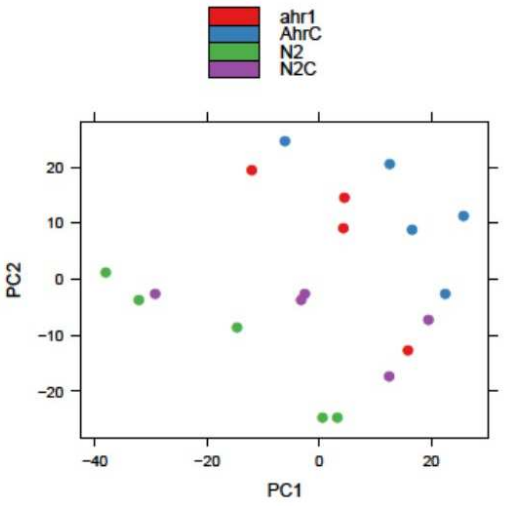

Figure S 7 Quality control of the microarray samples after normalization. Arrays, marked by checkbox selection are considered outliers. The quality control criteria were *1 Distances between arrays, *2 boxplots, *3 MA plots. A)

Quality control of the whole array with Principle Component Analysis. B) Quality control with Principle Component analysis after removing the sample ahr-1C5.

Table S 12 Differentially expressed genes between wild-type DMSO and *ahr-1(ju145)* DMSO. Genes down-regulated in *ahr-1(ju145)* vs. wild-type are listed on the left, genes up-regulated on the right. Genes are sorted by logFC.

Gene name	logFC	adj. p-value
R02F11.1	-2.30779	0.03124
hbl-1	-2.01333	0.017098
atf-2	-1.95801	0.022727
lpr-4	-1.83383	0.022727
K04H4.2	-1.83107	0.024807
egl-46	-1.82284	0.040615
T20F5.4	-1.80333	0.040013
ptr-4	-1.76648	0.016201
lpr-5	-1.75178	0.022727
dyf-7	-1.74257	0.022685
H42K12.3	-1.73433	0.042144
pqn-73	-1.72249	0.047445
lpr-3	-1.69339	0.055442
sqt-3	-1.67325	0.023111
mlt-11	-1.67191	0.022727
dpy-17	-1.62187	0.036339
acn-1	-1.62107	0.022727
F30H5.3	-1.61736	0.022727
R09E10.5	-1.61486	0.028534
K10D3.4	-1.60709	0.022727
cutl-28	-1.57051	0.011316
dpy-3	-1.55543	0.022727
wrt-2	-1.48601	0.031328
mlt-8	-1.48294	0.032648
gei-13	-1.45287	0.032648
R03H10.2	-1.44336	0.070443
cutl-16	-1.42889	0.053732
F43D9.1	-1.4232	0.054118
dma-1	-1.42216	0.042343
fmi-1	-1.40332	0.009804
Y62H9A.12	-1.35524	0.002324
clec-78	-1.33873	0.044472
ifa-3	-1.33389	0.021913
lpr-6	-1.33251	0.047322
K02E10.4	-1.33126	0.054118
F26A10.2	-1.33115	0.024807
dpy-14	-1.31322	0.050159
Y65B4BL.1	-1.28467	0.023111
dpy-2	-1.27411	0.022446
F49E10.2	-1.26419	0.09108
wrt-10	-1.25256	0.047322

Gene name	logFC	adj. p-value
irld-35	1.968438	0.001884
clec-209	1.881916	0.01817
F56A4.2	1.881916	0.01817
clec-209	1.881916	0.01817
F56A4.2	1.881916	0.01817
Y19D10A.16	1.670847	9.28E-09
C01B4.6	1.670847	9.28E-09
C01B4.6	1.670847	9.28E-09
Y19D10A.16	1.670847	9.28E-09
F56A4.3	1.659561	0.001279
srd-75	1.614213	7.35E-05
srd-61	1.614213	7.35E-05
srd-61	1.614213	7.35E-05
srd-75	1.614213	7.35E-05
C01B4.7	1.605505	0.002762
Y19D10A.4	1.605505	0.002762
Y19D10A.4	1.605505	0.002762
C01B4.7	1.605505	0.002762
Y19D10A.11	1.386083	0.002324
B0511.11	1.335108	0.044456
F56A4.12	1.318093	0.000953
H19N07.3	0.964753	0.001782
Y45G12C.16	0.961089	1.5E-07
C13B7.6	0.952915	1.5E-07
Y19D10A.5	0.842653	0.021913
C01B4.8	0.842653	0.021913
Y19D10A.5	0.842653	0.021913
C01B4.8	0.842653	0.021913
fbxa-2	0.726068	0.011316
T24D5.3	0.66301	0.022727
scl-6	0.602444	0.022727
T05F1.15	0.580452	0.079738
F44F4.9	0.548792	0.033875
Y73F8A.14	0.548626	0.040324
pho-10	0.524168	0.025675
C39D10.9	0.516259	0.075401
frm-8	0.510294	0.032369
R102.6	0.50414	0.031328
Y39G10AR.32	0.484483	0.022727
F09C6.12	0.463732	0.073814
gur-4	0.459782	0.070336

T06D8.3	-1.24527	0.062663
syd-9	-1.2291	0.009804
noah-2	-1.22174	0.071573
fbxa-192	-1.21906	0.005478
syg-2	-1.21812	0.017687
ces-2	-1.21702	0.055203
ugt-57	-1.21572	0.060811
noah-1	-1.20537	0.066586
ZK287.1	-1.19707	0.040013
T01D3.3	-1.19122	0.075969
unc-75	-1.1846	0.037936
dpy-10	-1.17934	0.022727
T03G6.1	-1.165	0.031323
hil-7	-1.16352	0.041096
C09F9.2	-1.1544	0.050159
zag-1	-1.13926	0.033983
F14B4.1	-1.12536	0.074999
C03A3.1	-1.12492	0.037936
ZK822.1	-1.11529	0.011468
F09F9.4	-1.11338	0.049162
F44E2.4	-1.09598	0.055442
unc-42	-1.08238	0.044456
atf-8	-1.07909	0.054344
M03D4.4	-1.07701	0.069382
pros-1	-1.07477	0.010534
fbn-1	-1.06833	0.053473
nab-1	-1.06541	0.033875
F54E2.2	-1.05788	0.077672
W04A8.4	-1.04237	0.022727
T19C4.1	-1.03974	0.073571
B0393.5	-1.02373	0.03698
tag-297	-1.02063	0.08972
igcm-1	-1.00601	0.037302
F53B1.4	-0.99462	0.089766
F15B9.8	-0.98362	0.09357
plx-2	-0.98273	0.060727
T19A5.3	-0.97232	0.024663
T04F8.9	-0.968	0.086018
Y71H2AM.15	-0.95867	0.047151
C35A5.11	-0.95295	0.053732
lgx-1	-0.94853	0.036621
F01D5.6	-0.92602	0.055442
jmjd-3.1	-0.92135	0.024807
let-4	-0.91826	0.068647
rga-2	-0.91792	0.038223
lam-3	-0.91077	0.037835
ceh-34	-0.89243	0.036339
sre-7	0.457319	0.081285
slc-17.5	0.455935	0.073571
Y76B12C.8	0.450049	0.079738
irld-52	0.435735	0.033875
C04E7.1	0.426115	0.032677
Y40H7A.3	0.425913	0.033983
ugt-9	0.409121	0.089273
fbxa-61	0.408477	0.09357
bath-21	0.3967	0.024807
nhr-239	0.392006	0.033875
T22D1.6	0.389992	0.088813
F19H6.3	0.385002	0.056634
T20D4.8	0.373778	0.047322
ttr-17	0.371511	0.033875
F29D10.1	0.369134	0.079738
rnh-1.2	0.353303	0.054655
spd-3	0.344498	0.050159
ugt-29	0.33968	0.037835
Y37A1B.4	0.33668	0.037936
K03B8.8	0.321934	0.088421
lec-4	0.314087	0.050687
pnk-1	0.238965	0.079738

prkl-1	-0.88965	0.022727
T26C5.2	-0.88676	0.017098
C14F11.6	-0.88141	0.024807
nhr-91	-0.88017	0.024807
lin-42	-0.87861	0.022727
cdh-5	-0.87701	0.048102
cdh-9	-0.87356	0.073889
nlr-1	-0.86968	0.032527
C06E7.4	-0.86948	0.033875
agr-1	-0.86231	0.017098
F23H12.5	-0.85845	0.059901
ZK512.1	-0.85359	0.011468
slt-1	-0.85106	0.048063
unc-129	-0.84814	0.017687
EEED8.2	-0.84748	0.087011
lron-2	-0.83913	0.024446
nlp-20	-0.8382	0.024807
lron-1	-0.83287	0.037936
ddr-2	-0.83195	0.079149
C03C10.9	-0.82946	0.040013
cwn-2	-0.81755	0.037936
F57B1.6	-0.80336	0.089766
C05A9.2	-0.80112	0.079738
ttx-1	-0.79408	0.06438
unc-86	-0.78987	0.055203
igcm-3	-0.78835	0.097793
tsp-17	-0.78013	0.079738
asns-2	-0.77728	0.082521
D2005.6	-0.75693	0.03698
catp-3	-0.74932	0.079249
dsl-6	-0.7478	0.024807
Y75B8A.6	-0.73437	0.064456
cfi-1	-0.73364	0.030044
W03G11.4	-0.73005	0.055203
Y110A2AL.4	-0.72786	0.070509
H08J11.2	-0.72659	0.022727
hum-6	-0.72419	0.022685
crb-1	-0.71926	0.092126
T05A7.11	-0.71311	0.024807
hhat-2	-0.70716	0.089273
sox-2	-0.69978	0.071803
his-24	-0.69969	0.086942
ZK154.1	-0.69831	0.088813
cutl-25	-0.68205	0.032037
ces-1	-0.672	0.054149
H19M22.3	-0.66311	0.055442
shn-1	-0.66005	0.093837

dlg-1	-0.65778	0.024807
F20D6.10	-0.65573	0.029611
dyb-1	-0.65552	0.017058
lev-8	-0.65493	0.025769
efn-2	-0.64681	0.022727
tbx-2	-0.64552	0.063755
cdh-3	-0.64503	0.068217
T25G12.11	-0.64499	0.063446
dsl-3	-0.64446	0.079738
ceh-30	-0.63426	0.098294
C14A4.9	-0.62923	0.022685
lact-5	-0.62031	0.047309
his-60	-0.61334	0.091699
his-50	-0.61334	0.091699
his-14	-0.61334	0.091699
his-64	-0.61334	0.091699
his-5	-0.61334	0.091699
his-38	-0.61334	0.091699
his-46	-0.61334	0.091699
his-10	-0.61334	0.091699
his-26	-0.61334	0.091699
his-67	-0.61334	0.091699
his-37	-0.61334	0.091699
his-31	-0.61334	0.091699
his-56	-0.61334	0.091699
his-18	-0.61334	0.091699
his-28	-0.61334	0.091699
his-1	-0.61334	0.091699
his-37	-0.61334	0.091699
his-18	-0.61334	0.091699
his-67	-0.61334	0.091699
his-60	-0.61334	0.091699
his-38	-0.61334	0.091699
his-26	-0.61334	0.091699
his-56	-0.61334	0.091699
his-14	-0.61334	0.091699
his-1	-0.61334	0.091699
his-5	-0.61334	0.091699
his-28	-0.61334	0.091699
his-64	-0.61334	0.091699
his-46	-0.61334	0.091699
his-10	-0.61334	0.091699
his-31	-0.61334	0.091699
his-50	-0.61334	0.091699
his-56	-0.61334	0.091699
his-26	-0.61334	0.091699
his-31	-0.61334	0.091699

his-50	-0.61334	0.091699
his-14	-0.61334	0.091699
his-37	-0.61334	0.091699
his-28	-0.61334	0.091699
his-38	-0.61334	0.091699
his-1	-0.61334	0.091699
his-46	-0.61334	0.091699
his-67	-0.61334	0.091699
his-18	-0.61334	0.091699
his-10	-0.61334	0.091699
his-64	-0.61334	0.091699
his-5	-0.61334	0.091699
his-60	-0.61334	0.091699
C33D9.6	-0.61047	0.089461
pha-4	-0.60475	0.048063
cdh-8	-0.59983	0.098941
C14A11.2	-0.59408	0.039506
rhgf-2	-0.58694	0.070443
Y34F4.1	-0.58475	0.022727
R57.2	-0.58454	0.042343
C02B10.3	-0.5831	0.055442
ceh-6	-0.58069	0.052559
Y39G10AR.11	-0.58015	0.055442
F42G4.7	-0.57638	0.065059
C40A11.6	-0.56746	0.073571
somi-1	-0.5643	0.022727
egl-43	-0.562	0.047309
mps-2	-0.55825	0.05597
cdh-1	-0.55763	0.037835
lgc-27	-0.55681	0.047445
C14B9.2	-0.55494	0.022727
F14B8.5	-0.55442	0.073571
mltn-9	-0.55213	0.090118
ZK836.3	-0.55137	0.048286
tlp-1	-0.54435	0.079249
insc-1	-0.54382	0.079738
Y62H9A.13	-0.54172	0.036339
ppt-1	-0.53798	0.079738
K07C11.4	-0.53393	0.09108
sup-12	-0.53363	0.045685
rpm-1	-0.52803	0.010541
cuti-1	-0.5268	0.025335
C35E7.4	-0.5229	0.022727
C02E7.6	-0.51741	0.054149
max-1	-0.51645	0.035784
F32D8.3	-0.51214	0.093077
Y37E11AL.6	-0.51119	0.055203

syg-1	-0.50627	0.040019
dsl-7	-0.50191	0.055203
C44H9.7	-0.50168	0.031323
rsf-1	-0.49849	0.03698
lim-7	-0.49843	0.018883
cutl-21	-0.49625	0.073571
ajm-1	-0.48294	0.005121
C06B8.7	-0.48106	0.050687
F38B6.6	-0.48102	0.091619
rgs-1	-0.47428	0.073571
K01A2.5	-0.47185	0.022727
cst-1	-0.46927	0.055212
tub-2	-0.46532	0.002762
madf-10	-0.46473	0.048402
cwn-1	-0.44977	0.089265
tbb-4	-0.44595	0.060727
ain-1	-0.43657	0.03698
bath-38	-0.43364	0.021913
skr-19	-0.42034	0.051674
F25F8.1	-0.41675	0.073571
tsp-14	-0.40871	0.089766
tag-278	-0.40812	0.089461
nid-1	-0.40313	0.017098
dre-1	-0.40091	0.046211
K10B4.3	-0.3993	0.061609
F53B1.6	-0.39296	0.097386
alg-1	-0.39074	0.086018
blmp-1	-0.37696	0.040013
Y55D5A.3	-0.3758	0.073571
F40G9.15	-0.36822	0.073889
pes-4	-0.36652	0.089273
oac-46	-0.36456	0.071573
aat-1	-0.36155	0.091699
Y59C2A.3	-0.35796	0.059901
lam-2	-0.35265	0.019015
slo-1	-0.34651	0.053732
T07A9.12	-0.34631	0.097793
cyn-6	-0.3457	0.069382
C49G9.2	-0.34403	0.044456
unc-44	-0.33731	0.055203
D1086.2	-0.32596	0.093837
fasn-1	-0.32288	0.050159
F57G12.1	-0.31849	0.079738
pdi-6	-0.3011	0.089766
F44E2.3	-0.28535	0.062833
his-59	-0.24457	0.079738
his-55	-0.24457	0.079738

his-49	-0.24457	0.079738
his-25	-0.24457	0.079738
his-40	-0.24457	0.079738
his-45	-0.24457	0.079738
his-27	-0.24457	0.079738
his-6	-0.24457	0.079738
his-32	-0.24457	0.079738
his-63	-0.24457	0.079738
his-9	-0.24457	0.079738
his-2	-0.24457	0.079738
his-17	-0.24457	0.079738
his-42	-0.24457	0.079738
his-13	-0.24457	0.079738
his-40	-0.24457	0.079738
his-25	-0.24457	0.079738
his-45	-0.24457	0.079738
his-63	-0.24457	0.079738
his-27	-0.24457	0.079738
his-49	-0.24457	0.079738
his-59	-0.24457	0.079738
his-13	-0.24457	0.079738
his-55	-0.24457	0.079738
his-32	-0.24457	0.079738
his-6	-0.24457	0.079738
his-42	-0.24457	0.079738
his-2	-0.24457	0.079738
his-17	-0.24457	0.079738
his-9	-0.24457	0.079738
his-44	-0.24331	0.089766
his-15	-0.24331	0.089766
his-29	-0.24331	0.089766
his-11	-0.24331	0.089766
his-34	-0.24331	0.089766
his-15	-0.24331	0.089766
his-11	-0.24331	0.089766
his-44	-0.24331	0.089766
his-29	-0.24331	0.089766
his-34	-0.24331	0.089766

Table S 13 Differentially expressed genes between wild-type DMSO and wild-type curcumin. Genes down-regulated in curcumin vs. DMSO are listed on the left, genes up-regulated on the right. Genes are sorted by logFC.

Gene name	logFC	adj. p-value
lys-7	-1.53802	0.08383
cyp-35A5	-1.08222	0.086568
C14A4.9	-0.54566	0.078675

Gene name	logFC	adj. p-value
pgp-1	2.735163	3.09E-08
clec-169	2.170259	0.000111
ZK742.3	2.056031	7.5E-07
C40H1.8	2.032371	0.017857

H43E16.1	1.533288	0.021518
numr-1	1.423363	0.033938
mul-1	1.340707	0.029289
oac-14	1.23861	0.085249
F58B4.5	1.214422	0.029726
comt-4	1.170796	0.028856
F09C8.1	1.077651	0.029302
ugt-48	1.069114	0.033938
cyp-13A5	1.055261	0.056763
T19C9.8	0.963534	0.08383
clec-57	0.958184	0.003751
comt-3	0.956545	0.044007
cat-4	0.918134	0.021518
C17H12.4	0.839035	0.01468
spp-18	0.836621	0.073749
bcmo-2	0.80457	0.096075
pcp-3	0.752507	0.010792
Y49E10.18	0.696275	0.034362
T24E12.5	0.693589	0.040098
C25F9.14	0.661462	0.065388
ZK185.5	0.655758	0.004585
slc-17.5	0.639008	0.021518
acl-7	0.623693	0.034362
asah-1	0.607172	0.086018
fpn-1.2	0.598783	0.056763
Y105C5B.15	0.590488	0.073749
C39H7.4	0.577595	0.045461
ugt-9	0.572564	0.028856
T28D9.3	0.564125	0.068977
F27E5.1	0.554622	0.036855
clec-198	0.547387	0.096075
clec-166	0.532278	0.073749
clec-143	0.523636	0.058163
B0035.13	0.521589	0.005849
F53A9.1	0.442009	0.081328
nhr-239	0.425716	0.036855
F46G10.1	0.366391	0.02623
ugt-29	0.357032	0.056763

Table S 14 Biological process GO terms enriched in *ahr-1(ju145)* vs. wild-type. P-values are corrected with Bonferroni step down. GO terms are sorted according to their GO group.

GO ID	GO Term	P-value	GO Groups	Associated Genes (%)	No. Genes	Associated Genes Found
GO:0007588	excretion	0.49	Group00	6.12	3	[ceh-6, lim-7, shn-1]
GO:0040034	regulation of development, heterochronic	0.11	Group01	16.67	3	[dre-1, hbl-1, lin-42]
GO:0060465	pharynx development	0.48	Group02	6.52	3	[lim-7, pha-4, tbx-2]

GO:0097376	interneuron axon guidance	0.00	Group03	60.00	3	[ddr-2, fmi-1, nid-1]
GO:1903311	regulation of mRNA metabolic process	0.37	Group04	5.88	3	[rpm-1, sup-12, unc-75]
GO:0048665	neuron fate specification	0.03	Group05	30.00	3	[sox-2, unc-42, unc-86]
GO:0048663	neuron fate commitment	0.04	Group05	27.27	3	[sox-2, unc-42, unc-86]
GO:0031589	cell-substrate adhesion	0.02	Group06	33.33	3	[B0393.5, R09E10.5, nid-1]
GO:0007160	cell-matrix adhesion	0.02	Group06	33.33	3	[B0393.5, R09E10.5, nid-1]
GO:0001708	cell fate specification	0.00	Group07	8.45	12	[ceh-34, cwn-1, cwn-2, dsl-3, dsl-6, dsl-7, pha-4, sox-2, tbx-2, tsp-14, unc-42, unc-86]
GO:0045165	cell fate commitment	0.00	Group07	7.53	14	[ceh-34, cfi-1, cwn-1, cwn-2, dsl-3, dsl-6, dsl-7, egl-46, pha-4, sox-2, tbx-2, tsp-14, unc-42, unc-86]
GO:0007156	homophilic cell adhesion via plasma membrane adhesion molecules	0.00	Group08	50.00	6	[cdh-1, cdh-3, cdh-5, cdh-8, cdh-9, fmi-1]
GO:0098742	cell-cell adhesion via plasma-membrane adhesion molecules	0.00	Group08	40.00	6	[cdh-1, cdh-3, cdh-5, cdh-8, cdh-9, fmi-1]
GO:0098609	cell-cell adhesion	0.00	Group08	15.38	6	[cdh-1, cdh-3, cdh-5, cdh-8, cdh-9, fmi-1]
GO:0045138	nematode male tail tip morphogenesis	0.08	Group09	7.50	6	[acn-1, cdh-3, plx-2, ptr-4, tsp-14, unc-129]
GO:0090598	male anatomical structure morphogenesis	0.09	Group09	7.14	6	[acn-1, cdh-3, plx-2, ptr-4, tsp-14, unc-129]
GO:0046661	male sex differentiation	0.13	Group09	6.38	6	[acn-1, cdh-3, plx-2, ptr-4, tsp-14, unc-129]
GO:0007548	sex differentiation	0.03	Group09	5.19	11	[acn-1, alg-1, blmp-1, cdh-3, ceh-30, dre-1, lim-7, plx-2, ptr-4, tsp-14, unc-129]
GO:0033563	dorsal/ventral axon guidance	0.04	Group10	16.00	4	[rpm-1, slt-1, unc-129, unc-44]
GO:0008045	motor neuron axon guidance	0.15	Group10	14.29	3	[ddr-2, rpm-1, unc-129]
GO:0043069	negative regulation of programmed cell death	0.40	Group10	7.50	3	[ceh-30, ces-1, rpm-1]
GO:0060548	negative regulation of cell death	0.43	Group10	6.00	3	[ceh-30, ces-1, rpm-1]
GO:0043067	regulation of programmed cell death	0.13	Group10	5.60	7	[ceh-30, ces-1, ces-2, cst-1, dre-1, rpm-1, unc-129]
GO:0010941	regulation of cell death	0.24	Group10	4.58	7	[ceh-30, ces-1, ces-2, cst-1, dre-1, rpm-1, unc-129]
GO:0042981	regulation of apoptotic process	0.43	Group10	4.46	5	[ceh-30, cst-1, dre-1, rpm-1, unc-129]
GO:0060560	developmental growth involved in morphogenesis	0.03	Group11	9.52	6	[dma-1, rpm-1, slt-1, syg-1, syg-2, zag-1]
GO:0048588	developmental cell growth	0.04	Group11	8.96	6	[dma-1, rpm-1, slt-1, syg-1, syg-2, zag-1]
GO:0007416	synapse assembly	0.18	Group11	8.70	4	[nab-1, rpm-1, syg-1, syg-2]
GO:0050808	synapse organization	0.05	Group11	8.45	6	[dyb-1, nab-1, nid-1, rpm-1, syg-1, syg-2]

GO:0007271	synaptic transmission, cholinergic	0.43	Group11	7.14	3	[dyb-1, nid-1, unc-75]
GO:0099177	regulation of trans-synaptic signaling	0.16	Group11	4.55	3	[dyb-1, slo-1, unc-75]
GO:0050804	modulation of chemical synaptic transmission	0.16	Group11	4.55	3	[dyb-1, slo-1, unc-75]
GO:0007267	cell-cell signaling	0.15	Group11	4.10	10	[cwn-1, cwn-2, dlg-1, dyb-1, lev-8, nid-1, slo-1, syg-1, syg-2, unc-75]
GO:0002064	epithelial cell development	0.00	Group12	19.23	5	[H42K12.3, T26C5.2, let-4, noah-1, noah-2]
GO:0042338	cuticle development involved in collagen and cuticulin-based cuticle molting cycle	0.00	Group12	19.23	5	[dpy-10, dpy-17, dpy-2, dpy-3, sqt-3]
GO:0042335	cuticle development	0.00	Group12	14.52	9	[H42K12.3, T26C5.2, dpy-10, dpy-17, dpy-2, dpy-3, noah-1, noah-2, sqt-3]
GO:0030855	epithelial cell differentiation	0.02	Group12	14.29	5	[H42K12.3, T26C5.2, let-4, noah-1, noah-2]
GO:0040002	collagen and cuticulin-based cuticle development	0.03	Group12	11.90	5	[dpy-10, dpy-17, dpy-2, dpy-3, sqt-3]
GO:0018996	molting cycle, collagen and cuticulin-based cuticle	0.00	Group12	9.90	10	[acn-1, dpy-10, dpy-17, dpy-2, dpy-3, dre-1, noah-1, noah-2, ptr-4, sqt-3]
GO:0060429	epithelium development	0.08	Group12	7.32	6	[H42K12.3, T26C5.2, cdh-3, let-4, noah-1, noah-2]
GO:0009888	tissue development	0.04	Group12	5.38	10	[H42K12.3, T26C5.2, blmp-1, cdh-3, ceh-30, ceh-34, let-4, noah-1, noah-2, tsp-14]
GO:0006334	nucleosome assembly	0.00	Group13	15.79	6	[hil-7, his-1, his-11, his-13, his-24, his-40]
GO:0031497	chromatin assembly	0.00	Group13	15.38	6	[hil-7, his-1, his-11, his-13, his-24, his-40]
GO:0006333	chromatin assembly or disassembly	0.00	Group13	15.00	6	[hil-7, his-1, his-11, his-13, his-24, his-40]
GO:0034728	nucleosome organization	0.00	Group13	14.29	6	[hil-7, his-1, his-11, his-13, his-24, his-40]
GO:0006323	DNA packaging	0.03	Group13	10.00	6	[hil-7, his-1, his-11, his-13, his-24, his-40]
GO:0065004	protein-DNA complex assembly	0.09	Group13	7.14	6	[hil-7, his-1, his-11, his-13, his-24, his-40]
GO:0071824	protein-DNA complex subunit organization	0.11	Group13	6.82	6	[hil-7, his-1, his-11, his-13, his-24, his-40]
GO:0071103	DNA conformation change	0.18	Group13	5.71	6	[hil-7, his-1, his-11, his-13, his-24, his-40]
GO:0055002	striated muscle cell development	0.38	Group14	8.11	3	[cst-1, dyb-1, slo-1]
GO:0055001	muscle cell development	0.39	Group14	7.89	3	[cst-1, dyb-1, slo-1]
GO:0051146	striated muscle cell differentiation	0.39	Group14	7.69	3	[cst-1, dyb-1, slo-1]
GO:0042692	muscle cell differentiation	0.24	Group14	7.55	4	[cst-1, dyb-1, slo-1, tbx-2]
GO:0007271	synaptic transmission, cholinergic	0.43	Group14	7.14	3	[dyb-1, nid-1, unc-75]
GO:0061061	muscle structure development	0.49	Group14	4.88	4	[cst-1, dyb-1, slo-1, tbx-2]

GO:0099177	regulation of trans-synaptic signaling	0.16	Group14	4.55	3	[dyb-1, slo-1, unc-75]
GO:0050804	modulation of chemical synaptic transmission	0.16	Group14	4.55	3	[dyb-1, slo-1, unc-75]
GO:0007267	cell-cell signaling	0.15	Group14	4.10	10	[cwn-1, cwn-2, dlg-1, dyb-1, lev-8, nid-1, slo-1, syg-1, syg-2, unc-75]
GO:0000122	negative regulation of transcription by RNA polymerase II	0.00	Group15	10.26	8	[atf-2, blmp-1, ces-1, cfi-1, hbl-1, lin-42, pros-1, zag-1]
GO:0045861	negative regulation of proteolysis	0.15	Group15	7.14	5	[F30H5.3, F54E2.2, K10D3.4, T01D3.3, mlt-11]
GO:0010466	negative regulation of peptidase activity	0.15	Group15	7.14	5	[F30H5.3, F54E2.2, K10D3.4, T01D3.3, mlt-11]
GO:0051253	negative regulation of RNA metabolic process	0.02	Group15	6.77	9	[atf-2, blmp-1, ces-1, cfi-1, hbl-1, lin-42, pros-1, rpm-1, zag-1]
GO:0045892	negative regulation of transcription, DNA-templated	0.04	Group15	6.61	8	[atf-2, blmp-1, ces-1, cfi-1, hbl-1, lin-42, pros-1, zag-1]
GO:1902679	negative regulation of RNA biosynthetic process	0.04	Group15	6.40	8	[atf-2, blmp-1, ces-1, cfi-1, hbl-1, lin-42, pros-1, zag-1]
GO:1903507	negative regulation of nucleic acid-templated transcription	0.04	Group15	6.40	8	[atf-2, blmp-1, ces-1, cfi-1, hbl-1, lin-42, pros-1, zag-1]
GO:0051346	negative regulation of hydrolase activity	0.21	Group15	6.33	5	[F30H5.3, F54E2.2, K10D3.4, T01D3.3, mlt-11]
GO:0052547	regulation of peptidase activity	0.24	Group15	5.95	5	[F30H5.3, F54E2.2, K10D3.4, T01D3.3, mlt-11]
GO:0045934	negative regulation of nucleobase-containing compound metabolic process	0.04	Group15	5.88	9	[atf-2, blmp-1, ces-1, cfi-1, hbl-1, lin-42, pros-1, rpm-1, zag-1]
GO:0045944	positive regulation of transcription by RNA polymerase II	0.02	Group15	5.39	11	[atf-8, blmp-1, ceh-30, ces-2, cfi-1, pha-4, pros-1, rhgf-2, ttx-1, unc-42, unc-86]
GO:2000113	negative regulation of cellular macromolecule biosynthetic process	0.04	Group15	5.35	10	[ain-1, alg-1, atf-2, blmp-1, ces-1, cfi-1, hbl-1, lin-42, pros-1, zag-1]
GO:0010558	negative regulation of macromolecule biosynthetic process	0.04	Group15	5.24	10	[ain-1, alg-1, atf-2, blmp-1, ces-1, cfi-1, hbl-1, lin-42, pros-1, zag-1]
GO:0045893	positive regulation of transcription, DNA-templated	0.04	Group15	4.98	11	[atf-8, blmp-1, ceh-30, ces-2, cfi-1, pha-4, pros-1, rhgf-2, ttx-1, unc-42, unc-86]
GO:0006357	regulation of transcription by RNA polymerase II	0.00	Group15	4.96	19	[atf-2, atf-8, blmp-1, ceh-30, ces-1, ces-2, cfi-1, egl-46, hbl-1, lin-42, pha-4, pros-1, rhgf-2, tbx-2, ttx-1, unc-129, unc-42, unc-86, zag-1]
GO:1902680	positive regulation of RNA biosynthetic process	0.04	Group15	4.95	11	[atf-8, blmp-1, ceh-30, ces-2, cfi-1, pha-4, pros-1, rhgf-2, ttx-1, unc-42, unc-86]
GO:1903508	positive regulation of nucleic acid-templated transcription	0.04	Group15	4.95	11	[atf-8, blmp-1, ceh-30, ces-2, cfi-1, pha-4, pros-1, rhgf-2, ttx-1, unc-42, unc-86]

GO:0051172	negative regulation of nitrogen compound metabolic process	0.00	Group15	4.92	16	[F30H5.3, F54E2.2, K10D3.4, T01D3.3, ain-1, alg-1, atf-2, blmp-1, ces-1, cfi-1, hbl-1, lin-42, mlt-11, pros-1, rpm-1, zag-1]
GO:0051254	positive regulation of RNA metabolic process	0.03	Group15	4.90	12	[atf-8, blmp-1, ceh-30, ces-2, cfi-1, pha-4, pros-1, rhgf-2, rpm-1, ttx-1, unc-42, unc-86]
GO:0031327	negative regulation of cellular biosynthetic process	0.07	Group15	4.81	10	[ain-1, alg-1, atf-2, blmp-1, ces-1, cfi-1, hbl-1, lin-42, pros-1, zag-1]
GO:0010951	negative regulation of endopeptidase activity	0.21	Group15	4.76	3	[F30H5.3, K10D3.4, mlt-11]
GO:0009890	negative regulation of biosynthetic process	0.08	Group15	4.74	10	[ain-1, alg-1, atf-2, blmp-1, ces-1, cfi-1, hbl-1, lin-42, pros-1, zag-1]
GO:0031324	negative regulation of cellular metabolic process	0.00	Group15	4.73	16	[F30H5.3, F54E2.2, K10D3.4, T01D3.3, ain-1, alg-1, atf-2, blmp-1, ces-1, cfi-1, hbl-1, lin-42, mlt-11, pros-1, rpm-1, zag-1]
GO:0045935	positive regulation of nucleobase-containing compound metabolic process	0.04	Group15	4.67	12	[atf-8, blmp-1, ceh-30, ces-2, cfi-1, pha-4, pros-1, rhgf-2, rpm-1, ttx-1, unc-42, unc-86]
GO:0043087	regulation of GTPase activity	0.32	Group15	4.49	4	[plx-2, rga-2, rgs-1, rhgf-2]
GO:0010557	positive regulation of macromolecule biosynthetic process	0.07	Group15	4.49	11	[atf-8, blmp-1, ceh-30, ces-2, cfi-1, pha-4, pros-1, rhgf-2, ttx-1, unc-42, unc-86]
GO:0032269	negative regulation of cellular protein metabolic process	0.19	Group15	4.47	8	[F30H5.3, F54E2.2, K10D3.4, T01D3.3, ain-1, alg-1, mlt-11, rpm-1]
GO:0043086	negative regulation of catalytic activity	0.43	Group15	4.46	5	[F30H5.3, F54E2.2, K10D3.4, T01D3.3, mlt-11]
GO:0006366	transcription by RNA polymerase II	0.00	Group15	4.45	19	[atf-2, atf-8, blmp-1, ceh-30, ces-1, ces-2, cfi-1, egl-46, hbl-1, lin-42, pha-4, pros-1, rhgf-2, tbx-2, ttx-1, unc-129, unc-42, unc-86, zag-1]
GO:0051248	negative regulation of protein metabolic process	0.19	Group15	4.44	8	[F30H5.3, F54E2.2, K10D3.4, T01D3.3, ain-1, alg-1, mlt-11, rpm-1]
GO:0051336	regulation of hydrolase activity	0.15	Group15	4.43	9	[F30H5.3, F54E2.2, K10D3.4, T01D3.3, mlt-11, plx-2, rga-2, rgs-1, rhgf-2]
GO:0009891	positive regulation of biosynthetic process	0.08	Group15	4.42	11	[atf-8, blmp-1, ceh-30, ces-2, cfi-1, pha-4, pros-1, rhgf-2, ttx-1, unc-42, unc-86]
GO:0031328	positive regulation of cellular biosynthetic process	0.08	Group15	4.42	11	[atf-8, blmp-1, ceh-30, ces-2, cfi-1, pha-4, pros-1, rhgf-2, ttx-1, unc-42, unc-86]
GO:0010628	positive regulation of gene expression	0.04	Group15	4.39	13	[atf-8, blmp-1, ceh-30, ces-2, cfi-1, pha-4, pros-1, rhgf-2, rpm-1, tlp-1, ttx-1, unc-42, unc-86]
GO:0052548	regulation of endopeptidase activity	0.10	Group15	4.11	3	[F30H5.3, K10D3.4, mlt-11]
GO:0044092	negative regulation of molecular function	0.41	Group15	4.00	5	[F30H5.3, F54E2.2, K10D3.4, T01D3.3, mlt-11]
GO:0033564	anterior/posterior axon guidance	0.03	Group16	30.00	3	[cwn-1, cwn-2, fmi-1]

GO:1905489	regulation of sensory neuron axon guidance	0.04	Group16	27.27	3	[cwn-1, rpm-1, slt-1]
GO:0097374	sensory neuron axon guidance	0.05	Group16	25.00	3	[cwn-1, rpm-1, slt-1]
GO:0008038	neuron recognition	0.00	Group16	23.81	5	[dma-1, plx-2, slt-1, syg-1, syg-2]
GO:0051271	negative regulation of cellular component movement	0.06	Group16	23.08	3	[blmp-1, rpm-1, slt-1]
GO:0045665	negative regulation of neuron differentiation	0.08	Group16	20.00	3	[rhgf-2, rpm-1, slt-1]
GO:0010977	negative regulation of neuron projection development	0.08	Group16	20.00	3	[rhgf-2, rpm-1, slt-1]
GO:0050768	negative regulation of neurogenesis	0.10	Group16	17.65	3	[rhgf-2, rpm-1, slt-1]
GO:0010770	positive regulation of cell morphogenesis involved in differentiation	0.04	Group16	16.67	4	[cwn-1, dma-1, plx-2, zag-1]
GO:0033563	dorsal/ventral axon guidance	0.04	Group16	16.00	4	[rpm-1, slt-1, unc-129, unc-44]
GO:0050772	positive regulation of axonogenesis	0.13	Group16	15.79	3	[cwn-1, plx-2, zag-1]
GO:0010976	positive regulation of neuron projection development	0.01	Group16	15.15	5	[cwn-1, ddr-2, dma-1, plx-2, zag-1]
GO:0031345	negative regulation of cell projection organization	0.13	Group16	15.00	3	[rhgf-2, rpm-1, slt-1]
GO:0051961	negative regulation of nervous system development	0.13	Group16	15.00	3	[rhgf-2, rpm-1, slt-1]
GO:0050769	positive regulation of neurogenesis	0.00	Group16	15.00	6	[cwn-1, cwn-2, ddr-2, dma-1, plx-2, zag-1]
GO:0097485	neuron projection guidance	0.00	Group16	14.74	14	[cwn-1, cwn-2, ddr-2, dma-1, efn-2, egl-46, fmi-1, nid-1, plx-2, rpm-1, slt-1, unc-129, unc-44, zag-1]
GO:0045666	positive regulation of neuron differentiation	0.02	Group16	14.29	5	[cwn-1, ddr-2, dma-1, plx-2, zag-1]
GO:0008045	motor neuron axon guidance	0.15	Group16	14.29	3	[ddr-2, rpm-1, unc-129]
GO:0007411	axon guidance	0.00	Group16	13.83	13	[cwn-1, cwn-2, ddr-2, efn-2, egl-46, fmi-1, nid-1, plx-2, rpm-1, slt-1, unc-129, unc-44, zag-1]
GO:0040013	negative regulation of locomotion	0.16	Group16	13.64	3	[blmp-1, rpm-1, slt-1]
GO:0051962	positive regulation of nervous system development	0.00	Group16	13.46	7	[cwn-1, cwn-2, ddr-2, dma-1, plx-2, rpm-1, zag-1]
GO:0007409	axonogenesis	0.00	Group16	13.18	17	[cwn-1, cwn-2, ddr-2, dma-1, efn-2, egl-46, fmi-1, lron-1, nid-1, plx-2, rpm-1, slt-1, syg-1, syg-2, unc-129, unc-44, zag-1]
GO:0031346	positive regulation of cell projection organization	0.02	Group16	13.16	5	[cwn-1, ddr-2, dma-1, plx-2, zag-1]

GO:0048667	cell morphogenesis involved in neuron differentiation	0.00	Group16	12.41	17	[cwn-1, cwn-2, ddr-2, dma-1, efn-2, egl-46, fmi-1, lron-1, nid-1, plx-2, rpm-1, slt-1, syg-1, syg-2, unc-129, unc-44, zag-1]
GO:1902667	regulation of axon guidance	0.08	Group16	12.12	4	[cwn-1, plx-2, rpm-1, slt-1]
GO:0030182	neuron differentiation	0.00	Group16	12.11	27	[cfi-1, cwn-1, cwn-2, ddr-2, dma-1, dyf-7, efn-2, egl-43, egl-46, fmi-1, lron-1, nid-1, plx-2, pros-1, rhgf-2, rpm-1, slt-1, sox-2, syg-1, syg-2, ttx-1, unc-129, unc-42, unc-44, unc-75, unc-86, zag-1]
GO:0000904	cell morphogenesis involved in differentiation	0.00	Group16	11.97	17	[cwn-1, cwn-2, ddr-2, dma-1, efn-2, egl-46, fmi-1, lron-1, nid-1, plx-2, rpm-1, slt-1, syg-1, syg-2, unc-129, unc-44, zag-1]
GO:0120039	plasma membrane bounded cell projection morphogenesis	0.00	Group16	11.97	17	[cwn-1, cwn-2, ddr-2, dma-1, efn-2, egl-46, fmi-1, lron-1, nid-1, plx-2, rpm-1, slt-1, syg-1, syg-2, unc-129, unc-44, zag-1]
GO:0048812	neuron projection morphogenesis	0.00	Group16	11.97	17	[cwn-1, cwn-2, ddr-2, dma-1, efn-2, egl-46, fmi-1, lron-1, nid-1, plx-2, rpm-1, slt-1, syg-1, syg-2, unc-129, unc-44, zag-1]
GO:0001764	neuron migration	0.03	Group16	11.90	5	[cwn-1, cwn-2, egl-46, nid-1, slt-1]
GO:0048858	cell projection morphogenesis	0.00	Group16	11.81	17	[cwn-1, cwn-2, ddr-2, dma-1, efn-2, egl-46, fmi-1, lron-1, nid-1, plx-2, rpm-1, slt-1, syg-1, syg-2, unc-129, unc-44, zag-1]
GO:0010721	negative regulation of cell development	0.20	Group16	11.54	3	[rhgf-2, rpm-1, slt-1]
GO:0032990	cell part morphogenesis	0.00	Group16	11.49	17	[cwn-1, cwn-2, ddr-2, dma-1, efn-2, egl-46, fmi-1, lron-1, nid-1, plx-2, rpm-1, slt-1, syg-1, syg-2, unc-129, unc-44, zag-1]
GO:0061564	axon development	0.00	Group16	11.41	17	[cwn-1, cwn-2, ddr-2, dma-1, efn-2, egl-46, fmi-1, lron-1, nid-1, plx-2, rpm-1, slt-1, syg-1, syg-2, unc-129, unc-44, zag-1]
GO:0048699	generation of neurons	0.00	Group16	11.07	27	[cfi-1, cwn-1, cwn-2, ddr-2, dma-1, dyf-7, efn-2, egl-43, egl-46, fmi-1, lron-1, nid-1, plx-2, pros-1, rhgf-2, rpm-1, slt-1, sox-2, syg-1, syg-2, ttx-1, unc-129, unc-42, unc-44, unc-75, unc-86, zag-1]
GO:0031175	neuron projection development	0.00	Group16	11.05	19	[cwn-1, cwn-2, ddr-2, dma-1, dyf-7, efn-2, egl-46, fmi-1, lron-1, nid-1, plx-2, rhgf-2, rpm-1, slt-1, syg-1, syg-2, unc-129, unc-44, zag-1]
GO:0022008	neurogenesis	0.00	Group16	10.67	27	[cfi-1, cwn-1, cwn-2, ddr-2, dma-1, dyf-7, efn-2, egl-43, egl-46, fmi-1, lron-1, nid-1, plx-2, pros-1, rhgf-2, rpm-1, slt-1, sox-2, syg-1, syg-2, ttx-1, unc-129, unc-42, unc-44, unc-75, unc-86, zag-1]
GO:0050767	regulation of neurogenesis	0.00	Group16	10.38	11	[cwn-1, cwn-2, ddr-2, dma-1, egl-43, plx-2, rhgf-2, rpm-1, slt-1, unc-75, zag-1]
GO:0048666	neuron development	0.00	Group16	10.26	20	[cwn-1, cwn-2, ddr-2, dma-1, dyf-7, efn-2, egl-46, fmi-1, lron-1, nid-1, plx-2, rhgf-2, rpm-1, slt-1, syg-1, syg-2, unc-129, unc-44, unc-86, zag-1]

GO:0045664	regulation of neuron differentiation	0.00	Group16	10.00	10	[cwn-1, ddr-2, dma-1, egl-43, plx-2, rhgf-2, rpm-1, slt-1, unc-75, zag-1]
GO:0010720	positive regulation of cell development	0.03	Group16	9.68	6	[cwn-1, cwn-2, ddr-2, dma-1, plx-2, zag-1]
GO:0060560	developmental growth involved in morphogenesis	0.03	Group16	9.52	6	[dma-1, rpm-1, slt-1, syg-1, syg-2, zag-1]
GO:0045596	negative regulation of cell differentiation	0.29	Group16	9.38	3	[rhgf-2, rpm-1, slt-1]
GO:0010975	regulation of neuron projection development	0.00	Group16	9.30	8	[cwn-1, ddr-2, dma-1, plx-2, rhgf-2, rpm-1, slt-1, zag-1]
GO:0050920	regulation of chemotaxis	0.08	Group16	9.26	5	[cwn-1, mps-2, plx-2, rpm-1, slt-1]
GO:0006935	chemotaxis	0.00	Group16	9.09	15	[cwn-1, cwn-2, ddr-2, dma-1, efn-2, egl-46, fmi-1, mps-2, nid-1, plx-2, rpm-1, slt-1, unc-129, unc-44, zag-1]
GO:0007399	nervous system development	0.00	Group16	9.09	30	[ceh-30, cfi-1, cwn-1, cwn-2, ddr-2, dlg-1, dma-1, dyf-7, efn-2, egl-43, egl-46, fmi-1, lron-1, nab-1, nid-1, plx-2, pros-1, rhgf-2, rpm-1, slt-1, sox-2, syg-1, syg-2, ttx-1, unc-129, unc-42, unc-44, unc-75, unc-86, zag-1]
GO:0120035	regulation of plasma membrane bounded cell projection organization	0.00	Group16	9.00	9	[cwn-1, ddr-2, dma-1, plx-2, rhgf-2, rpm-1, slt-1, ttx-1, zag-1]
GO:0048588	developmental cell growth	0.04	Group16	8.96	6	[dma-1, rpm-1, slt-1, syg-1, syg-2, zag-1]
GO:0051960	regulation of nervous system development	0.00	Group16	8.87	11	[cwn-1, cwn-2, ddr-2, dma-1, egl-43, plx-2, rhgf-2, rpm-1, slt-1, unc-75, zag-1]
GO:0007416	synapse assembly	0.18	Group16	8.70	4	[nab-1, rpm-1, syg-1, syg-2]
GO:0031344	regulation of cell projection organization	0.00	Group16	8.57	9	[cwn-1, ddr-2, dma-1, plx-2, rhgf-2, rpm-1, slt-1, ttx-1, zag-1]
GO:0010769	regulation of cell morphogenesis involved in differentiation	0.05	Group16	8.57	6	[cwn-1, dma-1, plx-2, rpm-1, slt-1, zag-1]
GO:0050808	synapse organization	0.05	Group16	8.45	6	[dyb-1, nab-1, nid-1, rpm-1, syg-1, syg-2]
GO:0042330	taxis	0.00	Group16	8.38	15	[cwn-1, cwn-2, ddr-2, dma-1, efn-2, egl-46, fmi-1, mps-2, nid-1, plx-2, rpm-1, slt-1, unc-129, unc-44, zag-1]
GO:0010171	body morphogenesis	0.05	Group16	8.33	6	[dpy-10, dpy-2, lim-7, rhgf-2, rpm-1, unc-44]
GO:0050770	regulation of axonogenesis	0.10	Group16	8.33	5	[cwn-1, plx-2, rpm-1, slt-1, zag-1]
GO:0030516	regulation of axon extension	0.39	Group16	7.89	3	[rpm-1, slt-1, zag-1]
GO:0120036	plasma membrane bounded cell projection organization	0.00	Group16	7.87	20	[cwn-1, cwn-2, ddr-2, dma-1, dyf-7, efn-2, egl-46, fmi-1, lron-1, nid-1, plx-2, rhgf-2, rpm-1, slt-1, syg-1, syg-2, ttx-1, unc-129, unc-44, zag-1]
GO:0060284	regulation of cell development	0.00	Group16	7.80	11	[cwn-1, cwn-2, ddr-2, dma-1, egl-43, plx-2, rhgf-2, rpm-1, slt-1, unc-75, zag-1]
GO:0045597	positive regulation of cell differentiation	0.07	Group16	7.79	6	[cwn-1, cwn-2, ddr-2, dma-1, plx-2, zag-1]

GO:0061387	regulation of extent of cell growth	0.39	Group16	7.69	3	[rpm-1, slt-1, zag-1]
GO:0030030	cell projection organization	0.00	Group16	7.60	20	[cwn-1, cwn-2, ddr-2, dma-1, dyf-7, efn-2, egl-46, fmi-1, lron-1, nid-1, plx-2, rhgf-2, rpm-1, slt-1, syg-1, syg-2, ttx-1, unc-129, unc-44, zag-1]
GO:0001558	regulation of cell growth	0.24	Group16	7.27	4	[dma-1, rpm-1, slt-1, zag-1]
GO:0048468	cell development	0.00	Group16	6.99	30	[H42K12.3, T26C5.2, cst-1, cwn-1, cwn-2, ddr-2, dma-1, dyb-1, dyf-7, efn-2, egl-43, egl-46, fmi-1, let-4, lron-1, nid-1, noah-1, noah-2, plx-2, rhgf-2, rpm-1, slo-1, slt-1, syg-1, syg-2, unc-129, unc-44, unc-75, unc-86, zag-1]
GO:1990138	neuron projection extension	0.28	Group16	6.90	4	[dma-1, rpm-1, slt-1, zag-1]
GO:0000902	cell morphogenesis	0.00	Group16	6.84	18	[cwn-1, cwn-2, ddr-2, dma-1, efn-2, egl-46, fmi-1, lron-1, nid-1, plx-2, rhgf-2, rpm-1, slt-1, syg-1, syg-2, unc-129, unc-44, zag-1]
GO:0032989	cellular component morphogenesis	0.00	Group16	6.67	20	[cwn-1, cwn-2, ddr-2, dma-1, dyb-1, efn-2, egl-46, fmi-1, lron-1, nid-1, plx-2, rhgf-2, rpm-1, slo-1, slt-1, syg-1, syg-2, unc-129, unc-44, zag-1]
GO:0032101	regulation of response to external stimulus	0.14	Group16	6.32	6	[cwn-1, ddr-2, mps-2, plx-2, rpm-1, slt-1]
GO:0030154	cell differentiation	0.00	Group16	6.27	46	[H42K12.3, T26C5.2, ceh-30, ceh-34, ceh-6, cfi-1, cst-1, cwn-1, cwn-2, ddr-2, dma-1, dsl-3, dsl-6, dsl-7, dyb-1, dyf-7, efn-2, egl-43, egl-46, fmi-1, jmjd-3.1, let-4, lin-42, lron-1, nid-1, noah-1, noah-2, pha-4, plx-2, pros-1, rhgf-2, rpm-1, slo-1, slt-1, sox-2, syg-1, syg-2, tbx-2, tsp-14, ttx-1, unc-129, unc-42, unc-44, unc-75, unc-86, zag-1]
GO:0051270	regulation of cellular component movement	0.09	Group16	6.09	7	[blmp-1, cwn-1, cwn-2, egl-43, plx-2, rpm-1, slt-1]
GO:0045595	regulation of cell differentiation	0.01	Group16	5.88	12	[cwn-1, cwn-2, ddr-2, dma-1, egl-43, plx-2, rhgf-2, rpm-1, slt-1, tsp-14, unc-75, zag-1]
GO:0048731	system development	0.00	Group16	5.87	38	[alg-1, blmp-1, ceh-30, cfi-1, cwn-1, cwn-2, ddr-2, dlg-1, dma-1, dre-1, dyf-7, efn-2, egl-43, egl-46, fmi-1, lim-7, lron-1, nab-1, nid-1, pha-4, plx-2, pros-1, rhgf-2, rpm-1, slt-1, sox-2, spd-3, syg-1, syg-2, tbx-2, tsp-14, ttx-1, unc-129, unc-42, unc-44, unc-75, unc-86, zag-1]
GO:0008361	regulation of cell size	0.27	Group16	5.66	3	[rpm-1, slt-1, zag-1]
GO:0048675	axon extension	0.27	Group16	5.66	3	[rpm-1, slt-1, zag-1]
GO:0010469	regulation of signaling receptor activity	0.30	Group16	5.08	3	[cwn-1, cwn-2, unc-129]
GO:0048638	regulation of developmental growth	0.18	Group16	5.00	7	[dma-1, dpy-2, rpm-1, slt-1, tsp-14, unc-44, zag-1]

GO:0040012	regulation of locomotion	0.03	Group16	4.94	12	[blmp-1, cwn-1, cwn-2, dyb-1, egl-43, lam-2, mps-2, plx-2, rhgf-2, rpm-1, slt-1, sup-12]
GO:0051094	positive regulation of developmental process	0.07	Group16	4.85	10	[blmp-1, cwn-1, cwn-2, ddr-2, dma-1, plx-2, rpm-1, tsp-14, unc-44, zag-1]
GO:0016477	cell migration	0.11	Group16	4.74	9	[blmp-1, cwn-1, cwn-2, dre-1, egl-43, egl-46, nid-1, slt-1, unc-129]
GO:0030334	regulation of cell migration	0.47	Group16	4.71	4	[blmp-1, cwn-1, cwn-2, egl-43]
GO:0009653	anatomical structure morphogenesis	0.00	Group16	4.65	29	[acn-1, cdh-3, ceh-34, cwn-1, cwn-2, ddr-2, dma-1, dpy-10, dpy-2, dyb-1, efn-2, egl-46, fmi-1, lim-7, lron-1, nid-1, pha-4, plx-2, ptr-4, rhgf-2, rpm-1, slo-1, slt-1, syg-1, syg-2, tsp-14, unc-129, unc-44, zag-1]
GO:2000145	regulation of cell motility	0.35	Group16	4.55	4	[blmp-1, cwn-1, cwn-2, egl-43]
GO:0048870	cell motility	0.14	Group16	4.52	9	[blmp-1, cwn-1, cwn-2, dre-1, egl-43, egl-46, nid-1, slt-1, unc-129]
GO:0042981	regulation of apoptotic process	0.43	Group16	4.46	5	[ceh-30, cst-1, dre-1, rpm-1, unc-129]
GO:0040008	regulation of growth	0.29	Group16	4.24	7	[dma-1, dpy-2, rpm-1, slt-1, tsp-14, unc-44, zag-1]
GO:0007275	multicellular organism development	0.00	Group16	4.23	63	[H42K12.3, T26C5.2, acn-1, ajm-1, alg-1, atf-8, blmp-1, cdh-3, ceh-30, ceh-34, ceh-6, ces-2, cfi-1, cst-1, cwn-1, cwn-2, ddr-2, dlg-1, dma-1, dpy-10, dpy-17, dpy-2, dpy-3, dre-1, dsl-3, dsl-6, dsl-7, dyf-7, efn-2, egl-43, egl-46, fmi-1, hbl-1, let-4, lim-7, lin-42, lron-1, nab-1, nid-1, noah-1, noah-2, pha-4, plx-2, ppt-1, pros-1, ptr-4, rhgf-2, rpm-1, slt-1, sox-2, spd-3, sqt-3, syg-1, syg-2, tbx-2, tsp-14, ttx-1, unc-129, unc-42, unc-44, unc-75, unc-86, zag-1]
GO:0051130	positive regulation of cellular component organization	0.28	Group16	4.22	7	[cwn-1, ddr-2, dma-1, egl-46, plx-2, rpm-1, zag-1]
GO:2000026	regulation of multicellular organismal development	0.06	Group16	4.18	13	[cwn-1, cwn-2, ddr-2, dma-1, egl-43, lin-42, plx-2, rhgf-2, rpm-1, slt-1, tsp-14, unc-75, zag-1]
GO:0090066	regulation of anatomical structure size	0.26	Group16	4.00	4	[let-4, rpm-1, slt-1, zag-1]

Table S 15 Biological process fused GO terms enriched in *ahr-1(ju145)* vs. wild-type. P-values are corrected with Bonferroni step down. GO terms are sorted according to their GO group in CytoScape.

GO ID	GO Term	P-value	GO Groups	Associated Genes (%)	No. Genes	Associated Genes Found
GO:0007160	cell-matrix adhesion	0.01	Group00	33.33	3	[B0393.5, R09E10.5, nid-1]
GO:0048665	neuron fate specification	0.02	Group01	30.00	3	[sox-2, unc-42, unc-86]
GO:0006334	nucleosome assembly	0.00	Group02	15.79	6	[hil-7, his-1, his-11, his-13, his-24, his-40]
GO:0097376	interneuron axon guidance	0.00	Group03	60.00	3	[ddr-2, fmi-1, nid-1]

GO:0007156	homophilic cell adhesion via plasma membrane adhesion molecules	0.00	Group04	50.00	6	[cdh-1, cdh-3, cdh-5, cdh-8, cdh-9, fmi-1]
GO:0045138	nematode male tail tip morphogenesis	0.03	Group05	7.50	6	[acn-1, cdh-3, plx-2, ptr-4, tsp-14, unc-129]
GO:0007548	sex differentiation	0.01	Group05	5.19	11	[acn-1, alg-1, blmp-1, cdh-3, ceh-30, dre-1, lim-7, plx-2, ptr-4, tsp-14, unc-129]
GO:0001708	cell fate specification	0.00	Group06	8.45	12	[ceh-34, cwn-1, cwn-2, dsl-3, dsl-6, dsl-7, pha-4, sox-2, tbx-2, tsp-14, unc-42, unc-86]
GO:0045165	cell fate commitment	0.00	Group06	7.53	14	[ceh-34, cfi-1, cwn-1, cwn-2, dsl-3, dsl-6, dsl-7, egl-46, pha-4, sox-2, tbx-2, tsp-14, unc-42, unc-86]
GO:0033564	anterior/posterior axon guidance	0.02	Group07	30.00	3	[cwn-1, cwn-2, fmi-1]
GO:0007409	axonogenesis	0.00	Group07	13.18	17	[cwn-1, cwn-2, ddr-2, dma-1, efn-2, egl-46, fmi-1, lron-1, nid-1, plx-2, rpm-1, slt-1, syg-1, syg-2, unc-129, unc-44, zag-1]
GO:0001764	neuron migration	0.02	Group07	11.90	5	[cwn-1, cwn-2, egl-46, nid-1, slt-1]
GO:0006935	chemotaxis	0.00	Group07	9.09	15	[cwn-1, cwn-2, ddr-2, dma-1, efn-2, egl-46, fmi-1, mps-2, nid-1, plx-2, rpm-1, slt-1, unc-129, unc-44, zag-1]
GO:0051270	regulation of cellular component movement	0.04	Group07	6.09	7	[blmp-1, cwn-1, cwn-2, egl-43, plx-2, rpm-1, slt-1]
GO:0002064	epithelial cell development	0.00	Group08	19.23	5	[H42K12.3, T26C5.2, let-4, noah-1, noah-2]
GO:0042338	cuticle development involved in collagen and cuticulin-based cuticle molting cycle	0.00	Group08	19.23	5	[dpy-10, dpy-17, dpy-2, dpy-3, sqt-3]
GO:0042335	cuticle development	0.00	Group08	14.52	9	[H42K12.3, T26C5.2, dpy-10, dpy-17, dpy-2, dpy-3, noah-1, noah-2, sqt-3]
GO:0018996	molting cycle, collagen and cuticulin-based cuticle	0.00	Group08	9.90	10	[acn-1, dpy-10, dpy-17, dpy-2, dpy-3, dre-1, noah-1, noah-2, ptr-4, sqt-3]
GO:0060429	epithelium development	0.04	Group08	7.32	6	[H42K12.3, T26C5.2, cdh-3, let-4, noah-1, noah-2]
GO:0009888	tissue development	0.02	Group08	5.38	10	[H42K12.3, T26C5.2, blmp-1, cdh-3, ceh-30, ceh-34, let-4, noah-1, noah-2, tsp-14]
GO:0000122	negative regulation of transcription by RNA polymerase II	0.00	Group09	10.26	8	[atf-2, blmp-1, ces-1, cfi-1, hbl-1, lin-42, pros-1, zag-1]
GO:0051253	negative regulation of RNA metabolic process	0.01	Group09	6.77	9	[atf-2, blmp-1, ces-1, cfi-1, hbl-1, lin-42, pros-1, rpm-1, zag-1]
GO:0045944	positive regulation of transcription by RNA polymerase II	0.01	Group09	5.39	11	[atf-8, blmp-1, ceh-30, ces-2, cfi-1, pha-4, pros-1, rhgf-2, ttx-1, unc-42, unc-86]

GO:2000113	negative regulation of cellular macromolecule biosynthetic process	0.02	Group09	5.35	10	[ain-1, alg-1, atf-2, blmp-1, ces-1, cfi-1, hbl-1, lin-42, pros-1, zag-1]
GO:0006357	regulation of transcription by RNA polymerase II	0.00	Group09	4.96	19	[atf-2, atf-8, blmp-1, ceh-30, ces-1, ces-2, cfi-1, egl-46, hbl-1, lin-42, pha-4, pros-1, rhgf-2, tbx-2, ttx-1, unc-129, unc-42, unc-86, zag-1]
GO:0051172	negative regulation of nitrogen compound metabolic process	0.00	Group09	4.92	16	[F30H5.3, F54E2.2, K10D3.4, T01D3.3, ain-1, alg-1, atf-2, blmp-1, ces-1, cfi-1, hbl-1, lin-42, mlt-11, pros-1, rpm-1, zag-1]
GO:0051254	positive regulation of RNA metabolic process	0.01	Group09	4.90	12	[atf-8, blmp-1, ceh-30, ces-2, cfi-1, pha-4, pros-1, rhgf-2, rpm-1, ttx-1, unc-42, unc-86]
GO:0031324	negative regulation of cellular metabolic process	0.00	Group09	4.73	16	[F30H5.3, F54E2.2, K10D3.4, T01D3.3, ain-1, alg-1, atf-2, blmp-1, ces-1, cfi-1, hbl-1, lin-42, mlt-11, pros-1, rpm-1, zag-1]
GO:0010628	positive regulation of gene expression	0.02	Group09	4.39	13	[atf-8, blmp-1, ceh-30, ces-2, cfi-1, pha-4, pros-1, rhgf-2, rpm-1, tlp-1, ttx-1, unc-42, unc-86]
GO:0008038	neuron recognition	0.00	Group10	23.81	5	[dma-1, plx-2, slt-1, syg-1, syg-2]
GO:0051271	negative regulation of cellular component movement	0.02	Group10	23.08	3	[blmp-1, rpm-1, slt-1]
GO:0010977	negative regulation of neuron projection development	0.03	Group10	20.00	3	[rhgf-2, rpm-1, slt-1]
GO:0010770	positive regulation of cell morphogenesis involved in differentiation	0.02	Group10	16.67	4	[cwn-1, dma-1, plx-2, zag-1]
GO:0033563	dorsal/ventral axon guidance	0.02	Group10	16.00	4	[rpm-1, slt-1, unc-129, unc-44]
GO:0010976	positive regulation of neuron projection development	0.01	Group10	15.15	5	[cwn-1, ddr-2, dma-1, plx-2, zag-1]
GO:0051962	positive regulation of nervous system development	0.00	Group10	13.46	7	[cwn-1, cwn-2, ddr-2, dma-1, plx-2, rpm-1, zag-1]
GO:0007409	axonogenesis	0.00	Group10	13.18	17	[cwn-1, cwn-2, ddr-2, dma-1, efn-2, egl-46, fmi-1, lron-1, nid-1, plx-2, rpm-1, slt-1, syg-1, syg-2, unc-129, unc-44, zag-1]
GO:0030182	neuron differentiation	0.00	Group10	12.11	27	[cfi-1, cwn-1, cwn-2, ddr-2, dma-1, dyf-7, efn-2, egl-43, egl-46, fmi-1, lron-1, nid-1, plx-2, pros-1, rhgf-2, rpm-1, slt-1, sox-2, syg-1, syg-2, ttx-1, unc-129, unc-42, unc-44, unc-75, unc-86, zag-1]
GO:0001764	neuron migration	0.02	Group10	11.90	5	[cwn-1, cwn-2, egl-46, nid-1, slt-1]
GO:0050767	regulation of neurogenesis	0.00	Group10	10.38	11	[cwn-1, cwn-2, ddr-2, dma-1, egl-43, plx-2, rhgf-2, rpm-1, slt-1, unc-75, zag-1]
GO:0048666	neuron development	0.00	Group10	10.26	20	[cwn-1, cwn-2, ddr-2, dma-1, dyf-7, efn-2, egl-46, fmi-1, lron-1, nid-1, plx-2, rhgf-2, rpm-1, slt-1, syg-1, syg-2, unc-129, unc-44, unc-86, zag-1]

GO:0060560	developmental growth involved in morphogenesis	0.01	Group10	9.52	6	[dma-1, rpm-1, slt-1, syg-1, syg-2, zag-1]
GO:0007399	nervous system development	0.00	Group10	9.09	30	[ceh-30, cfi-1, cwn-1, cwn-2, ddr-2, dlg-1, dma-1, dyf-7, efn-2, egl-43, egl-46, fmi-1, lron-1, nab-1, nid-1, plx-2, pros-1, rhgf-2, rpm-1, slt-1, sox-2, syg-1, syg-2, ttx-1, unc-129, unc-42, unc-44, unc-75, unc-86, zag-1]
GO:0120035	regulation of plasma membrane bounded cell projection organization	0.00	Group10	9.00	9	[cwn-1, ddr-2, dma-1, plx-2, rhgf-2, rpm-1, slt-1, ttx-1, zag-1]
GO:0048588	developmental cell growth	0.02	Group10	8.96	6	[dma-1, rpm-1, slt-1, syg-1, syg-2, zag-1]
GO:0010769	regulation of cell morphogenesis involved in differentiation	0.02	Group10	8.57	6	[cwn-1, dma-1, plx-2, rpm-1, slt-1, zag-1]
GO:0050808	synapse organization	0.02	Group10	8.45	6	[dyb-1, nab-1, nid-1, rpm-1, syg-1, syg-2]
GO:0010171	body morphogenesis	0.02	Group10	8.33	6	[dpy-10, dpy-2, lim-7, rhgf-2, rpm-1, unc-44]
GO:0120036	plasma membrane bounded cell projection organization	0.00	Group10	7.87	20	[cwn-1, cwn-2, ddr-2, dma-1, dyf-7, efn-2, egl-46, fmi-1, lron-1, nid-1, plx-2, rhgf-2, rpm-1, slt-1, syg-1, syg-2, ttx-1, unc-129, unc-44, zag-1]
GO:0048468	cell development	0.00	Group10	6.99	30	[H42K12.3, T26C5.2, cst-1, cwn-1, cwn-2, ddr-2, dma-1, dyb-1, dyf-7, efn-2, egl-43, egl-46, fmi-1, let-4, lron-1, nid-1, noah-1, noah-2, plx-2, rhgf-2, rpm-1, slo-1, slt-1, syg-1, syg-2, unc-129, unc-44, unc-75, unc-86, zag-1]
GO:0000902	cell morphogenesis	0.00	Group10	6.84	18	[cwn-1, cwn-2, ddr-2, dma-1, efn-2, egl-46, fmi-1, lron-1, nid-1, plx-2, rhgf-2, rpm-1, slt-1, syg-1, syg-2, unc-129, unc-44, zag-1]
GO:0032989	cellular component morphogenesis	0.00	Group10	6.67	20	[cwn-1, cwn-2, ddr-2, dma-1, dyb-1, efn-2, egl-46, fmi-1, lron-1, nid-1, plx-2, rhgf-2, rpm-1, slo-1, slt-1, syg-1, syg-2, unc-129, unc-44, zag-1]
GO:0030154	cell differentiation	0.00	Group10	6.27	46	[H42K12.3, T26C5.2, ceh-30, ceh-34, ceh-6, cfi-1, cst-1, cwn-1, cwn-2, ddr-2, dma-1, dsl-3, dsl-6, dsl-7, dyb-1, dyf-7, efn-2, egl-43, egl-46, fmi-1, jmjd-3.1, let-4, lin-42, lron-1, nid-1, noah-1, noah-2, pha-4, plx-2, pros-1, rhgf-2, rpm-1, slo-1, slt-1, sox-2, syg-1, syg-2, tbx-2, tsp-14, ttx-1, unc-129, unc-42, unc-44, unc-75, unc-86, zag-1]
GO:0051270	regulation of cellular component movement	0.04	Group10	6.09	7	[blmp-1, cwn-1, cwn-2, egl-43, plx-2, rpm-1, slt-1]
GO:0045595	regulation of cell differentiation	0.00	Group10	5.88	12	[cwn-1, cwn-2, ddr-2, dma-1, egl-43, plx-2, rhgf-2, rpm-1, slt-1, tsp-14, unc-75, zag-1]

GO:0048731	system development	0.00	Group10	5.87	38	[alg-1, blmp-1, ceh-30, cfi-1, cwn-1, cwn-2, ddr-2, dlg-1, dma-1, dre-1, dyf-7, efn-2, egl-43, egl-46, fmi-1, lim-7, lron-1, nab-1, nid-1, pha-4, plx-2, pros-1, rhgf-2, rpm-1, slt-1, sox-2, spd-3, syg-1, syg-2, tbx-2, tsp-14, ttx-1, unc-129, unc-42, unc-44, unc-75, unc-86, zag-1]
GO:0040012	regulation of locomotion	0.01	Group10	4.94	12	[blmp-1, cwn-1, cwn-2, dyb-1, egl-43, lam-2, mps-2, plx-2, rhgf-2, rpm-1, slt-1, sup-12]
GO:0051094	positive regulation of developmental process	0.03	Group10	4.85	10	[blmp-1, cwn-1, cwn-2, ddr-2, dma-1, plx-2, rpm-1, tsp-14, unc-44, zag-1]
GO:0009653	anatomical structure morphogenesis	0.00	Group10	4.65	29	[acn-1, cdh-3, ceh-34, cwn-1, cwn-2, ddr-2, dma-1, dpy-10, dpy-2, dyb-1, efn-2, egl-46, fmi-1, lim-7, lron-1, nid-1, pha-4, plx-2, ptr-4, rhgf-2, rpm-1, slo-1, slt-1, syg-1, syg-2, tsp-14, unc-129, unc-44, zag-1]
GO:0007275	multicellular organism development	0.00	Group10	4.23	63	[H42K12.3, T26C5.2, acn-1, ajm-1, alg-1, atf-8, blmp-1, cdh-3, ceh-30, ceh-34, ceh-6, ces-2, cfi-1, cst-1, cwn-1, cwn-2, ddr-2, dlg-1, dma-1, dpy-10, dpy-17, dpy-2, dpy-3, dre-1, dsl-3, dsl-6, dsl-7, dyf-7, efn-2, egl-43, egl-46, fmi-1, hbl-1, let-4, lim-7, lin-42, lron-1, nab-1, nid-1, noah-1, noah-2, pha-4, plx-2, ppt-1, pros-1, ptr-4, rhgf-2, rpm-1, slt-1, sox-2, spd-3, sqt-3, syg-1, syg-2, tbx-2, tsp-14, ttx-1, unc-129, unc-42, unc-44, unc-75, unc-86, zag-1]
GO:2000026	regulation of multicellular organismal development	0.02	Group10	4.18	13	[cwn-1, cwn-2, ddr-2, dma-1, egl-43, lin-42, plx-2, rhgf-2, rpm-1, slt-1, tsp-14, unc-75, zag-1]

Table S 16 Molecular function fused GO terms enriched in *ahr-1(ju145)* vs. wild-type. P-values are corrected with Bonferroni step down. GO terms are sorted according to their GO group in CytoScape.

GO ID	GO Term	P-value	GO Groups	Associated Genes (%)	No. Genes	Associated Genes Found
GO:0030414	peptidase inhibitor activity	0.01	Group0	7.35	5	[F30H5.3, F54E2.2, K10D3.4, T01D3.3, mlt-11]
GO:0004867	serine-type endopeptidase inhibitor activity	0.03	Group0	6.12	3	[F30H5.3, K10D3.4, mlt-11]
GO:0046983	protein dimerization activity	0.04	Group1	4.14	6	[asns-2, his-1, his-11, his-13, his-40, syg-2]
GO:0046982	protein heterodimerization activity	0.01	Group1	8.70	4	[his-1, his-11, his-13, his-40]
GO:0000981	RNA polymerase II transcription factor activity, sequence-specific DNA binding	0.00	Group2	8.20	10	[atf-2, atf-8, ceh-30, ces-2, cfi-1, egl-46, hbl-1, pha-4, pros-1, unc-86]
GO:0000982	transcription factor activity, RNA polymerase II proximal promoter sequence-specific DNA binding	0.00	Group2	21.05	4	[atf-2, atf-8, ces-2, pros-1]

GO:0001228	transcriptional activator activity, RNA polymerase II transcription regulatory region sequence-specific DNA binding	0.01	Group2	11.76	4	[atf-8, ceh-30, ces-2, cfi-1]
GO:0044212	transcription regulatory region DNA binding	0.00	Group2	7.48	11	[atf-2, atf-8, blmp-1, ceh-30, ces-1, ces-2, cfi-1, hbl-1, sox-2, ttx-1, unc-86]